Study On Conformation And Ultrafast Dynamics In Biomolecular Recognition With Optical Laser Spectroscopy

THESIS

SUBMITTED FOR THE DEGREE OF

DOCTOR OF PHILOSOPHY (SCIENCE)

BY

SUSOBHAN CHOUDHURY

DEPARTMENT OF BIOCHEMISTRY

UNIVERSITY OF CALCUTTA

2017

To My Parents
and Brother

Acknowledgements

Completion of this doctoral dissertation would never have been possible without the support and guidance of several people. Though it will not be enough to express my gratitude in words to all those people, I would still like to give my many, many thanks to all these people.

First and foremost, I would like to express my gratitude to my supervisor, Prof. Samir Kumar Pal for his valuable guidance, scholarly inputs and consistent encouragement which I have received throughout the research work. This feat was possible only because of the unconditional support provided by him. A person with an amicable and positive disposition, Sir has always made himself available for innumerous helpful discussions and to clarify my doubts. I consider it as a great opportunity to do my doctoral programme under his guidance and to learn from his instrumental expertise, insight into various experimental problems, wisdom and inspiration. He has also provided me a wonderful scientific environment to work and gain scientific experience. He has allowed me to explore new areas of research, interact and collaborate with talented researchers from various national and international institutes. Thank you Sir, for all your kind help and support for me.

I would also like to thank Prof. Siddhartha Roy of Bose Institute, India; Prof. Thalappil Pradeep, of Department of Chemistry, IIT Madras, India; Prof. Gautam Basu of Bose Institute, India; Prof. Peter Lemmens of Braunschweig University of Technology, Germany; Prof. Ramaprasad Mukhopadhyay of BARC, India, Prof. Santasree Mazumdar of Department of Biochemistry, Calcutta University, India and Prof. Ranjan Das of Department of Chemistry, West Bengal State University, India. Special mention is given to Prof. Roy for his valuable advices and for reviewing my works. For support and discussions, I am gratified to the lab members of the Prof. Roy's group specially Dr. Raka Ghose and Basushree Ghose.

I also appreciate for the beautiful work culture and environment in the lab maintained by my seniors and colleagues. The members of the Prof. Pal's group have contributed immensely to my personal and professional time at S. N. Bose Centre. The direction of my Ph.D. work has been strongly influenced by the members of the Prof. Pal's group, notably Dr. Subrata Batabyal, Dr. Prasanna kumar Mondal and Dr. Tanumoy Mondal. I acknowledge Priya for working with me in a significant portion of my thesis. I would like to acknowledge my other colleagues (Samim, Nabarun, Siddhi Di, Prasenjit, Damayanti, Jayeta, Aniruddha, Prabir, Tuhin, Ramesh, Poulomi, Animesh da, Surajit da, Nirmal da, Soma di, and Soumendra Da) for providing me a homely and cheerful environment. I am, especially, thankful to Samim, Nabarun, Aniruddhha and Ramesh who shared glorious moments over a long period of time, supported my work annoyances, and also for the good moments of fun!

I gratefully acknowledge the Council of Scientific & Industrial Research of India for providing me fellowship. My work was also supported by the Department of Science and Technology (DST). I express my gratitude to the members of my thesis committee. I must acknowledge all the teaching and non-teaching staff of S. N. Bose National Centre for Basic Sciences for their kind helps at various phases of this research.

Last but not the least, I would like to pay high regards to my beloved parents, for their devotions, sincere encouragement, support and inspiration throughout my research work that have made me more courageous, dedicated and patient. I owe everything to them and they are the reasons for what I am today. I feel myself very fortunate to have them as parents and Soumen as brother. It is their unconditional love, well wishes and confidence on me that have made this thesis a success.

Date:

Department of Chemical, Biological and Macromolecular Sciences,
S. N. Bose National Centre for Basic Sciences,
Salt Lake, Kolkata 700106, *(Susobhan Choudhury)*
India.

CONTENTS

Chapter 1

Introduction

1.1. Scope of the study on conformation and ultrafast dynamics in biomolecular recognition with optical laser spectroscopy:

Highly specific and tightly regulated interactions between biological macromolecules are referred as biomolecular interactions. Molecular recognition is a fundamental step in any biological process [1-2]. Enzyme catalysis, cellular signalling, protein-protein association, protein crowding, reactant transport, and the noncovalent binding of a receptor with a ligand molecule, to name only a few, involve the recognition between two or more molecular binding partners, leading either to their association or to their rejection [3-7]. Molecular association is most widely investigated, as it generally leads to biological function. Various weak noncovalent interactions, for examples, hydrophobic, electrostatic, van der Waals and hydrogen bonding govern the binding processes during protein-DNA, protein/DNA-drug interactions [8-10]. The protein-DNA interactions can be formed by different domains, such as the zinc finger or the helix-turn-helix [11]. These interactions are involved in a variety of biological processes including DNA replication, DNA repair, viral infection, DNA packing, and DNA modifications [12-15]. Among them, transcription factors (TFs), for examples, lambda repressor protein (cI and Cro), Gal repressor and Lac repressor are the best characterized [16-21]. When a TF binds to specific DNA sequences in promoters, they can promote or repress the transcription of genes [22]. On the other hand drugs (ligand) interact with biomolecules at the latter's active site generally following Emli Fischer's "Lock and Key" model along with other a higher degree of complementarities of thermodynamic parameters for efficient biological activity [23]. Again, a large number of clinically important drugs/ligands and antibiotics

are believed to exert their primary biological action by means of noncovalent interactions with protein and DNA. In view of tremendous number of potential vital interactions occurring in the biological environment, the mechanism underlying the formation of molecular complexes is a key aspect that needs to be rigorously described, not only for advancing our knowledge of chemistry and biology, but also in the development of therapeutics for the treatment of disease.

Till recently, the conventional concepts of affinity and standard kinetic constants were being used frequently to deal with biomolecular recognition processes in protein-DNA interactions [24]. However, during last decades, it appeared that these concepts were insufficient to understand completely the mechanism of biomolecular recognitions [25-26]. Indeed, the outcomes of these interactions were found also depend on other factors and that are not currently accounted for, such as molecular crowding, solvent polarity, distance and orientations among the biomolecules and so on. Biomolecular recognition is also strongly influenced by the conformation and dynamics of the corresponding biomolecules and the environment in which the biomolecules are embedded. Elucidating the role of these conformation and dynamics of biomolecular interactions and the time scales involved provide insights into the mechanism of molecular recognition [27]. A thorough knowledge of the structural, dynamical and energetic parameters that dictate such molecular interactions can find immense use in the modulations of the ligand-macromolecular recognition process which may have enormous application in medicine. In this respect, time resolved fluorescence spectroscopy is an efficient tool to study the process of molecular recognition. In comparison to sophisticated nuclear magnetic resonance (NMR) spectroscopy and X-ray crystallography, fluorescence laser spectroscopy has several advantages, for example due to some of its salient features related to the requirement of low sample concentration, solution phase data collection, noninvasiveness, and cost-effectiveness, has been useful in providing data on

faster experimental time frame of biomacromolecule's structure and dynamics efficiently during biomolecular interactions.

Host-Guest complex formation requires two important criteria to be satisfied; namely, proper conformation of the biomolecules vis-à-vis the ultrafast dynamical flexibility of the biological macromolecules at the interface. In this direction more prominent example is the allosteric regulation, where one effector controls the conformation and dynamics of the active site of the enzyme by binding at the distant site [28-29]. Allosteric regulation is used as a very efficient mechanism to control protein activity in most biological processes, including signal transduction, metabolism, catalysis and gene regulation. Classical biochemistry has taught us that allosteric proteins exist typically in two states, for example active and inactive, and inter-conversion between these two states is modulated by the allosteric signal. There is still considerable debate as to the fundamental mechanisms underlying the function of allosteric systems. However, fast growing lists of examples illustrate the intimate link between internal motions over a wide range of time scales (from femtosecond to nanosecond) and function in protein–ligand interactions [30]. The early crystallographic work on allosteric systems helped to advance and establish a purely structural, 'mechanical' view. However, to insight more details about the contribution of conformation change (enthalpic contribution) and dynamical fluctuations (entropic contribution) fluorescence spectroscopy is the obvious choice [31]. Fluorescence spectroscopy, among other techniques, has been used to explore the different motions of proteins involved in the propagation of long range allosteric signal. Fluorescence spectroscopy, in addition to providing structural information of a biological system in solution, is unique in providing information about the amplitude of motions taking place on a wide range of time scales. To investigate the effect of other external factors like molecular crowding, solvent polarity, and population

heterogeneity on biomolecular interactions fluorescence spectroscopy has been used very frequently.

The key focus of this thesis is to understand the role of conformation and ultrafast dynamics on different type of biomolecular interactions. The structure and dynamics of the individual biomolecules play very crucial role in the biomolecular recognition processes. Several X-ray crystallography and NMR studies have been reported for the structural properties of the interface of some biologically active complexes [32-33]. Very few studies on the interfacial dynamics of the biologically relevant complexes are reported with femtosecond to nanosecond resolution. Fluorescence probing of biomacromolecular dynamics is a popular technique, as it does not suffer from artifacts due to the use of higher concentration of the samples. However, the selection of fluorophore is very crucial to such investigation. In this regard, to explore the coupling between hydration dynamics and structural fluctuations and their effect on molecular recognition, we have studied the photo physical studies of Coumarin 500 with model sodium dodecyl sulfate (SDS) and sodium dodcely benzene sulfonate (SDBS) micelles. SDBS micelles have DNA like π-stacking which is absent in SDS micelles [34-35]. The study was carried out with an anticipation to understand the effect of π-stacking in molecular recognition. A long standing debate in biochemistry is to determine whether the biomolecular interactions proceed through conformational selection (of pre-existing isoforms) or induced fit (ligand-induced 3D reshaping) [36-39]. In this regard, we have used molecular modelling together with experiments to investigate the time scales associated with the conformational flexibility of the protein which plays a key role in the selection of a pathway in biomolecular recognition, is a central event in all biological processes. Another aspect of the present thesis is to study on the dynamical processes involved in molecular recognition in protein-protein and protein-DNA interactions. We have tried to intervene into certain protein-DNA or protein-protein interactions which

are crucial mechanisms in signaling cascades leading to cellular events like regulation of gene expression and transcription. In this regard, we choose galactose repressor protein and different operator DNA (O_E and O_I) to observe the molecular recognition as well as allosteric interaction. We have observed that the DNA sequence changes sub-nanosecond motions in a distant site of a transcription factor (DNA-binding protein) which is likely to have functional consequence in protein-protein interactions and eventually towards the regulation of gene expression [40-41]. Förster resonance energy transfer (FRET) was employed to monitor the distance between donor (tryptophan) and acceptor (IAEDANS) and hence the dynamical and structural fluctuation over the time. Again with another protein, lambda Cro-repressor, we have studied the role of DNA flexibility during specific protein-DNA recognition. We have extensively performed numerous spectroscopic studies to understand the recognition of specific operator DNA sequences (O_R3 and O_R2) by lambda Cro repressor protein, which regulates the lytic cycle of bacteriophage lambda. We also explored the interfacial water dynamics and DNA side chain flexibility using Hoechst 33258 (H258), a well-known DNA minor groove binder, in a well known DNA-CTMA biomaterial. We have investigated the role of water dynamics in the efficacy of the DNA-CTMA biomaterial in bio-LEDs.

1.2. Objective:

Molecular recognition process refers to the weak noncovalent interaction, which takes place selectively and specifically between small ligand molecules with biological macromolecules. Understanding of such recognition in biological and biomimetic milieu is the central attraction for drug designing, which is crucial for the improvement of human healthcare. A thorough knowledge of the structural, dynamical and energetic parameters that dictate such molecular interactions can find immense use in the modulations of the ligand-macromolecule recognition process. DNA is a biomolecule that carries the genetic instructions used in the

growth, development, functioning and reproduction of all known living organisms. To understand the role of π-stacking within the DNA in the course of biomolecular recognition is very much essential for drug designing and for the discovery of new medicines to benefit human health. Dynamic supramolecular assemblies like micelles and reverse micelles are excellent biomimetics for exploration of biological membranes, or protein/DNA interface. SDBS surfactant possesses one benzene moiety, which offers additional rigidity to SDBS micelles through π-stacking. The objective is to rationalize the coupling between structural fluctuation and the dynamics of associated water molecules of biological macromolecules and their effect on molecular recognition. The comparative study on biomimetic using the probe explores the possibility of drug delivery and other therapeutic applications.

In the past decade there has been an intensive effort to develop photonic devices based on biomaterials. From the rich world of organic materials, biomaterials are of particular interest as they often have unusual properties that are not easily replicated in conventional organic or inorganic materials. Furthermore, natural biomaterials are a renewable resource and are inherently biodegradable. DNA−cationic surfactant complexes (cetyltrimethylammonium; CTMA) become promising material in biomaterials-based optoelectronic devices including bio-LEDs. Charge migration along DNA molecules is a key factor in these optoelectronic devices. The association of a significant amount of water molecules in DNA-based materials for the intactness of the DNA structure and their dynamic role in the charge-transfer (CT) dynamics is less documented in contemporary literature. In the present study, we have investigated the role of water dynamics in the efficacy of the charge transfer mechanism in the DNA-CTMA biomaterial.

The binding of a ligand molecule to a protein is often accompanied by conformational changes of the protein. A central question is whether the ligand

induces the conformational change (induced-fit), or rather selects and stabilizes a complementary conformation from a pre-existing equilibrium of ground and excited states of the protein (selected-fit). Although some theoretical hypotheses are there regarding this debate, no direct experimental evidences are present in the contemporary literature. In this regard, we have perturbed the conformational equilibrium simply by changing the pH of the medium and using fluorescence spectroscopy in a microfluidics channel, we have observed that molecular recognition of α-Chymotrypsin in hydrous surroundings at two different pH values (3.6 and 6.3) follows two distinctly different pathways. Whereas one corroborates an induced-fit model (pH 3.6), the other one (pH 6.3) is consistent with the selected-fit model of biomolecular recognition.

Protein–DNA and protein-protein interactions play a crucial role in central biological processes, ranging from the mechanism of replication, transcription and recombination to enzymatic events utilizing nucleic acids as substrates. Various external and internal factors influence the interaction between protein-DNA and protein-protein. While considering the binding nature and extent of interaction, one need to account the allosteric regulation, hydrophobic effect, DNA base pair sequences, hydrogen bonding, shape complementarity, van der Waals interactions etc. In this context, the present study exploits the unique opportunity to study a model protein-DNA complex comprising of galactose repressor (GalR) protein and the two operator DNA sites, O_E and O_I and their consequences in protein-protein (tetramerization) to form a DNA loop encompassing the promoter segment. The study aims to reveal the dynamical behaviour of allostery regulation from N-terminal protein-DNA interaction to C-terminal protein-protein interactions. As a continuation of the above work, in another report, we have studied the role of DNA dynamics in specific protein-DNA interactions. We have investigated the role of dynamics of the minor groove water molecules and also the side chain flexibility of the two operator DNAs (O_R3 and O_R2) in the processes of specific binding to lambda Cro-repressor protein. These dynamical studies are

expected to enhance our understanding of the corresponding biological function of biomolecular recognition.

1.3. Summary of the work done:

1.3.1. Spectroscopic studies on ultrafast structural fluctuation of DNA-like biomimetic systems in molecular recognition:

1.3.1.1. Direct observation of coupling between structural fluctuation and ultrafast hydration dynamics of fluorescent probes in anionic micelles [42]: The coupling of structural fluctuation and the dynamics of associated water molecules of biological macromolecules is vital for various biological activities. Although a number of molecular dynamics (MD) studies on proteins/DNA predicted the importance of such coupling, experimental evidence of variation of hydration dynamics with controlled structural fluctuation even in model macromolecule is sparse and raised controversies in the contemporary literature. Here, we have investigated dynamics of hydration at the surfaces of two similar anionic micelles sodium dodecyl sulfate (SDS) and sodium dodecylbenzenesulfonate (SDBS) as model macromolecules using coumarin 500 (C500) as spectroscopic probe with femtosecond to picosecond time resolution up to 20 ns time window. The constituting surfactants SDS and SDBS are structurally similar except one benzene moiety in the SDBS may offer additional rigidity to the SDBS micelles through π-stacking and added bulkiness. The structural integrity of the micelles in the aqueous medium is confirmed in dynamic light scattering (DLS) studies. A variety of studies including polarization gated fluorescence spectroscopy and quasielastic neutron scattering (QENS) have been used to confirm differential structural fluctuation of SDS and SDBS micelles. We have also employed femtosecond-resolved Förster resonance energy transfer (FRET) in order to study binding of a cationic organic ligand ethidium bromide (EtBr) salt at the micellar surfaces. The distance distribution of the donor (C500)−acceptor (EtBr) in the micellar media reveals the manifestation of the structural flexibility of the micelles. Our studies on

dynamical coupling of the structural flexibility with surface hydration in the nanoscopic micellar media may find the relevance in the "master−slave" type water dynamics in biologically relevant macromolecules.

1.3.2. Spectroscopic studies on the interfacial dynamics at DNA-surfactant interface:

1.3.2.1. Ultrafast dynamics of solvation and charge transfer in a DNA-based biomaterial [43]: Charge migration along DNA molecules is a key factor for DNA-based devices in optoelectronics and biotechnology. The association of a significant amount of water molecules in DNA-based materials for the intactness of the DNA structure and their dynamic role in the charge-transfer (CT) dynamics is less documented in contemporary literature. In the present study, we have used a genomic DNA–cetyltrimethyl ammonium chloride (CTMA) complex, a technological important biomaterial, and Hoechest 33258 (H258), a well-known DNA minor groove binder, as fluorogenic probe for the dynamic solvation studies. The CT dynamics of CdSe/ZnS quantum dots (QDs; 5.2 nm) embedded in the as-prepared and swollen biomaterial have also been studied and correlated with that of the timescale of solvation. We have extended our studies on the temperature-dependent CT dynamics of QDs in a nanoenvironment of an anionic, sodium bis(2-ethylhexyl)- sulfosuccinate reverse micelle (AOT RMs), whereby the number of water molecules and their dynamics can be tuned in a controlled manner. A direct correlation of the dynamics of solvation and that of the CT in the nanoenvironments clearly suggests that the hydration barrier within the Arrhenius framework essentially dictates the charge-transfer dynamics.

1.3.3. Spectroscopic studies on the role of ultrafast conformational dynamics in the molecular recognition of a protein:

1.3.3.1. Direct observation of kinetic pathways of biomolecular recognition [44]: The pathways of molecular recognition, which is a central event in all biological processes, belong to the most important subjects of contemporary research in biomolecular science. By using fluorescence spectroscopy in a microfluidics channel, it can be determined that molecular recognition of α-Chymotrypsin in hydrous surroundings at two different pH values (3.6 and 6.3) follows two distinctly different pathways. Whereas one corroborates an induced-fit model (pH 3.6), the other one (pH 6.3) is consistent with the selected-fit model of biomolecular recognition. The role of massive structural perturbations of differential recognition pathways could be ruled out by earlier XRD studies, rather was consistent with the femtosecond-resolved observation of dynamic flexibility of the protein at different pH values. At low concentrations of ligands, the selected-fit model dominates, whereas increasing the ligand concentration leads to the induced-fit model. From molecular modelling and experimental results, the timescale associated with the conformational flexibility of the protein plays a key role in the selection of a pathway in biomolecular recognition.

1.3.4. Spectroscopic investigation on the role of ultrafast allostery in specific protein-DNA recognition:

1.3.4.1. Modulation of ultrafast conformational dynamics in allosteric interaction of Gal repressor protein with different operator DNA sequences [45]: Although all forms of dynamical behavior of a protein under allosteric interaction with effectors are predicted, little evidence of ultrafast dynamics in the interaction has been reported. Here, we demonstrate the efficacy of a combined approach involving picosecond-resolved FRET and polarization-gated fluorescence for the exploration of ultrafast dynamics in the allosteric interaction

of the Gal repressor (GalR) protein dimer with DNA operator sequences O_E and O_I. FRET from the single tryptophan residue to a covalently attached probe AEDANS at a cysteine residue in the C-terminal domain of GalR shows structural perturbation and conformational dynamics during allosteric interaction. Polarization-gated fluorescence spectroscopy of AEDANS and another probe (FITC) covalently attached to the operator directly revealed the essential dynamics for co-operativity in the protein–protein interaction. The ultrafast resonance energy transfer from AEDANS in the protein to FITC also revealed different dynamic flexibility in the allosteric interaction. An attempt was made to correlate the dynamic changes in the protein dimers with O_E and O_I with the consequent protein–protein interaction (tetramerization) to form a DNA loop encompassing the promoter segment.

1.3.5. Spectroscopic studies on ultrafast conformational DNA-dynamics in specific protein-DNA recognition:

1.3.5.1. Ultrafast differential flexibility of Cro-protein binding domains of two operator DNAs with different sequences [46]: The nature of the interface of specific protein–DNA complexes has attracted immense interest in contemporary molecular biology. Although extensive studies on the role of flexibility of DNA in the specific interaction in the genetic regulatory activity of lambda Cro (Cro-protein) have been performed, the exploration of quantitative features remains deficient. In this study, we have mutated (site directed mutagenesis: SDM) Cro-protein at the 37th position with a cysteine residue (G37C) retaining the functional integrity of the protein and labeled the cysteine residue, which is close to the interface, with a fluorescent probe (AEDANS), for the investigation of its interface with operator DNAs (O_R3 and O_R2). We have employed picosecond resolved polarization gated fluorescence spectroscopy and the well known strategy of solvation dynamics for the exploration of physical motions of the fluorescent

probes and associated environments, respectively. Even though this particular probe on the protein (AEDANS) shows marginal changes in its structural flexibility upon interaction with the DNAs, a non-covalent DNA bound probe (DAPI), which binds to the minor groove, shows a major differential alteration in the dynamical flexibility in the O_R3–Cro complex when compared to that of the O_R2 complex with the Cro-protein. We attempt to correlate the observed significant structural fluctuation of the Cro-protein binding domain of O_R3 for the specificity of the protein to the operator DNA.

1.4. Plan of thesis:

The plan of the thesis is as follows:

Chapter 1: This chapter gives a brief introduction to the scope and motivation behind the thesis work. A brief summary of the work done is also included in this chapter.

Chapter 2: This chapter provides a brief overview of the steady-state and dynamical tools, the structural aspects of biologically important systems (proteins, operator DNA, biomimetic etc.) and fluorescent probes used in the experiments.

Chapter 3: Details of instrumentation, data analysis and experimental procedures have been discussed in this chapter.

Chapter 4: Spectroscopic studies on ultrafast structural fluctuation of DNA-like biomimetic systems in molecular recognition have been elaborated in this chapter.

Chapter 5: Role of water molecules in the charge transfer process in the DNA-based biomaterials have been addressed in this chapter. Spectroscopic studies on the interfacial dynamics at DNA-surfactant interface.

Chapter 6: Spectroscopic studies on the role of ultrafast conformational dynamics in the molecular recognition of a protein is discussed in this chapter.

Chapter 7: In this chapter, the role of ultrafast allostery in specific protein-DNA recognition is elaborated.

Chapter 8: Spectroscopic studies on ultrafast conformational DNA-dynamics in specific protein-DNA recognition is discussed in this chapter.

References

[1] M. R. Lockett, H. Lange, B. Breiten, A. Heroux, W. Sherman, D. Rappoport, P. O. Yau, P. W. Snyder and G. M. Whitesides, The binding of benzoarylsulfonamide ligands to human carbonic anhydrase is insensitive to formal fluorination of the ligand, *Angew. Chem. Int. Ed.* **52**, (2013), 7714.

[2] B. Breiten, M. R. Lockett, W. Sherman, S. Fujita, M. Al-Sayah, H. Lange, C. M. Bowers, A. Heroux, G. Krilov and G. M. Whitesides, Water networks contribute to enthalpy/entropy compensation in protein–ligand binding, *J. Am. Chem. Soc.* **135**, (2013), 15579.

[3] D. Fiedler, D. H. Leung, R. G. Bergman and K. N. Raymond, Selective molecular recognition, C-H bond activation, and catalysis in nanoscale reaction vessels, *Acc. Chem. Res.* **38**, (2005), 349.

[4] G. D. Brown, Dectin-1: A signalling non-tlr pattern-recognition receptor, *Nat. Rev. Immunol.* **6**, (2006), 33.

[5] L. L. Conte, C. Chothia and J. Janin, The atomic structure of protein-protein recognition sites, *J. Mol. Biol.* **285**, (1999), 2177.

[6] R. E. Babine and S. L. Bender, Molecular recognition of protein−ligand complexes: Applications to drug design, *Chem. Rev.* **97**, (1997), 1359.

[7] N. Zacharias and D. A. Dougherty, Cation–pi interactions in ligand recognition and catalysis, *Trends Pharmacol. Sci.* **23**, (2002), 281.

[8] C. G. Kalodimos, N. Biris, A. M. Bonvin, M. M. Levandoski, M. Guennuegues, R. Boelens and R. Kaptein, Structure and flexibility adaptation in nonspecific and specific protein-DNA complexes, *Science* **305**, (2004), 386.

[9] G. Orphanides and D. Reinberg, A unified theory of gene expression, *Cell* **108**, (2002), 439.

[10] C. Muller, P. Calsou, P. Frit and B. Salles, Regulation of the DNA-dependent protein kinase (DNA-PK) activity in eukaryotic cells, *Biochimie* **81**, (1999), 117.

[11] B. Alberts, A. Johnson, J. Lewis, M. Raff, K. Roberts and P. Walter, *DNA-binding motifs in gene regulatory proteins*, **2002**, Garland Science, New York, USA.

[12] I. Haq, Thermodynamics of drug–DNA interactions, *Arch. Biochem. Biophys.* **403**, (2002), 1.

[13] J. B. Chaires, A thermodynamic signature for drug–DNA binding mode, *Arch. Biochem. Biophys.* **453**, (2006), 26.

[14] Q. Liu, M. Kasuga, Y. Sakuma, H. Abe, S. Miura, K. Yamaguchi-Shinozaki and K. Shinozaki, Two transcription factors, $DREB_1$ and $DREB_2$, with an $EREBP/AP_2$ DNA binding domain separate two cellular signal transduction pathways in drought and low-temperature-responsive gene expression, respectively, in arabidopsis, *Plant Cell* **10**, (1998), 1391.

[15] T. Hai and T. Curran, Cross-family dimerization of transcription factors Fos/Jun and ATF/CREB alters DNA binding specificity, *Proc. Natl. Acad. Sci. USA* **88**, (1991), 3720.

[16] M. Ptashne, *A genetic switch: Phage lambda and higher organisms,* **1992**, Cell Press, Boston, USA.

[17] Z. Humayun, D. Kleid and M. Ptashne, Sites of contact between λ operators and λ repressor, *Nucleic Acids Res.* **4**, (1977), 1595.

[18] A. D. Johnson, B. J. Meyer and M. Ptashne, Interactions between DNA-bound repressors govern regulation by the λ phage repressor, *Proc. Natl. Acad. Sci. USA* **76**, (1979), 5061.

[19] S. Malik and R. G. Roeder, The metazoan mediator co-activator complex as an integrative hub for transcriptional regulation, *Nature Rev. Genet.* **11**, (2010), 761.

[20] A. Majumdar and S. Adhya, Probing the structure of gal operator-repressor complexes. Conformation change in DNA, *J. Biol. Chem.* **262**, (1987), 13258.

[21] S. Semsey, M. Geanacopoulos, D. E. Lewis and S. Adhya, Operator-bound galr dimers close DNA loops by direct interaction: Tetramerization and inducer binding, *EMBO J.* **21**, (2002), 4349.

[22] M. E. Massari and C. Murre, Helix-loop-helix proteins: Regulators of transcription in eucaryotic organisms, *Mol. Cell. Biol.* **20**, (2000), 429.

[23] G. Frenkel, D. L. Nelson, B. C. Soltvedt and A. L. Lehninger, *Test bank for nelson and cox, lehninger principles of biochemistry*, **2000**, Worth Publishers, New York, USA.

[24] M. Oda and H. Nakamura, Thermodynamic and kinetic analyses for understanding sequence-specific DNA recognition, *Genes Cells* **5**, (2000), 319.

[25] K. Wollschläger, K. Gaus, A. Körnig, R. Eckel, S. D. Wilking, M. McIntosh, Z. Majer, A. Becker, R. Ros and D. Anselmetti, Single-molecule experiments to elucidate the minimal requirement for DNA recognition by transcription factor epitopes, *Small* **5**, (2009), 484.

[26] R. Eckel, S. D. Wilking, A. Becker, N. Sewald, R. Ros and D. Anselmetti, Single–molecule experiments in synthetic biology: An approach to the affinity ranking of DNA–binding peptides, *Angew. Chem. Int. Ed.* **44**, (2005), 3921.

[27] T. Mondol, S. Banerjee, S. Batabyal and S. K. Pal, Study of biomolecular recognition using time-resolved optical spectroscopy, *IREBIC* **2**, (2011), 211.

[28] M. Karplus and J. Kuriyan, Molecular dynamics and protein function, *Proc. Natl. Acad. Sci. USA* **102**, (2005), 6679.

[29] H. Frauenfelder, B. H. McMahon, R. H. Austin, K. Chu and J. T. Groves, The role of structure, energy landscape, dynamics, and allostery in the enzymatic function of myoglobin, *Proc. Natl. Acad. Sci. USA* **98**, (2001), 2370.

[30] W. A. Eaton, V. Muñoz, S. J. Hagen, G. S. Jas, L. J. Lapidus, E. R. Henry and J. Hofrichter, Fast kinetics and mechanisms in protein folding, *Annu. Rev. Biophys. Biomol. Struct.* **29**, (2000), 327.

[31] D. D. Boehr, R. Nussinov and P. E. Wright, The role of dynamic conformational ensembles in biomolecular recognition, *Nat. Chem. Biol.* **5**, (2009), 789.

[32] M. Akke, NMR methods for characterizing microsecond to millisecond dynamics in recognition and catalysis, *Curr. Opin. Struct. Biol.* **12**, (2002), 642.

[33] N. Tjandra and A. Bax, Direct measurement of distances and angles in biomolecules by nmr in a dilute liquid crystalline medium, *Science* **278**, (1997), 1111.

[34] F. Palazzesi, M. Calvaresi and F. Zerbetto, A molecular dynamics investigation of structure and dynamics of SDS and SDBS micelles, *Soft Matter* **7**, (2011), 9148.

[35] V. Sharma, S. Mitra, M. Johnson and R. Mukhopadhyay, Dynamics in anionic micelles: Effect of phenyl ring, *J. Phys. Chem. B* **117**, (2013), 6250.

[36] J. D. Bryngelson, J. N. Onuchic, N. D. Socci and P. G. Wolynes, Funnels, pathways and the energy landscape of protein folding: A synthesis, *Proteins Struct. Funct. Bioinf.* **21**, (1995), 167.

[37] T. R. Weikl and C. von Deuster, Selected-fit versus induced-fit protein binding: Kinetic differences and mutational analysis, *Proteins Struct. Funct. Bioinf.* **75**, (2009), 104.

[38] C. Tang, C. D. Schwieters and G. M. Clore, Open-to-closed transition in apo maltose-binding protein observed by paramagnetic NMR, *Nature* **449**, (2007), 1078.

[39] A. Mittermaier and L. E. Kay, New tools provide new insights in NMR studies of protein dynamics, *Science* **312**, (2006), 224.

[40] C. Zwieb, J. Kim and S. Adhya, DNA bending by negative regulatory proteins: Gal and lac repressors, *Genes Dev.* **3**, (1989), 606.

[41] M. Brenowitz, E. Jamison, A. Majumdar and S. Adhya, Interaction of the escherichia coli Gal repressor protein with its DNA operators in vitro, *Biochemistry* **29**, (1990), 3374.

[42] S. Choudhury, P. K. Mondal, V. Sharma, S. Mitra, V. G. Sakai, R. Mukhopadhyay and S. K. Pal, Direct observation of coupling between structural fluctuation and ultrafast hydration dynamics of fluorescent probes in anionic micelles, *J. Phys. Chem. B* **119**, (2015), 10849.

[43] S. Choudhury, S. Batabyal, T. Mondol, D. Sao, P. Lemmens and S. K. Pal, Ultrafast dynamics of solvation and charge transfer in a DNA-based biomaterial, *Chem. Asian J.* **9**, (2014), 1395.

[44] S. Choudhury, S. Batabyal, P. K. Mondal, P. Singh, P. Lemmens and S. K. Pal, Direct observation of kinetic pathways of biomolecular recognition, *Chem. Eur. J.* **21**, (2015), 16172.

[45] S. Choudhury, G. Naiya, P. Singh, P. Lemmens, S. Roy and S. K. Pal, Modulation of ultrafast conformational dynamics in allosteric interaction of Gal repressor protein with different operator DNA sequences, *ChemBioChem*, **17**, (2016) 605.

[46] S. Choudhury, B. Ghosh, P. Singh, R. Ghosh, S. Roy and S. K. Pal, Ultrafast differential flexibility of Cro-protein binding domains of two operator DNAs with different sequences, *Phys. Chem. Chem. Phys.* **18**, (2016), 17983.

Chapter 2

An overview of experimental techniques and systems

In order to investigate the various processes involved in the course of study on conformation and ultrafast dynamics in biomolecular recognition, different steady-state and dynamical tools have been employed. These include solvation dynamics, fluorescence anisotropy, Förster resonance energy transfer (FRET), determination of activation energy barrier using Arrhenius theory, diffusion studies, and Circular dichroism (CD). In this chapter, brief discussions about these tools and an overview of various systems used in our studies have been provided.

2.1. Steady-state and dynamical tools:

2.1.1. Solvation dynamics:

2.1.1.1. Theory: Solvation dynamics refer to the process of reorganization of solvent dipoles around a dipole created instantaneously or an electron/proton injected suddenly in a polar liquid. In order to understand the meaning and scope of solvation dynamics, let us first visualize the physical essence of the dynamical process involved for a solute molecule in a polar solvent [1]. A change in the probe (solute) is made at time t=0, by an excitation pulse, which leads to the creation of a dipole. This dipole gives rise to an instantaneous electric field on the solvent molecules. The interaction of permanent dipoles of the solvent with the instantaneously created electric field, shifts the free energy minimum of the solvent to a non-zero value of the polarization. The solvent motion is crucial (Figure 2.1). Since the probe is excited instantaneously (a Franck-Condon transition as far as the nuclear degrees of freedom are concerned), the solvent molecules at t=0 find themselves in a relatively high-energy configuration. Subsequently, the solvent molecules begin to move and rearrange themselves to

reach their new equilibrium positions (Figure 2.2). The nuclear motion involved can be broadly classified into rotational and translational motions.

When the solvent is bulk water, rotational motion would also include hindered rotation and libration, while translation would include the intermolecular vibration due to the extensive hydrogen bonding. The two specific motions, libration and intermolecular vibration, are relatively high in frequency and are expected to play a dominant role in the initial part of solvation [2]. The molecular motions involved are shown schematically in

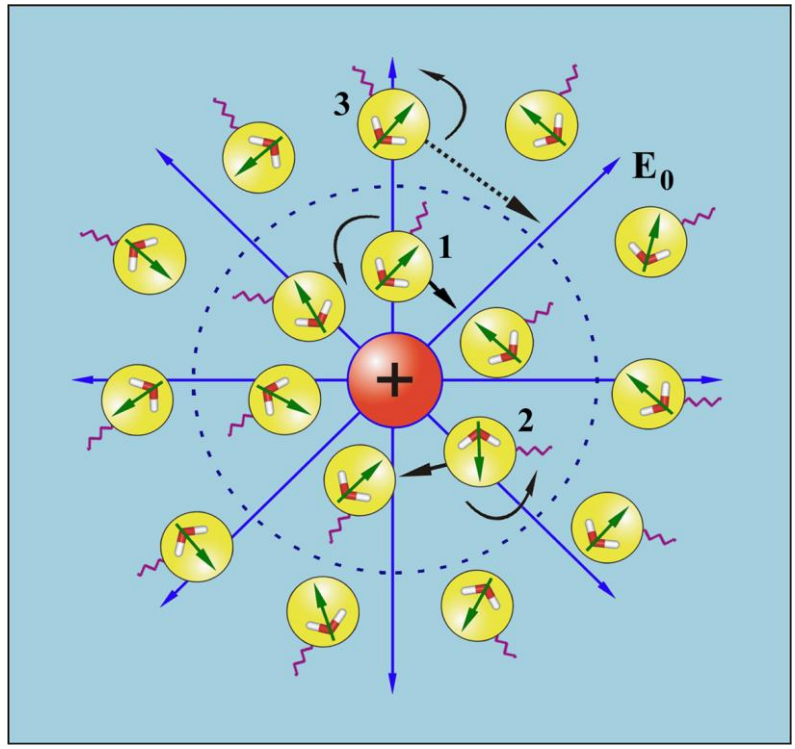

Figure 2.1. *Schematic illustration of solvation of an ion (or dipole) by water. The neighboring molecules (numbered 1 and 2) can either rotate or translate to attain the minimum energy configuration. On the other hand, distant water molecule 3 can only rotate to attain minimum energy configuration. The field is shown as* E_0*. The springs connected to the molecules are meant to denote hydrogen bonding.*

Figure 2.1, and in Figure 2.3 a typical solvation time correlation function is depicted. For clarity, we approximate the motions responsible for the decay in different regions.

A simple way to address the dynamics of polar solvation is to start with the following expression for the solvation energy, $E_{solv}(t)$ [3],

$$E_{solv}(t) = -\frac{1}{2}\int dr\, E_0(r)\cdot P(r,t) \tag{2.1}$$

where $E_0(r)$ is the instantaneously created, position-dependent electric field from the ion or the dipole of the solute and $P(r,t)$ is the position and time-dependent polarization.

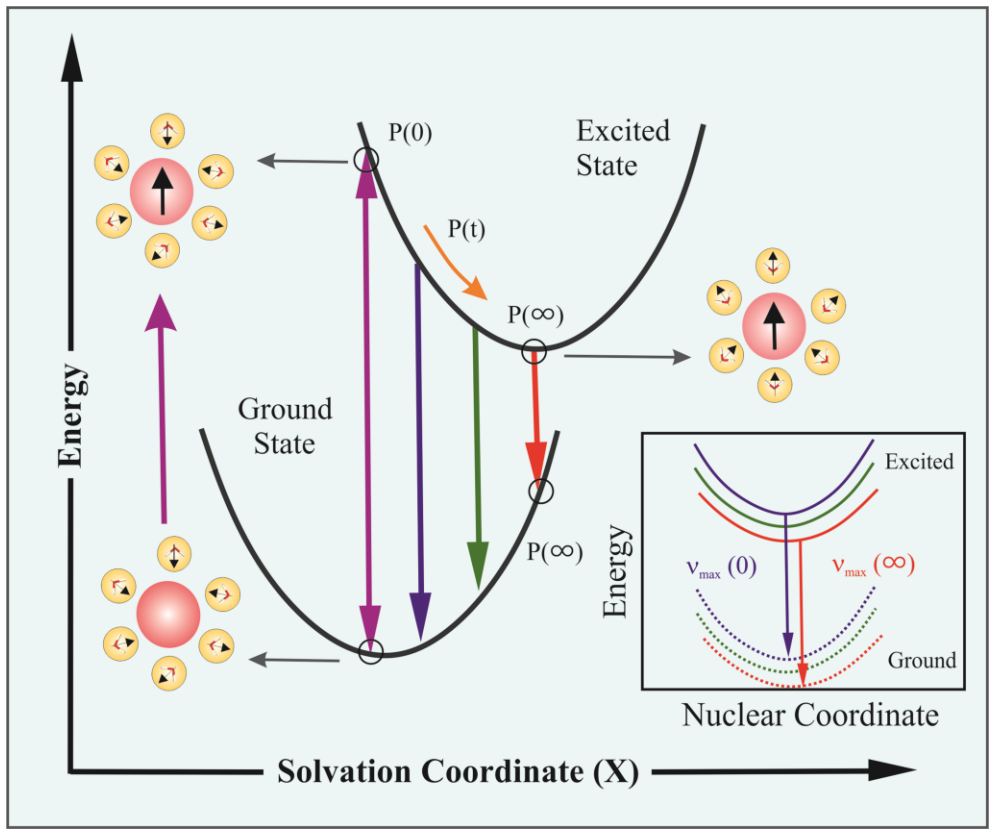

Figure 2.2. *Schematic representation of the potential energy surfaces involved in solvation dynamics showing the water orientational motions along the solvation coordinate together with instantaneous polarization P. In the inset we show the change in the potential energy along the intramolecular nuclear coordinate. As solvation proceeds the energy of the solute comes down giving rise to a red shift in the fluorescence spectrum. Note the instantaneous P, e.g., P(∞), on the two connected potentials.*

The latter is defined by the following expression,

$$P(r,t) = \int d\Omega\, \mu(\Omega)\, \rho\,(r,\Omega,t) \tag{2.2}$$

where $\mu(\Omega)$ is the dipole moment vector of a molecule at position r, and $\rho(r,\Omega,t)$ is the position, orientation and time-dependent density. Therefore, the time dependence of the solvation energy is determined by the time dependence of polarization that is in turn determined by the time dependence of the density. If the perturbation due to the probe on dynamics of bulk water is negligible, then the time dependence of polarization is dictated by the natural dynamics of the liquid. The theoretical analysis of the time-dependent density is usually carried out using a molecular hydrodynamic approach that is based on the basic conservation (density, momentum and energy) laws and includes the effects of intermolecular (both spatial and orientational) correlations. The latter provides the free energy surface on which solvation proceeds. The equation of motion of the density involves both orientational and translational motions of the solvent molecules.

The details of the theoretical development are reported in literature [1]; here we shall present a simple physical picture of the observed biphasic solvation dynamics. Within linear response theory, the solvation correlation function is directly related to the solvation energy as,

$$\mathrm{C(t)} = \frac{\langle \delta E(0) \cdot \delta E(t) \rangle}{\langle \delta E^2 \rangle} = \frac{\langle E(t) \rangle - \langle E(\infty) \rangle}{\langle E(0) \rangle - \langle E(\infty) \rangle} \tag{2.3}$$

where δE is the fluctuation of solvation energy from the average, equilibrium value. Note that the equality in equation (2.3) indicates the direct relation for the average of the fluctuations over the equilibrium distribution (left) and the non-equilibrium function (right) which relates to observables; without $\langle E(\infty) \rangle$ the correspondence is clear, and $\langle E(\infty) \rangle$ is rigorously the result of the equilibrium term in the numerator and for normalization in the denominator.

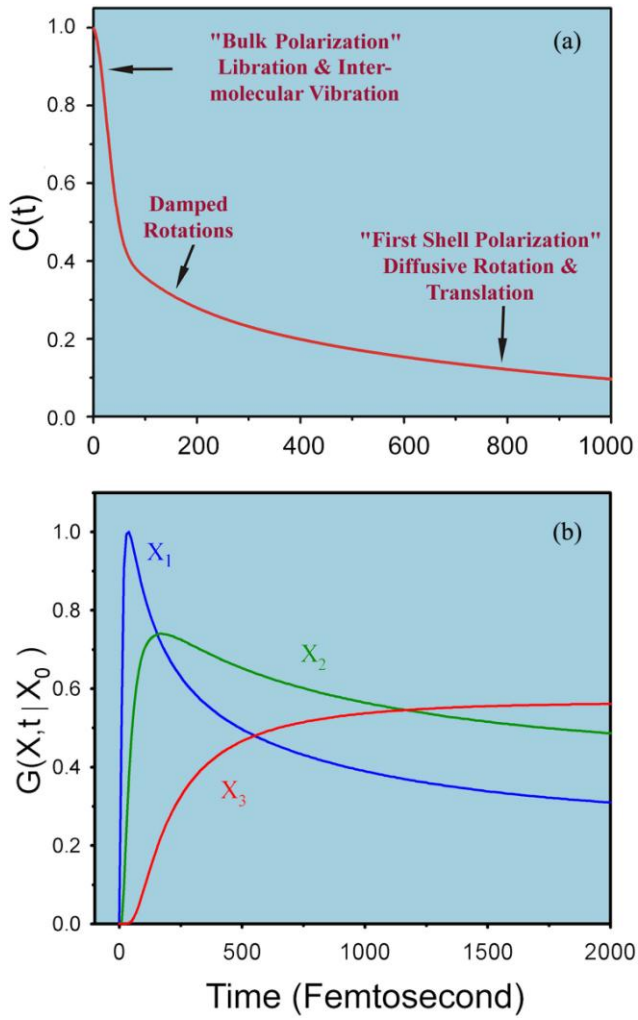

Figure 2.3. *(a) A typical solvation time correlation function for water is shown here. The time correlation function exhibits three distinct regions: The initial ultrafast decay, an intermediate decay of about 200 fs and the last slow decay with time constant of 1 ps. The physical origin of each region is indicated on the plot itself; see text. (b) Green's function G(X, t | X_0) for population relaxation along the solvation coordinate (X) is plotted against time in femtosecond. In G, X_0 is the initial position at t = 0. This Figure shows the position and time dependence of the population fluorescence intensity. At early times (when the population is at X_1) there is ultrafast rise followed by an ultrafast decay. At intermediate times (when the population is at X_2) there is a rise followed by a slow decay as shown by the green line. At long times when the population is nearly relaxed (position X_3, red line) we see only a rise.*

The ultrafast component in the solvation time correlation function (see Figure 2.3a), originates from the initial relaxation in the steep collective solvation potential. The collective potential is steep because it involves the total polarization of the system [1, 4]. This initial relaxation couples mainly to the hindered rotation (i.e., libration) and the hindered translation (i.e., the intermolecular vibration),

which are the available high frequency modes of the solvent; neither long amplitude rotation nor molecular translation are relevant here. The last part in the decay of the solvation correlation function involves larger amplitude rotational and translational motions of the nearest neighbor molecules in the first solvation shell. In the intermediate time, one gets contributions from the moderately damped rotational motions of water molecules. In a sense, with the above description one recovers the famous Onsager's "inverse snow-ball" picture of solvation [5]. The slowest time constant is ~1 ps, which is determined by the individual rotational and translational motions of the molecules in the "first solvation shell" nearly close to the probe. The femtosecond component is dominated by the high frequency hindered rotational and translational (vibration) polarization [6].

Figure 2.2 shows a schematic of the solvation potential and the orientational motions for the water molecules involved. From the shape of the potential, it can be seen that the transient behavior for the population during solvation should be a decay function on the blue edge of the spectrum and a rise function on the red edge. These wavelength-dependent features can be explained nicely within a generalized model of relaxation in which a Gaussian wave packet relaxes on a harmonic surface. The relaxation is non-exponential and a Green's function can describe the approach of the wave packet along the solvation coordinate, X, to its equilibrium value. For the general non-Markovian case it is given by [7],

$$G(X,t|X_0) = \frac{1}{\sqrt{2\pi\langle X^2\rangle[1-C^2(t)]}} \exp\left[-\frac{[X - X_0C(t)]^2}{2\langle X^2\rangle[1-C^2(t)]}\right] \qquad (2.4)$$

where $\langle X^2\rangle$ is the equilibrium mean square fluctuation of the polarization coordinate in the excited state surface, *C(t)* is the solvation correlation function described in equation (2.3) and X_0 is the initial value of the packet on the solvation coordinate. Equation (2.4) describes the motion of the wave packet (polarization density) beginning at $t = 0$ (X_0) as a delta function and according to the solvation

time correlation function. As $t \rightarrow \infty$, $C(t) \rightarrow 0$ and we recover the standard Gaussian distribution. Initially, ($t \rightarrow 0$), the exponential is large, so the decay is ultrafast, but at long times, the relaxation slows down, ultimately to appear as a rise. In Figure 2.3b, we present calculations of $G(X, t \mid X_0)$ at different positions along the solvation coordinate giving decays at X_1 and X_2, but with different time constants, and a rise at X_3, as demonstrated experimentally.

2.1.1.2. Experimental methods: In order to study solvation stabilization of a probe in an environment, a number of fluorescence transients are taken at different wavelengths across the emission spectrum of the probe. As described earlier, blue and red ends of the emission spectrum are expected to show decay and rise, respectively in the transients. The observed fluorescence transients are fitted by using a nonlinear least square fitting procedure to a function,

$$\left(X(t) = \int_0^t E(t')R(t-t')dt' \right) \tag{2.5}$$

comprising of convolution of the instrument response function (IRF) ($E(t)$) with a sum of exponentials,

$$\left(R(t) = A + \sum_{i=1}^{N} B_i \exp\left(-t/\tau_i\right) \right) \tag{2.6}$$

with pre-exponential factors (B_i), characteristic lifetimes (τ_i) and a background (A). Relative concentration in a multiexponential decay is finally expressed as;

$$\alpha_n = \frac{B_n}{\sum_{i=1}^{N} B_i} \tag{2.7}$$

The relative contribution of a particular decay component (f_n) in the total fluorescence is defined as,

$$f_n = \frac{\tau_n B_n}{\sum_{i=1}^{N} B_i \tau_i} \times 100. \tag{2.8}$$

The quality of the curve fitting is evaluated by reduced chi-square (0.9-1.1) and residual data. The purpose of the fitting is to obtain the decays in an analytical form suitable for further data analysis.

To construct time resolved emission spectra (TRES) we follow the technique described in references [8]. As described above, the emission intensity decays are analyzed in terms of the multiexponential model,

$$I(\lambda,t) = \sum_{i=1}^{N} \alpha_i(\lambda) \exp\left(-t/\tau_i(\lambda)\right) \tag{2.9}$$

where $\alpha_i(\lambda)$ are the pre-exponential factors, with $\Sigma\alpha_i(\lambda)$ = 1.0. In this analysis we compute a new set of intensity decays, which are normalized so that the time-integrated intensity at each wavelength is equal to the steady-state intensity at that wavelength. Considering $F(\lambda)$ to be the steady-state emission spectrum, we calculate a set of $H(\lambda)$ values using,

$$H(\lambda) = \frac{F(\lambda)}{\int_0^\infty I(\lambda,t)dt} \tag{2.10}$$

which for multiexponential analysis becomes,

$$\mathrm{H}(\lambda) = \frac{\mathrm{F}(\lambda)}{\sum_i \alpha_i(\lambda)\tau_i(\lambda)} \tag{2.11}$$

Then, the appropriately normalized intensity decay functions are given by,

$$I'(\lambda,t) = H(\lambda)I(\lambda,t) = \sum_{i=1}^{N} \alpha_i'(\lambda) \exp\left(-t/\tau_i(\lambda)\right) \tag{2.12}$$

where $\alpha'_i(\lambda) = H(\lambda)\alpha_i(\lambda)$. The values of $I'(\lambda,t)$ are used to calculate the intensity at any wavelength and time, and thus the TRES. The values of the emission maxima and spectral width are determined by nonlinear least-square fitting of the spectral shape of the TRES. The spectral shape is assumed to follow a lognormal line shape [8-9],

$$I(\bar{\nu}) = I_0 \exp\left\{-\left[\ln 2\left(\frac{\ln(\alpha+1)}{b}\right)^2\right]\right\} \tag{2.13}$$

with $\alpha = \frac{2b(\bar{\nu} - \overline{\nu_{\max}})}{\Delta} - 1$ where I_0 is amplitude, $\bar{\nu}_{max}$ is the wavenumber of the emission maximum and spectral width is given by, $\Gamma = \Delta\left[\frac{\sinh(b)}{b}\right]$. The terms b and Δ are asymmetry and width parameters, respectively and equation (2.9) reduces to a Gaussian function for b=0.

The time-dependent fluorescence Stokes shifts, as estimated from TRES are used to construct the normalized spectral shift correlation function or the solvent correlation function *C(t)* and is defined as,

$$C(t) = \frac{\bar{\nu}(t) - \bar{\nu}(\infty)}{\bar{\nu}(0) - \bar{\nu}(\infty)} \tag{2.14}$$

where, $\bar{\nu}(0)$, $\bar{\nu}(t)$ and $\bar{\nu}(\infty)$ are the emission maxima (in cm^{-1}) of the TRES at time zero, t and infinity, respectively. The $\bar{\nu}(\infty)$ value is considered to be the emission frequency beyond which insignificant or no spectral shift is observed. The *C(t)* function represents the temporal response of the solvent relaxation process, as occurs around the probe following its photoexcitation and the associated change in the dipole moment.

In order to further investigate possible heterogeneity in the positional distribution of fluoroprobes at the interfaces of biomimicking self-assemblies we follow time-resolved area normalized emission spectroscopy (TRANES), which is a well-established technique [10-11] and is a modified version of TRES. TRANES were constructed by normalizing the area of each spectrum in TRES such that the area of the spectrum at time t is equal to the area of the spectrum at t = 0. A useful feature of this method is the presence of an isoemissive point in the spectra involves emission from two species, which are kinetically coupled either irreversibly or reversibly or not coupled at all.

2.1.2. Fluorescence anisotropy: Anisotropy is defined as the extent of polarization of the emission from a fluorophore. Anisotropy measurements are commonly

used in biochemical applications of fluorescence. It provides information about the size and shape of proteins or the rigidity of various molecular environments. Anisotropy measurements have also been used to measure protein-protein associations, fluidity of membranes and for immunoassays of numerous substances. These measurements are based on the principle of photoselective excitation of those fluorophore molecules whose absorption transition dipoles are parallel to the electric vector of polarized excitation light. In an isotropic solution, fluorophores are oriented randomly. However, upon selective excitation, partially oriented population of fluorophores with polarized fluorescence emission results. The relative angle between the absorption and emission transition dipole moments determines the maximum measured anisotropy (r_0). The fluorescence anisotropy (r) and polarization (P) are defined by,

$$r = \frac{I_{II} - I_{\perp}}{I_{II} + 2I_{\perp}} \tag{2.15}$$

$$P = \frac{I_{II} - I_{\perp}}{I_{II} + I_{\perp}} \tag{2.16}$$

where the fluorescence intensities of vertically and horizontally polarized emission when the fluorophore is excited with vertically polarized light. Polarization and anisotropy are interrelated as,

$$r = \frac{2P}{3 - P} \tag{2.17}$$

$$P = \frac{3r}{2 + r} \tag{2.18}$$

Although polarization and anisotropy provides the same information, anisotropy is preferred since the latter is normalized by total fluorescence intensity ($I_T = I_{II} + 2I_{\perp}$) and in case of multiple emissive species anisotropy is additive while polarization is not. Several phenomena, including rotational diffusion and energy transfer, can decrease the measured anisotropy to values lower than maximum theoretical values. Following a pulsed excitation the fluorescence anisotropy, $r(t)$ of a sphere is given by,

$$r(t) = r_0 \exp(-t/\tau_{rot}) \tag{2.19}$$

where r_0 is the anisotropy at time t = 0 and τ_{rot} is the rotational correlation time of the sphere.

2.1.2.1. Theory: For a radiating dipole the intensity of light emitted is proportional to the square of the projection of the electric field of the radiating dipole onto the transmission axis of the polarizer. The intensity of parallel and perpendicular projections are given by,

$$I_{II}(\theta,\psi) = \cos^2\theta \tag{2.20}$$

$$I_{\perp}(\theta,\psi) = \sin^2\theta \sin^2\psi \tag{2.21}$$

where θ and ψ are the orientational angles of a single fluorophore relative to the z and y-axis, respectively (Figure 2.4a). In solution, fluorophores remain in random distribution and the anisotropy is calculated by excitation photoselection. Upon photoexcitation by polarized light, the molecules having absorption transition moments aligned parallel to the electric vector of the polarized light have the highest probability of absorption. For the excitation polarization along z-axis, all molecules having an angle ψ with respect to the y-axis will be excited. The population will be symmetrically distributed about the z-axis. For experimentally accessible molecules, the value of ψ will be in the range from 0 to 2π with equal probability. Thus, the ψ dependency can be eliminated.

$$\langle \sin^2\psi \rangle = \frac{\int_0^{2\pi} \sin^2\psi \, d\psi}{\int_0^{2\pi} d\psi} = \frac{1}{2} \tag{2.22}$$

$$\text{and } I_{II}(\theta) = \cos^2\theta \tag{2.23}$$

$$I_{\perp}(\theta) = \frac{1}{2}\sin^2\theta \tag{2.24}$$

Consider a collection of molecules oriented relative to the z-axis with probability $f(\theta)$. Then, measured fluorescence intensities for this collection after photoexcitation are,

$$I_{II} = \int_0^{\pi/2} f(\theta)\cos^2\theta d\theta = k\left\langle \cos^2\theta \right\rangle \tag{2.25}$$

$$\mathrm{I}_{\perp} = \frac{1}{2}\int_0^{\pi/2} f(\theta)\ \sin^2\theta d\theta = \frac{k}{2}\left\langle \sin^2\theta \right\rangle \tag{2.26}$$

where $f(\theta)d\theta$ is the probability that a fluorophore is oriented between θ and $\theta + d\theta$ and is given by,

$$f(\theta)d\theta = \cos^2\theta \sin\theta d\theta \tag{2.27}$$

k is the instrumental constant. Thus, the anisotropy (r) is defined as,

$$r = \frac{3\left\langle \cos^2\theta \right\rangle - 1}{2} \tag{2.28}$$

when $\theta = 54.7^0$ i.e. when $cos^2\theta = 1/3$, the complete loss of anisotropy occurs. Thus, the fluorescence taken at $\theta = 54.7^0$ with respect to the excitation polarization is expected to be free from the effect of anisotropy and is known as magic angle emission. For collinear absorption and emission dipoles, the value of $\langle cos^2\theta \rangle$ is given by the following equation,

$$\left\langle \cos^2\theta \right\rangle = \frac{\int_0^{\pi/2} \cos^2\theta f(\theta) d\theta}{\int_0^{\pi/2} f(\theta) d\theta} \tag{2.29}$$

Substituting equation (2.27) in equation (2.29) one can get the value of $\langle cos^2\theta \rangle = 3/5$ and anisotropy value to be 0.4 (from equation (2.28)). This is the maximum value of anisotropy obtained when the absorption and emission dipoles are collinear and when no other depolarization process takes place. However, for most fluorophore, the value of anisotropy is less than 0.4 and it is dependent on the excitation wavelength. It is demonstrated that as the displacement of the

absorption and emission dipole occurs by an angle γ relative to each other, it causes further loss of anisotropy (reduction by a factor 2/5) [12] from the value obtained from equation (2.28). Thus, the value of fundamental anisotropy, r_0 is given by,

$$r_0 = \frac{2}{5}\left(\frac{3\cos^2\gamma - 1}{2}\right) \tag{2.30}$$

For any fluorophore randomly distributed in solution, with one-photon excitation, the value of r_0 varies from -0.20 to 0.40 for γ values varying from 90^0 to 0^0.

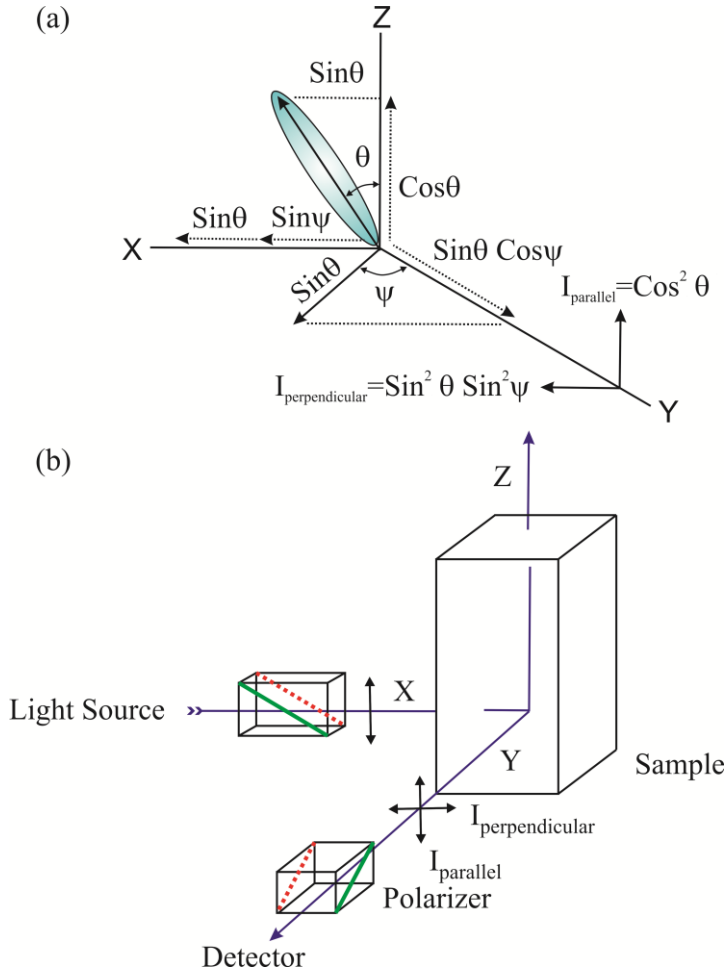

Figure 2.4. *(a) Emission intensity of a single fluorophore (blue ellipsoid) in a coordinate system. (b) Schematic representation of the measurement of fluorescence anisotropy.*

2.1.2.2. Experimental methods: For time resolved anisotropy (*r(t)*) measurements (Figure 2.4b), emission polarization is adjusted to be parallel and perpendicular to that of the excitation polarization. Spencer and Weber [13] have derived the relevant equations for the time dependence of $I_{II}(t)$ (equation (2.31)) and $I_{\perp}(t)$ (equation (2.32)) for single rotational and fluorescence relaxation times, τ_{rot} and τ_f, respectively,

$$I_{II}(t) = \exp\left(-t/\tau_f\right)\left(1 + 2r_0 \exp\left(-t/\tau_{rot}\right)\right) \tag{2.31}$$

$$I_{\perp}(t) = \exp\left(-t/\tau_f\right)\left(1 - r_0 \exp\left(-t/\tau_{rot}\right)\right) \tag{2.32}$$

The total fluorescence is given by,

$$F(t) = I_{II}(t) + 2I_{\perp}(t) = 3\exp\left(-t/\tau_f\right) = F_0 \exp\left(-t/\tau_f\right) \tag{2.33}$$

The time dependent anisotropy, *r(t)* is given by,

$$r(t) = \frac{I_{II}(t) - I_{\perp}(t)}{I_{II}(t) + 2I_{\perp}(t)} = r_0 \exp\left(-t/\tau_{rot}\right) \tag{2.34}$$

F(t) depends upon τ_f and *r(t)* depends upon τ_{rot} so that these two lifetimes can be separated. This separation is not possible in steady-state measurements. It should be noted that the degree of polarization (*P*) is not independent of τ_f and is therefore not as useful quantity as *r*. For reliable measurement of *r(t)*, three limiting cases can be considered.

(a) If $\tau_f < \tau_{rot}$, the fluorescence decays before the anisotropy decays, and hence only r_0 can be measured.

(b) If $\tau_{rot} < \tau_f$, in contrast to steady-state measurements, τ_{rot} can be measured in principle. The equations (2.31) and (2.32) show that the decay of the parallel and perpendicular components depends only upon τ_{rot}. The only experimental disadvantage of this case is that those photons emitted after the period of a few times τ_{rot} cannot contribute to the determination of τ_{rot}, but provided the signal-to-noise ratio is favorable, this need not be of great concern.

(c) If $\tau_{rot} \approx \tau_f$, then it becomes the ideal situation since almost all photons are counted within the time (equal to several rotational relaxation times) in which *r(t)* shows measurable changes.

For systems with multiple rotational correlation times, *r(t)* is given by,

$$r(t) = r_0 \sum_i \beta_i e^{-t/\tau_i} \tag{2.35}$$

where $\sum_i \beta_i = 1$ It should be noted that the instrument monitoring the fluorescence, particularly the spectral dispersion element, responds differently to different polarizations of light, thus emerging the need for a correction factor. For example, the use of diffraction gratings can yield intensities of emission, which depend strongly upon orientation with respect to the plane of the grating. It is inevitably necessary when using such instruments to correct for the anisotropy in response. This instrumental anisotropy is usually termed as G-factor (grating factor) and is defined as the ratio of the transmission efficiency for vertically polarized light to that for horizontally polarized light ($G = I_{II} + I_{\perp}$). Hence, values of fluorescence anisotropy, *r(t)* corrected for instrumental response, would be given by [12],

$$r(t) = \frac{I_{II}(t) - GI_{\perp}(t)}{I_{II}(t) + 2GI_{\perp}(t)} \tag{2.36}$$

The G-factor at a given wavelength can be determined by exciting the sample with horizontally polarized excitation beam and collecting the two polarized fluorescence decays, one parallel and other perpendicular to the horizontally polarized excitation beam. G-factor can also be determined following longtime tail matching technique [12]. If $\tau_{rot} < \tau_f$, it can be seen that the curves for $I_{II}(t)$ and $I_{\perp}(t)$ should become identical. If in any experiment they are not, it can usually be assumed that this is due to a nonunitary G-factor. Hence normalizing the two decay curves on the tail of the decay eliminates the G-factor in the anisotropy measurement.

2.1.3. Estimation of microviscosity from Stokes-Einstein-Debye equation: The interfacial microviscosity, η_m as experienced by probe molecule in the biological/biomimicking systems like protein cavities, reverse micelle/micelle, can be estimated from the time-resolved fluorescence anisotropy using the modified Stokes-Einstein-Debye equation (SED) [14-15],

$$\tau_r = \frac{\eta_m V_h}{k_B T} \tag{2.37}$$

where k_B is the Boltzmann constant, T is the absolute temperature. Hydrodynamic volume of the probe (V_h) can be calculated as:

$$V_h = V_m fC \tag{2.38}$$

where f is the shape factor (f = 1 for a spherical probe) and C represents solute-solvent coupling constant (C = 1 for "stick" condition and C < 1 for "slip" condition) and V_m is the molecular volume of the probe [16]. In case of f = C = 1, equation (2.37) reduces to the original simple SED equation,

$$\tau_r = \frac{\eta_m V_m}{k_B T} \tag{2.39}$$

For probe molecules with prolate ellipsoid shape, the value of f is calculated using the equation [14-15],

$$f = \frac{2}{3} \frac{1-p^4}{[(2-p^2)p^2(1-p^2)^{-1/2} \ln \frac{1+(1-p^2)^{1/2}}{p}] - p^2} \tag{2.40}$$

where p is the axial ratio (ratio of minor axis to major axis) of the prolate ellipsoid. The energy barrier, E_η for the viscous flow is estimated according to the relation [17],

$$\eta_m = \eta_0 \exp(\frac{E_\eta}{RT}) \tag{2.41}$$

2.1.4. Arrhenius theory of activation energy: The dynamics of solvation at a biomolecular interface can be exploited to give information about the energetics of the participating water molecules [3]. Water present at the surface of biomolecules

or biomimetic can broadly be distinguished as bound type (water hydrogen bonded to the interface, BW) and free type water (FW). In the water layer around the surface, the interaction with water involves hydrogen bonding to the polar and charged groups of the surface. When strongly bonded to the biomacromolecules or biomimicking surfaces, the water molecules cannot contribute to solvation dynamics because they can neither rotate nor translate. However, hydrogen bonding is transient and there exists a dynamic equilibrium between the free and the bound water molecules. The potential of the interaction can be represented by a double-well structure to symbolize the processes of bond breaking and bond forming. In general, the bonded water molecules become free by translational and rotational motions. The equilibrium between bound and free water can be written as [17],

$$(\text{water})_{\text{free state}} \leftrightarrow (\text{water})_{\text{bound state}} \tag{2.42}$$

Using the dynamic exchange model, an expression for this equilibrium can be derived. In a coupled diffusion-reaction equation the rate constant $k_{\pm}$ can be written as,

$$k_{\pm} = 0.5[-B \pm (B^2 - 4D_R k_{bf})^{1/2}] \tag{2.43}$$

where $B = 2D_R + k_{bf} + k_{fb}$ and D_R is the rotational diffusion constant, k_{bf} is the rate constant of the bound to free transition and k_{fb} is that of the reverse process. Typically, the rate constant of free to bound reaction, is larger than that for the reverse process. It can be shown that, when the rates of interconversion between "bound" and "free" water molecules are small as compared to $2D_R$, then,

$$\tau_{slow} \approx k_{bf}^{-1} \tag{2.44}$$

and from the activated complex theory one can have,

$$k_{bf} = (k_B T / h) \exp(-\Delta G^0 / RT) \tag{2.45}$$

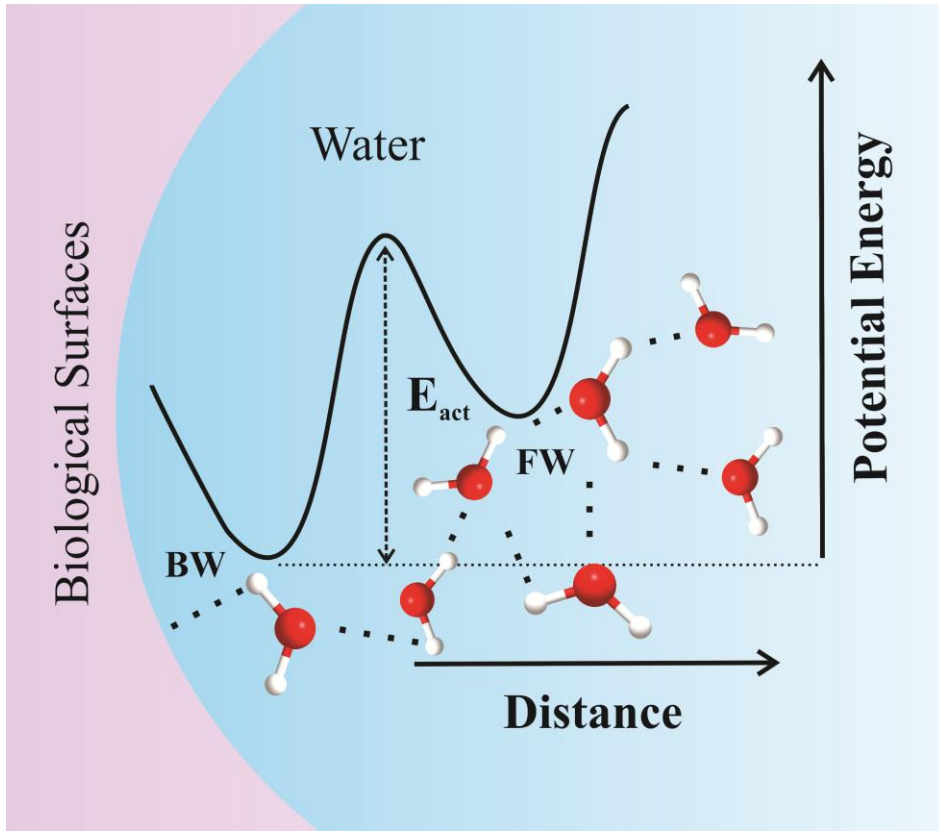

***Figure* 2.5.** *Schematic representation of different types of water molecules (BW and FW) present at various bimolecular interfaces and the corresponding activation energy barrier.*

If the transition process (equation (2.42)) follows a typical Arrhenius type of energy barrier crossing model, one can write,

$$\tau_{slow}^{-1} \approx k_{bf} = A\exp(-E_{act}/RT) \tag{2.46}$$

where 'E_{act}' is the activation energy for the transition process and 'A' is the pre-exponential factor. A plot of $ln(1/\tau_{slow})$ against $1/T$ produces a straight line and from the slope of the line E_{act} can be calculated. The temperature dependence of the solvation follows the Arrhenius equation and yields the activation energy needed for the conversion of bound and free forms [18].

2.1.5. Förster resonance energy transfer (FRET): FRET is an electrodynamic phenomenon involving the nonradiative transfer of the excited state energy from the donor dipole (D) to an acceptor dipole (A) in the ground state (Figure 2.6a). FRET has got wide applications in all fluorescence applications including medical

diagnostics, DNA analysis and optical imaging. Since FRET can measure the size of a protein molecule or the thickness of a membrane, it is also known as 'spectroscopic ruler' [19]. FRET is very often used to measure the distance between two sites on a macromolecule [20]. Basically, FRET is of two types: (i) homo-molecular FRET and (ii) hetero-molecular FRET. In the former case the same fluorophore acts both as energy donor and acceptor, while in the latter case two different molecules act as donor and acceptor.

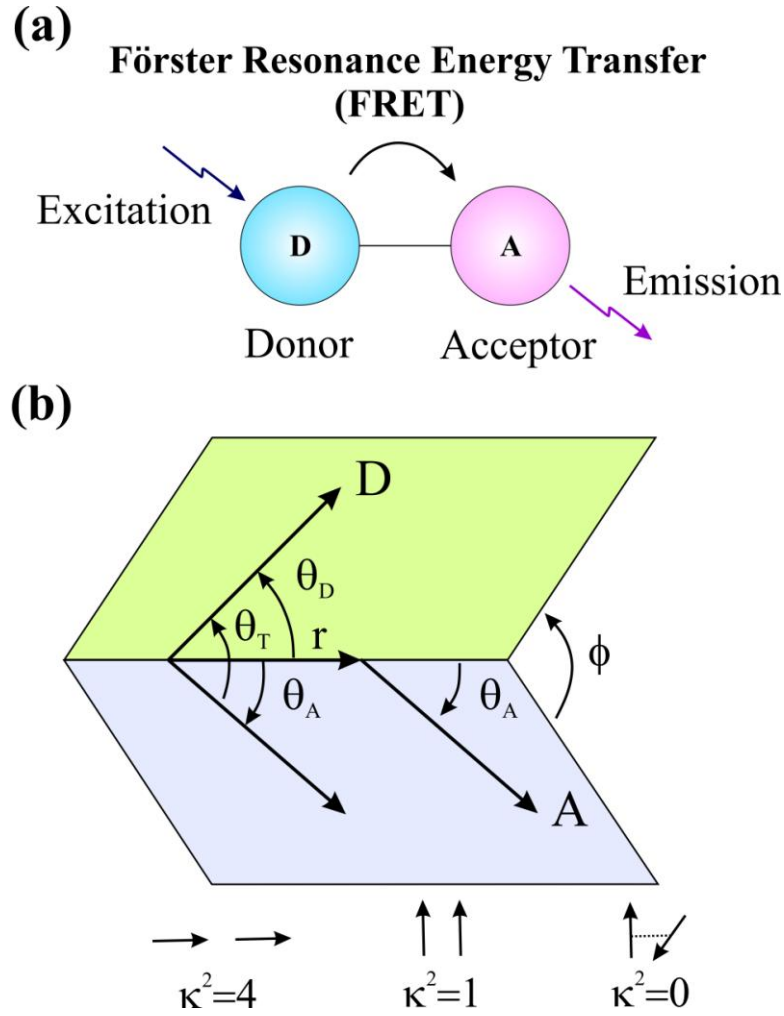

Figure 2.6. *(a) Schematic illustration of the FRET process. (b) Dependence of the orientation factor* κ^2 *on the directions of the emission and absorption dipoles of the donor and acceptor, respectively.*

Each donor-acceptor (D-A) pair participating in FRET is characterized by a distance known as Förster distance (R_0) i.e., the D-A separation at which energy transfer is 50% efficient. The R_0 value ranges from 20 to 60 Å. The rate of resonance energy transfer (k_T) from donor to an acceptor is given by [12],

$$k_T = \frac{1}{\tau_D}\left(\frac{R_0}{r}\right)^6 \tag{2.47}$$

where τ_D is the lifetime of the donor in the absence of acceptor and r is the donor to acceptor (D-A) distance. The rate of transfer of donor energy depends upon the extent of overlap of the emission spectrum of the donor with the absorption spectrum of the acceptor ($J(\lambda)$), the quantum yield of the donor (Q_D), the relative orientation of the donor and acceptor transition dipoles (κ^2) and the distance between the donor and acceptor molecules (r) (Figure 2.6b). In order to estimate FRET efficiency of the donor and hence to determine distances between donor-acceptor pairs, the methodology described below is followed [12]. R_0 is given by,

$$R_0 = 0.211\left[\kappa^2 n^{-4} Q_D J(\lambda)\right]^{1/6} \text{ (in Å)} \tag{2.48}$$

where n is the refractive index of the medium, Q_D is the quantum yield of the donor and $J(\lambda)$ is the overlap integral. κ^2 is defined as,

$$\kappa^2 = \left(\cos\theta_T - 3\cos\theta_D \cos\theta_A\right)^2 = \left(\sin\theta_D \sin\theta_A \cos\varphi - 2\cos\theta_D \cos\theta_A\right)^2 \tag{2.49}$$

where θ_T is the angle between the emission transition dipole of the donor and the absorption transition dipole of the acceptor, θ_D and θ_A are the angles between these dipoles and the vector joining the donor and acceptor and φ is angle between the planes of the donor and acceptor (Figure 2.6b). κ^2 value can vary from 0 to 4. For collinear and parallel transition dipoles, $\kappa^2 = 4$; for parallel dipoles, $\kappa^2 = 1$; and for perpendicularly oriented dipoles, $\kappa^2 = 0$. For donor and acceptors that randomize by rotational diffusion prior to energy transfer, the magnitude of κ^2 is assumed to be 2/3. However, in systems where there is a definite site of attachment of the donor and acceptor molecules, to get physically relevant results, the value of κ^2 has to be estimated from the angle between the donor emission and

acceptor absorption dipoles [21]. $J(\lambda)$, the overlap integral, which expresses the degree of spectral overlap between the donor emission and the acceptor absorption, is given by,

$$J(\lambda) = \frac{\int_0^\infty F_D(\lambda)\varepsilon_A(\lambda)\lambda^4 d\lambda}{\int_0^\infty F_D(\lambda) d\lambda} \tag{2.50}$$

where $F_D(\lambda)$ is the fluorescence intensity of the donor in the wavelength range of λ to $\lambda+d\lambda$ and is dimensionless. $\varepsilon_A(\lambda)$ is the extinction coefficient (in $M^{-1}cm^{-1}$) of the acceptor at λ. If λ is in nm, then $J(\lambda)$ is in units of $M^{-1}\,cm^{-1}\,nm^4$.

Once the value of R_0 is known, the efficiency of energy transfer can be calculated. The efficiency of energy transfer (E) is the fraction of photons absorbed by the donor which are transferred to the acceptor and is defined as,

$$E = \frac{k_T(r)}{\tau_D^{-1} + k_T(r)} \tag{2.51}$$

$$\text{or, } E = \frac{R_0^6}{r^6 + R_0^6} \tag{2.52}$$

For D-A systems decaying with multiexponential lifetimes, E is calculated from the amplitude weighted lifetimes $\langle\tau\rangle = \sum_i \alpha_i \tau_i$ of the donor in absence (τ_D) and presence (τ_{DA}) of the acceptor as,

$$E = 1 - \frac{\tau_{DA}}{\tau_D} \tag{2.53}$$

The D-A distances can be measured using equations (2.52) and (2.53).

Distance distribution between donor and acceptor was estimated according to the procedure described in the literature [12, 22]. The observed fluorescence transients of the donor molecules in absence of acceptor were fitted using a

nonlinear least-squares fitting procedure (software SCIENTIST) to the following function,

$$I_D(t) = \int_0^t E(t')\, p(t'-t)dt' \tag{2.54}$$

which comprises the convolution of the instrument response function (IRF) ((*E(t)*) with exponential $(p(t) = \sum_i \alpha_{Di} \exp(-t/\tau_{Di}))$. The convolution of the distance distribution function *P(r)* in the fluorescence transients of donor in presence of acceptor in the system under studies is estimated using the same software (SCIENTIST) in the following way.

The intensity decay of D-A pair, spaced at a distance *r*, is given by

$$I_{DA}(r,t) = \sum_i \alpha_{Di} \exp\left[-\frac{t}{\tau_{Di}} - \frac{t}{\tau_{Di}}\left(\frac{R_0}{r}\right)^6 \right] \tag{2.55}$$

and the intensity decay of the sample considering distance distribution probablity function, *P(r)* is given by,

$$I_{DA}(t) = \int_{r=0}^{\infty} P(r) I_{DA}(r,t) dr \tag{2.56}$$

where *P(r)* consist of the folowing terms:

$$P(r) = \frac{1}{\sigma\sqrt{2\pi}} \exp\left[-\frac{1}{2}\left(\frac{\bar{r} - r}{\sigma}\right)^2 \right] \tag{2.57}$$

In this equation $\bar{r}$ is the mean of the Gaussian with a standard deviation of σ. Usually distance distributions are described by the full width at half maxima (*hw*). This half width is given by $hw = 2.354\sigma$.

2.1.6. Circular dichroism (CD): CD is now a routine tool in many laboratories with applications to determine whether a chiral molecule has been synthesized or resolved into pure enantiomers and probing the structures of biomolecules, in particular determining the α-helical content of proteins [23-24].

2.1.6.1. Theory: When a plane polarized light passes through an optically active substance, not only do the left (L) and right (R) circularly polarized light rays travel at different speeds, $c_L \neq c_R$, but these two rays are absorbed to a different extent, i.e. $A_L \neq A_R$. The difference in the absorbance of the left and right circularly polarized light, i.e., $\Delta A = A_L - A_R$, is defined as circular dichroism (CD). Circular dichroism spectroscopy follows Beer-Lambert law. If I_0 is the intensity of light incident on the cell, and I, that of emergent light, then absorbance is given by,

$$A = \log_{10}\left(\frac{I_0}{I}\right) = \varepsilon c l \tag{2.58}$$

i.e., A is proportional to concentration (c) of optically active substance and optical path length (l). If 'c' is in moles litre^{-1} and 'l' is in cm, then ε is called the molar absorptivity or molar extinction coefficient. In an optically active medium, two absorbances, A_L and A_R are considered, where $A_L = \log_{10}\left(I_0/I_L\right)$ and $A_R = \log_{10}\left(I_0/I_R\right)$. At the time of incidence on the sample, intensity of left and right circularly polarized light are same, i.e. $I_0 = I_L = I_R$. Any dicrograph passes periodically changing light through the medium, oscillating between left and right circular polarization, and the difference in absorbances are recorded directly.

$$\Delta A = A_L - A_R = \log_{10}\left(\frac{I_0}{I_L}\right) - \log_{10}\left(\frac{I_0}{I_R}\right) = \log_{10}\left(\frac{I_R}{I_L}\right) \tag{2.59}$$

$$\Delta A = \left(\Delta\varepsilon\right) c l \tag{2.60}$$

As seen from equation (2.59), I_0 does not appear in this final equation, so there is no need for a reference beam. The instruments are, therefore, of single beam type.

After passing through an optically active substance, light is changed in two aspects. The maximal amplitude of intensity is no longer confined to a plane; instead it traces out an ellipse. Ellipticity is defined as the arctangent of the ratio of minor axis to the major axis of the ellipse (Figure 2.7). The orientation of ellipse is another aspect. The major axis of the ellipse no longer remains parallel to the

polarization of the incident light. Thus, after passing through an optically active substance, neither do the absorbance nor do the radii of the emergent left and right circularly polarized light remains same. Hence, CD is equivalent to ellipticity.

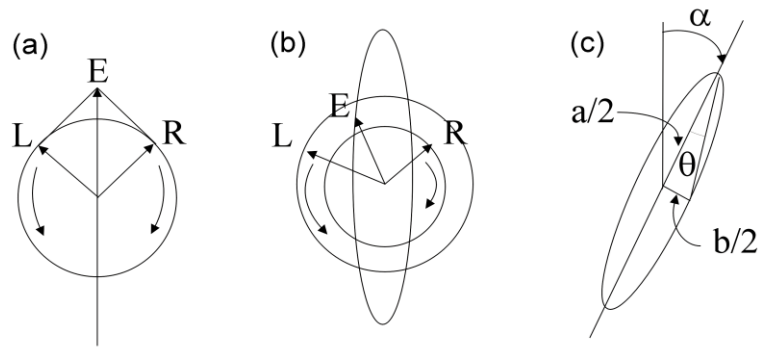

***Figure* 2.7.** *(a) Left (L) and right (R) circularly polarized light component having same intensities and phases lying in one plane and oscillating with same magnitude, (b) R component being less intense (more absorbed) than L component leading to elliptically polarized light and (c) θ, ellipticity is the angle made by semi-major and semi-minor axes of the ellipse. The major axis has rotated through angle α corresponding to optical rotation.*

Most of the CD spectropolarimeters, although they measure differential absorption, produce a CD spectrum in units of ellipticity (θ) expressed in milli-degrees versus λ, rather than ΔA versus λ. The relation between ellipticity and CD is given by,

$$\theta = \frac{2.303 \times 180 \times \left(A_L - A_R\right)}{4\pi} \text{ (in degrees)} \tag{2.61}$$

to compare the results from different samples, optical activity is computed on a molar or residue basis. Molar ellipticity, $[\theta]$ is defined as,

$$[\theta] = \frac{\theta}{cl} \tag{2.62}$$

where (θ) is in degrees, 'c' is in moles per litre and 'l' is in cm. The unit of molar ellipticity is deg.M^{-1}.cm^{-1}. Sometimes, CD is reported as $\Delta\varepsilon = \Delta\varepsilon_L - \Delta\varepsilon_R$. From Beer-Lambert law and molar ellipticity relation it can be shown that,

$$[\theta] = 3300.\Delta\varepsilon \tag{2.63}$$

2.1.6.2. Experimental methods: In biophysical studies, CD is mostly used to determine the secondary structures of proteins and nucleic acids and the changes in secondary structures upon recognition by small molecules and other biomolecules. Through CD spectropolarimeter, we obtain CD spectrograph having a plot of optical rotation in millidegrees versus wavelength in nm. In order to obtain information about the secondary structures of proteins, the graph is fitted with non-linear least square fitting method using freely available software. The percentages of different secondary structures are calculated by matching the experimental data with that of reference standard. In proteins, the secondary structural content includes α–helix, β–sheet, β–turn and random coil while for DNA, CD is used to determine the structures of different A, B, Z and condensed forms of DNA. The CD spectrum of α–helix contains two negative peaks, one at 208 nm (π–π* transition) and 222 nm (n–π* transition). β–sheet has a negative band at 216 nm and a positive band of similar magnitude at 195 nm. β–turn has weak negative peak at 225 nm (n–π* transition), a strong positive peak between 200 nm and 205 nm due to π–π* transition and a strong negative band between 180 nm and 190 nm. Random coil or unordered conformation has a strong negative band below 200 nm; a positive band at 218 nm and in some cases has a very weak negative band at 235 nm. A positive band centered at 275 nm and a negative band at 240 nm with crossover at 258 nm characterizes B-DNA. Under high salt condition, the band at 275 nm collapse due to reduction in number of base pairs per turn. A-DNA has a positive band at 260 nm, a very weak band at 190 nm and fairly intense negative band at 210 nm. Z-form DNA has a negative and a positive band at 290 nm and 260 nm, which are mirror images of B-DNA spectrum. Condensed DNA has a negative peak between 250 nm and 260 nm and long stretching positive molar ellipticity above 300 nm, not observed for normal B-form DNA.

2.1.7. Twisted intramolecular charge transfer (TICT): While interpretation of solvent-dependent emission spectra appears simple, this is a very complex topic. The complexity is due to the variety of interactions that can result in spectral shifts. The theory for general solvent effects is often inadequate for explaining the detailed behavior of fluorophores in a variety of environments.

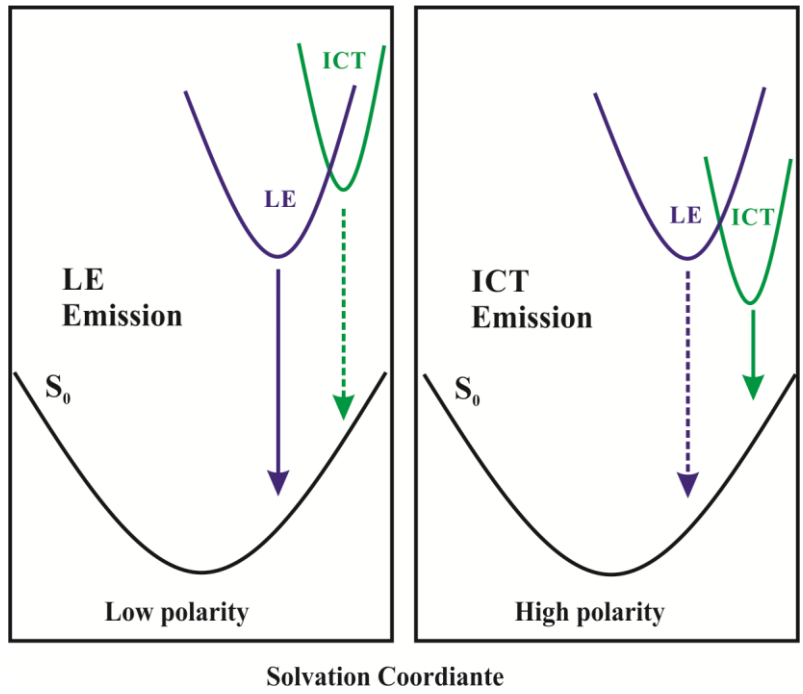

***Figure 2.8**. Effect of solvent polarity on the energies of locally excited (LE) and ICT states [9].*

The Jablonski diagram for solvent effects should also reflect the possibility of specific solvent–fluorophore interactions that can lower the energy of the excited state. In addition to specific solvent–fluorophore interactions, many fluorophores can form an internal charge transfer (ICT) state, or a twisted internal charge transfer (TICT) state (Figure 2.8). For instance, suppose the fluorophore contains both an electron-donating and an electron-accepting group. Such groups could be amino and carbonyl groups, respectively, but numerous other groups are known. Following excitation there can be an increase in charge separation within the fluorophore. If the solvent is polar, then a species with charge separation (the

ICT state) may become the lowest energy state. In a nonpolar solvent the species without charge separation, the so-called locally excited (LE) state, may have the lowest energy. Hence, the role of solvent polarity is not only to lower the energy of the excited state due to general solvent effects, but also to govern which state has the lowest energy. In some cases, formation of the ICT state requires rotation of groups on the fluorophore to form the TICT state. Formation of ICT states is not contained within the theory of general solvent effects. Some probes display charge transfer in the excited state. In a highly viscous environment, the molecule cannot distort as needed for charge transfer, and the decay is radiative. In a less viscous environment, the molecule displays internal rotation and charge transfer, which results in radiation less decay.

2.1.8. Microfluidics theory: The flow of a fluid through a microfluidic channel can be characterized by the Reynolds number, defined as,

$$R_e = \frac{LV_{avg}\rho}{\mu} \tag{2.64}$$

where L is the most relevant length scale, μ is the viscosity, ρ is the fluid density, and V_{avg} is the average velocity of the flow. For microchannels, L is equal to $4A/P$ where A is the cross sectional area of the channel and P is the wetted perimeter of the channel. Due to the small dimensions of microchannels, the R_e is usually much less than 100. In this Reynolds number regime, flow is completely laminar and no turbulence occurs. The transition to turbulent flow generally occurs in the range of Reynolds number 2000. Laminar flow provides a means by which molecules can be transported in a relatively predictable manner through microchannels.

Due to laminar flow in the microchannel, the transport of the mass of the subjected species within the microchannel follows the diffusion law. Figure 2.10 depicts the molecular diffusion of the species under study in the microchannel. The diffusion coefficient is estimated according to the procedure described by in

the literature [25]. Considering the two-dimensional diffusion law, Einstein's equation of Brownian motion states that,

$$\tau = \frac{d^2}{2D} \tag{2.65}$$

where, d is the root mean square distance traversed by a molecule during the time interval for a given diffusion coefficient D.

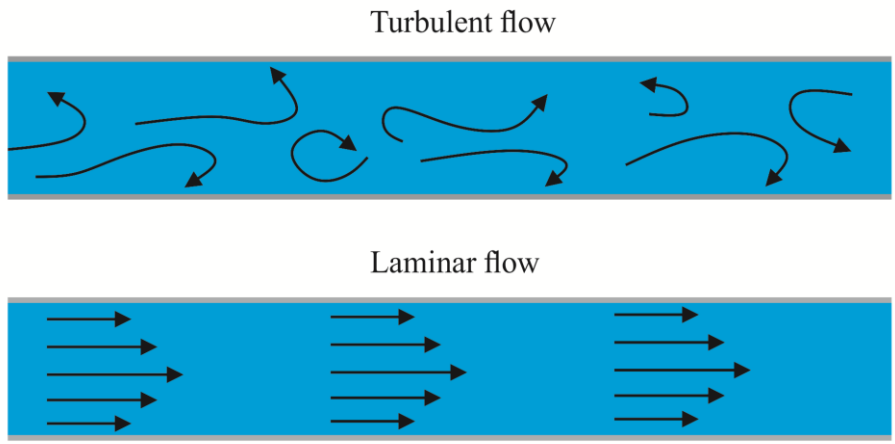

Figure 2.9. *Graphical representation of turbulent and laminar flow within a microchannel.*

The kinetics of molecular recognition/interaction was analyzed by measuring the fluorescence intensity of fluoroprobe along the microchannel. For a single step first order reaction, reactants will produce products as follows:

$$\text{Reactants} \xrightarrow{k} \text{Products}$$

The rate equation can be written as [26],

$$x = a(1 - e^{-kt}) \tag{2.66}$$

where, 'x' corresponds to the product concentration at time t and k is the first-order rate constant. Considering a reaction having an intermediate step, i.e. $A \xrightarrow{k_1} I \xrightarrow{k_2} P$, the product concentration at time, t would be [26],

$$x = a(1 + \frac{k_1 e^{-k_2 t} - k_2 e^{-k_1 t}}{k_2 - k_1}) \tag{2.67}$$

Where, 'a' denotes the initial concentration at time t=0 and k_1, k_2 are the respective rate constants. The precision of the measurement of the kinetics parameter will depend on the

uniformity and accuracy of the flow velocity and the signal-to-noise ratio in the fluorescence measurement.

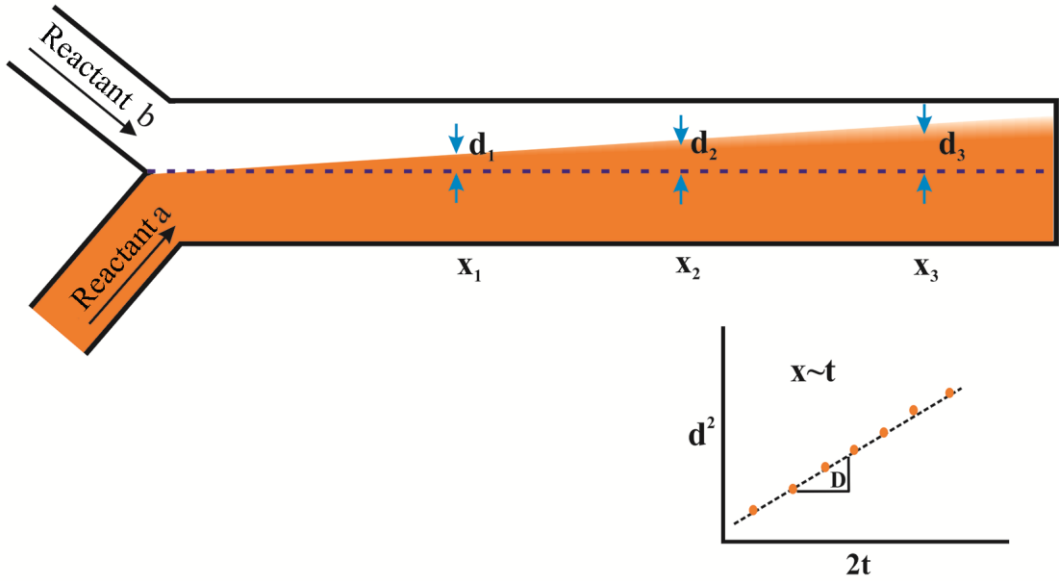

Figure 2.10. *Measurement of the diffusion of the subjected species by monitoring the spreading width at different time interval is graphically represented.*

2.2. Systems:

2.2.1. Organized assemblies (biomimetics): Amphiphilic molecules like surfactant aggregates to form macromolecular assemblies, like micelles and reverse micelles, which very often resemble the structural properties of biomolecules. In the following section, we will discuss about these entities.

2.2.1.1. Micelles: Micelles are spherical or nearly spherical aggregates of amphiphilic surfactant molecules formed in aqueous solution above a concentration known as critical micellar concentration (CMC). Micelles are formed above a critical temperature called "Kraft point" which is different for different surfactants. Micellar aggregates have diameter varying within 10 nm and the aggregation number, i.e., the number of surfactant molecules per micelle, ranges from 20 to 200. Israelachvili et al. [27] have proposed that surfactant molecular packing considerations are determinant in the formation of large surfactant

aggregates. In particular, it is considered that the surfactant packing parameter θ ($\theta = v/\sigma l$, where v is the surfactant molecular volume, σ is the area per polar head, and l is the length of hydrophobic part) gives a good idea of the shape of aggregates which will form spontaneously [27]. It is considered that normal or direct rod-like micelles are formed when $2<\theta<3$ [28]. Micelles can be both neutral (triton X-100) and ionic (sodium dodecyl sulfate, SDS (anionic) and cetyl trimethyl ammonium bromide, CTAB (cationic)). The structure of a typical micelle is schematically shown in Figure 2.11. The core of a micelle is essentially "dry" and consists of the hydrocarbon chains with the polar and charged head groups projecting outward toward the bulk water. The stern layer, surrounding the core, comprises of the ionic or polar head groups, bound counter ions and water molecules. Between the stern layer and the bulk water there is a diffused Guoy-Chapman (GC) layer, which contains the free counter ions and water molecules.

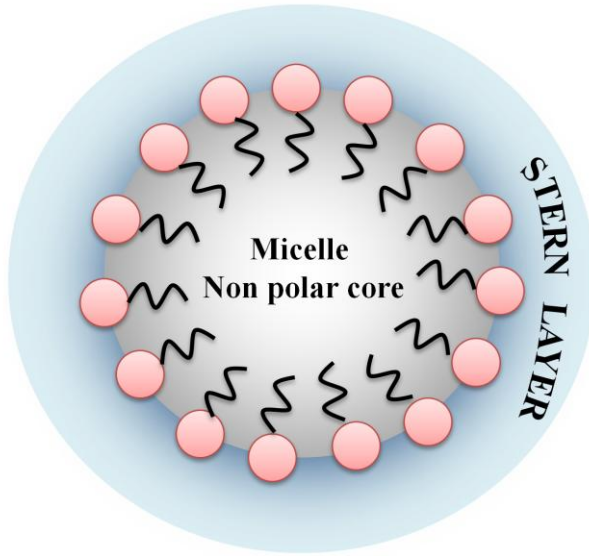

Figure 2.11. *The schematic representation of the structure of a micelle.*

In non-ionic polyoxyethylated surfactants e.g. triton X-100 (TX-100), the hydrocarbon core is surrounded by a palisade layer, which consists of the

polyoxyethylene groups hydrogen-bonded to water molecules [29]. Small angle X-ray and neutron scattering have provided detailed information on the structure of the CTAB micelles [30-31]. According to these studies, CMC and aggregation number of CTAB micelle are 0.8 mM and 52 respectively and the thickness of the stern layer is 6-9 Å. The overall radius of CTAB micelle is about 50 Å. For TX-100 micelle, the CMC, thickness of the palisade layer and overall radius of the hydrophobic core are reported to be 0.1 mM, 51 Å and 25-27 Å, respectively and that of SDS micelles are 8.6 mM [32], 33 Å [33] and 5 Å, respectively [34].

2.2.1.2. Reverse micelles: Reverse micelles (RMs) or water-in-oil microemulsions (Figure 2.12) are nanopools of polar solvent protected by a monolayer of surfactant molecules at the periphery with polar head groups pointing inward into the polar solvent, and the hydrocarbon tails directed toward the non-polar organic solvents [35-36]. RMs with water nanopools resemble the water pockets found in various bio-aggregates such as proteins, membranes, and mitochondria. Thus, these systems are very often considered as templates for the synthesis of nanoparticles and as excellent biomimetic for exploration of biological membranes and biologically confined water molecules [37]. Aqueous RMs are generally characterized by the degree of hydration (w_0), which is the ratio of molar concentration of water to that of surfactant, where the radius of the water pool (r in $\mathring{A}$) is empirically defined as, $r = 2\times w_0$ [38]. Shapes and sizes of the surfactant aggregates depend strongly on the type and concentration of the surfactant, and on the nature of counterion and external solvent. In principle, reverse micelles can be formed in the presence and in the absence of solubilized water. However, it has generally been proposed that if the medium is completely water-free, there is not a well-defined CMC (critical micelle concentration), and the aggregates formed are very small and polydisperse, indicating minimum cooperativity in the surfactant association.

This has been particularly established for surfactant bis (2-ethylhexyl) sulfosuccinate sodium salt (AOT) in several organic solvents. RMs with w_0 values

less than 20 are stable and mono disperse over a wide range of temperatures. The AOT-alkane-water system is interesting as the solution is homogeneous and optically transparent over a wide range of temperature, pressure, and pH. The AOT-RMs can compartmentalize a large amount of water in its central core, and the nanoscale aggregation process is fairly well characterized with respect to size and shape at various water contents. The CMC of AOT in hydrocarbon solvent is about 0.1 mM. In liquid alkanes, AOT-RMs (w_0 = 0) are completely associated and each micelle contains 23 monomers. The structures of these RMs are slightly asymmetric and are of round cylindrical nature. Spherical RMs are generally formed by surfactants with high values of the packing parameter, θ>3. AOT RMs can dissolve large amounts of water, being able to reach w_0 values as large as 40-60, depending on the surrounding non-polar organic medium and temperature [39]. At low w_0 values, the systems are usually referred to as RMs, whereas the term water-in-oil microemulsion is frequently used for higher w_0 values. Fluorescence spectroscopy has been extensively used to study the AOT-RMs system. Fluorescent probes have been used to determine the viscosity, binding site, rigidity and proximity within the water pool. These studies have shown that water inside the RMs is generally of two types: i) interfacial (bound) and ii) core (free) water. One of the studies [40] has shown the existence of third type of water (trapped) molecules present between the polar head groups of the individual surfactant molecules. Thus, the interior of RMs is extremely heterogeneous. Dielectric relaxation studies [41] indicate the presence of 7 ns component for bound water in RM, very similar to those of water molecules in the close vicinity of biological macromolecules (biological water). In contrast to AOT which does not require any cosurfactant to form RMS, cationic surfactants do not form RMs in the absence of cosurfactants. Several non-ionic or neutral surfactants (TX-100) have been reported to form RMs in pure and mixed hydrocarbon solvents [42].

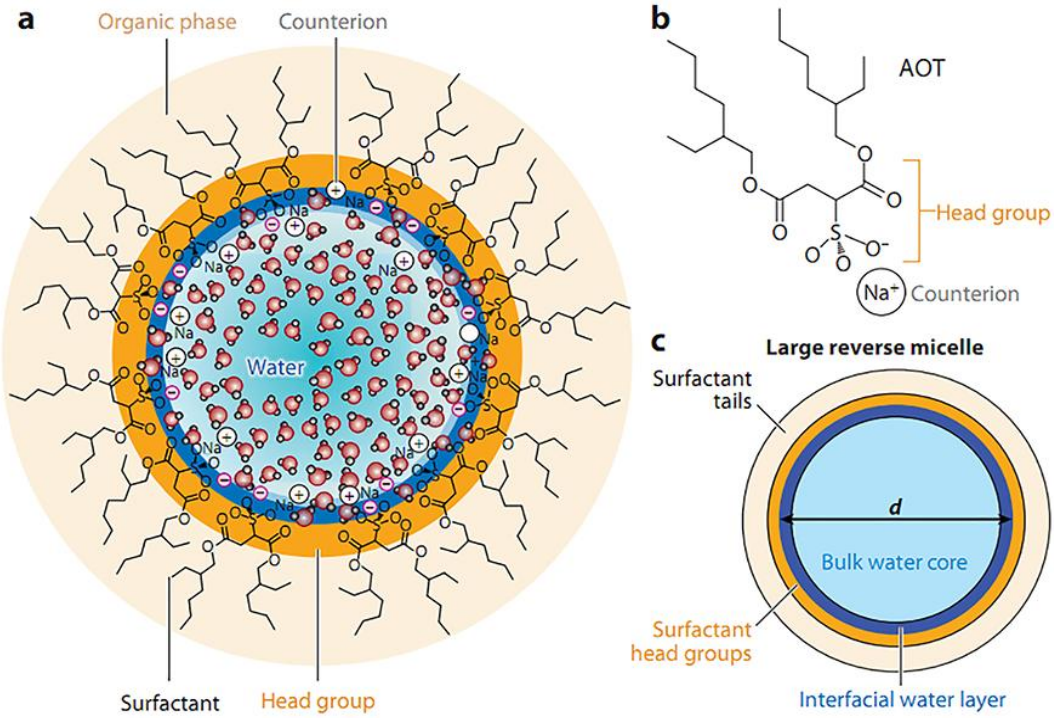

Figure 2.12. *(a) Schematic depiction of a potential structure of a reverse micelle. Water molecules reside in the interior, sometimes interacting with head groups and counterions. Surfactant tails reside in contact with the continuous, nonpolar, organic supporting phase. (b) Chemical structure of Aerosol OT (AOT; sodium bis(2-ethylhexyl) sulfosuccinate (c) Schematic of a large reverse micelle showing important features of the structure.*

2.2.2. Proteins: Three types of proteins; alpha chymotrypsin (CHT), galactose repressor protein (GalR) and Cro-repressor have been used in our study.

2.2.2.1. α-Chymotrypsin (CHT): α-Chymotrypsin (Figure 2.13) isolated from bovine pancreas, is a member of the family serine endopeptidase (molecular weight of 25,191 Da) catalysing the hydrolysis of peptides in the small intestine [43]. The three dimensional structure of CHT was solved by David Blow [44]. The molecule is a three-dimensional ellipsoid of dimensions 51 × 40 × 40 Å and comprises of 245 amino acid residues. CHT contains several antiparallel β-pleated sheet regions and little α-helix. Physiological activity of CHT is determined by the pH. The enzyme is not active at lower pH, but the activity increases nonmonotonically with pH [45]; in the duodenum (low pH), it is inactive, whereas in the lower small intestinal track (high pH), it becomes active. The inactivity of

the enzyme at lower pH is known to be related to the protonation of the residues of the catalytic triad [45]. From spectroscopic studies [46-47], it was suggested that the degree of mobility of water molecules, not hydrophobicity, may be the important factor for the change with pH.

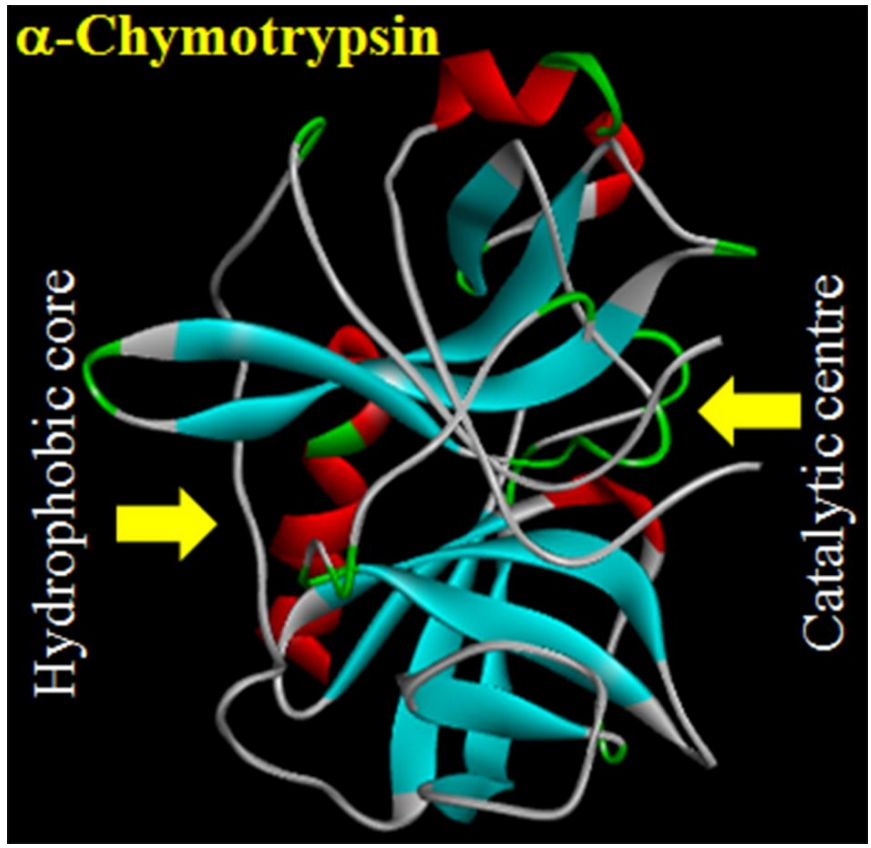

Figure 2.13. *X-ray crystallographic structure (PDB code: 2CHA) of CHT depicting the different domains.*

2.2.2.2. Galactose repressor protein: In the classical negative control of gene expression, a repressor protein binds to cognate operator element(s) in DNA at or near the promoter and inhibits transcription initiation. It was originally proposed and commonly believed that repressor prevents RNA polymerase from binding to the promoter site. *E. coli* galactose repressor (GalR) is a repressor protein, which represses the transcription of *gal operon* by two promoters P_1 and P_2, upon binding to two operator DNAs, O_E and O_I. O_E is located immediately upstream to two

promoters P_1 and P_2 of *gal operon*, whereas O_I is separated from O_E by 114 bp and is in fact located inside the first structural gene, GalE [48]. Several evidences suggest that the binding of the repressor protein to the target DNA sequences is in the dimeric form. Although high resolution X-ray crystallographic/NMR structure of the repressor protein (GalR) and its complexes are not evident till date, the protein is concluded to be similar in structure and function to another repressor protein Lac-repressor. The GalR is a single polypeptide chain of 343 amino acids. Homology modeled structure of GalR (performed with I-tasser software) with the tryptophan and cysteine residues highlighted is shown in Figure 2.14. One of the unique features of the repressor protein is that the operator is in the class of single tryptophan residue containing protein (Trp165) offering excellent opportunity for the spectroscopic investigation on the intrinsic tryptophan probe.

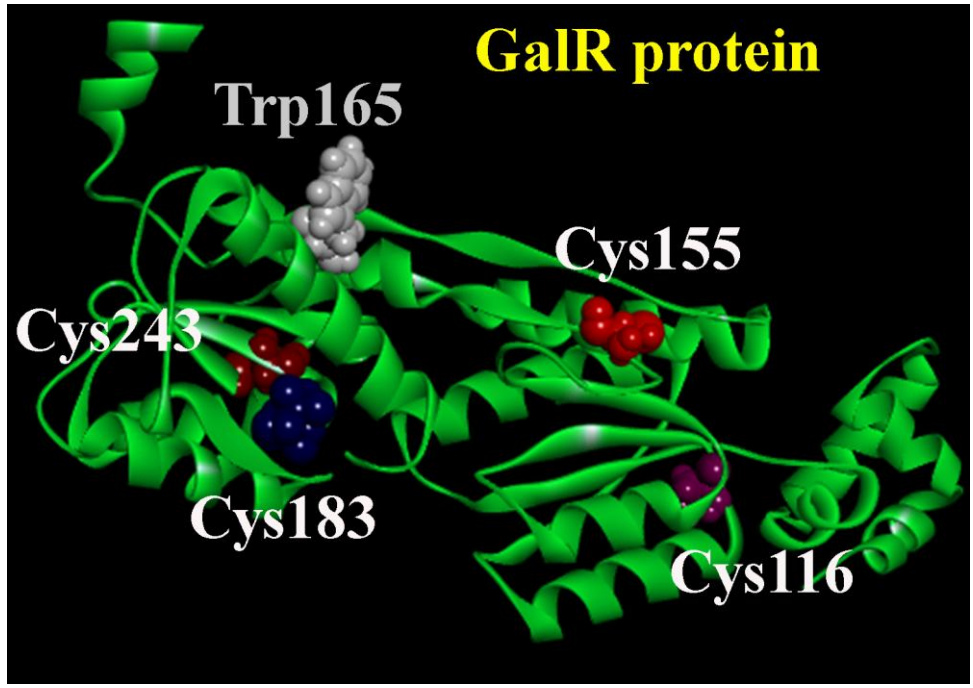

Figure 2.14. *Homology model (performed with I-tasser software) of GalR showing the tryptophan and cysteine residues.*

2.2.2.2. Cro-repressor protein: Bacteriophage lambda has been a useful model system for studying the role of specific protein-DNA and protein-protein

interaction in maintaining complex gene regulatory circuits. Bacteriophage lambda encodes two repressors: Cro repressor (Cro) and lambda (or cI) repressor. Mark Ptashne and coworkers have established the λ genetic switch, which is governed by λ-repressor and Cro-repressor (Figure 2.15). The switching system consists of three contiguous 17 base pair sequences known as the right operator sites, O_R1, O_R2 and O_R3, and two proteins λ-repressor and Cro-repressor. This collection of operator sites known as right operator or O_R, also contains two promoters P_{RM} and P_R. The structural gene of λ-repressor (cI) is under the control of P_{RM} and the structural gene of cro is under the control of the promoter P_R. Cro binds to the three operator sites, cooperatively, in the order of decreasing affinity $O_R3>O_R1>O_R2$ [49]. In the lytic state, Cro dimer occupies O_R3 and O_R2 and activates the promoter P_R repressing the promoter P_{RM}. Thus, it shuts off cro synthesis and activates λ-repressor synthesis.

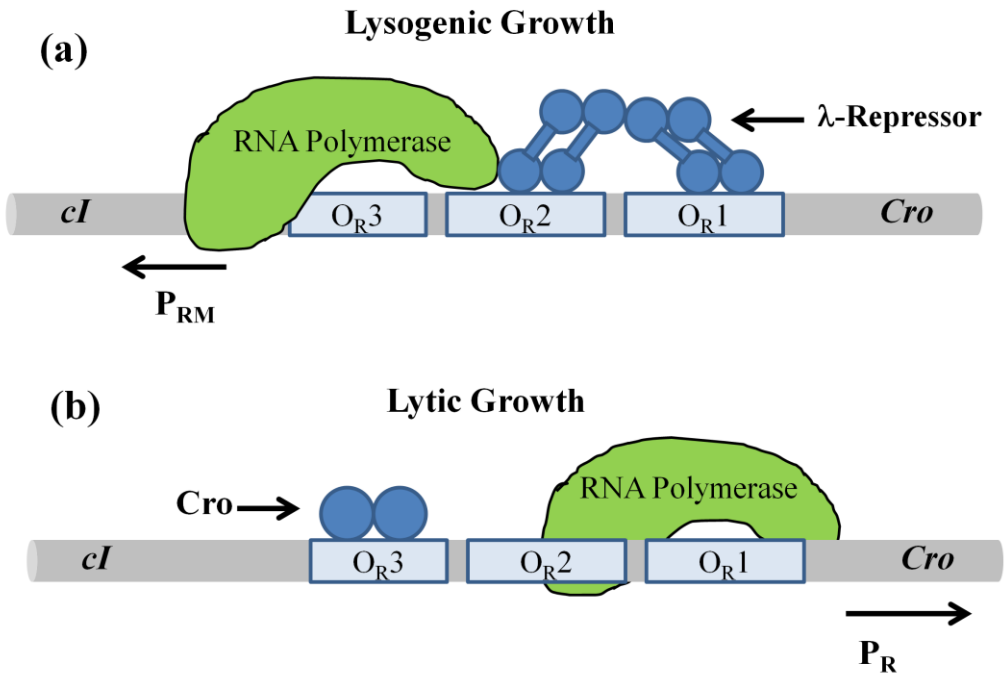

Figure 2.15. *The λ phage genetic switch depicting (a) Lysogenic cycle and (b) Lytic cycle.*

Lambda Cro is a basic, dimeric protein consisting of 66-amino acid residues. The three dimensional structure (Figure 2.16) of this important protein has been solved both in absence [50] and presence of cognate DNA [51]. The structure of Cro protein monomer is very simple, consisting of three strands of aniparallel β-sheets (residues 2-6, 39-45 and 48-55) and three α-helices (7-14, 15-23 and 27-36). It has been proposed that Cro protein binds DNA by penetrating the α-helices into the DNA major groove, allowing the amino acids of Cro to form sequence-specific H bonds with the exposed parts of bases (1-3).

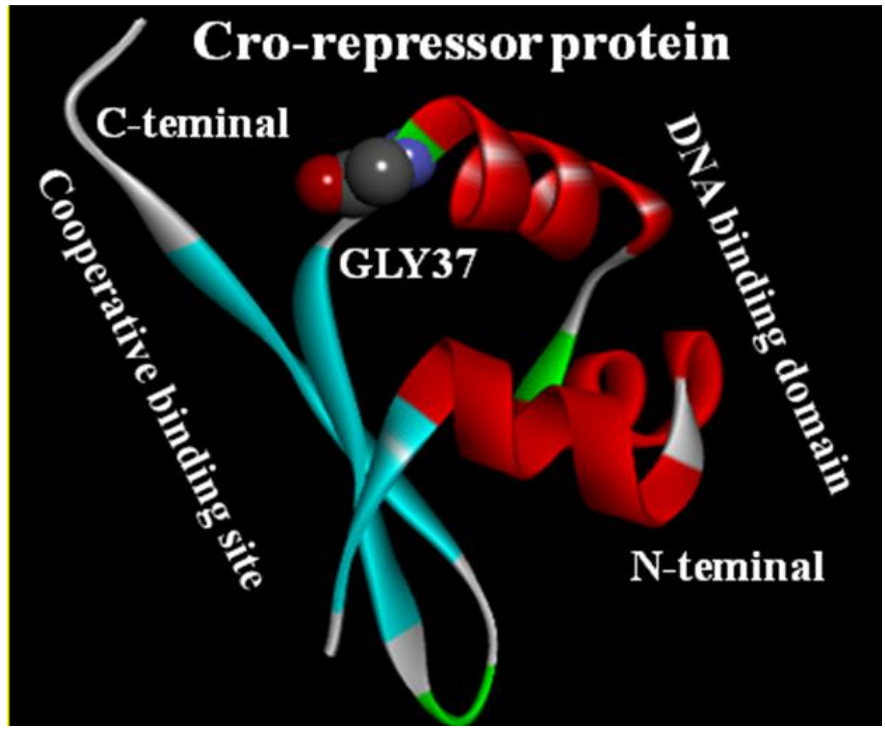

Figure 2.16. *X-ray crystallographic structure of Cro-repressor (PDB code: 6CRO), depicting the different domains.*

2.2.3. Deoxyribonucleic acid: Deoxyribonucleic acids (DNA) are polynucleotide with each nucleotide comprising of deoxyribose sugar, purine and pyrimidine bases and phosphate groups. The main bases whose intermolecular hydrogen bonding holds the DNA strands together are adenine, guanine, thymine and cytosine. DNA serves as carrier of genetic information [52-53]. The classic example

of how biological function follows from biomolecular structure comes from the elucidation of double helical structure of DNA by Watson and Crick [54]. There are generally three forms of DNA-A, B and Z-form. Natural DNA, however, exists in B-form. Natural DNA is about meter long and comprises of hundreds of base pairs. The distance between two base pairs in B-DNA is 3.4 Å [55]. In about 4 M NaCl, B-form assumes Z-form. DNA structures consist of major and minor grooves and intercalation spaces through which DNA interacts with ligands. There are two modes of interaction between DNA and ligands: (i) intercalation, where the planar polycyclic hetero-aromatic ligands sit in between the base pairs of DNA and interact through π–π interaction [56-57], and (ii) groove binding, where the ligands bind in the major and minor grooves of DNA [58]. The water molecules at the surface of DNA are critical for the molecular recognition and maintaining the structure. The DNA codes for proteins and that code is copied into messenger RNA during a process called transcription. Transcription is the first step leading to gene expression and an intricate regulation of this step is critical for the complex functioning of a living cell. The process of transcription is carried out by an enzyme called the RNA polymerase and is tightly regulated by a class of proteins called the transcription factors. Transcription factors are proteins that bind specifically to target DNA sequences upstream or downstream of a particular gene and thereby influence its expression pattern. The basic principle of transcription regulation was established in 1960, primarily by the pioneering work of Francois Jacob and Jacque Monod. The fundamental units of gene regulation in prokaryotes are three types of DNA sequences that determine the level of gene expression under physiological conditions.

(a) Promoters: Originally defined as elements that determine the maximum potential level of gene expression. Promoters are recognized by RNA polymerase, and contain all the information necessary for accurate transcription initiation.

(b) Operators: These are sequences recognized by transcription factors which inhibit transcription that would otherwise occur from the promoters.

(c) Some positive control DNA elements are recognized by activator proteins that stimulate transcription from the promoter. The function of activators and repressors can be modulated by specific physiological conditions thereby regulating expression of the cognate genes.

We have used right operators DNA (O_R3 and O_R2) of λ phage genome, in our studies. O_R3 (5'-TATCACCGCAAGGGATA-3') and its complementary oligonucleotide, O_R2 (5′TACAACACGCACGGTGTTAT3′) and its complementary oligonucleotide were used in our experiments. We have also used O_E and O_I operator DNAs for Gal repressor protein. 5′-C_6 amino linked O_E (5′-GCGTGTAAACGATTCCACGC-3′) operator DNA and its complementary, and 5′-C_6 amino linked O_I (5′-GCGTG GTAGC GGTTA CATGC-3′) and its complimentary. We have used 5′-C_6 amino linked oligonucleotides to attach an amino reactive molecular probe to them for ultrafast dynamical investigation. The schematic of operator DNA is represented in Figure 2.17. We have also used Calf thymus DNA for studying the DNA drug interaction.

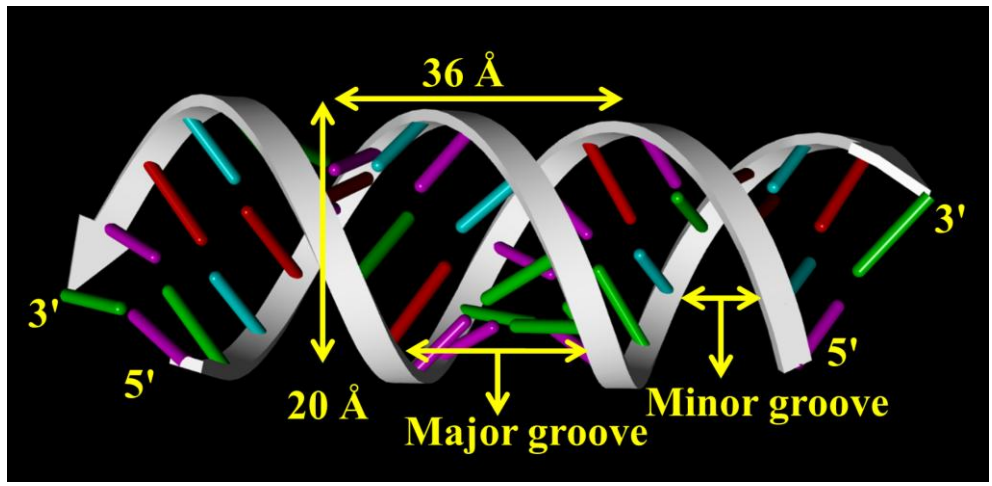

Figure 2.17. *Schematic representation of deoxyribonucleic acid (DNA).*

2.2.4. Molecular probes: In this section we will discuss about the different probe molecules that have been used in the course of study.

2.2.4.1. 2′-(4-Hydroxyphenyl)-5-(4-methyl-1-piperazinyl)-2,5′-bi-1H benzimidazole (Hoechst 33258): The commercially available probe Hoechst 33258 (Figure 2.18a) is widely used as fluorescent cytological stain of DNA. Since it has affinity for the double stranded DNA. Hoechst 33258 is soluble in water. In bulk water the absorption peak and emission peaks of Hoechst 33258 are at 366 and 500 nm [59], respectively and it is sensitive to the polarity of the medium. The significant solvochromic effect (solvation) in the absorption and emission spectra of H258 makes the dye an attractive solvation probe for microenvironments [60].

2.2.4.2. 5-({2-[(iodoacetyl)amino]ethyl}amino)naphthalene-1-sulfonic acid (IAEDANS): IAEDANS is an thiol-reactive organic fluorophore (Figure 2.18b). It is widely used as a protein marker in fluorescence spectroscopy as near-neutral (physiological) pH IAEDANS can be covalently attached with thiol groups (cysteine) of the protein selectively in the presence of amine groups. Actually IAEDANS is a probe containing haloalkyl moiety along with a naphthalene ring. The carbon atom attached to iodine group will react to the sulfhydryl group (S-H) to form covalent attachment as follows:

$$\underset{\text{Haloacetamide (X=I, Br)}}{R^1CH_2X} + R^2SH \longrightarrow \underset{\text{Thioether}}{R^1CH_2\text{-}SR^2} + HX \qquad (2.68)$$

Only cysteine amino acid has sulfhydryl group, which leads the IAEDNS to interact selectively to cysteine. During attachment iodine group of IAEDANS has been substituted by sulfhydril group and it becomes AEDANS. IAEDANS has a peak excitation wavelength of 336 nm and a peak emission wavelength of 490 nm in buffer (pH 7). It can also be used as a solvation probe to monitor the hydration dynamics around the protein. The absorption spectrum of IAEDANS overlaps well with the emission spectrum of tryptophan, making it useful as an acceptor in FRET experiments. It can also be used as a resonance energy donor to fluorophores such as fluorescein, Alexa Fluor 488, Oregon Green [61].

2.2.4.3. Coumarin 500 (C500): The solvation probe C500 (Figure 2.18c) is sparingly soluble in water and shows reasonably good solubility in isooctane. In bulk water the absorption peak (400 nm) is significantly red shifted compared to that in isooctane (360 nm). The emission peak of C500 in bulk water (500 nm) also shows a 90 nm red shift compared to that in isooctane (excitation at 350 nm). The significantly large solvochromic effect in the absorption and emission spectra of C500 makes the dye an attractive solvation probe for microenvironments. The photophysics of the probe have also been studied in detail [62].

2.2.4.4. 1-anilino-8-naphthalenesulfonic acid, ammonium salt (ANS): ANS is a well-known solvation probe [63] which binds selectively to the native state of certain proteins and enzymes in their hydrophobic as well as polar sites (Figure 2.18d). In aqueous solution, the emission quantum yield of ANS is very small (0.004) with emission peak at ~520 nm and a lifetime of ~0.25 ns. The steady-state emission is quenched dramatically in polar solvents. Because of its bichromophoric structure, ANS is known to undergo charge transfer (CT) from one aromatic moiety to the other ring and solvation. In nonpolar solvents, the emission is strong and is mostly from the locally excited state i.e., before charge separation. In polar solvents, the fluorescence decreases and is dominated by emission from the CT state. The solvent polarity and rigidity determine the wavelength and yield of emission and that is why ANS is a useful biological probe. In the protein solutions, the steady-state fluorescence intensity is much larger than in the water solution. ANS is known to bind rigidly at a single site on the surface of the enzyme protein bovine pancreatic α–Chymotrypsin (CHT) near the cysteine-1–122 disulfide bond. This ANS binding site is almost opposite in position to the enzymatic centre of CHT. With femtosecond time resolution Zewail and coworkers have reported ultrafast hydration dynamics at the surface of the enzyme CHT, when the protein is in its physiologically active or inactive states using ANS as the fluorescent probe [45].

2.2.4.5. Tryptophan [(2S)-2-amino-3-(1H-indol-3-yl) propanoic acid]: Tryptophan (Figure 2.18e) is one of the 22 standard amino acids and an essential amino acid in the human diet. Only the L-stereoisomer of tryptophan is found in enzymes and proteins. However, the D-stereoisomer is occasionally found in naturally produced peptides. Tryptophan has large bulky aromatic side chain. Tryptophan is significantly more polar than other aromatic amino acids, because of the nitrogen of the tryptophan indole ring. Tryptophan is rare amino acid and has a single codon. It absorbs light at 280 nm. The molar extinction coefficient value of tryptophan in water is 5,579 M^{-1} cm^{-1} at 278 nm. The fluorescence emission peak of tryptophan dissolved in water is at ~355 nm and the quantum yield of this molecule is 0.14 [64].

2.2.4.6. Fluorescein 5-Isothiocyanate (FITC): Fluorescein has an absorption maximum at 494 nm and emission maximum of 521 nm (in water). Fluorescein 5-isothiocyanate (FITC) is a derivative of fluorescein used in wide-ranging applications (Figure 2.18f). FITC is the original fluorescein molecule functionalized with an isothiocyanate reactive group, replacing a hydrogen atom on the bottom ring of the structure. FITC has excitation and emission spectrum peaks at approximately 495 nm and 521 nm respectively. The molar extinction coefficient is 72,000 M^{-1} cm^{-1} in aqueous buffer, pH 8. FITC is among the most simple and commonly used reagents for protein fluorescent labeling. These isothiocyanates react to amino, sulfhydryl, imidazoyl, tyrosyl or carbonyl groups on proteins; however, only the derivatives of primary and secondary amines generally yield stable products. Reactions are most efficient at pH 8-9 and must be performed in an amine-free buffer such as carbonate/bicarbonate.

2.2.4.7. 4',6-Diamidino-2-phenylindole (DAPI): The dye DAPI (Figure 2.18g) is another commercially available fluorescent cytological stain for DNA. Studies on the DAPI-DNA complexes show that the probe exhibits a wide variety of interactions of different strength and specificity with DNA [65]. The dye exhibits

intramolecular proton transfer as an important mode of excited state relaxation at physiological pH [66], which takes place from the amidino to the indole moiety.

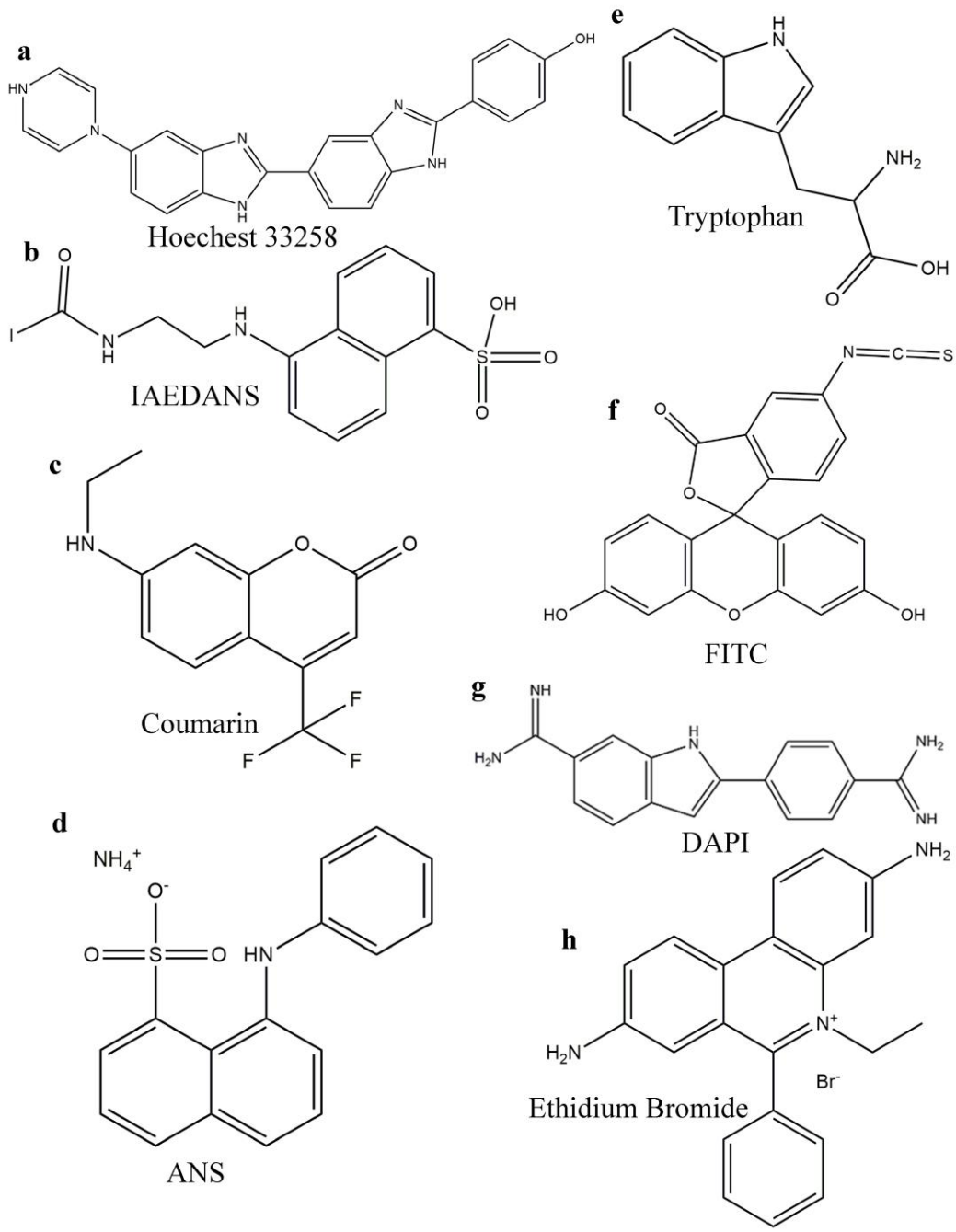

Figure 2.18. *Molecular structure of (a) Hoechst 33258, (b) IAEDANS, (c) Coumarin 500, (d) ANS, (e) Tryptophan, (f) FITC, (g) DAPI, (h) Ethidium bromide.*

Supression of this excited state pathway leads to enhancement of fluorescence quantum yield and hence the fluorescence intensity in hydrophobic restricted environments.

2.2.4.8. Ethidium bromide (EtBr): EtBr is a well-known fluorescent probe (Figure 2.18h) for DNA, which readily intercalates into the DNA double helix [67]. Compared to bulk water, the emission intensity and lifetime of EtBr increases significantly when EtBr intercalates into the double helix of DNA [68]. This remarkable fluorescence enhancement of EtBr is utilized to study the motion of DNA segments, and the interaction of DNA with surfactants and drug [69]. Absorption maxima of EtBr in aqueous solution are at 285 nm and 480 nm, after excitation EtBr emits orange light with wavelength maxima at 620 nm [70].

2.2.5. Quantum dots (QDs): QDs are semiconductors whose excitons are confined in all three spatial dimensions. Amongst the various types of nanomaterials, QDs have been widely investigated and are quite understandable [71-72]. They exhibit size-tunable band gaps and luminescence energies owing to the "quantum-size effect". In order to understand that effect, first consider an electron excited from the valence band by the absorption of a quantum of light moves to the conduction band, leaving behind a hole in the valence band. Together, the bound state of the electron and the electron hole which are attracted by coulombic force is called exciton. Taking a simple Bohr model picture of the exciton, the electron and hole orbit each other at a distance known as the Bohr radius, which varies depending on the material, ranging from a few to tens of nanometers. In a semiconductor crystallite whose diameter is smaller than the size of its excitons Bohr radius, the excitons are squeezed, leading to quantum confinement [71]. Compared with the organic fluorophores that were previously used for biological labelling, quantum dots are much brighter and do not photobleach. They also provide a readilyaccessible range of colours. As fluorophores, high quality QDs are extremely bright, with quantum yields (QYs) approaching unity. QDs have been

used for a wide variety of applications, such as light emitting diodes, lasers and solar cells, staining and lighting up cells for visualization, photocatalysis etc. However, with regard to biological applications toxicity remains a complicated

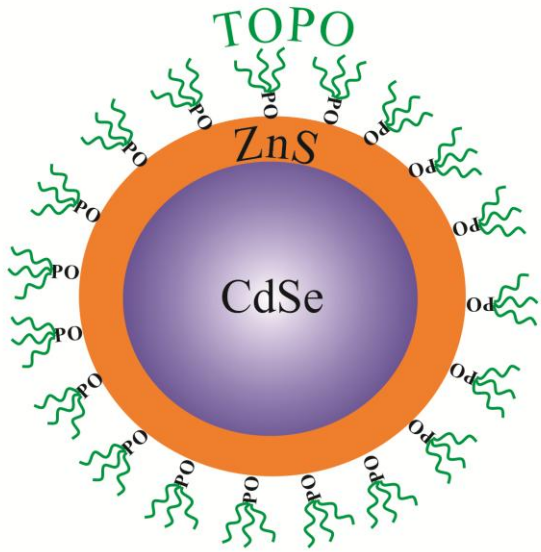

Figure 2.19. *Schematic representation of a core-shell quantum dots. The core consists of CdSe and shell consists of ZnS. Trioctylphosphine oxide (TOPO) is used a capping ligand.*

question. Additionally, cellular uptake of QDs is extremely complex, varying not only with size but with QD surface properties as well as cell type [73]. In our study we have mainly used Trioctylphosphine oxide (TOPO) capped CdSe/ZnS QDs dispersed in toluene solution.

References

[1] B. Bagchi and R. Biswas, Polar and nonpolar solvation dynamics, ion diffusion and vibrational relaxation: Role of biphasic solvent response in chemical dynamics, *Adv. Chem. Phys.* **109**, (1999), 207.

[2] R. Jimenez, G. R. Fleming, P. V. Kumar and M. Maroncelli, Femtosecond solvation dynamics of water, *Nature* **369**, (1994), 471.

[3] S. K. Pal, J. Peon, B. Bagchi and A. H. Zewail, Biological water: Femtosecond dynamics of macromolecular hydration, *J. Phys. Chem. B* **106**, (2002), 12376.

[4] B. Bagchi, Dynamics of solvation and charge transfer reactions in dipolar liquids, *Ann. Rev. Phys. Chem.* **40**, (1989), 115.

[5] L. Onsager, Comments on "effects of phase density on the ionization process and electron localization in fluids" by J. Jortner and A. Gathon, *Can. J. Chem.* **55**, (1977), 1819.

[6] R. M. Stratt and M. Maroncelli, Nonreactive dynamics in solution: The emerging molecular view of solvation dynamics and vibrational relaxation, *J. Phys. Chem.* **100**, (1996), 12981.

[7] J. T. Hynes, Outer-sphere electron transfer reactions and frequency-dependent friction, *J. Phys. Chem.* **90**, (1986), 3701.

[8] M. L. Horng, J. A. Gardecki, A. Papazyan and M. Maroncelli, Subpicosecond measurements of polar solvation dynamics: Coumarin 153 revisited, *J. Phys. Chem.* **99**, (1995), 17311.

[9] J. R. Lakowicz, *Principles of flourescence spectroscopy*, 2nd ed., **1999**, Kluwer Academic/Plenum Publishers, New York, USA.

[10] N. Periasamy and A. S. R. Koti, Time resolved fluorescence spectroscopy: TRES and TRANES, *Proc. Indian Natn. Sci. Acad.* **69**, (2003), 41.

[11] A. S. R. Koti, M. M. G. Krishna and N. Periasamy, Time-resolved area-normalized emission spectroscopy (TRANES): A novel method for

confirming emission from two excited states, *J. Phys. Chem. A* **105**, (2001), 1767.

[12] J. R. Lakowicz, *Principles of Fluorescence Spectroscopy*, 2nd ed., **2006**, Kluwer Academic/Plenum, New York, USA.

[13] R. D. Spencer and G. Weber, Measurements of subnanosecond fluorescence lifetimes with a cross-correlation phase fluorometer, *Ann. N. Y. Acad. Sci* **158**, (1969), 361.

[14] L. A. Philips, S. P.Webb and J. H. Clark, High-pressure studies of rotational reorientation dynamics: The role of dielectric friction, *J. Chem. Phys.* **83**, (1985), 5810.

[15] B. Kalman, N. Clarke and L. B. A. Johansson, Dynamics of a new fluorescent probe, 2,5,8,11-tetra-tert-butylperylene in solution, cubic lyotropic liquid crystals, and model membranes, *J. Phys. Chem.* **93**, (1989), 4608.

[16] N. Ito, O. Kajimoto and K. Hara, Picosecond time-resolved fluorescence depolarization of p-terphenyl at high pressures, *Chem. Phys. Lett.* **318**, (2000), 118.

[17] R. Zana, Microviscosity of aqueous surfactant micelles: Effect of various parameters, *J. Phys. Chem. B* **103**, (1999), 9117.

[18] N. Nandi and B. Bagchi, Dielectric relaxation of biological water, *J. Phys. Chem. B* **101**, (1997), 10954.

[19] L. Stryer, Fluorescence energy transfer as a spectroscopic ruler, *Ann. Rev. Biochem.* **47**, (1978), 819.

[20] P. K. Verma and S. K. Pal, Ultrafast resonance energy transfer in bio-molecular systems, *Eur. Phys. J. D* **60**, (2010), 137.

[21] D. Banerjee and S. K. Pal, Simultaneous binding of minor groove binder and intercalator to dodecamer DNA: Importance of relative orientation of donor and acceptor in FRET, *J. Phys. Chem. B* **111**, (2007), 5047.

[22] S. Batabyal, T. Mondol and S. K. Pal, Picosecond-resolved solvent reorganization and energy transfer in biological and model cavities, *Biochimie* **95**, (2013), 1127.

[23] A. Rodger and B. Norden, *Circular dichroism and linear dichroism*, **1997**, Oxford University Press, Oxford, UK.

[24] N. Berova, K. Nakanishi and R. W. Woody, *Circular dichroism*, 2nd ed., **2000**, Wiley-VCH, New York, USA.

[25] R. F. Ismagilov, A. D. Stroock, P. J. A. Kenis, G. Whitesides and H. A. Stone, Experimental and theoretical scaling laws for transverse diffusive broadening in two-phase laminar flows in microchannels, *Appl. Phys. Lett.* **76**, (2000), 2376.

[26] K. J. Laidler, *Chemical Kinetics*, 3 ed., **1987**, Prentice Hall, UK.

[27] J. N. Israelachvili, D. J. Mitchell and B. W. Ninham, Theory of self-assembly of hydrocarbon amphiphiles into micelles and bilayers, *J. Chem. Soc., Faraday Trans.* **272**, (1976), 1525.

[28] D. J. Mitchell and B. W. Ninham, Micelles, vesicles and microemulsions, *J. Chem. Soc., Faraday Trans.* **77**, (1981), 601.

[29] H. H. Paradies, Shape and size of a nonionic surfactant micelle. Triton X-100 in aqueous solution, *J. Phys. Chem.* **84**, (1980), 599.

[30] S. S. Berr, Solvent isotope effects on alkytrimethylammonium bromide micelles as a function of alkyl chain length, *J. Phys. Chem.* **91**, (1987), 4760.

[31] S. S. Berr, E. Caponetti, J. S. Johnson, J. R. R. M. Jones and L. J. Magid, Small-angle neutron scattering from hexadecyltrimethylammonium bromide micelles in aqueous solutions, *J. Phys. Chem.* **90**, (1986), 5766.

[32] N. J. Turro, X.-G. Lei, K. P. Ananthapadmanabhan and M. Aronson, Spectroscopic probe analysis of protein-surfactant interactions: The BSA/SDS system, *Langmuir* **11**, (1995), 2525.

[33] P. A. Hassan, S. R. Raghavan and E. W. Kaler, Microstructural changes in SDS micelles induced by hydrotropic salt, *Langmuir* **18**, (2002), 2543.

[34] A. K. Shaw and S. K. Pal, Activity of subtilisin carlsberg in macromolecular crowding, *J. Photochem. Photobiol., B* **86**, (2007), 199.

[35] P. L. Luisi, M. Giomini, M. P. Pileni and B. H. Robinson, Reverse micelles as hosts for proteins and small molecules, *BBA-Rev. Biomembranes* **947**, (1988), 209.

[36] K. E. Tettey and D. Lee, Effect of thermal treatment and moisture content on the charge of silica particles in non-polar media, *Soft Matter* **9**, (2013), 7242.

[37] B. Cohen, D. Huppert, K. M. Solntsev, Y. Tsfadia, E. Nachliel and M. Gutman, Excited state proton transfer in reverse micelles, *J. Am. Chem. Soc.* **124**, (2002), 7539.

[38] M. P. Pileni, Water in oil colloidal droplets used as microreactors, *Adv. Colloid Interface Sci.* **46**, (1993), 139.

[39] C. Petit, P. Lixon and M. P. Pileni, Structural study of divalent metal bis(2-ethylhexyl) sulfosuccinate aggregates, *Langmuir* **7**, (1991), 2620.

[40] T. K. Jain, M. Varshney and A. Maitra, Structural studies of aerosol ot reverse micellar aggregates by FTIR spectroscopy, *J. Phys. Chem.* **93**, (1989), 7409.

[41] M. A. Middleton, R. S. Schechter and K. P. Johnston, Dielectric-properties of anionic and nonionic surfactant microemulsions, *Langmuir* **6**, (1990), 920.

[42] D. M. Zhu, X. Wu and Z. A. Schelly, Reverse micelles and water in oil microemulsions of triton x-100 in mixed-solvents of benzene and n-hexane. Dynamic light-scattering and turbidity studies, *Langmuir* **8**, (1992), 1538.

[43] D. L. Nelson and M. M. Cox, *Lehninger principles of biochemistry*, **2000**, W.H. Freeman & Co., New York, USA.

[44] J. J. Birktoft and D. M. Blow, Structure of crystalline α-chymotrypsin, *J. Mol. Biol.* **68**, (1972), 187.

[45] S. K. Pal, J. Peon and A. H. Zewail, Ultrafast surface hydration dynamics and expression of protein functionality: α-chymotrypsin, *Proc. Natl. Acad. Sci. USA* **99**, (2002), 15297.

[46] J. D. Johnson, M. A. El-Bayoumi, L. D. Weber and A. Tulinsky, Interaction of. α-chymotrypsin with the fluorescent probe 1-anilinonaphthalene-8-sulfonate in solution, *Biochemistry* **18**, (1979), 1292.

[47] L. D. Weber, A. Tulinsky, J. D. Johnson and M. A. El-Bayoumi, Expression of functionality of. α-chymotrypsin. The structure of a fluorescent probe-. alpha.-chymotrypsin complex and the nature of its pH dependence, *Biochemistry* **18**, (1979), 1297.

[48] A. Majumdar and S. Adhya, Probing the structure of gal operator-repressor complexes. Conformation change in DNA, *J. Biol. Chem.* **262**, (1987), 13258.

[49] A. D. Johnson, B. J. Meyer and M. Ptashne, Interactions between DNA-bound repressors govern regulation by the λ phage repressor, *Proc. Natl. Acad. Sci. USA* **76**, (1979), 5061.

[50] D. H. Ohlendorf, D. E. Tronrud and B. W. Matthews, Refined structure of Cro repressor protein from bacteriophage λ suggests both flexibility and plasticity, *J. Mol. Biol.* **280**, (1998), 129.

[51] R. A. Albright and B. W. Matthews, Crystal structure of λ-Cro bound to a consensus operator at 3.0 Å resolution, *J. Mol. Biol.* **280**, (1998), 137.

[52] A. D. Hershey and M. Chase, Independent functions of viral protein and nucleic acid in growth of bacteriophage, *J. Gen. Physiol.* **36**, (1952), 39.

[53] O. Avery, C. Macleod and M. MacCarty, Studies on the chemical nature of the substances inducing transformation of pneumococcal types, *J. Expt. Med.* **7**, (1944), 137.

[54] J. D. Watson and F. H. C. Crick, Molecular structure of nucleic acids. A structure for deoxyribose nucleic acid, *Nature* **171**, (1953), 737.

[55] D. L. Nelson and M. M. Cox, *Lehninger principles of biochemistry*, **2000**, W.H. Freeman & Co., New York.

[56] L. S. Lerman, The structure of the DNA-acridine complex, *Proc. Natl. Acad. Sci. USA* **49**, (1963), 94.

[57] M. B. Lyles and I. L. Cameron, Interactions of the DNA intercalator acridine orange, with itself, with caffeine, and with double stranded DNA, *Biophys. Chem.* **96**, (2002), 53.

[58] P. B. Dervan, Molecular recognition of DNA by small molecules, *Bioorg. Med. Chem.* **9**, (2001), 2215.

[59] R. Saha, S. Rakshit, D. Majumdar, A. Singha, R. Mitra and S. Pal, Nanostructure, solvation dynamics, and nanotemplating of plasmonically active SERS substrate in reverse vesicles, *J. Nanopart. Res.* **15**, (2013), 1576.

[60] D. Banerjee, S. S. Sinha and S. K. Pal, Interplay between hydration and electrostatic attraction in ligand binding: Direct observation of hydration barrier at reverse micellar interface, *J. Phys. Chem. B* **111**, (2007), 14239.

[61] S. Chatterjee, Y.-N. Zhou, S. Roy and S. Adhya, Interaction of Gal repressor with inducer and operator: Induction of gal transcription from repressor-bound DNA, *Proc. Natl. Acad. Sci. USA* **94**, (1997), 2957.

[62] S. Nad and H. Pal, Photophysical properties of coumarin-500 (C500): Unusual behavior in nonpolar solvents, *J. Phys. Chem. A* **107**, (2003), 501.

[63] R. P. DeToma, J. H. Easter and L. Brand, Dynamic interactions of fluorescence probes with the solvent environment, *J. Am. Chem. Soc.* **98**, (1976), 5001.

[64] P. G. Wu and L. Brand, Resonance energy transfer: Methods and applications, *Anal. Biochem.* **218**, (1994), 1.

[65] W. D. Wilson, F. A. Tanious, H. J. Barton, R. L. Jones, K. Fox, R. L. Wydra and L. Strekowski, DNA sequence dependent binding modes of 4',6-diamidino-2-phenylindole (DAPI), *Biochemistry* **29**, (1990), 8452.

[66] M. L. Barcellona and E. Gratton, A molecular approach to 4′,6-diamidine-2-phenylindole (DAPI) photophysical behaviour at different pH values, *Biophys. Chem.* **40**, (1991), 223.

[67] D. P. Millar, R. J. Robbins and A. H. Zewail, Torsion and bending of nucleic acids studied by subnanosecond time-resolved fluorescence depolarization of intercalated dyes, *J. Chem. Phys.* **76**, (1982), 2080.

[68] J. Olmsted and D. R. Kearns, Mechanism of ethidium bromide fluorescence enhancement on binding to nucleic acids, *Biochemistry* **16**, (1977), 3647.

[69] R. Sarkar and S. K. Pal, Ligand-DNA interaction in a nanocage of reverse micelle, *Biopolymers* **83**, (2006), 675.

[70] S. K. Pal, D. Mandal and K. Bhattacharyya, Photophysical processes of ethidium bromide in micelles and reverse micelles, *J. Phys. Chem. B* **102**, (1998), 11017.

[71] J. A. Smyder and T. D. Krauss, Coming attractions for semiconductor quantum dots, *Mater. Today* **14**, (2011), 382.

[72] Y. Yin and A. P. Alivisatos, Colloidal nanocrystal synthesis and the organic-inorganic interface, *Nature* **437**, (2005), 664.

[73] T.-G. Iversen, T. Skotland and K. Sandvig, Endocytosis and Intracellular Transport of Nanoparticles: Present Knowledge and Need for Future Studies, *Nano Today* **6**, (2011), 176.

Chapter 3

Instrumentation and sample preparation

In this chapter the details of instrumental setup and sample preparation techniques used in our studies have been described.

3.1. Instrumental setups:

3.1.1. Steady-State UV-Vis absorption and emission measurement: Steady-state UV-Vis absorption and emission spectra of the probe molecules were measured with Shimadzu UV-2450 spectrophotometer and Jobin Yvon Fluoromax-3 fluorimeter, respectively. Schematic ray diagrams of these two instruments are shown in Figures 3.1 and 3.2.

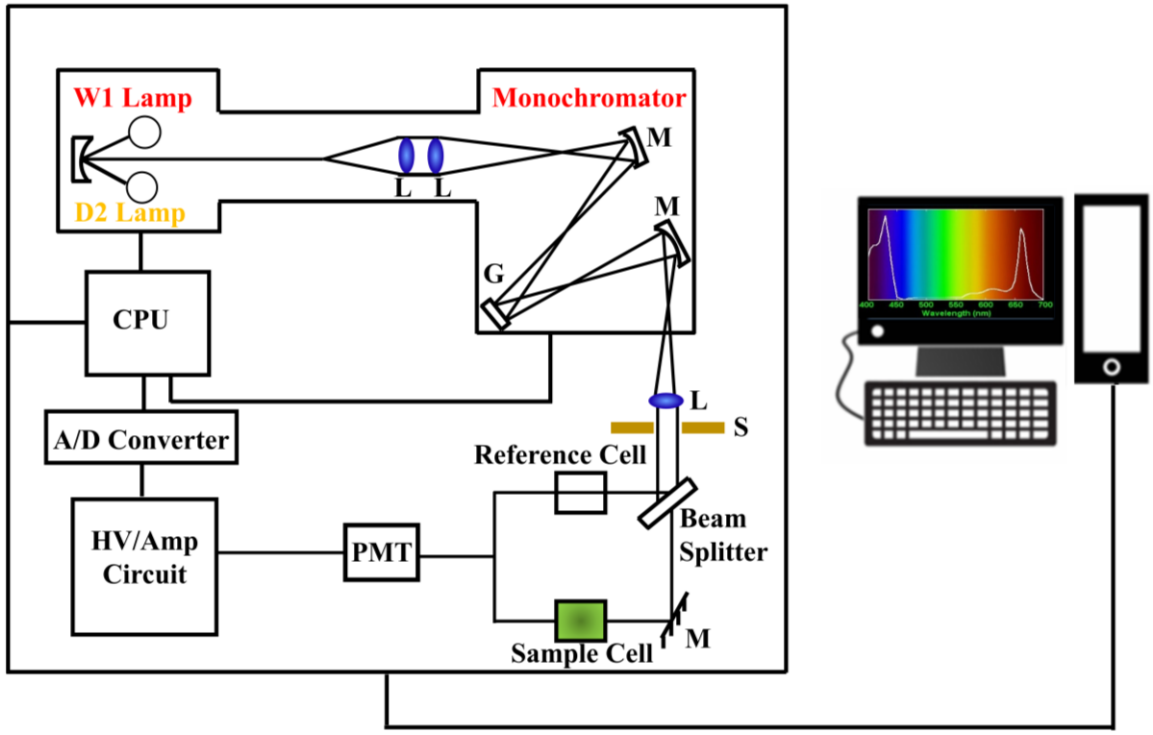

Figure 3.1. *Schematic ray diagram of an absorption spectrophotometer. Tungsten halogen (W1) and deuterium lamps (D2) are used as light sources in the visible and UV regions, respectively. M, G, L, S, PMT designate mirror, grating, lens, shutter and photomultiplier tube, respectively. CPU, A/D converter and HV/amp indicate central processing unit, analog to digital converter and high-voltage/amplifier circuit, respectively.*

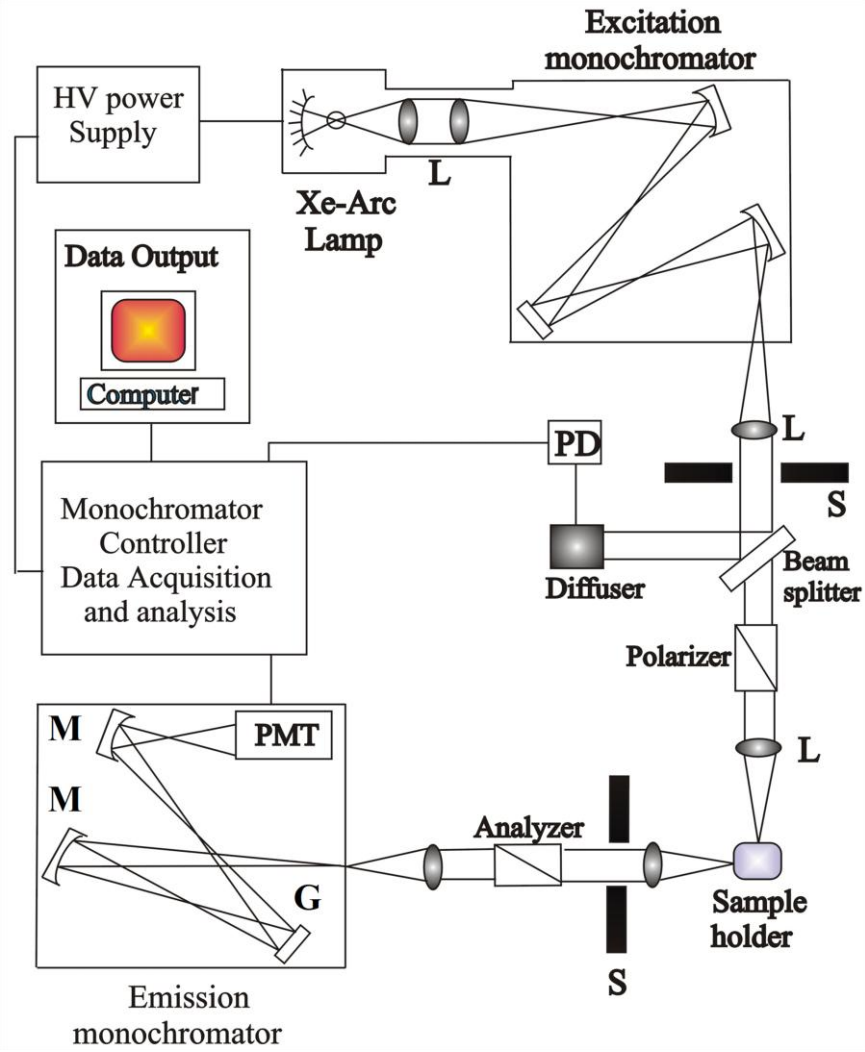

Figure 3.2. *Schematic ray diagram of an emission spectrofluorimeter. M, G, L, S, PMT and PD represent mirror, grating, lens, shutter, and photomultiplier tube and reference photodiode, respectively.*

3.1.2. Circular dichroism (CD) measurement: CD is a form of spectroscopy based on the differential absorption of left and right-handed circularly polarized light. It can be used to determine the structure of macromolecules (including the secondary structure of proteins and the handedness of DNA). The CD measurements were done in a JASCO spectropolarimeter with a temperature controller attachment (Peltier) (Figure 3.3). The CD spectra were acquired using quartz cells of 0.1 and 1.0 cm path length. For proteins and DNA the typical concentration used for CD measurements were within 10 μM.

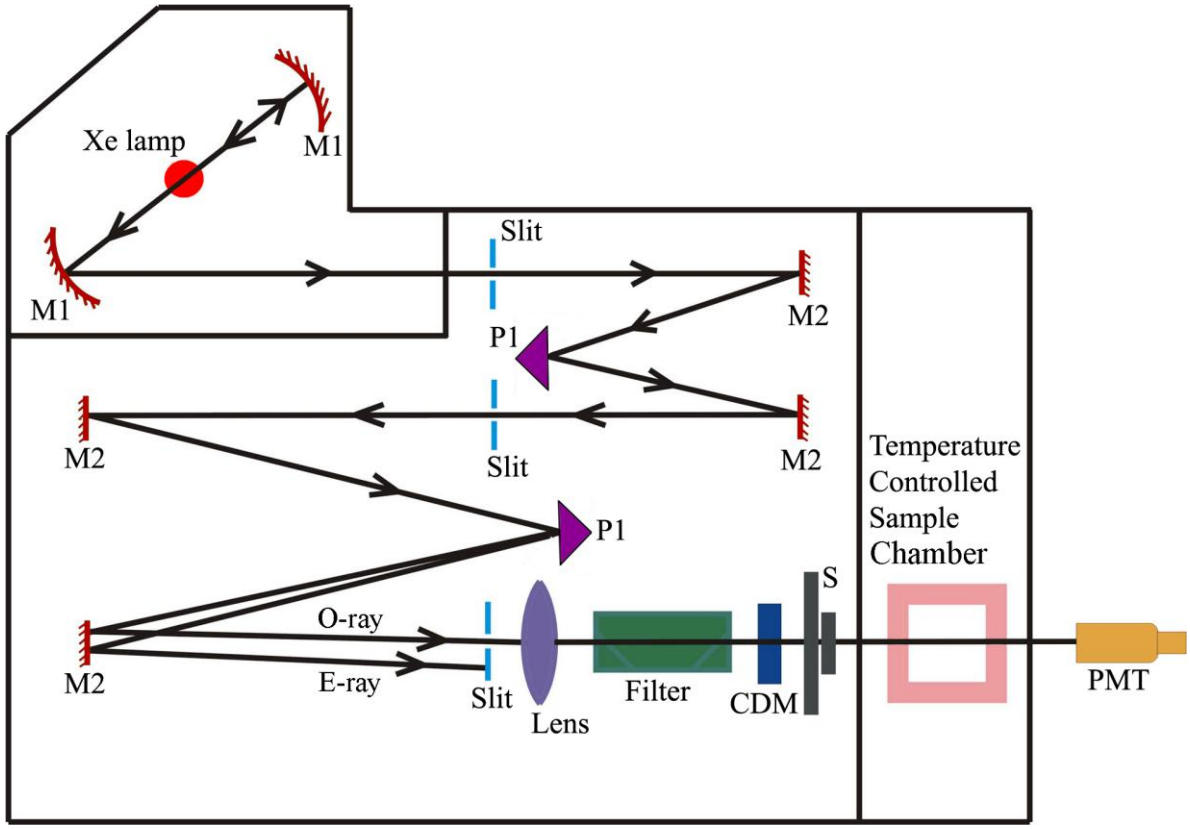

Figure 3.3. *Schematic ray diagram of a circular dichroism (CD) spectropolarimeter. M1, M2, P1, S, PMT, CDM, O-ray and E-ray represent concave mirror, plain mirror, reflecting prism, shutter, photomultiplier tube, CD-modulator, ordinary ray and extraordinary ray, respectively.*

3.1.3. Time-correlated single photon counting (TCSPC) technique: All the picosecond-resolved fluorescence transients were recorded using TCSPC technique. The schematic block diagram of a TCSPC system is shown in Figure 3.4. TCSPC setup from Edinburgh instruments, U.K., was used during fluorescence decay acquisitions. The instrument response functions (IRFs) of the laser sources at different excitation wavelengths varied between 70 ps to 80 ps. The fluorescence from the sample was detected by a photomultiplier after dispersion through a grating monochromator [1]. For all transients, the polarizer in the emission side

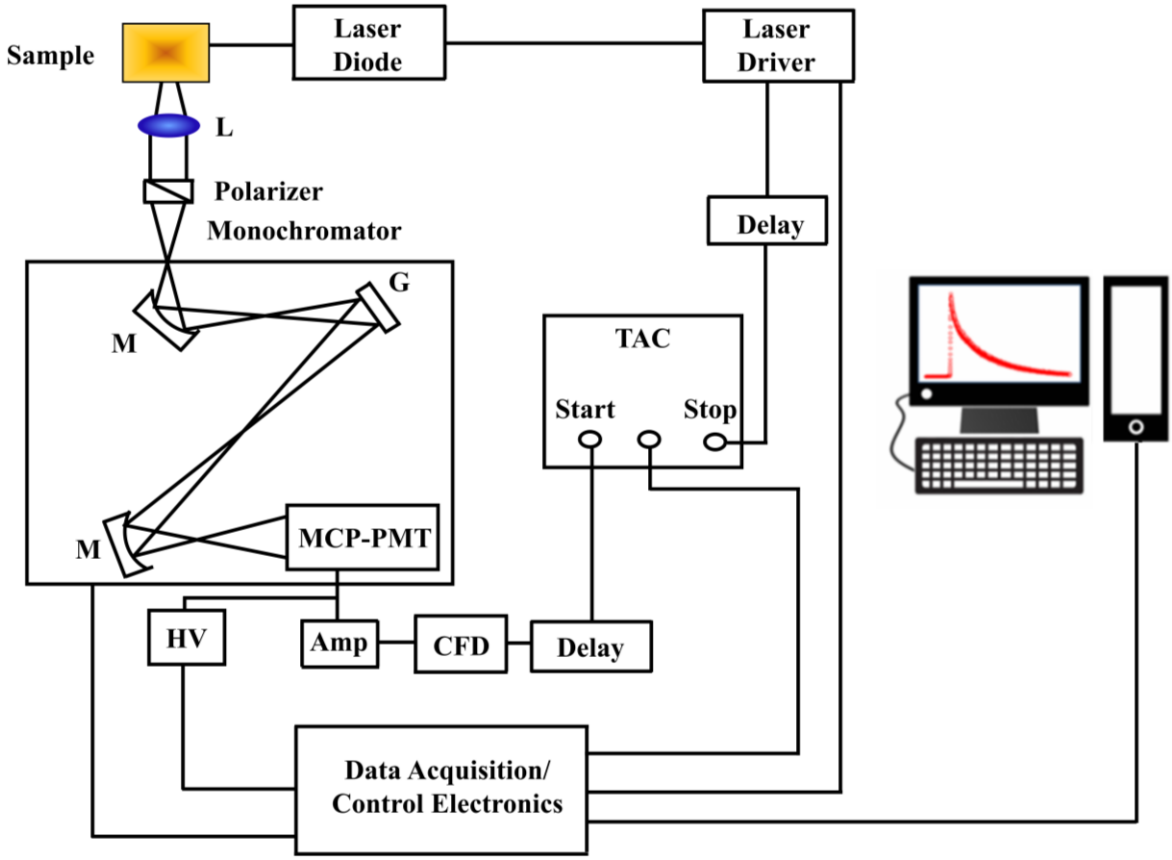

Figure 3.4. *Schematic ray diagram of a time correlated single photon counting (TCSPC) spectrophotometer. A signal from microchannel plate photomultiplier tube (MCP-PMT) is amplified (Amp) and connected to start channel of time to amplitude converter (TAC) via constant fraction discriminator (CFD) and delay. The stop channel of the TAC is connected to the laser driver via a delay line. L, M, G and HV represent lens, mirror, grating and high voltage source, respectively.*

was adjusted to be at 54.7^0 (magic angle) with respect to the polarization axis of excitation beam. In order to measure anisotropy, fluorescent transients were taken with emission polarizer aligned in parallel and perpendicular directions with respect to vertical polarization of excitation light. For tryptophan excitation of protein, femtosecond-coupled TCSPC setup were employed in which the sample was excited by the third harmonic laser beam (300 nm) of the 900 nm (0.5 nJ per pulse) using a mode-locked Ti-sapphire laser with an 80 MHz repetition rate (Tsunami, spectra physics), pumped by a 10 W Millennia (Spectra physics) followed by a pulse-peaker (rate 8 MHz) and a third harmonic generator (Spectra-physics, model 3980). The third harmonic beam was used for excitation of the

sample inside the TCSPC instrument (IRF = 70 ps) and the second harmonic beam was collected as for the start pulse.

3.1.4. Femtosecond resolved fluorescence upconversion technique: The femtosecond-resolved fluorescence spectroscopy was carried out using a femtosecond upconversion setup (FOG 100, CDP, Figure 3.5) in which the sample

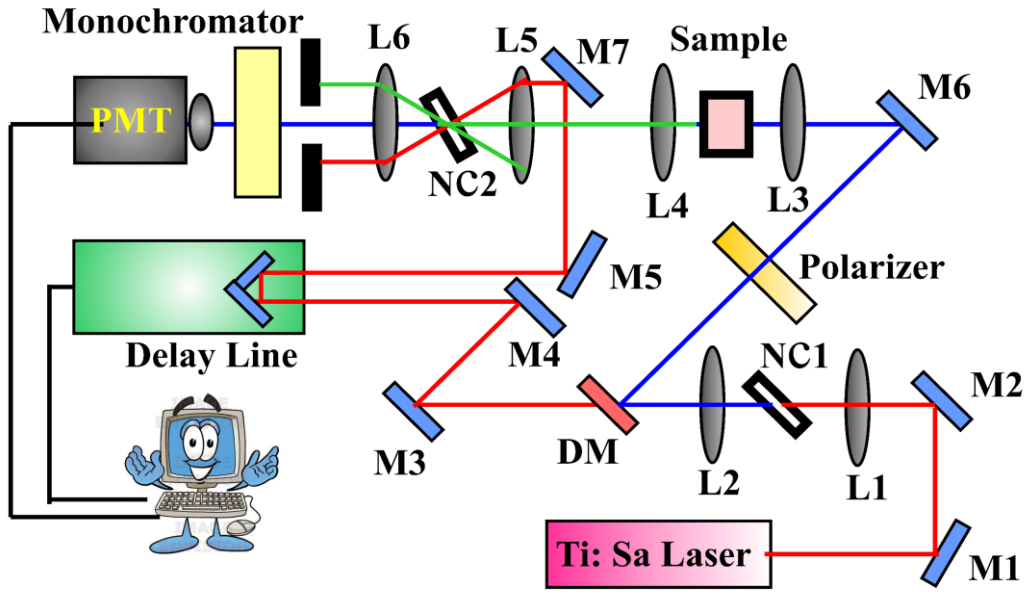

Figure 3.5. *Schematic diagram of a femtosecond fluorescence upconversion experimental setup. A BBO crystal (NC1) is used for second harmonic generation, which provides a pump beam in the UV region. Another BBO crystal (NC2) generates the upconversion signal of pump and probe beams. L and M indicate lenses and mirrors, respectively. M1, M2, M3, M4, M5, and M7 are IR mirrors whereas M6 is a UV mirror. DM is dichroic mirror, and P is periscope.*

was excited at 385 nm, using the second harmonic of a mode-locked Ti-sapphire laser with 80 MHz repetition rate (Tsunami, Spectra Physics), pumped by 10 W Millennia (Spectra Physics). The fundamental beam was passed through a periscopic arrangement (P) (Figure 3.5) before getting frequency doubled in a nonlinear crystal, NC1 (1 mm BBO, $\theta = 25°$, $\phi = 90°$). This beam was then sent into

a rotating circular cell of 1 mm thickness containing the sample via a dichroic mirror (DM), a polarizer and a mirror (M6). The resulting fluorescence emission was collected, refocused with a pair of lenses (L4 and L5) and mixed with the fundamental beam (770 nm) coming through a delay line to yield an upconverted photon signal in a nonlinear crystal, NC2 (0.5 mm BBO (β-barium borate), $\theta = 10°$, $\phi = 90°$). The upconverted light was dispersed in a double monochromator and detected using photon counting electronics. A cross-correlation function obtained using the Raman scattering from water displayed a full width at half maximum (FWHM) of 165 fs. The femtosecond fluorescence decays were fitted using a Gaussian shape for the exciting pulse.

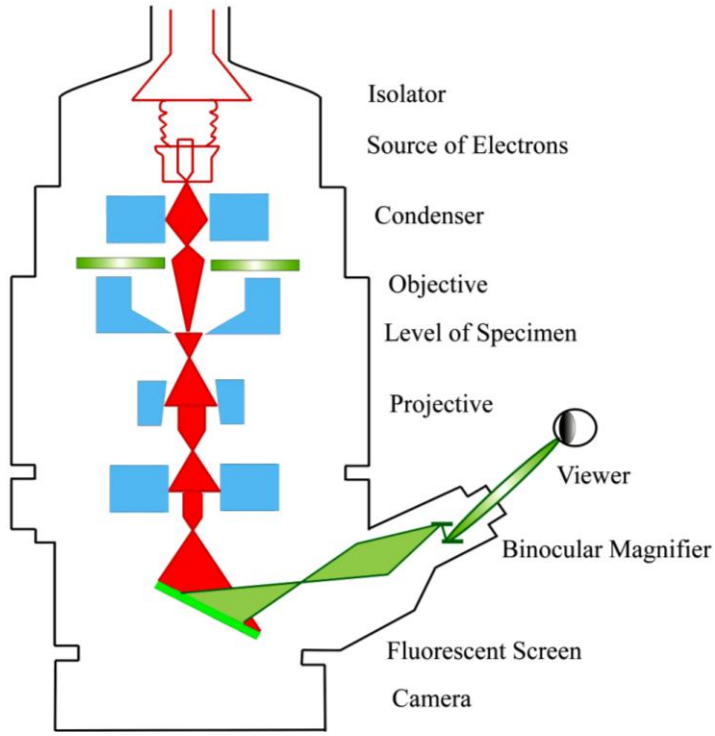

Figure 3.6. *Schematic diagram of a typical transmission electron microscope (TEM). After the transmission of electron beam through a specimen, the magnified image is formed either in the fluorescent screen or can be detected by a CCD camera.*

3.1.5. Transmission electron microscope (TEM): A FEI TecnaiTF-20 field-emission high-resolution TEM (Figure 3.6) equipped with an energy dispersive X-ray

(EDAX) spectrometer was used to characterize the microscopic structures of samples and to analyze their elemental composition. The sizes of the quantum dots (QDs) were determined from the TEM images obtained at 200 kV acceleration voltage of the microscope. Samples for TEM were prepared by placing a drop of the QDs solution on a carbon-coated copper grid and allowing the film to evaporate overnight at room-temperature.

3.1.6. Quasielastic Neutron Scattering (QENS). A 0.3 M micellar solution was prepared separately in D2O (99.9% atom D purity) for both surfactants. Experiments were carried out using the IRIS time-of-flight spectrometer at the ISIS pulsed neutron facility, U.K. IRIS is an inelastic neutron scattering instrument that works on inverted geometry with an array of pyrolytic graphite analyzer crystals situated near backscattering geometry. PG (002) analyzer provides an elastic resolution of 17.5 μeV at a final energy of 1.84 meV over wave vector transfer (Q) range from 0.44 to 1.83 Å−1 with an energy window from 0.35 to 1.2 meV (in offset configuration). In order to achieve no more than 10% scattering, the samples were placed in a cylindrical aluminum can with an internal spacing of 1 mm. QENS measurements were carried out on a micellar solution in D2O at temperatures of 300 K. Since we are interested in the dynamics of the micelles, we subtract the scattering contribution from D2O after measuring the QENS spectra for pure D2O. Data reduction involving background subtraction and detector efficiency corrections were performed by using the ISIS data analysis package, MODES [2].

3.1.7. Microfluidics methodology: Figure 3.7 portrays the used microfluidics (MF) system, represented as the Y-shaped MF chip. The specially designed MF chip with the connectors and the syringe pumps (Atlas-ASP011) were bought from Dolomite, UK and Syrris Ltd., UK respectively. The specially designed MF chip consists of two inlets and a common outlet. The chip was made out of optically transparent glass, which can sustain higher temperature if required. The diameter of the microchip (440 μm) was designed to withstand high flow rates. A small

special region just after the confluence (X region) with a diameter of 150 μm and a length scale around 2200 μm was deliberately added in the design, after which it expands to 440 μm (Y region). The small diameter guarantees a higher fluid front velocity with reasonably low Reynolds number. The special geometry empowers to study very fast kinetics with a time resolution in the order of nanoseconds. For the study of slow kinetics in the range of millisecond to microsecond, the other portion of the microchannel with a diameter of 440 μm is suitable. The two inlets were attached to a syringe pump by capillary tubes.

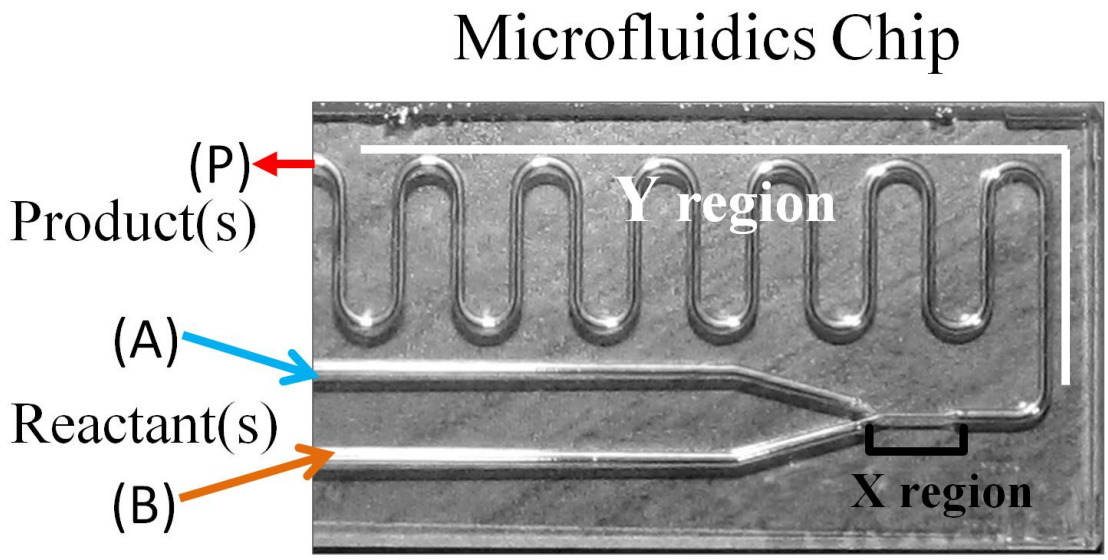

Figure 3.7. *Custom designed microfluidics chip to monitor fast reaction. Two specific regions are shown: X, for fast sub-100 ns kinetics and Y, for slower kinetics [3].*

The capillaries were passed through the shaft of the holder prior to connection with the MF chip. The reagents were propelled using the syringe pump and the total volumetric flow rate was adjusted according to the requirements. The term "flow rate" refers to the combined volumetric flow rate of the reagents through the micro-channel. The schematic of the MF channel is presented as a tube with a cross section S, length L, and total volume V=SL (Figure 3.8). The streams converge and their mixing starts in the micro-channel junction, position X_0 in the

Figure 3.8. The total length of the flow path of the micro-channel is around 10 cm. Fluorescence images were captured with a fluorescence microscope (BX-51, Olympus America, Inc.) equipped with a 100 W mercury arc lamp which was used as the excitation source (UV light excitation) and a DP72 CCD camera (Figure 3.8). The excitation light was cut off by using a standard filter and the fluorescence was

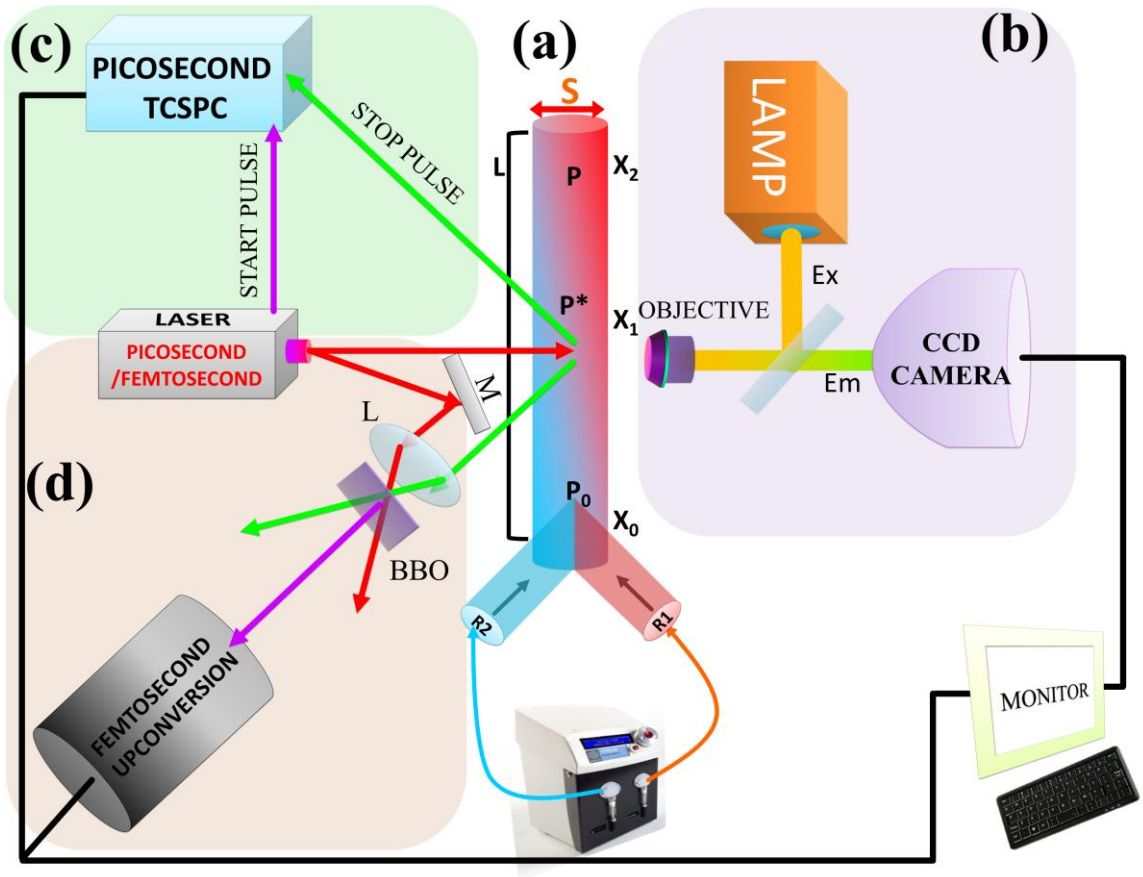

Figure 3.8. *(a) Schematic presentation of the developed microfluidics platform. L denotes the flow path length, X_i are the positions for measurements along the channel and S is the cross section of the micro-channel. (b) The fluorescence microscope coupled to the microfluidics channel. A CCD camera captures images of the ongoing reactions inside the micro-channel. (c) Picosecond resolved fluorescence technique for the collection of decay profiles along the micro-channel. (d) Femtosecond upconversion technique combined with the microfluidics platform for studying ultrafast dynamics.*

collected through a 10× objective. The image processing and analysis were done by the 'analySIS' software provided with the microscope. A region of interest (ROI) was selected at a specific height and width. This ROI was used to obtain an

intensity profile along the microchannel. Intensity profiles were acquired at a particular microchannel distance from the initial mixing confluence. The RGB analysis was performed wherever required. This channel distance was converted into the reaction time (t_n) by dividing it by the velocity of the flow (U [m/s]), obtained from the known volumetric flow rate and cross-section (S) of the micro-channel [3-4].

3.1.8. Fluorescence microscope: Commercially available fluorescence microscope (BX-51, Olympus America, Inc.) was used in our study. The light source is usually a mercury-vapor lamp. For bright field, Tungsten-halogen lamp was used. In particular, an inverted setup with a mercury-vapor lamp as light source is shown.

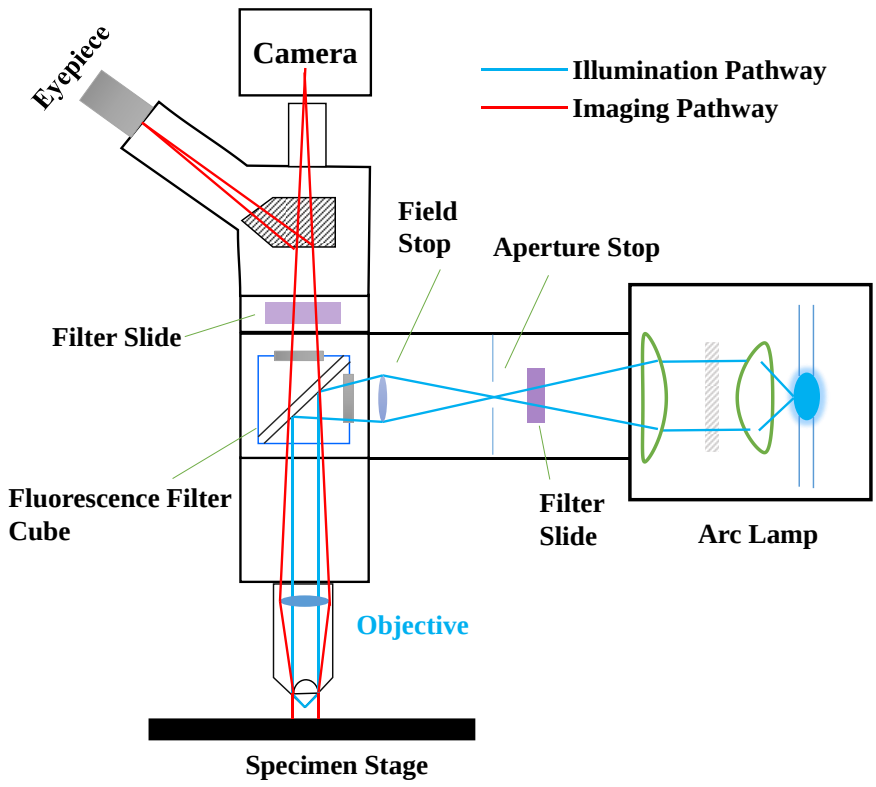

Figure 3.9. Schematic presentation of the fluorescence microscope.

The dichroic mirror, excitation and emission filter are joined together within the filter cube (Figure 3.9). Since mercury-vapor lamps emit light over the whole optical spectrum as well as in the ultraviolet range, an optical excitation filter is used to isolate one specific wavelength. Due to the Stokes shift, it is possible to separate excitation and emission light in the same light path optically via a dichroic mirror. This way, only the emission light is collected by the objective. An emission filter helps to suppress unwanted background light.

3.2. Sample preparation: In this section the different sample preparation methods have been discussed.

3.2.1. Chemicals used: The chemicals, spectroscopic probes, and proteins were procured from the following sources. Double distilled water was used to prepare all the aqueous solutions. The chemicals calf thymus DNA, bis (2-ethylhexyl) sulphosuccinate (AOT), Sodium dodecyl sulfate (SDS), sodium dodecyl benzenesulfonate, cetyl trimethyl ammonium chloride (CTMA), 8-anilino-1-naphthalenesulfonic acid ammonium salt (ANS), potassium phosphate monobasic, potassium chloride, EDTA, Streptomycin sulfate, acrylamide, bisacrylmide, TEMED, poly(ethyleneimine) and phenylmethanesulfonyl fluoride (PMSF), ethidium bromide, bromophenol blue, coomassie brilliant blue, ampicillin reduced glutathione, poly(ethyleneimine) and potassium hydroxide were purchased from Sigma Aldrich. The fluorescent probes 2′-(4-hydroxyphenyl)-5-(4-methyl-1-piperazinyl)-2,5′-Bi-1H-benzimidazole trihydrochloride hydrate (H258), ethidium bromide (EtBr), 4′,6-diamidino-2-phenylindole (DAPI), fluorescein-5-isothiocyanate (FITC) and 5-({2-[(iodoacetyl)amino]ethyl}amino)naphthalene-1-sulfonic acid (IAEDANS) were purchased from Molecular probes. Coumarin 500 (C500) is from Exciton. Polyethylene glycol p-(1,1,3,3-tetramethylbutyl)-phenyl ether (TX-100) was purchased from ROMIL. *p*-Benzoquinone (BQ) was from Alfa Aesar. Sodium hydroxide and phenolphthalein were purchased from Merck. Acrylamide and isopropyl β-D-thiogalactopyranoside (IPTG) were purchased

from Sigma Chemical Co. Bacto-tryptone, bacto-agar, and yeast extract were purchased from Difco Laboratories (Detroit, MI). β-Mercaptoethanol and glycerol were purchased from Aldrich Chemical Co. Isooctane was from Spectrochem. Birch yellow QDs, which is a suspension of CdSe QDs with a ZnS shell and TOPO capping, was purchased from Evidots. O_R3 (5'-TATCACCGCAAGGGATA-3') and its complementary oligonucleotide, O_R2 (5′-TACAACACGCACGGTGTTAT-3′) and its complementary oligonucleotide for Cro-repressor protein and 5′-C_6 amino linked O_E (5′-GCGTGTAAACGATTCCACGC-3′) operator DNA and its complementary, and 5′-C_6 amino linked O_I (5′-GCGTG GTAGC GGTTA CATGC-3′) and its complimentary were purchased from Trilink (USA). 100 mM phosphate buffer (pH 7) was prepared by using sodium dihydrogen phosphate (50 mM), di-sodium hydrogen phosphate (50 mM) in millipore water and the sample solutions were prepared in the same. All other reagents were of highest analytical grade quality.

3.2.2. Cro-repressor isolation and purification: Full length Cro (Enterobacteria phage lambda) cDNA was cloned in-frame into the EcoR1 and Sal1 site located downstream of the GST gene in the pGEX-4T-1 vector. Then the vector was transformed into BL21 cells and the cells were grown in Luria broth containing 100 mg ml1 ampicillin at 37 ^{0}C until A_{600} reached 0.5–0.6. After that cells were induced by 1 mM IPTG for 5 h at 32 ^{0}C. Cells were harvested by centrifugation. The cell pellet was suspended in lysis buffer (50 mM Tris–HCl, 500 mM NaCl, 5 mM EDTA, 10% glycerol, pH 8.6 and 1 mM PMSF). After sonication on ice, the lysate was cleared by centrifugation (14 000 rpm, 45 min, 4 ^{0}C). The supernatant was loaded onto a GST-Sepharose (GE Healthcare) column that was pre-equilibrated with lysis buffer. The column was washed subsequently with lysis buffer and wash buffer (50 mM Tris–HCl, 200 mM NaCl, 10% glycerol, pH 8.6). The GST-tagged fusion protein was eluted with elution buffer (30 mM reduced glutathione, 50 mM Tris–HCl, 100 mM NaCl, 10% glycerol, pH 8.6). Then the

protein was dialysed with 50 mM Tris–HCl, 100 mM NaCl, 10% glycerol, pH 8.6 and digested with thrombin at 16 1C for 1.5 h and loaded onto a benzamidine-Sepharose (GE Healthcare) column which was preequilibrated with 50 mM Tris–HCl, 100 mM NaCl, 10% glycerol, pH 8.6 for removal of thrombin. The digested protein was then further purified by FPLC on a mono-S column to get pure Cro-protein. Finally the protein was dialysed with 50 mM Tris–HCl, 100 mM NaCl, and 5% glycerol buffer of pH 7.2 and confirmed by gel electrophoresis [5].

3.2.3. **Site directed mutagenesis (SDM):** The point mutant of Cro-protein, CroG37C, was made by sitedirected mutagenesis (QuikChange II XL site-directed mutagenesis kit; Stratagene) as per the manufacturer's instructions. The mutant was confirmed by sequencing. Expression and purification of the mutant protein was carried out as described for wild-type cro-repressor protein above.

3.2.4. Gal-repressor isolation and purification: Escherichia coli strain DH5α bearing pSEM1026 or pSEM1051 was grown in superbroth containing 50 µg/ml ampicillin. After the optical density at 600 nm reached 0.4, the culture was induced with 0.2% arabinose for 5 h. The cells were harvested by centrifugation and stored at −80 ^{0}C. The frozen cells were resuspended in 1/40 volume of lysis I buffer (50 mM sodium phosphate pH 8.0, 0.5 mg/ml lysozyme) and stored on ice for 30 min. An equal volume of lysis II buffer (50 mM sodium phosphate pH 8.0, 2 M NaCl, 8 mM imidazole, 20% glycerol, 1% Triton X-100) was added and incubated for 30 min on ice. The cell debris was removed by centrifugation at 10000 *g* for 1 h. Addition of 3% Ni-NTA slurry (Qiagen) to the solution was followed by 1 h incubation at 4 ^{0}C. A Poly-Prep Chromatography Column (Bio-Rad) was used to collect the protein bound to Ni-NTA–agarose from the mixture. Twenty column volumes of washing buffer (50 mM sodium phosphate pH 8.0, 600 mM NaCl, 60 mM imidazole, 10% glycerol) were allowed to flow through the column. GalR was eluted by four column volumes of elution buffer

(50 mM sodium phosphate pH 8, 600 mM NaCl, 10% glycerol) containing 250 and 500 mM imidazole for wild-type and mutant GalR, respectively, and stored at −80 ^{0}C in 100 µl aliquots. Approximately 2.5 mg of protein was eluted from 1 ml of Ni-NTA–agarose in each case [6].

3.2.5. Preparation of reverse micelles: Reverse micellar solutions of specific degree of hydration (w_0) were prepared by addition of calculated volume of aqueous solution of the probe in known volume of 100 mM AOT solution in isooctane [7]. In order to ensure that each reverse micelle contains not more than one probe molecule, the overall probe concentration was kept less than that of reverse micellar concentration.

3.2.6. Preparation of synthetic and genomic DNA solutions: In order to reassociate the single strand DNA into self-complimentary double stranded DNA (ds DNA), thermal annealing was performed as per the methodology prescribed by the vendor. Aqueous sample solutions of genomic DNA were prepared in phosphate buffer (pH ~7). The nucleotide concentrations were determined by absorption spectroscopy using the average extinction coefficient per nucleotide of the DNA (6600 $M^{-1}cm^{-1}$ at 260 nm) [8].

3.2.7. Chemical modification of Cro-repressor and Gal-repressor with IAEDANS: IAEDANS is a thiol-reactive fluorescence probe. At near-neutral (physiological) pH protein can be coupled with thiol groups selectively in the presence of other amine groups. The site of reaction is an active cysteine in the protein. Repressor protein (11 µM) and IAEDANS (50 µM) were incubated in phosphate buffer (0.1 M, pH 8) overnight in the dark and extensively dialysed against the same phosphate buffer before use. Using absorbance at 280 nm and 363 nm for protein and IAEDANS, respectively, the labeling efficiency of IAEDANS has been calculated.

3.2.8. DNA labeling with FITC: For preparation of FITC labeled, oligonucleotides were labeled in 500 ml solution containing 1 M sodium carbonate/ bicarbonate buffer (pH 9): DMF:water [high-performance liquid chromatography (HPLC) grade] = 5:2:3. Reaction was carried out for 20 h at 25 ^{0}C. After incubation, the reaction was loaded onto a Sephadex G-25 column [pre-equilibrated in 0.1 M phosphate buffer (pH 8.0)] and eluted with same buffer. The oligonucleotides and their complementary strands were annealed by heating at 80 ^{0}C followed by cooling slowly at room temperature [9].

3.2.9. Preparation of DNA-CTMA thin film and labeling with QDs: A 50 mm phosphate buffer (pH 7) was prepared by using potassium phosphate monobasic salt. An aqueous solution of DNA was prepared in phosphate buffer (50 mm). The DNA solution was sonicated to reduce the chain length of DNA. The H258-DNA solution was prepared by adding the requisite volume of probe solution (aqueous) to a DNA solution with a 20 mm base pair concentration so that final concentration of the probe was 2 mm with continuous stirring for 4–5 h. DNA–surfactant complexes were prepared according to the reported literature [8]. Briefly, drug-bound DNA aqueous solution was mixed with CTMA aqueous solution in a 1:1 stoichiometric combination, which led to a highly organized complex. The insoluble complex was collected by filtration, washed with distilled water, and was then lyophilized to form freezedried powder. To avoid the adsorption of air moisture, the white powders of DNA–CTMA complexes were kept in a desiccator. The powder was dissolved in n-butanol, and the solution was uniformly spread on a quartz plate to prepare the thin film. The swollen DNA–CTMA film was prepared by soaking the film under water for 30 min and finally removing the excess amount of surface water. The incorporation of QDs into the thin film was carried out by adding the QDs in butanol prior to dissolving the DNA–CTMA matrix into the butanol solution and thereafter following the same procedure as described above [10].

3.2.10. COMSOL simulation: The fluid dynamics simulation was carried out by using the COMSOL multiphysics software (v4.3a) with a finite element method. A 3D geometry was created based on the dimensions (length 12.5 mm, radius 100 mm) of the microchannel used in our experiment with two inlets and one outlets (T shaped channel). Herein, we used two models for two pH values. For pH 3.6, we chose the model A+C→B→P, in which A, C, B, and P were ANS, CHT, intermediate complexes of the ANS–CHT, and the final ANS–CHT product. For high pH (6.3), the model was different leading to C→C*→P, in which C* was another conformation of CHT. To simulate the fluid flow in the microchannel, a model of laminar flow was added to the simulation. By considering diffusion of the species, the convection and diffusion model (transport of diluted species) was coupled to the fluid flow physics. The rate of product formation in the system equalled the rate of substrate depletion. Concentration profiles generated in COMSOL were exported as text files.

References

[1] D. V. O'Conner and D. Philips, *Time correlated single photon counting*, **1984**, Academic Press, London.

[2] S. Choudhury, P. K. Mondal, V. Sharma, S. Mitra, V. G. Sakai, R. Mukhopadhyay and S. K. Pal, Direct observation of coupling between structural fluctuation and ultrafast hydration dynamics of fluorescent probes in anionic micelles, *J. Phys. Chem. B* **119**, (2015), 10849.

[3] S. Batabyal, S. Rakshit, S. Kar and S. K. Pal, An improved microfluidics approach for monitoring real-time interaction profiles of ultrafast molecular recognition, *Rev. Sci. Instrum.* **83**, (2012), 043113.

[4] S. Choudhury, S. Batabyal, P. K. Mondal, P. Singh, P. Lemmens and S. K. Pal, Direct observation of kinetic pathways of biomolecular recognition, *Chem. Eur. J.* **21**, (2015), 16172.

[5] S. K. Pal, S. Choudhury, B. Ghosh, P. Singh, R. Ghosh and S. Roy, Ultrafast differential flexibility of cro-protein binding domains of two operator dnas with different sequences, *Phys. Chem. Chem. Phys.* **18**, (2016), 17983.

[6] S. Choudhury, G. Naiya, P. Singh, P. Lemmens, S. Roy and S. K. Pal, Modulation of ultrafast conformational dynamics in allosteric interaction of gal repressor protein with different operator DNA sequences, *ChemBioChem*, **17**, (2016), 605.

[7] R. Saha, S. Rakshit, P. K. Verma, R. K. Mitra and S. K. Pal, Protein-cofactor binding and ultrafast electron transfer in riboflavin binding protein under the spatial confinement of nanoscopic reverse micelles, *J. Mol. Recognit.* **26**, (2013), 59.

[8] G. Cosa, K.-S. Focsaneanu, J. R. N. McLean, J. P. McNamee and J. C. Scaiano, Photophysical properties of fluorescent DNA dyes bound to single and double stranded DNA in aqueous buffered solution, *Photochem. Photobiol.* **73**, (2001), 585.

[9] A. Maiti and S. Roy, Switching DNA-binding specificity by unnatural amino acid substitution, *Nucleic Acids Res.* **33**, (2005), 5896.

[10] S. Choudhury, S. Batabyal, T. Mondol, D. Sao, P. Lemmens and S. K. Pal, Ultrafast dynamics of solvation and charge transfer in a DNA-based biomaterial, *Chem. Asian J.* **9**, (2014), 1395.

Chapter 4

Spectroscopic studies on ultrafast structural fluctuation of DNA-like biomimetic systems in molecular recognition

4.1. Introduction: Exchange of dynamical information between biological macromolecules and water molecules in their vicinity (hydration water) is found to be key for the biological function of water as the "matrix of life" [1-4]. The ubiquitous dynamical role of hydration water in various biological processes including charge transfer [5-7], productive enzyme substrate complex formation [8-9] and protein folding [10-11] is well documented in the early and recent literature. Master role of water molecules at surface [12] and interior [13] of biologically relevant macromolecules in the control of macromolecular dynamics has also been proposed. Whereas the influence of hydration water on the dynamics and function of several biologically relevant macromolecules is evidenced [14], and believed to be slaved to those of the solvent, yet to date, how dynamical coupling between the hydration water and biologically relevant macromolecules occurs remain unclear [15-18]. This is because of experimental difficulties in directly accessing hydration water dynamics [15, 19]. The usefulness of femtosecond resolved electronic spectroscopy in the exploration of the dynamics of hydration in various biological macromolecules is evidenced and reviewed [14, 20].

In the present work we have used two anionic micelles sodium dodecyl sulfate (SDS; $C_{12}H_{25}SO_4Na$) and sodium dodecyl benzene sulfonate (SDBS; $C_{12}H_{25}C_6H_4SO_3Na$) as model macromolecules. SDBS monomer has the same alkyl moiety as SDS with an extra phenyl ring linked to a sulfonate group. Although SDBS and SDS the micelles are very similar from structural point of view, their dynamical behaviour differs significantly. Dynamic Light Scattering (DLS) studies confirm structural integrity of the micelles in our experimental

condition. Recent molecular dynamics [21] studies clearly show that the dynamics of SDBS micelles are more restricted compared to SDS micelles. The structure factor indicates that the alkyl chains are more flexible in SDS compared with SDBS [22]. The restricted structural flexibility of the SDBS micelles is believed to be due to the π-stacking of two benzene moieties of two adjacent surfactants [23], though other possibilities including increase in the molar mass of SDBS cannot be completely ruled out. Results of our QENS study reveal restricted internal motion in the case of SDBS micelles compared to that of the SDS micelles.

We have employed temperature dependent polarization gated fluorescence anisotropy of a well know fluorescence probe coumarin 500 (C500) [24] in the micelles revealing microviscosity of the immediate probe environments and associated energetics. The strategy of investigating water dynamics in similar micellar systems using time resolved dynamics stokes shift is well documented in the literature [25]. Femtosecond resolved stokes shifts of a well known solvation probe C500 in the micelles have been followed for the investigation of hydration dynamics at the micellar surface. A coupling of the structural flexibility of the micelles with their dynamics of hydration is evident from our studies. We have also employed femtosecond resolved Förster resonance energy transfer (FRET) for the investigation of nonspecific binding of a cationic dye ethidium bromide (EtBr) salt to the micellar surface. A strong spectral overlap of the emission of C500 with the absorption spectrum of EtBr reveals the possibility of energy transfer from C500 (donor) to the acceptor EtBr through dipole-dipole coupling [26]. The distribution of the donor-acceptor distances in the micelles clearly reveals a correlation of the structural flexibility of the micelles in their molecular recognition by a small organic ligand (EtBr). Overall, our present study is an attempt to explore the coupling of structural flexibility with the dynamics of hydration of nanoscopic micellar systems using femtosecond to picosecond resolved electronic spectroscopy.

4.2. Results and discussion:

4.2.1. Direct observation of coupling between structural fluctuation and ultrafast hydration dynamics of fluorescent probes in anionic micelles: Figure 4.1a shows steady state absorption and emission spectra of the probe (C500) in solvents of different degrees of polarity. The emission peak in

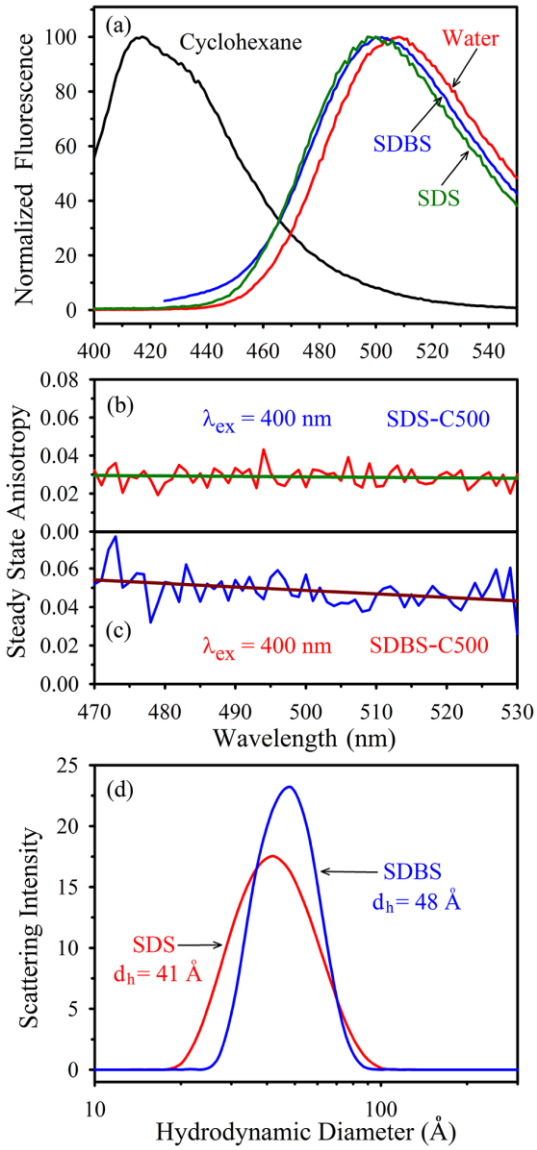

Figure 4.1. *(a) Steady state emission spectra of fluorescence probe C500 in various solvent and in SDS and SDBS micelles. Steady state anisotropy of the probe in SDS and SDBS micelles are shown in (b) and (c), respectively. (d) Typical DLS spectra of both micelles showing their corresponding hydrodynamic diameter.*

cyclohexane at 417 nm moves to 510 nm in water. The absorption spectra of the probe in the two solvents do not show much change (data not shown) revealing significantly larger transition dipole moment upon excitation [27]. The emission maxima of the probe C500 in the SDS and SDBS micelles are found to be 505 nm and 508 nm respectively indicating the location of the probe at the micellar interface. Similar spectral width of the emission profiles of the probe C500 in the micellar media and bulk water, rules out significant heterogeneity in the location of the probe in the micelles. A slight but reproducible shift of emission spectrum of the probe C500 in SDBS compared to that in SDS is indicative of more polar environment in the vicinity of the probe in SDBS micelles. Relatively higher steady state fluorescence anisotropy value of the probe C500 in SDBS micelles (~0.05) compared to that in SDS micelles (~0.03) is evident from Figure 4.1b, which suggests a more restricted environment of the probe in the former medium. The persistency of the steady state anisotropy values in a range of emission wavelengths (470-530 nm) in the micelles is also indicative of less heterogeneity in the probe's micro-environments in the micelles. Dynamics light scattering (DLS) experiments on the micelles (Figure 4.1c) reveals similar and almost mono-dispersed distribution of the SDS and SDBS micelles with hydrodynamic diameters of 4.1 nm and 4.8 nm, respectively, consistent with earlier reported values [28-29].

Neutron scattering data from a micellar system have dominant contribution from hydrogen atoms present due to their high incoherent cross-section compared to other elements. The measured scattering intensity can therefore be written as [30]

$$I = \frac{\partial^2 \sigma}{\partial \Omega \partial \omega} \propto \frac{k_i}{k_f} \sigma_{inc} S_{inc}(Q, \omega) \tag{4.1}$$

where $S_{inc}(Q,\omega)$ is the dynamical scattering function describing single particle motion. Here, Q (=k_i-k_f), is the wave vector transfer, k_i and k_f are the incident and scattered neutron wave vectors, respectively and $\hbar\omega$ is the energy transfer. To minimize the scattering contribution from the solvent, deuterated water was used. In order to obtain the contribution from the micelles alone, data from the

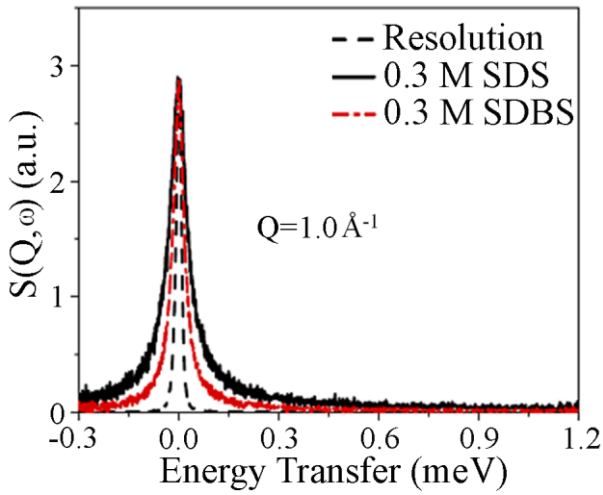

Figure 4.2. *Typical QENS spectra for 0.3 M SDS and SDBS micellar solution at Q=1.0 Å^{-1}. The instrument resolution is shown by dashed line. All the spectra are normalized to peak intensities.*

pure solvent were subtracted from that of the micellar solution. Figure 4.2 shows QENS spectra measured for SDS and SDBS micelles (contribution of D_2O subtracted) at Q =1.0 Å^{-1}. Observed quasielastic broadening for SDS micelles is found to be significantly larger in SDS compared to SDBS suggesting slower dynamics in SDBS compared to SDS micelles.

Varieties of motions are plausible in a micellar system, such as global motion (which includes translational and rotation of the micelles), internal motions of different CH_2 units and fast torsional motion within the micelles [31]. The dynamical processes are expected to contribute within the time scales of the neutron scattering technique used (10^{-9} - 10^{-12} sec). Therefore, QENS spectra shown in Figure 4.2 consist of all these motions and to find out the contribution from different dynamical processes, we need to model the total dynamical scattering function. Assuming that these dynamical processes are independent of each other, the scattering law, $S_{micelles}(Q,\omega)$ can be expressed as convolution of the global and internal motions of the micelles [22]. It may be noted that "global" motions of the micelles involve both translational and rotational motion of the whole micelles. It has been shown that the total scattering law comprising both translational and rotational motion can be

described by a single Lorentzian function for a dispersed spherical nanometer sized macromolecules [32]. Therefore, the scattering law for global motion can be written as [30]

$$S_G(Q,\omega) = L_G(\Gamma_G,\omega) = \frac{1}{\pi}\frac{\Gamma_G}{\Gamma_G^2+\omega^2} \tag{4.2}$$

Here Γ_G is the half width at half maxima (HWHM) of the Lorentzian function corresponding to global motion and is proportional to the global diffusivity, D_G, of the micelles. Perez et al. [32] have also showed numerically that the D_G, obtained with single Lorentzian description, is higher compared to the self diffusion coefficient, D_s.

Apart from the global motion the data also has contribution from internal motion of the surfactant monomers. This scattering law consists of an elastic component and a quasielastic component. The scattering law for the internal motion, $S_{in}(Q, \omega)$ can be expressed as [22]

$$S_{\text{in}}(Q,\omega) = A(Q)\,\delta(\omega) + \big(1-A(Q)\big)L_{in}(\Gamma_{\text{in}},\omega) \tag{4.3}$$

The quasielastic component is approximated as a single Lorentzian function, $L_{in}(\Gamma_{\text{in}}, \omega)$ with HWHM, Γ_{in}. Elastic Incoherent Structure Factor (EISF), defined as the fraction of the elastic scattering out of total scattering is useful to understand the geometry of a dynamical motion [22] and can be identified as $A(Q)$ in equation (4.3). As mentioned above the scattering law for micelles is the convolution product of the global and internal motions which can be written as [22],

$$S_{micelles}(Q,\omega) = \Big[A(Q)\,L_G(\Gamma_G,\omega) + \big(1-A(Q)\big)L_{tot}(\Gamma_{tot},\omega)\Big] \tag{4.4}$$

Here, L_{tot} (Γ_{tot},ω) represents the total contribution from global and internal motions and $\Gamma_{tot}=\Gamma_G + \Gamma_{\text{in}}$. The program DAVE [33] developed at the NIST Center for Neutron Research is used to analyse the QENS data. The parameters A(Q), Γ_G and Γ_{tot} are obtained by least squares fit with the measured data after

convoluting the above scattering law (equation 4.4) with the instrumental resolution function. It is found that the model function (equation 4.4) could fit

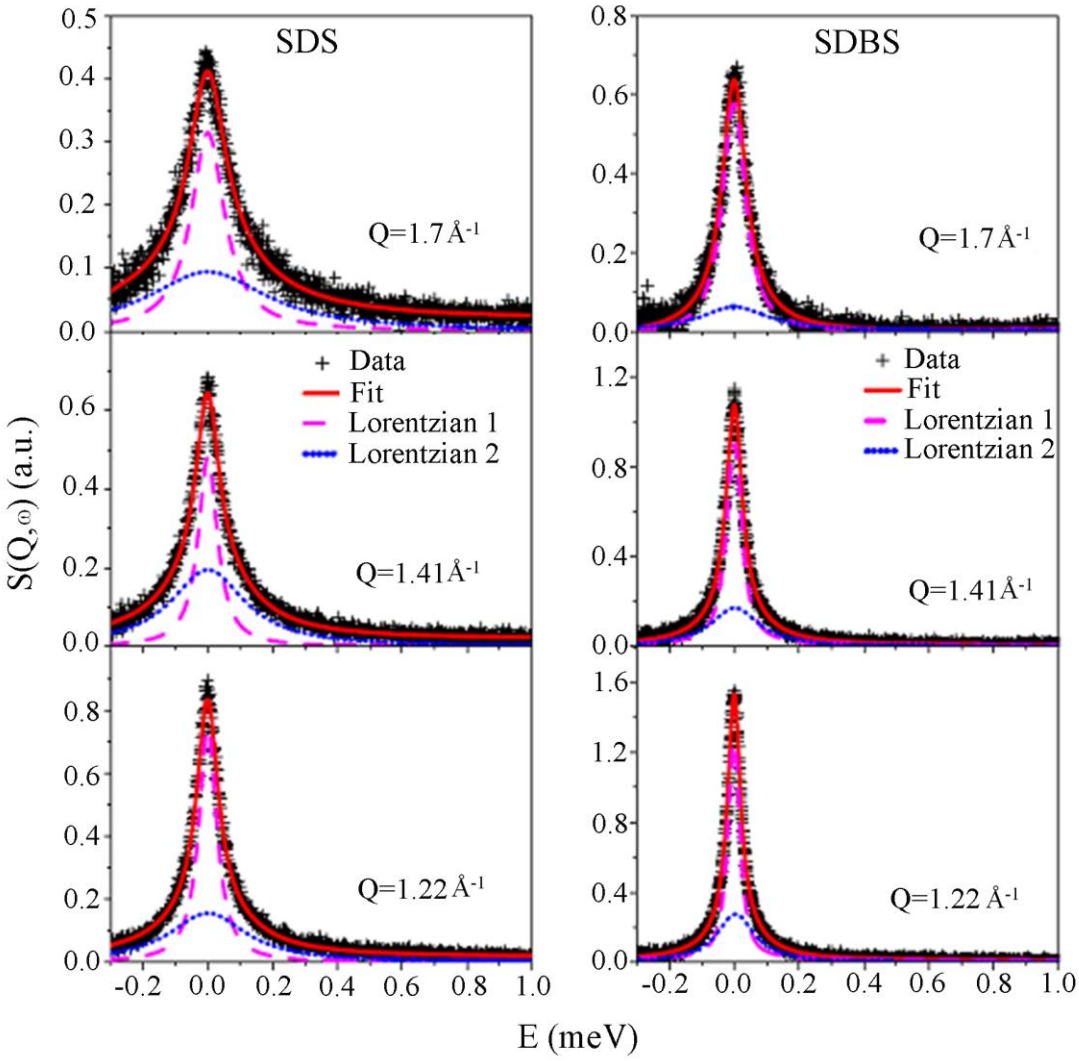

Figure 4.3. *Typical fitted S(Q, ω) for 0.3 M SDS and SDBS micelles at different Q values, assuming the scattering function given in equation 4.4.*

the observed QENS spectra very well at all the Q values. Typical fitted spectra for SDS and SDBS micelles are shown in Figure 4.3 at some typical Q values. The variation of the HWHM, Γ_G, of the 1st Lorentzian for SDBS is shown in Figure 4.4a along with that of SDS micelles. Larger Γ_G for SDS suggests that the global motion is faster in SDS than SDBS micelles. It is clear that the global diffusion follows Fick's law ($\Gamma_G = D_G Q^2$, D_G being the global diffusion coefficient) for both the micellar systems as shown by solid lines in Figure 4.4a.

D_G =1.9 (± 0.30 × 10^{-6} cm^2/sec is obtained for SDBS, whereas for SDS micelles, it is found to be 3.4 (± 0.4) ×10^{-6} cm^2/sec [22]. Self diffusion constant for pure translational motion of the micelles, D_s, can be calculated using Stokes-Einstein relation, $D_s=k_BT/6\pi\eta R$. Here R, η and T are the hydrodynamic radius of micelles, viscosity of D_2O and the temperature of the solution, respectively. For SDS micelles having radius, R=20.5 Å, η_{D2O}=0.9 cP [34] at T= 300 K, the value of

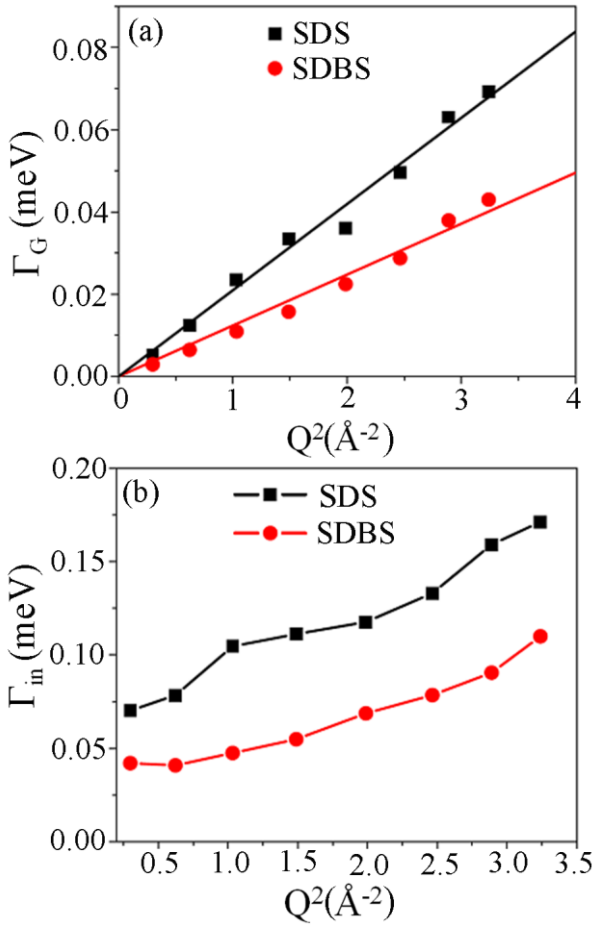

Figure 4.4. *(a) Variation of half width at half maxima (HWHM), Γ_G, corresponds to global motion, with Q^2 for SDBS and SDS micelles. (b) Variation of the HWHM, Γ_{in}, which correspond to the internal motion of the monomer for SDS and SDBS micelles with Q^2.*

D_s obtained as 1.2 × 10^{-6} cm^2/sec which is between the value reported by Hayter and Penfold [35] and the present work. Although several studies including MD simulation studies [21] on SDS and SDBS estimated the similar

sizes of SDS and SDBS micelles, global diffusivities obtained from QENS study are found to be significantly different in SDS and SDBS micelles.

Γ_{in} corresponding to internal motion is obtained by subtracting Γ_G (as already known from the first Lorentzian in equation 4.4) from Γ_{tot}. The values of Γ_{in} obtained for SDS and SDBS are shown in Figure 4.4b. It is evident from the figure that the internal motion is faster in SDS than SDBS. More compact or denser hydrophobic core of the SDBS micelles compared to SDS micelles leads to the constriction in the internal motion in SDBS micelles. As stated earlier, the π–stacking between the aromatic rings of the adjacent surfactants is one of the possibilities for the compactness. In effect, more "viscous" (dense) medium in SDBS micelles (because of increase in packing density), provide the basis for constrained dynamics of mobile protons in SDBS than in SDS.

The obtained A(Q), which represents the EISF for the internal motion for both the micelles is shown in Figure 4.5. It is evident that the EISF for SDBS micelles are higher than that of SDS micelles indicating that alkyl chains in SDS

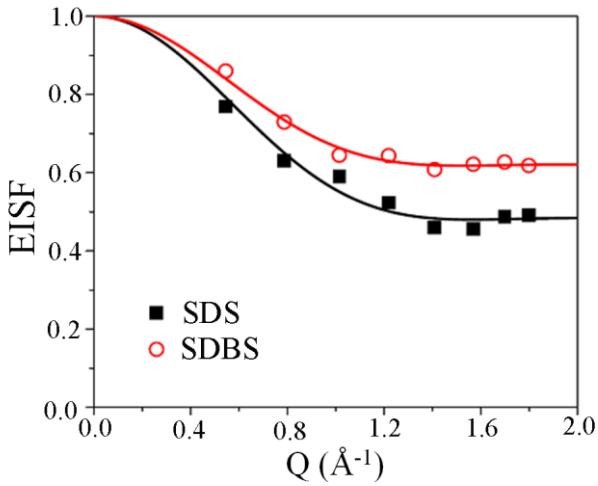

Figure 4.5. *Variation of EISF for SDS and SDBS micellar solution with Q. Solid lines are fitted curves assuming equation 4.5.*

are more dynamic than in SDBS micelles. The main feature of the internal motions in a structured system is the confinement of the species within a certain volume of space. The exact shape of this volume is not well-known but in a first approximation is assumed as spherical. Volino and Dianoux [36] had

derived the scattering law for diffusion of particles within a sphere with an impermeable surface. It may be noted that all the hydrogen atoms might not be dynamically active at a given temperature, considering the same, a factor P_x is introduced, representing fraction of hydrogen atoms which are dynamically inactive at a given temperature. This methodology is widely used in a number of systems including vesicles [37], proteins [32], haemoglobin [38] etc. to describe the hydrogen mobility in long chain systems. The modified EISF can then be written as

$$EISF = P_x + (1 - P_x)\left[\frac{3j_1(Qa)}{(Qa)}\right]^2 \tag{4.5}$$

Here, $j_1(Qa)$ is the spherical Bessel function of the first order and a is the radius of the confining volume. Solid lines in Figure 4.5 shows the least squares fit of the experimentally obtained EISF using the above equation. It is found that in case of SDS micelles, about 48 (± 2) % of the hydrogen atoms are dynamically inactive, while in case of SDBS micelles it is about 62 (± 2) %. The radius of confinement for both SDS and SDBS is found to be 2.9 (± 0.2) Å. This suggests that the spatial domain of dynamics of the hydrogen atoms is ~ 6 Å in both the micellar systems.

In order to investigate the physical movement of the probe C500 in the micelles during the course of hydration relaxation around the probe, we have measured the fluorescence anisotropy of the probe in the micelles as shown in Figure 4.6a and 4.6b. The fluorescence anisotropy decays depict rotational relaxation time constants of C500 in SDS and SDBS micelles are 280 ps and 340 ps, respectively. The observed time constants are much slower and are consistent with those measured from picoseconds resolved time correlated single photon counting (TCSPC) technique. In order to calculate π-stacking energy in case of SDBS micelles we have measured temperature dependent anisotropy of both the micelles with TCSPC. Figure 4.6c and 4.6d show the anisotropy decay of the probe in SDS and SDBS micelles at 293K temperature, respectively. The corresponding parallel and perpendicular polarisation gated

decays are shown in the respective insets. Anisotropy at 278K and 343K of both the SDS and SDBS micelles are shown in the inset of

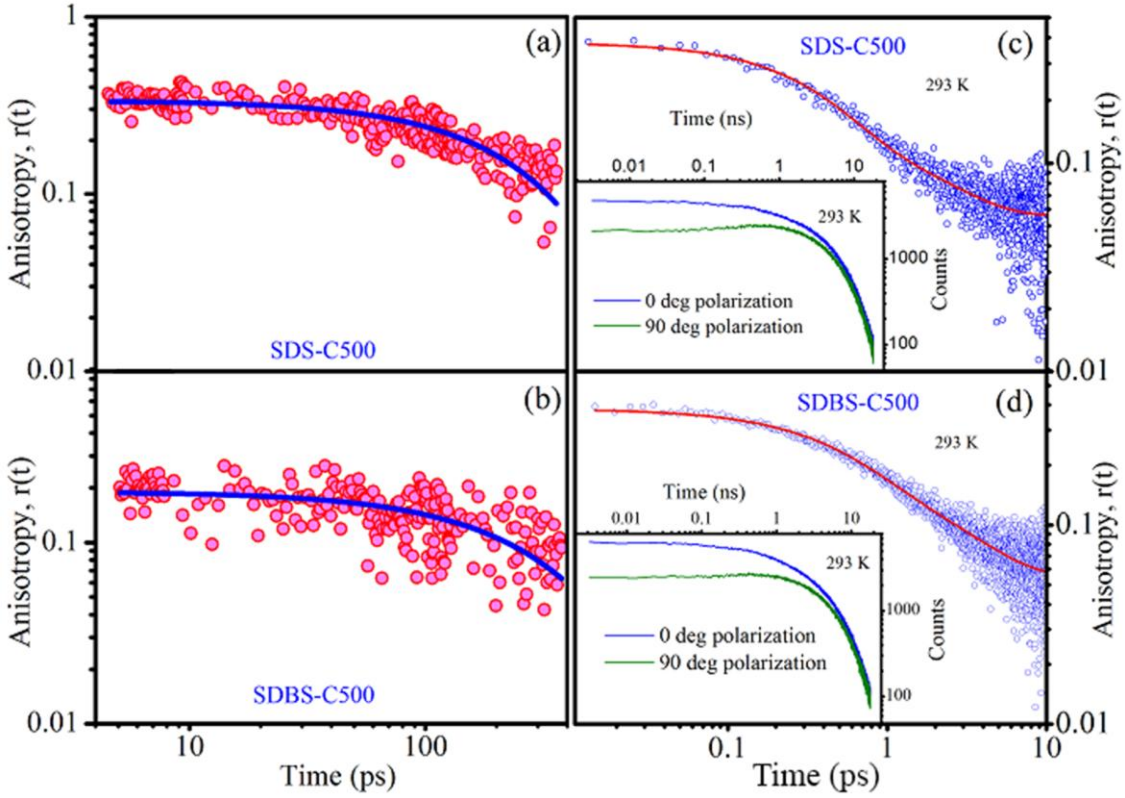

Figure 4.6. *Femtosecond fluorescence anisotropy decays of C500 in SDS (a) and SDBS (b) are shown in log-log plot. The room temperature picoseconds resolved anisotropy of C500 in SDS (c) and SDBS (d) are also shown. Insert shows parallel and perpendicular polarization gated decay for the corresponding systems.*

Figure 4.7a and 4.7b, respectively. As observed from the Figure 4.7a and 4.7b rotational time constant (τ_{rot}) becomes faster upon increasing temperature for both systems. We have estimated microviscosities at different temperature for the corresponding systems, given the hydrodynamics diameter of the probe is 7.6 Å as reported earlier [39] and plotted with 1/T (K^{-1}) as shown in Figure 4.7c. The plots are distinct and out of the experimental uncertainty (5%). Linear fit of both plots provide activation energy 22.8 (±1.1) KJ/mole and 24.1 (±1.2) KJ/mole for SDS and SDBS, respectively, using the equation $\eta = \eta_0 \exp\left(\frac{E_\eta}{RT}\right)$,

where E_η is the energy barrier for viscous flow [40]. The relatively higher

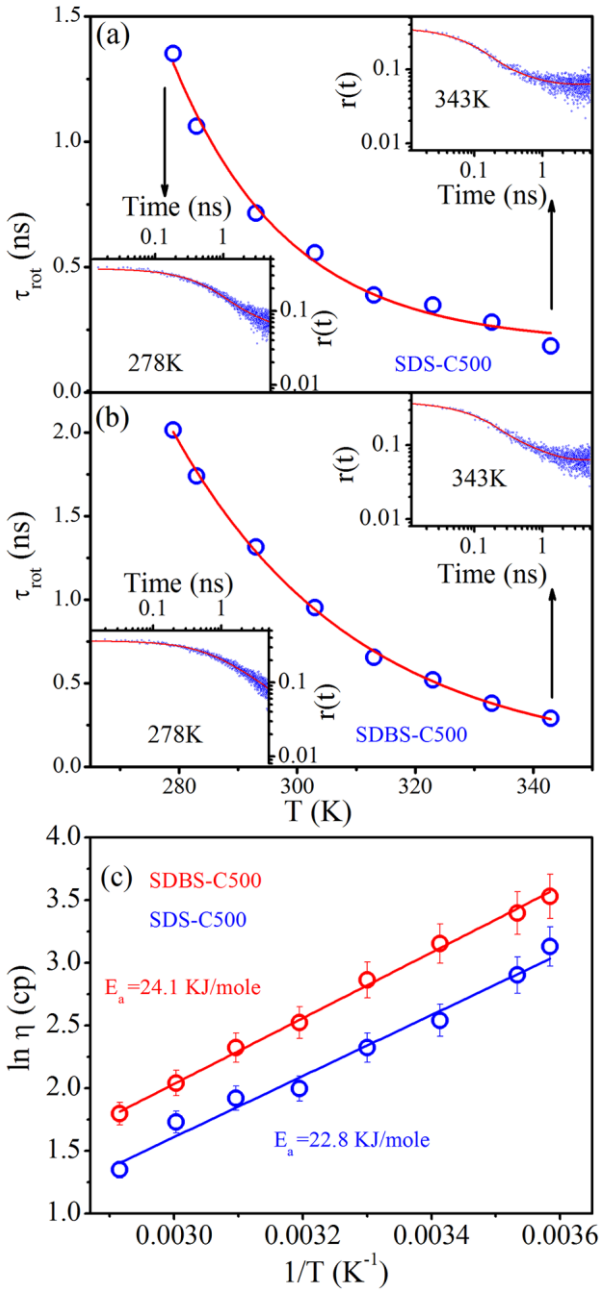

Figure 4.7. *Plot of rotational time constant (τ_{rot}) against temperature for SDS (a) and SDBS (b) micelles. Inserts are showing anisotropy at initial and final temperature for the respective systems. (c) Arrhenius plots of microviscosity for SDS and SDBS micelles are shown (with 5% error bar).*

activation energy in the SDBS micelles compared to that in SDS micelles is probably the manifestation of less flexibility of the alkyl chains due to π-stacking (1.3 KJ/mole) in the former medium [41].

To correlate the fluctuations with hydration dynamics of the micelles, we have performed femtosecond solvation dynamics of both the micelles. The femtosecond resolved fluorescence transients of C500 in SDS and SDBS micelles at three characteristic wavelengths (440 nm, 480 nm and 560 nm) across the emission wavelengths are shown in Figure 4.8a and 4.8b,

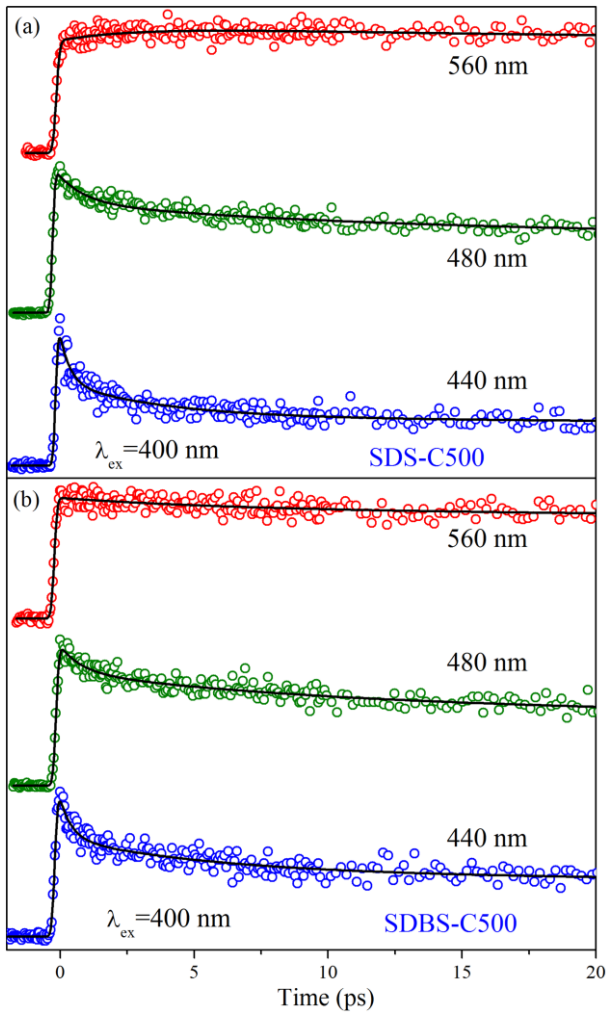

Figure 4.8. *Femtosecond resolved fluorescence transients of C500 in three representative detection wavelengths (440 nm, 480 nm and 560 nm) for SDS (a) and SDBS (b) micelles are shown. The circles are experimental data, and the solid lines are best multi-exponential fit.*

respectively. An ultrafast decay component in the blue end is eventually converted in to a rise component of similar time constant in the red end for both the micelles. The observation is consistent with the solvation of the probe C500 in the media [24]. The constructed time dependent stokes shift (TDSS) of

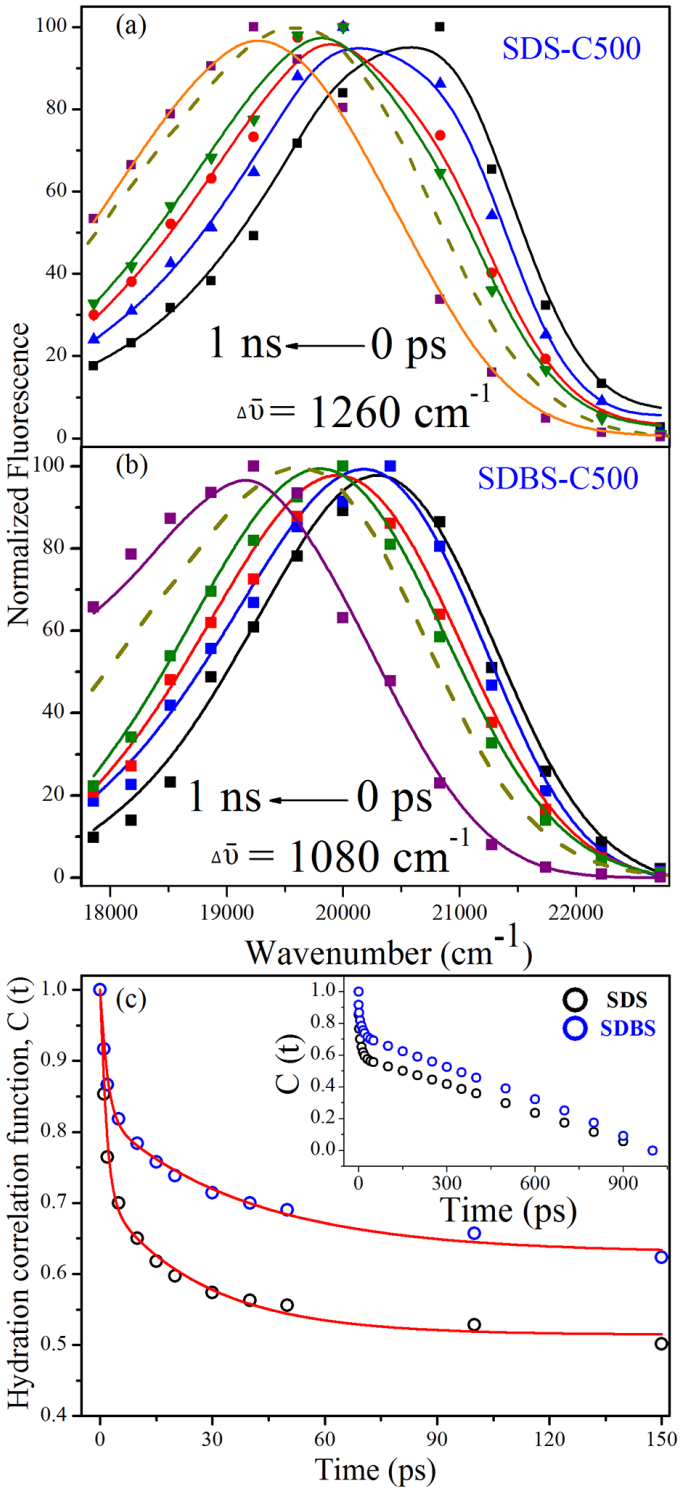

Figure 4.9. *Time dependent emission spectra (TRES) of fluorescent probe C500 in SDS (a) and SDBS (b) micelles are shown. The dotted lines are the steady state fluorescence spectra of the corresponding systems* $\Delta\bar{\upsilon}$ *is the spectral shift for the micellar system in 1 ns time window. (c) Hydration correlation functions for the SDS and SDBS are shown up to 150 ps. The solid lines are the best bi-exponential fit to C(t). Insert shows the correlation function in long time range.*

the C500 emission at different time are shown in Figure 4.9a and 4.9b, with a spectral shift of 1260 cm^{-1} and 1080 cm^{-1} for SDS and SDBS micelles respectively, in an 1 ns time window. The hydration correlation functions [C(t)] for the SDS and SDBS micelles upto 150 ps as shown in Figure 4.9c can be fitted with bi-exponential decay functions. C(t) upto 1 ns for SDS and SDBS as shown in inset are non-exponential due to contribution of fluctuation of micellar head group. Up to 150 ps for SDS micelles the decay time constants are 1.48 ps (59%) and 27 ps (41%) and for SDBS micelles the obtained time constants are 1.75 ps (48%) and 39 ps (52%). Our result is consisting with earlier femtosecond resolved study [42] on the dynamics of hydration in TX-100 micelles reported hydration time constants of 2.9 ps (45%) and 58 ps (55%) [43]. It has to be noted that the correlation functions for both the micelles show non-exponential behaviour after 150 ps up to a time window of 1 ns. The non exponential behaviour of biologically relevant macromolecules including DNA has been well documented at a time window from femtosecond to microsecond [44]. Earlier it has been concluded that the faster response in the C(t) is the consequence of the movement of counter ions away from their average position through the electric field at the probe. On the other hand relatively slower components are from various kinds of motions of the host system itself [44-45]. Overall, a variety of dynamical events are likely to be included in the solvation response and the relaxation dynamics must be treated as a collective response of the whole system. The faster dynamics of hydration in SDS than that in SDBS micelles is clearly evident from the study. The structural flexibility of the SDS and SDBS micelles is also evident from polarization gated fluorescence anisotropy studies (Figure 4.6), revealing higher rigidity in the latter case. Thus, our observation of faster hydration dynamics in structurally flexible SDS micelles may find a correlation between the dynamics of hydration water and internal motion of the micelles.

In Figure 4.10 we have shown the molecular complexation of a cationic dye EtBr with the anionic micelles SDS and SDBS using FRET techniques [46]. Figure 4.10a shows the overlap (overlap integral value of 3.37×10^{14} M^{-1} cm^{-1}

nm⁴) between the emission spectrum of C500 (donor) and the absorption spectrum of EtBr (acceptor) in the SDS micelles. The overlap for the SDBS

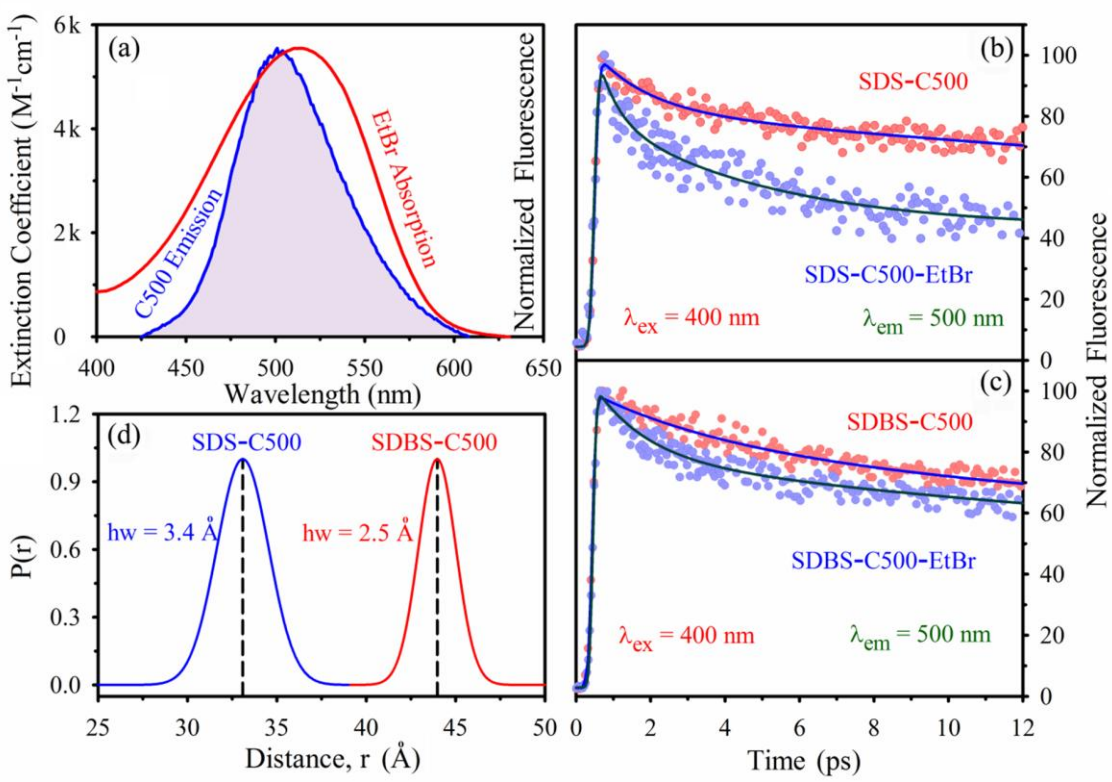

Figure 4.10. *Spectral overlap of C500 emission and EtBr absorption in SDS micelles is shown in (a). The (b) and (c) show fluorescence transients of C500 in the micelles at 500 nm, before and after complexation with cationic dye EtBr. The (d) shows distribution of donor-acceptor distances in the two micelles.*

micelles remains almost unchanged (overlap integral value of 3.1 × 10^{14} M^{-1} cm^{-1} nm^4; data not shown in the figure). Femtosecond resolved fluorescence transients of C500 at 500 nm in the micelles before and after the complexation with the acceptor EtBr is shown in the Figures 4.10b and 4.10c. A significant faster component of 410 fs (32%) in the case of SDS micelles upon complexation with EtBr is clearly evident. In case of SDBS micelles the faster component is found to be 475 fs (10%). The estimated Förster distance (R_0) values of the donor-acceptor pair for the SDS and SDBS micelles are 34.6 Å and 34.1 Å, respectively. The calculated donor-acceptor distances in the two micelles are found to be 33.6 Å and 45.0 Å, respectively. The higher donor-acceptor distance

in the case of SDBS compared to that in SDS micelles may not be due to the distant location of the donor C500 from the micellar surface, as the fluorescence spectrum of the donor probe shows similar characteristics revealing insignificant change in the polarity around the probe. In the case of deep insertion of the probe from the surface, lower polarity around the probe is unavoidable. Thus, the observation can be rationalized in terms of different position of the acceptor EtBr at the surface of the SDBS micelles compared to that of the SDS. The intrinsic micellar fluctuation, as evidenced in microviscosity (described above) is also substantiated in our FRET studies on the molecular recognition of EtBr by the two micellar systems. The distribution of donor-acceptor distances in the micelles is also shown in Figure 4.10d revealing relatively less broadening in the case of SDBS (half width = 2.5 Å) compared to that in SDS (half width = 3.4 Å). The observation of high width in the donor acceptor distance distribution in case of SDS micelles compared to SDBS micelles can be rationalised in terms of dynamical fluctuations of the host micelles [47-48]. The calculated half width values, revealing heterogeneity or fluctuations in the observed distances between the donor and the acceptor, thus correlated with the dynamics of hydration. The overall picture which emerges from our studies is depicted in Figure 4.11.

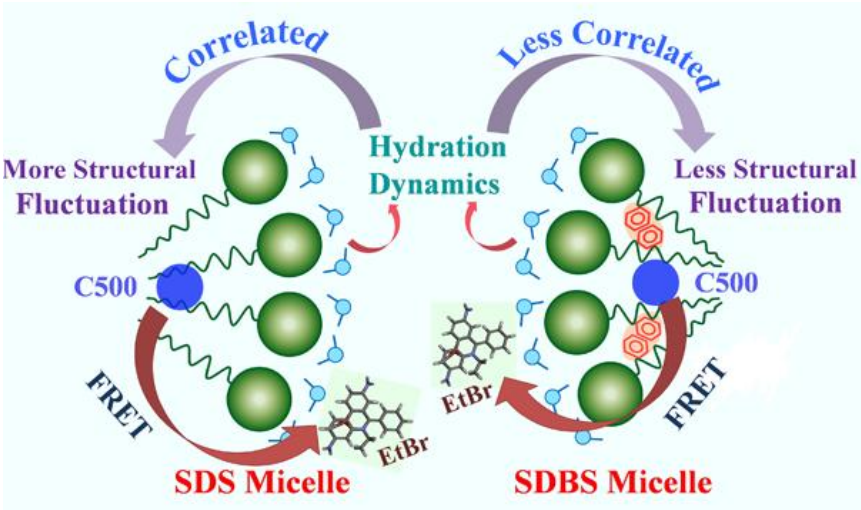

Figure 4.11. *Schematic representation of the coupling between intrinsic fluctuations and hydration dynamics of the SDS and SDBS micelles is shown.*

4.3. Conclusion: Here we have employed femtosecond resolved electronic spectroscopy for the exploration of hydration dynamics of a well known solvation probe C500 in two structurally similar anionic micelles SDS and SDBS. Dynamic light scattering (DLS) reveals the structural integrity of the micelles. We have used polarization gated fluorescence anisotropy for the estimation of structural flexibility of the micelles. We have found SDBS is more compact than SDS. The extracted dynamics of hydration in the micelles reveal slower water motion at the less flexible SDBS micelle compared to that in SDS micelle. The comparison of the dynamics of hydration across two micelles of different compactness reveals a gradient of coupling between hydration water and internal micellar motions, which is stronger in relatively flexible SDS and weaker in compact SDBS micelles. Slower internal motion in SDBS compared to SDS micelles is also confirmed from QENS studies. We have also used femtosecond resolved FRET in order to investigate the molecular recognition of the micelles by a small cationic ligand EtBr. Relatively broad distribution of EtBr at the micellar surfaces with respect to the probe C500 in the case of SDS micelles compared to that in SDBS micelles is evident. The observation is correlated with the internal flexibility of the micelles. Thus, our present study can be considered as an exploration of a coherent picture of structure, dynamics and function of molecular recognition at physiologically relevant important nanoscopic micellar environments [49].

References

[1] S. K. Pal and A. H. Zewail, Dynamics of water in biological recognition, *Chem. Rev.* **104**, (2004), 2099.

[2] P. Ball, Water as an active constituent in cell biology, *Chem. rev.* **108**, (2008), 74.

[3] L. Wang, X. Yu, P. Hu, S. Broyde and Y. Zhang, A water-mediated and substrate-assisted catalytic mechanism for sulfolobus solfataricus DNA polymerase IV, *J. Am. Chem. Soc.* **129**, (2007), 4731.

[4] C. Zong, G. A. Papoian, J. Ulander and P. G. Wolynes, Role of topology, nonadditivity, and water-mediated interactions in predicting the structures of α/β proteins, *J. Am. Chem. Soc.* **128**, (2006), 5168.

[5] K. Pechstedt, T. Whittle, J. Baumberg and T. Melvin, Photoluminescence of colloidal CdSe/ZnS quantum dots: The critical effect of water molecules, *J. Phys. Chem. C* **114**, (2010), 12069.

[6] A. Migliore, S. Corni, R. Di Felice and E. Molinari, Water-mediated electron transfer between protein redox centers, *J. Phys. Chem. B* **111**, (2007), 3774.

[7] S. Choudhury, S. Batabyal, T. Mondol, D. Sao, P. Lemmens and S. K. Pal, Ultrafast dynamics of solvation and charge transfer in a DNA-based biomaterial, *Chem. Asian J.* **9**, (2014), 1395.

[8] J. A. Rupley and G. Careri, Protein hydration and function, *Adv. Protein Chem.* **41**, (1991), 37.

[9] J. Kornblatt and M. Kornblatt, Water as it applies to the function of enzymes, *Int. Rev. Cytol.* **215**, (2002), 49.

[10] Y. Levy and J. N. Onuchic, Water mediation in protein folding and molecular recognition, *Annu. Rev. Biophys. Biomol. Struct.* **35**, (2006), 389.

[11] S. J. Kim, B. Born, M. Havenith and M. Gruebele, Real-time detection of protein–water dynamics upon protein folding by terahertz absorption spectroscopy, *Angew. Chem., Int. Ed.* **47**, (2008), 6486.

[12] F. Zhou and K. Schulten, Molecular dynamics study of a membrane-water interface, *J. Phys. Chem.* **99**, (1995), 2194.

[13] V. Helms, Protein dynamics tightly connected to the dynamics of surrounding and internal water molecules, *ChemPhysChem* **8**, (2007), 23.

[14] K. Bhattacharyya, Nature of biological water: A femtosecond study, *Chem. Comm.*, (2008), 2848.

[15] F.-X. Gallat, A. Laganowsky, K. Wood, F. Gabel, L. Van Eijck, J. Wuttke, M. Moulin, M. Härtlein, D. Eisenberg and J.-P. Colletier, Dynamical coupling of intrinsically disordered proteins and their hydration water: Comparison with folded soluble and membrane proteins, *Biophys. J.* **103**, (2012), 129.

[16] J. Qvist, G. Ortega, X. Tadeo, O. Millet and B. Halle, Hydration dynamics of a halophilic protein in folded and unfolded states, *J. Phys. Chem. B* **116**, (2012), 3436.

[17] V. Conti Nibali, G. D Angelo, A. Paciaroni, D. J. Tobias and M. Tarek, On the coupling between the collective dynamics of proteins and their hydration water, *J. Phys. Chem. Lett.* **5**, (2014), 1181.

[18] M. Heyden and D. J. Tobias, Spatial dependence of protein-water collective hydrogen-bond dynamics, *Phys. Rev. Lett.* **111**, (2013), 218101.

[19] M. Tarek and D. J. Tobias, Single-particle and collective dynamics of protein hydration water: A molecular dynamics study, *Phys. Rev. Lett.* **89**, (2002), 275501.

[20] S. K. Pal, L. Zhao and A. H. Zewail, Water at DNA surfaces: Ultrafast dynamics in minor groove recognition, *Proc. Natl. Acad. Sci. USA* **100**, (2003), 8113.

[21] F. Palazzesi, M. Calvaresi and F. Zerbetto, A molecular dynamics investigation of structure and dynamics of SDS and SDBS micelles, *Soft Matter* **7**, (2011), 9148.

[22] V. Sharma, S. Mitra, M. Johnson and R. Mukhopadhyay, Dynamics in anionic micelles: Effect of phenyl ring, *J. Phys. Chem. B* **117**, (2013), 6250.

[23] M. Islam, E. Rojas, D. Bergey, A. Johnson and A. Yodh, High weight fraction surfactant solubilization of single-wall carbon nanotubes in water, *Nano Lett.* **3**, (2003), 269.

[24] S. Rakshit, R. Saha, P. K. Verma and S. K. Pal, Role of solvation dynamics in excited state proton transfer of 1-naphthol in nanoscopic water clusters formed in a hydrophobic solvent, *Photochem. Photobiol.* **88**, (2012), 851.

[25] N. Nandi, K. Bhattacharyya and B. Bagchi, Dielectric relaxation and solvation dynamics of water in complex chemical and biological systems, *Chem. Rev.* **100**, (2000), 2013.

[26] P. Majumder, R. Sarkar, A. K. Shaw, A. Chakraborty and S. K. Pal, Ultrafast dynamics in a nanocage of enzymes: Solvation and fluorescence resonance energy transfer in reverse micelles, *J. Colloid Interface Sci.* **290**, (2005), 462.

[27] J. Lewis and M. Maroncelli, On the (uninteresting) dependence of the absorption and emission transition moments of coumarin 153 on solvent, *Chem. Phys. Lett.* **282**, (1998), 197.

[28] C. D. Bruce, M. L. Berkowitz, L. Perera and M. D. Forbes, Molecular dynamics simulation of sodium dodecyl sulfate micelle in water: Micellar structural characteristics and counterion distribution, *J. Phys. Chem. B* **106**, (2002), 3788.

[29] D. C. Cheng and E. Gulari, Micellization and intermicellar interactions in aqueous sodium dodecyl benzene sulfonate solutions, *J. Colloid Interface Sci.* **90**, (1982), 410.

[30] M. Bee, *Quasielastic Neutron Scattering*, **1988,** Bristol, UK.

[31] V. K. Sharma, S. Mitra, V. Garcia Sakai, P. A. Hassan, J. Peter Embs and R. Mukhopadhyay, The dynamical landscape in CTAB micelles, *Soft Matter* **8**, (2012), 7151.

[32] J. Pérez, J.-M. Zanotti and D. Durand, Evolution of the internal dynamics of two globular proteins from dry powder to solution, *Biophys. J.* **77**, (1999), 454.

[33] R. T. Azuah, L. R. Kneller, Y. Qiu, P. L. Tregenna-Piggott, C. M. Brown, J. R. Copley and R. M. Dimeo, Dave: A comprehensive software suite for the reduction, visualization, and analysis of low energy neutron spectroscopic data, *J. Res. Natl. Inst. Stand. Technol.* **114**, (2009), 341.

[34] V. Castelletto, I. W. Hamley, Z. Yang and W. Haeussler, Neutron spin-echo investigation of the dynamics of block copolymer micelles, *J. Chem. Phys.* **119**, (2003), 8158.

[35] J. B. Hayter and J. Penfold, *J. Chem. Soc., Faraday Trans. I* **77**, (1981), 1851.

[36] F. Volino and A. Dianoux, Neutron incoherent scattering law for diffusion in a potential of spherical symmetry, *J. Mol. Phys.* **41**, (1980), 271.

[37] Y. Gerelli, V. G. Sakai, J. Ollivier and A. Deriu, Conformational and segmental dynamics in lipid-based vesicles, *Soft Matter* **7**, (2011), 3929.

[38] C. Caronna, F. Natali and A. Cupane, Incoherent elastic and quasi-elastic neutron scattering investigation of hemoglobin dynamics, *Biophys. Chem.* **116**, (2005), 219.

[39] D. Banerjee, P. K. Verma and S. K. Pal, Temperature-dependent femtosecond-resolved hydration dynamics of water in aqueous guanidinium hydrochloride solution, *Photochem. Photobiol. Sci.* **8**, (2009), 1441.

[40] R. K. Mitra, P. K. Verma and S. K. Pal, Exploration of the dynamical evolution and the associated energetics of water nanoclusters formed in a hydrophobic solvent, *J. Phys. Chem. B* **113**, (2009), 4744.

[41] R. G. Huber, M. A. Margreiter, J. E. Fuchs, S. von Grafenstein, C. S. Tautermann, K. R. Liedl and T. Fox, Heteroaromatic ıı-stacking energy landscapes, *J. Chem. Inf. Model.* **54**, (2014), 1371.

[42] S. K. Pal, J. Peon and A. H. Zewail, Biological water at the protein surface: Dynamical solvation probed directly with femtosecond resolution, *Proc. Natl. Acad. Sci. USA* **99**, (2002), 1763.

[43] S. K. Pal, D. Sukul, D. Mandal, S. Sen and K. Bhattacharyya, Solvation dynamics of dcm in micelles, *Chem. Phys. Lett.* **327**, (2000), 91.

[44] D. Andreatta, J. L. Pérez Lustres, S. A. Kovalenko, N. P. Ernsting, C. J. Murphy, R. S. Coleman and M. A. Berg, Power-law solvation dynamics in DNA over six decades in time, *J. Am. Chem. Soc.* **127**, (2005), 7270.

[45] E. B. Brauns, M. L. Madaras, R. S. Coleman, C. J. Murphy and M. A. Berg, Complex local dynamics in DNA on the picosecond and nanosecond time scales, *Phys. Rev. Lett.* **88**, (2002), 158101.

[46] S. K. Pal, D. Mandal and K. Bhattacharyya, Photophysical processes of ethidium bromide in micelles and reverse micelles, *J. Phys. Chem. B* **102**, (1998), 11017.

[47] S. Chaudhuri, S. Batabyal, N. Polley and S. K. Pal, Vitamin B_2 in nanoscopic environments under visible light: Photosensitized antioxidant or phototoxic drug?, *J. Phys. Chem. A* **118**, (2014), 3934.

[48] S. Nag, B. Sarkar, M. Chandrakesan, R. Abhyanakar, D. Bhowmik, M. Kombrabail, S. Dandekar, E. Lerner, E. Haas and S. Maiti, A folding transition underlies the emergence of membrane affinity in amyloid-β, *Phys. Chem. Chem. Phys.* **15**, (2013), 19129.

[49] S. Choudhury, P. K. Mondal, V. Sharma, S. Mitra, V. G. Sakai, R. Mukhopadhyay and S. K. Pal, Direct observation of coupling between structural fluctuation and ultrafast hydration dynamics of fluorescent probes in anionic micelles, *J. Phys. Chem. B* **119**, (2015), 10849.

Chapter 5

Spectroscopic studies on the interfacial dynamics at DNA-surfactant interface

5.1. Introduction: A significant development of DNA-based materials in the field of nano-photonics and optoelectronics has been evident in recent years [1-5]. A class of DNA-based thin film is made of a genomic DNA-cationic surfactant (cetyltrimethyl ammonium chloride: CTMA) complex, which acts as efficient electron-blocking layers (EBL) [6-7] in the development of bio-LED (light emitting diode). Remarkably, as evident from the circular dichroism (CD) spectroscopic studies, DNA retains its physiological B-form in the thin film [8]. To unravel the role of DNA in the thin film for electronics applications, the exploration of the charge transfer (CT) mechanism of DNA in the thin film is unavoidable. In a series of earlier studies, it has been suggested that π–π interaction between base-pair stacking of double stranded DNA could be responsible for the one-dimensional CT along the DNA chain [9]. The CT mechanism in DNA matrix and classification of the matrix in insulators [8], semiconductors [10], conductors [11] or even superconductors [12] invited several debates in the early and recent literature [13]. A significant portion of the experimental evidence including the lack of anisotropy of conduction in spun-fiber sample, suggest that the mechanism is not consistent with the one-dimensional "molecular wire" type charge transport within the base-pair core, but rather rapid charge migration in the outer mantle of the B-DNA superstructure [9].

It has long been reported that the equilibrium structure, structural integrity and biochemical function of a DNA duplex are strongly dependent on the degree of DNA hydration [14]. High-resolution X-ray crystallographic analysis [15-17], neutron diffraction measurement [14] and solution NMR spectroscopic study [18] of the B form DNA revealed that the 'spine of

hydration' exists in the narrow minor groove of physiological active DNA. One of the previous studies suggests that decreasing humidity triggers the structural transition of DNA from B to Z form owing to volatilization of bound water molecules [8]. The role of water in the structural integrity of DNA is important because phosphate-phosphate electrostatic repulsion [19] is diminished by the high dielectric constant of water. In addition to the very existence of such water molecules in the DNA structure, the dynamics of these water molecules also play a pivotal role in maintaining DNA structure and functionality [20-21]. The observation of existence of water molecules within the DNA-CTMA film during thermo-gravimetric analysis (TGA) studies [8] probably points to the the intactness of B-form DNA in the DNA-CTMA film given the widely accepted fact that water is the integral part of biomolecular systems [22-26].

The time scale related to charge migration in the DNA moiety is found to be ultrafast and ranges from few picoseconds to several tens of nanoseconds [27-29]. To participate in the CT processes, the water molecules in the close vicinity of the DNA molecule (water of hydration) are expected to offer a similar solvation time scale. A series of ultrafast spectroscopic investigations reveal solvation time scales of the hydration water on similar orders [28]. Although the DNA-CTMA material is frequently used in the optoelectronics and has been found to be a promising materials for future technology [4, 6], surprisingly, the role of the water molecules in the material is absent in contemporary literature [30]. The dependence of device performance on the dynamics of the integrated water molecule within the DNA thin film is also sparsely documented in literature and this is the motive of our present study.

Here, we have prepared DNA-CTMA thin films, generally used in designing bio-LEDs [7, 31] by following the procedure reported elsewhere [8]. A well-characterized DNA minor groove binder dye, Hoechst 33258 (H258) [32-33] is used as a doping probe for spectroscopic investigation of the material. A detail characterization involving CD, FTIR, UV-Vis absorption and steady-

state fluorescence spectroscopy was used to confirm structural integrity of the DNA molecule and localization of the probe H258 in the DNA-minor groove in the biomaterial. Our picosecond-resolved time-correlated single photon counting (TCSPC) technique reveals the time scale associated with the solvation of the water molecules in the vicinity of DNA in the as-prepared material and after swelling. We have also investigated the ultrafast CT dynamics from embedded CdSe/ZnS quantum dots (QDs) in the thin film and compared it with that in the swollen material. The steady state and time

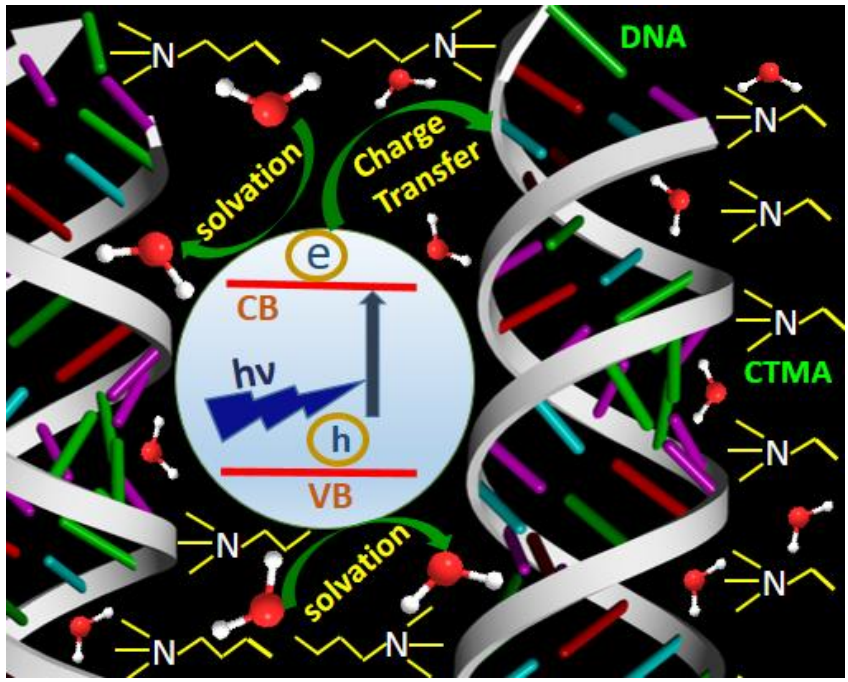

Figure 5.1. *Schematic representation of DNA-CTMA thin film. Embeded quantum dots (CdSe/ZnS) upon photoexcitation and charge transfer/solvation are also shown.*

resolved quenching of a fluorescence probe (here the QDs) in a DNA matrix is well documented as the manifestation of CT from/to the probe in the matrix as shown in Figure 5.1 [34-35]. To investigate the role of water molecules in the CT processes of the embedded QDs within the material, we have also studied the CT dynamics of the QDs in anionic sodium bis (2-ethylhexyl) sulfosuccinate reverse micelles (AOT RMs), in which the degree of hydration (number of water molecules) and dynamics of water molecules [36-37] around the entrapped QDs can be tuned in a controlled manner. The temperature

dependent dynamic light scattering (DLS) and picosecond-resolved CT dynamics of the entrapped QDs in the RMs clearly reveal the role of dynamics of the water molecules in the DNA materials. The studies are expected to have a profound effect on the key areas of research for developing superior biomaterials-based optoelectronic devices.

5.2. Results and discussion:

5.2.1. Ultrafast dynamics of solvation and charge transfer in a DNA-based biomaterial: Figure 5.2 shows the absorption and emission spectra of as-prepared H258 doped as prepared and swelled DNA-CTMA thin film on a

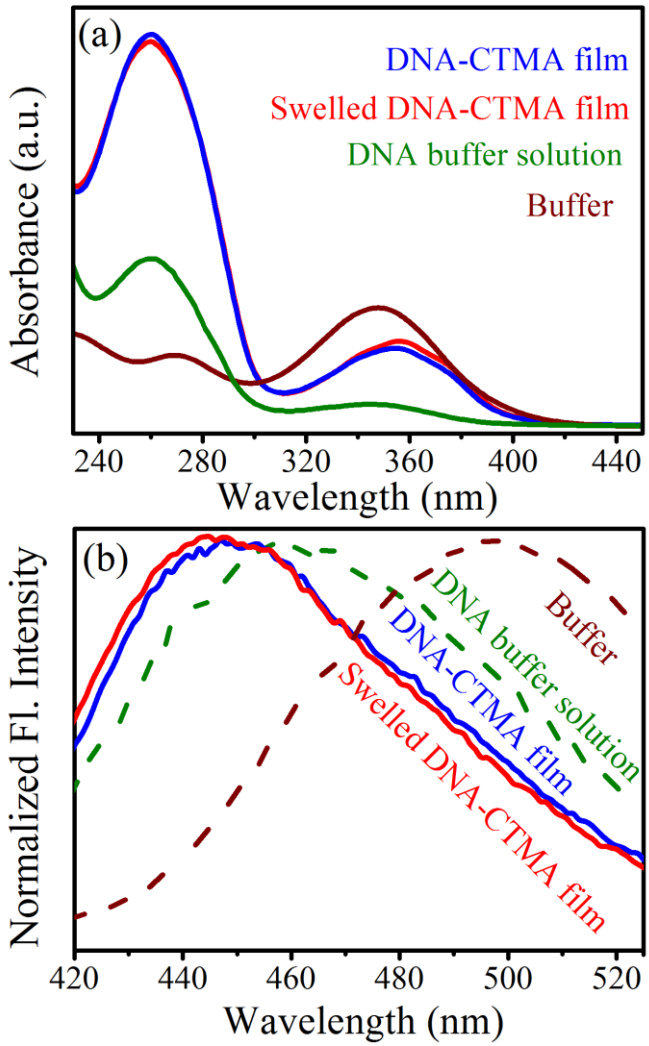

Figure 5.2. *(a) Absorption spectra of H258 in Buffer, DNA (solution), DNA-CTMA thin film and swelled DNA-CTMA thin film. (b) Emission spectra of H258 in buffer, DNA (solution), DNA-CTMA thin film and swelled DNA-CTMA thin film.*

quartz plate. The figure also shows the corresponding spectra of the probe H258 in the aqueous solution. A slight red shift in absorption spectra of H258 in the as-prepared and swelled thin films (355 nm) relative to the probe in buffer solution (347 nm)confirms the ground state complexation of the probe in the minor groove of the DNA in the film [38]. A significant blue shift in the emission spectrum (447 nm) of the probe in the thin film with respect to that in aqueous buffer solution (460 nm) is also consistent with location of the probe in the DNA minor groove (reported peak at 460 nm) [39]. No significant difference between the absorption and emission spectra of the probe in the as-prepared and swelled film is consistent with the fact that the immediate environment of the minor groove binding probe H258 remains unperturbed in the presence of additional water molecules in the film. Figure 5.3a shows circular dichroism (CD) spectra of the as-prepared and swelled films in which the positive peaks at 280 nm and negative peaks at 245 nm are the signature of the B-form of DNA in the films [40-41]. The CD spectrum for the DNA in aqueous solution is also shown in the figure as a reference. The structural integrity of the DNA (B-form) in the films with respect to that in the aqueous buffer solution is clearly evident from the figure. It has to be noted that the difference of the peak intensities of the films with respect to that in the DNA in aqueous buffer solution is due to relatively lower concentration in the latter sample.

To confirm the presence of strongly interacting water molecules in the film that leading to the monomeric form of the water [42-43], we performed FTIR experiment the results of which are shown in Figure 5.3b. The different C-H stretching modes of the DNA and the CTMA counterions (at 2851 cm^{-1} and 2921 cm^{-1}) [44] and O-H stretching frequencies of bulk water (at 3302 cm^{-1} and 3472 cm^{-1}) are consistent with those in the reported in the literature [45-46]. In the case of DNA fiber without CTMA, the O-H stretching frequencies can be deconvoluted with essentially two peaks, in which one at 3468 cm^{-1} consistent with a bulk type and another at 3590 cm^{-1} corroborate with the monomeric form of water molecules. The peak at 3204 cm^{-1} reveals an N-H stretching

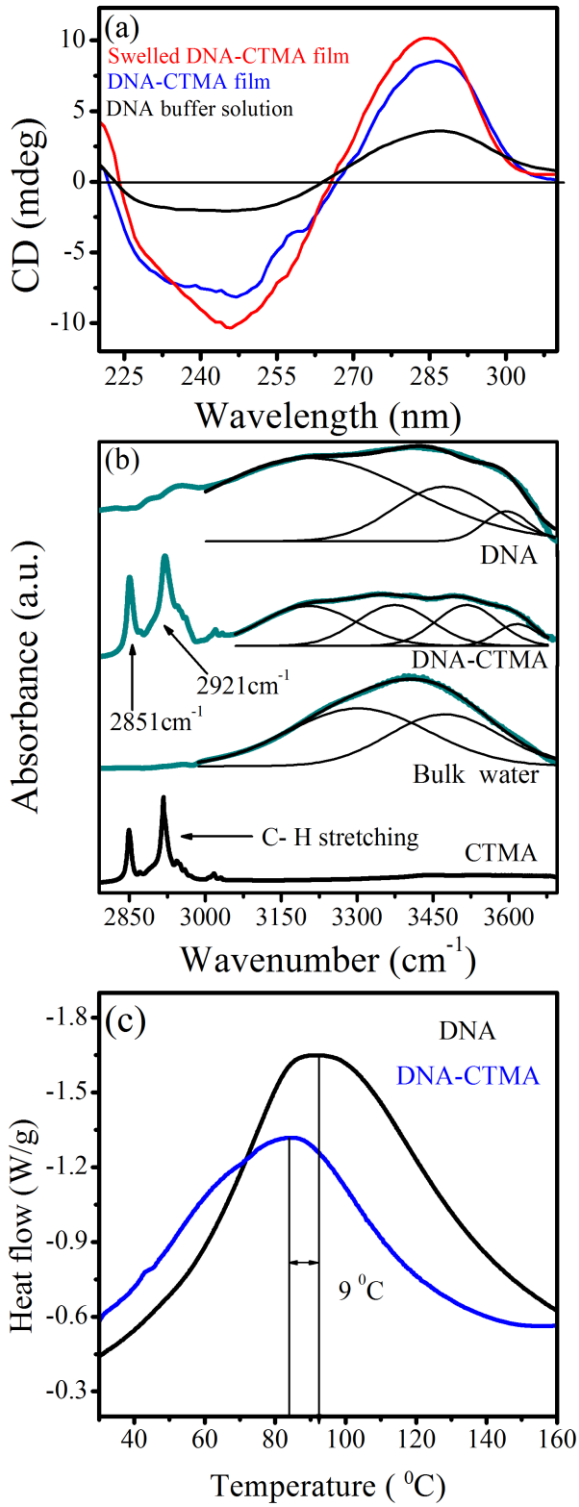

Figure 5.3. *(a) CD spectra of DNA in aqueous buffer solution, DNA-CTMA thin film (as-prepared and swelled). (b) FTIR spectra of DNA fiber, DNA-CTMA biomaterials, bulk water, and CTMA. To identify various types of water structures in the DNA and other systems, spectral deconvolution according to the Gaussian model was performed. (c) DSC scan (10 °C/min) of DNA and DNA-CTMA complex. The endothermic maximum is due to the denaturation process of DNA.*

frequency in the DNA sample. In the case of the DNA-CTMA sample, the deconvoluted peaks at 3199 cm^{-1} and 3607 cm^{-1} can be assigned to the stretching frequencies of N-H and monomeric water O-H, respectively. Two additional peaks at 3367 cm^{-1} and 3508 cm^{-1} are similar to bulk-type water molecules in the sample [47]. Our FTIR studies reveal the existence of different types of water molecules in the biomaterial including strongly interacting (essentially associated to DNA/CTMA) water molecules in the material.

Additional evidence of structural integrity of DNA in the biomaterial comes from thermometric studies of the films. In Figure 5.3c, differential scanning calorimetric (DSC) plots of DNA and DNA-CTMA complex are shown in the temperature range from 30 to 160 ^{0}C. Endothermic maxima around 90 ^{0}C for DNA and the DNA-CTMA complex correspond to the melting of DNA. A closer look at the thermogram shows that the endothermic peak for the DNA-CTMA film is at least 9 ^{0}C lower than that of the pure DNA fiber. It has been reported earlier that the melting of DNA molecule very much depends on the degree of hydration of the biomolecules [48]. The study that involving DNA melting in controlled humidity clearly showed that lower hydration leads to a relatively lower melting temperature of DNA. Thus our DSC study is consistent with the presence of water molecules in the biomaterial, yet they are lower in number than pure DNA fiber.

After confirmation of structural integrity of DNA and the association of significant water molecules in the vicinity of DNA in the biomaterial, we investigated the dynamic time scales of the water molecules. Picosecond-resolved fluorescence transient of H258 bound to DNA in DNA-CTMA film (both as-prepared and swelled) have been measured at a number of wavelengths across the emission spectrum of H258 in the film. Figure 5.4a and 5.4b show the decay transient of as-prepared and swelled DNA-CTMA film at three characteristic wavelengths from the blue to the red end of the fluorescence spectrum (410 nm, 460 nm and 530 nm). The fluorescence transient detected in the blue region (410 nm) of the fluorescence spectrum is

characterized by a faster picosecond decay component. The fluorescence transients become slower as the detection wavelengths increase and reveal a rise component at 530 nm. The nature of the wavelength dependent transients across the emission spectrum of the probe H258 in the DNA matrix signifies solvation stabilization of the probe in the DNA environments [21, 49].

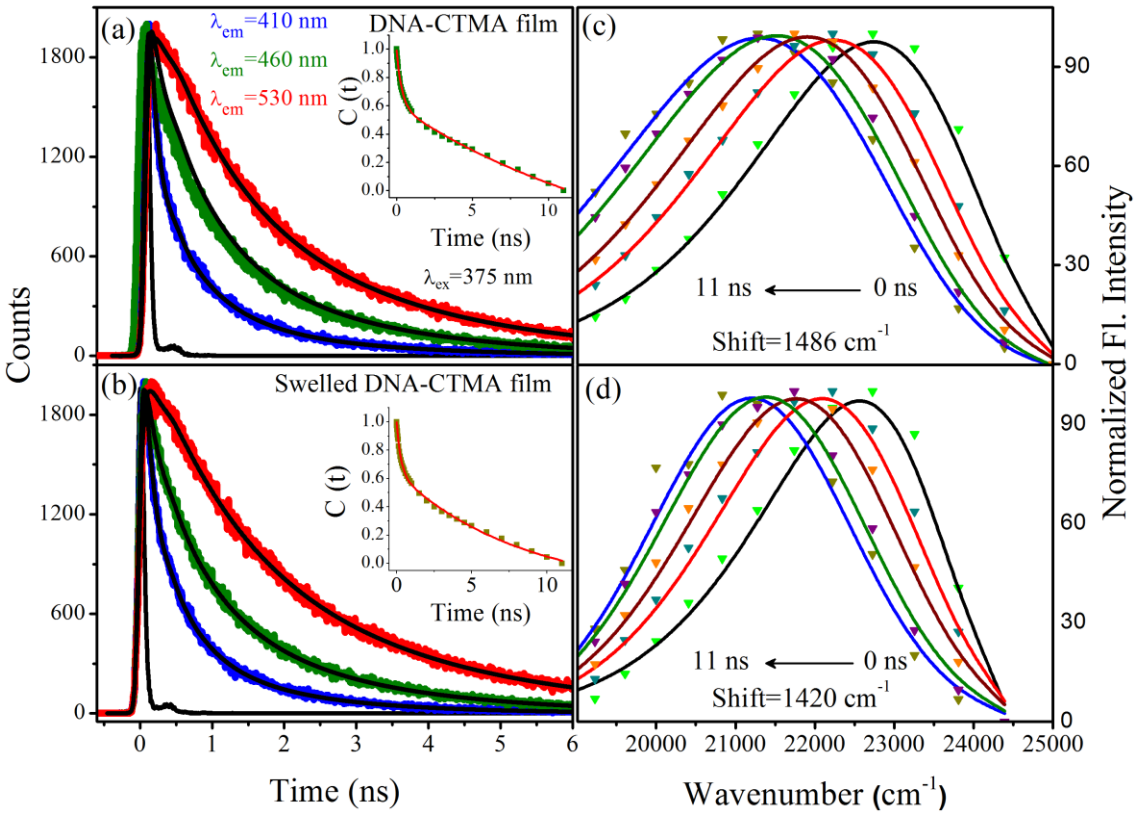

Figure 5.4. *Picosecond-resolved transient of H258 at three different wavelengths in (a) as-prepared DNA-CTMA and (b) Swelled DNA-CTMA biomaterial films. (c), (d) Time-resolved emission spectra (TRES) of corresponding systems are shown. Insets depict the corresponding solvation correlation decay profile of H258.*

However, the increase becomes more prominent in case of swelled DNA-CTMA thin film as shown in Figure 5.4a and Figure 5.4b. Figure 5.4c and 5.4d show the constructed time-resolved emission spectra (TRES) of H258 with a spectral shift of 1486 cm^{-1} and 1420 cm^{-1} for as-prepared and swelled biomaterial, respectively, in an 11 ns time window, which indicates that H258 is stabilized due to the solvation by the minor groove water molecules in the excited state [28]. The observed salvation correlation decay profile with time for corresponding systems are shown in the inset of Figure 5.4a and 5.4b, thus

revealing temporal excited state energy relaxation of the fluorophore in the DNA environments. Two component exponential decay fitting of the solvation correlation decay profile of H258 bound to DNA in DNA-CTMA film (inset) yields time components of 0.230 ns (28%) and 8.83 ns (72%). For swelled DNA-CTMA film, the two time components were estimated to be 0.220 ns (29%) and

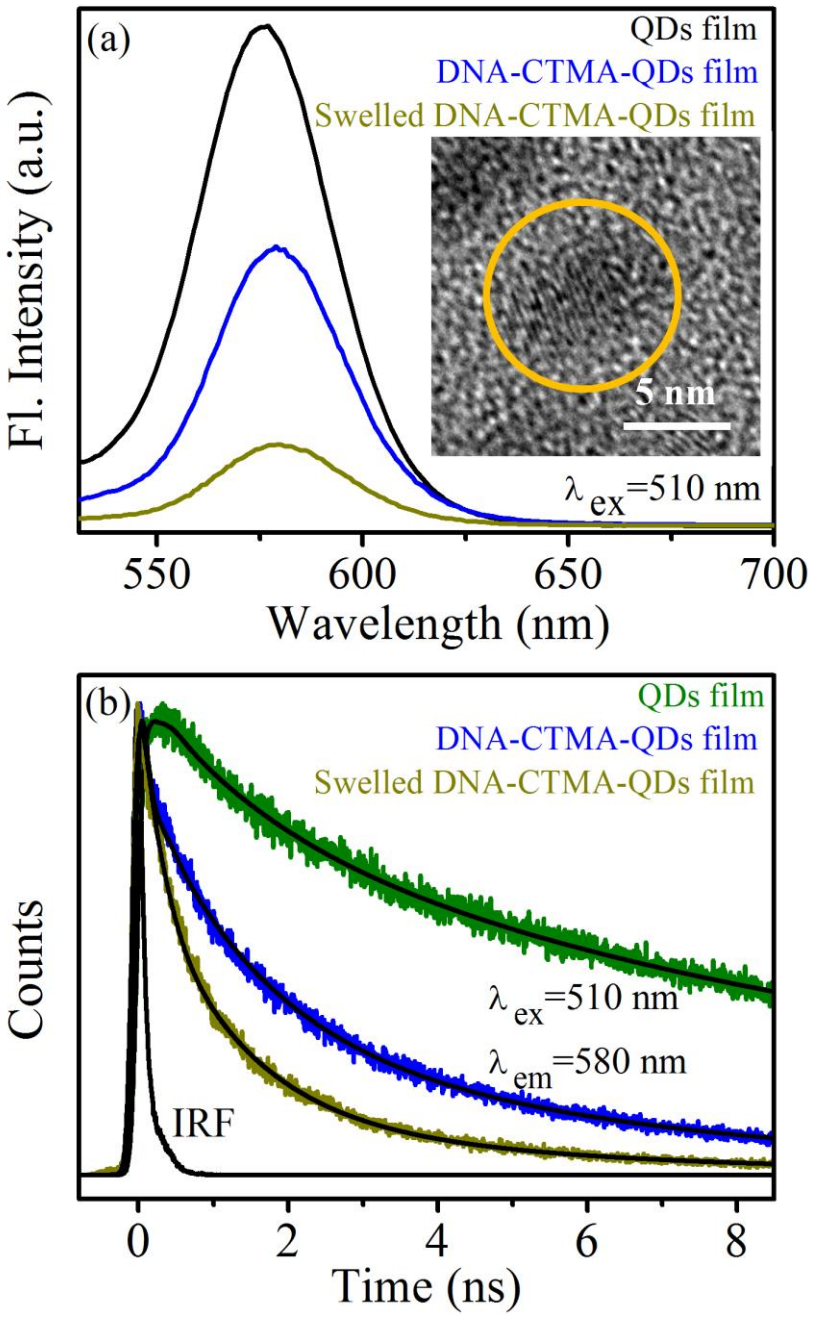

Figure 5.5. *(a)Fluorescence spectra of CdSe/ZnS QDs, QDs in as-prepared and swelled DNA-CTMA matrix. Inset depicts HRTEM image of QDs (5.2 nm). (b)Fluorescence decay transient of QDs, QDs in as-prepared and swelled DNA-CTMA matrix.*

6.50 ns (71%), which are consistent with our previous studies on solvation dynamics of DNA [28, 39]. The longer components in both cases are due to the relaxation of DNA itself. The observation indicates that upon swelling some water molecules can access the DNA film, which allows the DNA molecule to become more flexible, thus leading to a faster stabilization of the probe H258 and results in a decrease of water relaxation time.

In a recent report, the effect of water molecules on the stabilization of excited state of CdSe/ZnS QDs and the consequence of the water molecule stabilized state on the photoluminescence properties of the QDs has been reported [50]. In our studies we have used CdSe/ZnS QDs with a diameter of 5.2 nm as a CT probe in the DNA material. Figure 5.5a shows the steady-state fluorescence quenching of CdSe/ZnS QDs in the DNA matrix. The fluorescence of QDs in the matrix further quenches upon swelling of the film. The quenching of the excited state lifetime of the QDs in the films before and after swelling is further confirmed by the picosecond-resolved fluorescence studies as shown in Figure 5.5b. The fluorescence lifetime of QDs in the quartz plate (with average lifetime 12.47 ns) becomes significantly faster in the as-prepared biomaterial (4.49 ns). Upon swelling of the film, the lifetime of QDs becomes even faster (2.40 ns).The details are tabulated in Table 5.1. The faster excited-state lifetime of the QDs in the biomaterial could be the manifestation

Table 5.1. *The fluorescence lifetimes (τ_i) of QD in as-prepared and swelled DNA-CTMA films.*

System	τ_1 ns(%)	τ_2 ns(%)	τ_3 ns(%)	τ_{avg} ns
QDs film	-	1.78 (6)	13.16 (94)	12.48
QD-DNA film	0.06 (4)	1.52 (29)	6.04 (67)	4.49
Swelled QD-DNA film	0.054 (8)	0.88 (40)	3.93 (52)	2.40

of a photoinduced CT process from the embedded QDs to the DNA-bound water molecules in the matrix [50]. The apparent rate constants, k_{nr}, are

determined for the excited state non-radiative processes by comparing lifetimes of the QDs in the absence (τ_0) and in presence (τ) of the DNA-CTMA complex by using the following equation [51-52],

$$k_{nr} = {}^{1}\!/_{\langle\tau\rangle} - {}^{1}\!/_{\langle\tau_0\rangle} \tag{5.1}$$

For the DNA-CTMA complex, the rate constant for the non-radiative process

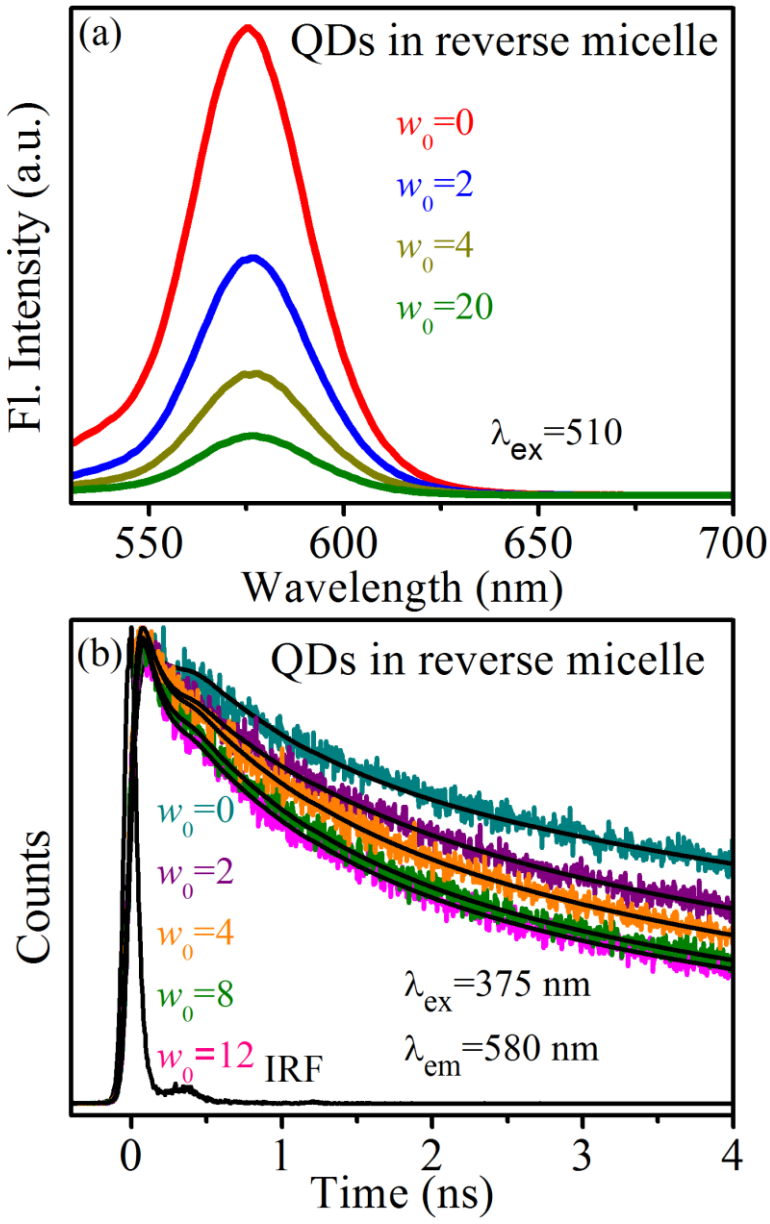

Figure 5.6. *(a) Steady-state fluorescence spectra of QDs in AOT RMs with increasing w_0 (w_0 =0, 2, 4, and 20 with λ_{ex} =510 nm). (b) Fluorescence decay transients of QDs in the AOT RMs at different w_0 values (w_0 =0, 2, 4, 8 and 12 with λ_{ex} =375 nm and λ_{em} =580 nm).*

was found to be 1.4×10^8 s^{-1}, whereas for the swelled system it is estimated to be 2.9×10^8 s^{-1}, indicating a faster CT from QDs to the water molecules in case of swelled DNA-CTMA film.

To investigate conclusive the role of the dynamics of water molecules in the CT mechanism for QDs, we extended our studies with the model biomimetic, AOT RMs, whereby the number of water molecules (w_0) and the dynamics can be controlled (by tuning the temperature) precisely. Figure 5.6a shows that with an increase in water content (w_0=2 to w_0=20) the fluorescence intensity of QDs entrapped in AOT RMs gradually decreases. The fluorescence decay transients of QDs in AOT RMs at different w_0 are shown in Figure 5.6b. Faster excited state lifetime of the QDs with increasing w_0 value from w_0=0 to w_0=20 (water pool size from 1.6 nm to 9.6 nm) revealing average lifetime from 7.4 ns (at w_0=0) to 2.69 ns (at w_0=20, details are in Table 5.2) is evident from the

Table 5.2. *Solvation correlation data for C500 and the fluorescence lifetimes (τ_i) data of QDs in AOT RMs at different w_0 values.*

System	Solvation of C-500			QDs in RM				
w_0	τ_1 ns (%)	τ_2 ns (%)	τ_{sol} ns	τ_1 ns (%)	τ_2 ns (%)	τ_3 ns (%)	τ_4 ns (%)	τ_{avg} ns
w_0=0	-	-	-	0.84 (34)	10.80 (66)	-	-	7.4
w_0=2	0.34 (25)	4.13 (75)	3.18	0.12 (26)	0.84 (17)	2.36 (18)	10.8 (39)	4.80
w_0=4	0.29 (35)	2.68 (65)	1.83	0.09 (30)	0.84 (22)	3.32 (22)	10.8 (26)	3.69
w_0=8	0.19 (38)	1.59 (62)	1.06	0.09 (32)	0.84 (27)	3.78 (24)	10.8 (17)	2.98
w_0=12	0.16 (35)	1.49 (65)	1.03	0.10 (36)	0.84 (25)	3.70 (24)	10.8 (15)	2.77
w_0=20	0.13 (33)	1.35 (67)	0.95	0.11 (34)	0.84 (26)	3.65 (26)	10.8 (14)	2.69

figure. To determine a correlation between the dynamics of CT of the QDs in the RMs at various degree of hydration (w_0) and the solvation dynamics of the RMs, we have measured solvation correlation functions of the RMs using C500 as fluorophore by following a procedure as reported earlier [53]. Linear

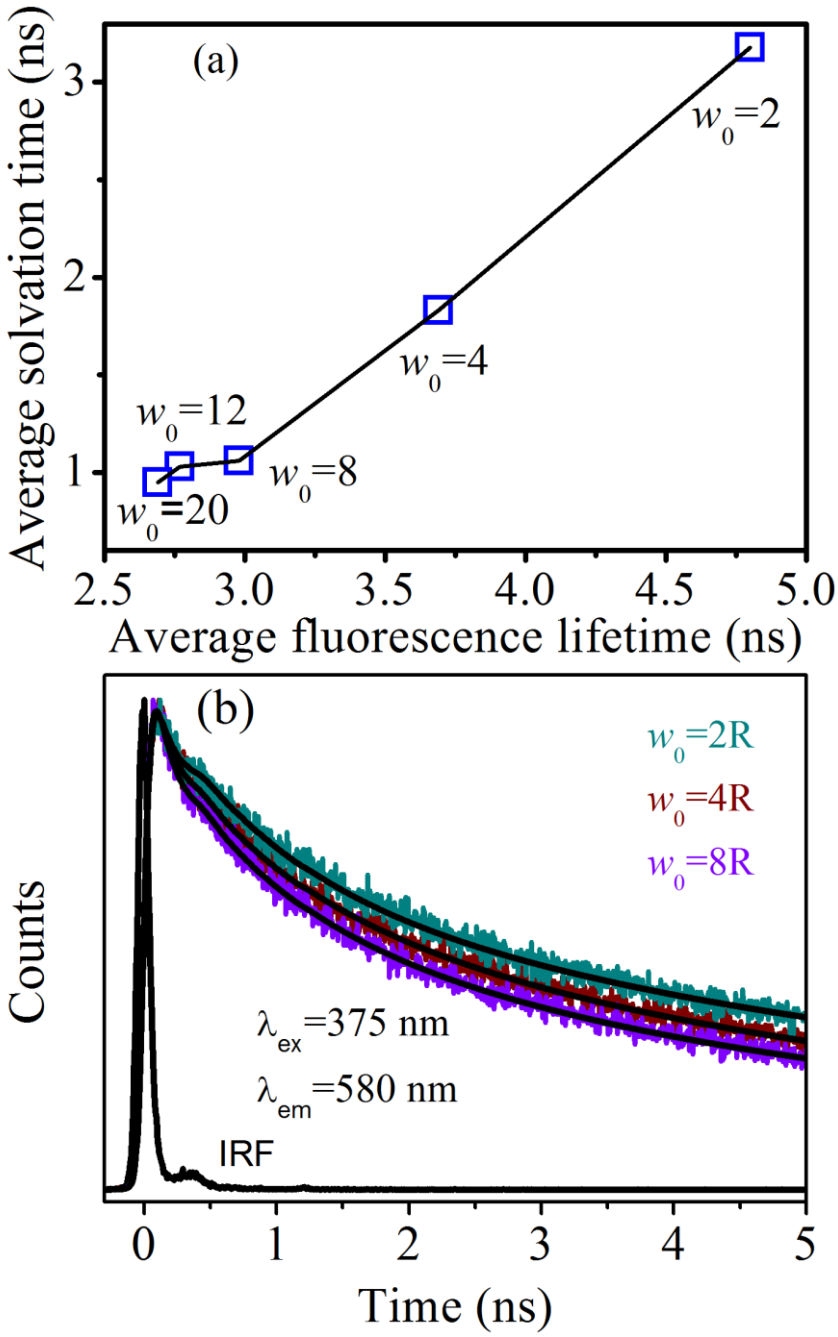

Figure 5.7. *(a) Plot of solvation time (τ_s) C-500 probe against average fluorescence lifetime (τ_{avg}) of the QDs at different w_0 values (b) Reversibility of fluorescence lifetime of QDs upon controlled reduction of RM size (w_0=8R, 4R, and 2R; R stands for reversible with λ_{ex}=375 nm and λ_{em} =580 nm).*

correlation of the average solvation time constant (τ_s) and excited state lifetime (τ_{avg}) of the QDs in the RMs upto w_0=8 is clearly evident from Figure 5.7a. It is well-known that upto w_0=8, there is an insignificant possibility of bulk type water and all the water molecules are strongly interacting with reverse micellar surface [54-55]. Further increase in the w_0 value begins to reveal two different types of water (bulk and bound type) and bulk type water might cause permanent and irreversible surface damage to reveal an irrecoverable fluorescence of the entrapped QDs [50]. The reversibility of the fluorescence (both steady state and time-resolved) of the QDs in the RMs from w_0=8 to w_0=2 has also been confirmed (Figure 5.7b and Table 5.3).

Table 5.3. *The fluorescence lifetimes (τ_i) of QD in AOT RM sat different w_0 values (R indicates reversible).*

System	τ_1 ns (%)	τ_2 ns (%)	τ_3 ns (%)	τ_4 ns (%)	τ_{avg} ns
w_0=2R	0.11 (22)	0.84 (24)	2.41 (15)	10.80 (39)	4.78
w_0=4R	0.09 (27)	0.84 (28)	3.37 (16)	10.80 (29)	3.89
w_0=8R	0.01 (32)	0.84 (30)	3.74 (18)	10.80 (20)	3.07
w_0=12R	0.14 (30)	0.84 (24)	3.14 (22)	10.80 (24)	3.54
w_0=20R	0.12 (31)	0.84 (23)	3.20 (23)	10.80 (23)	3.42

Our observation of a faster rate of CT dynamics of QDs in the RMs of higher w_0 values and a distinct correlation with the solvation dynamics confirm the role of water molecules in the tuning of the CT rate in the nano-environments. However, the observation raises question about the involvement of water molecules in the CT processes through dynamical flexibility of the water molecules or through the hydration number. To confirm the dynamic role of the water molecules in controlling CT processes, we studied the QDs in a particular RM with w_0= 5 at various temperatures. As shown in Figure 5.8a the DLS studies on the RM (w_0=5) with the QDs at different temperatures reveal an almost unaltered size of the RM and are consistent with our earlier

observation [53]. However, the non-radiative rate of the CT dynamics of the QDs follows the Arrhenius law up to 60 ^{0}C (Figure 5.8b). Corresponding lifetime values are tabulated in Table 5.4. The calculated barrier energy from

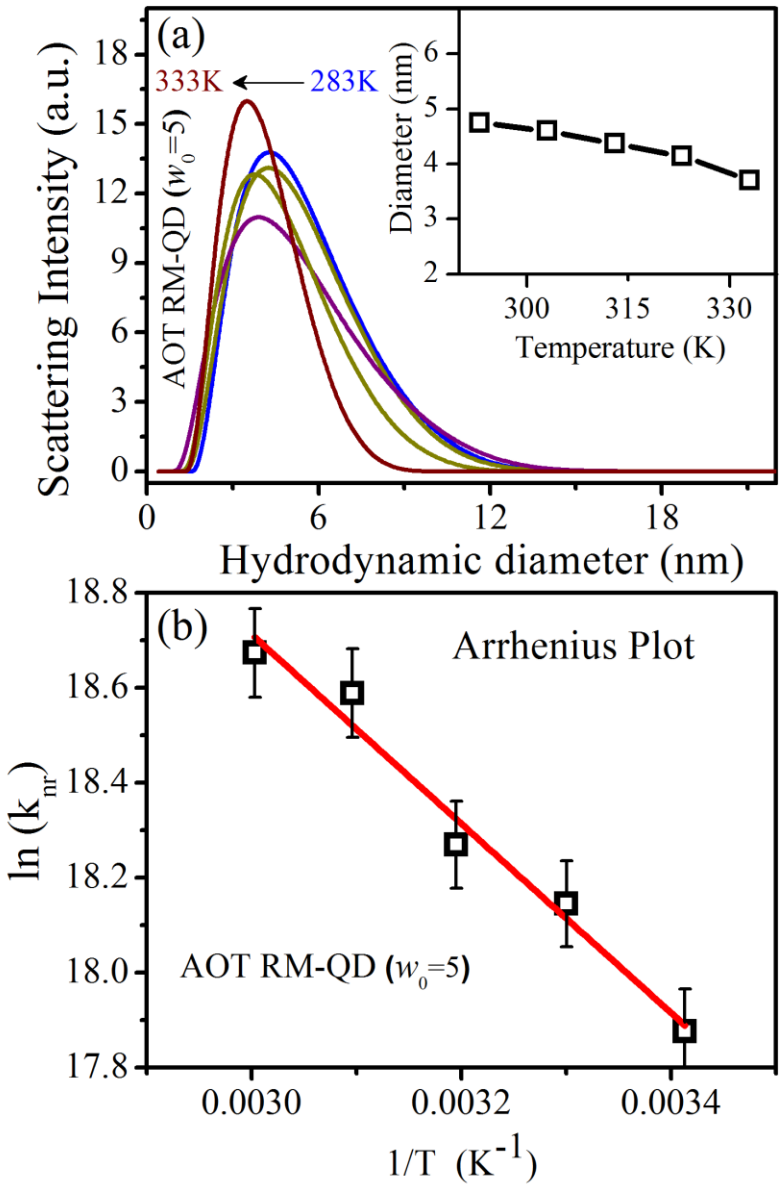

Figure 5.8. *(a) Typical DLS signals (scattering intensity) for w_0=5 AOT RMs systems at different temperatures (293K-333K) are presented. The inset reveals hydrodynamic diameters (d_h) of reverse micelles for different temperatures. (b) The Arrhenius plot of ln(k_{nr}) against 1/T for QDs in AOT RMs with w_0=5 and its linear fit (red line).*

the Arrhenius plot is 3.95 kcal/mol. Remarkably, it is noted that the solvation barrier for this kind of RMs (w_0=5) was estimated to be 2.4-4 kcal/mol from

molecular dynamics simulation [56] and experimentally measured to be around 5 kcal/mol [53]. Our observation of the barrier crossing type CT reaction of the QDs in the RMs and the similarity of the barrier with that of the solvation clearly unravel the role of the solvation barrier in the CT of the QDs in the RM [57].

Table 5.4. *The fluorescence lifetimes (τ_i) of QDs in AOT RMs (w_0 =5) at different temperatures.*

System	τ_1 ns (%)	τ_2 ns (%)	τ_3 ns (%)	τ_{avg} ns
293K	0.21 (31)	1.48 (30)	9.77 (39)	4.35
303K	0.19 (31)	1.38 (31)	9.37 (38)	4.04
313K	0.20 (33)	1.44 (31)	9.29 (36)	3.88
323K	0.18 (36)	1.32 (30)	8.79 (34)	3.44
333K	0.16 (35)	1.21 (31)	8.41 (34)	3.32

5.3. Conclusion: In summary, we have investigated solvation dynamics of DNA bound water in a technologically important biomaterial that consists of a DNA-CTMA self-assembly. The role of the dynamics in the excited-state CT process of QDs-embedded biomaterial has also been explored. Our studies on the solvation dynamics of water molecules in a controlled nano-environment of RMs and the CT of the QDs in that environment clearly reveal that the dynamic barrier (solvation) is the rate-limiting step for the CT process of the entrapped QDs. An interesting correlation of the dynamics of CT and solvation in the thin films (as-prepared and swelled) as well as in the RMs with different degree of hydration up to w_0=8, is evident from our studies. The solvation rate in the RMs of w_0=2 to w_0=8 (swelled RMs) gradually increases from 3.1×10^8 s^{-1} to 9.4×10^8 s^{-1}, respectively, thereby revealing the increase in the CT rate from 2.0×10^8 s^{-1} to 3.8×10^8 s^{-1}. In the case of the DNA-CTMA thin film, the rate of solvation upon swelling increases from 1.6×10^8 s^{-1} to 2.1×10^8 s^{-1} and

corresponding increase in the CT rate is from 2.2×10^{8} s^{-1} to 4.1×10^{8} s^{-1}, respectively. It is noteworthy that the dynamics of solvation and CT are essentially governed by the "bound type" biological water [26, 49] and the increase of the CT rate with respect to that of the solvation in the case of RMs and the biomaterial upon swelling are found to be 4.5 and 3.8, respectively. The surprising correlation in both systems clearly justifies the role of biological water in the CT dynamics. Our finding might find relevance in the QDs-based devices in which one can effectively tune the efficiency by controlling the humidity level.

References

[1] N. C. Seeman, DNA in a material world, *Nature* **421**, (2003), 427.

[2] Y. W. Kwon, C. H. Lee, D. H. Choi and J. I. Jin, Materials science of DNA, *J. Mater. Chem.* **19**, (2009), 1353.

[3] P. V. Kamat, Quantum dot solar cells: Semiconductor nanocrystals as light harvesters, *J. Phys. Chem. C* **112**, (2008), 18737.

[4] A. J. Steckl, DNA - a new material for photonics?, *Nat. Photonics* **1**, (2007), 3.

[5] T. Singh, N. Sariciftci and J. Grote, *Bio-organic optoelectronics devices using DNA*, **2010**, Springer, Berlin, Germany.

[6] Q. Sun, G. Subramanyam, L. Dai, M. Check, A. Campbell, R. Naik, J. Grote and Y. Wang, Highly efficient quantum-dot light-emitting diodes with DNA−CTMA as a combined hole-transporting and electron-blocking layer, *ACS Nano* **3**, (2009), 737.

[7] Q. Sun, D. W. Chang, L. Dai, J. Grote and R. Naik, Multilayer white polymer light-emitting diodes with deoxyribonucleic acid-cetyltrimetylammonium complex as a hole-transporting/electron-blocking layer, *Appl. Phys. Lett.* **92**, (2008), 251108.

[8] L. Wang, J. Yoshida, N. Ogata, S. Sasaki and T. Kajiyama, Self-assembled supramolecular films derived from marine deoxyribonucleic acid (DNA)−cationic surfactant complexes: Large-scale preparation and optical and thermal properties, *Chem. Mater.* **13**, (2001), 1273.

[9] J. M. Warman, M. P. de Haas and A. Rupprecht, DNA: A molecular wire?, *Chem. Phys. Lett.* **249**, (1996), 319.

[10] Y. G. Yang, P.-G. Yin, X.-Q. Li and Y. Yan, Kinetic study for hopping conduction through deoxyribonucleic acid molecules, *Appl. Phys. Lett.* **86**, (2005), 203901.

[11] H. W. Fink and C. Schonenberger, Electrical conduction through DNA molecules, *Nature* **398**, (1999), 407.

[12] A. Y. Kasumov, M. Kociak, S. Guéron, B. Reulet, V. T. Volkov, D. V. Klinov and H. Bouchiat, Proximity-induced superconductivity in DNA, *Science* **291**, (2001), 280.

[13] K. Kawai, H. Kodera, Y. Osakada and T. Majima, Sequence-independent and rapid long-range charge transfer through DNA, *Nat. Chem.* **1**, (2009), 156.

[14] S. Arai, T. Chatake, T. Ohhara, K. Kurihara, I. Tanaka, N. Suzuki, Z. Fujimoto, H. Mizuno and N. Niimura, Complicated water orientations in the minor groove of the B-DNA decamer d(ccattaatgg)$_2$ observed by neutron diffraction measurements, *Nuc. Acids Res.* **33**, (2005), 3017.

[15] H. R. Drew and R. E. Dickerson, Structure of a B-DNA dodecamer: III. Geometry of hydration, *J. Mol. Biol.* **151**, (1981), 535.

[16] X. Shui, L. McFail-Isom, G. G. Hu and L. D. Williams, The B-DNA dodecamer at high resolution reveals a spine of water on sodium, *Biochemistry* **37**, (1998), 8341.

[17] V. Tereshko, G. Minasov and M. Egli, A "hydrat-ion" spine in a B-DNA minor groove, *J. Am. Chem. Soc.* **121**, (1999), 3590.

[18] E. Liepinsh, G. Otting and K. Wüthrich, NMR observation of individual molecules of hydration water bound to DNA duplexes: Direct evidence for a spine of hydration water present in aqueous solution, *Nuc. Acids Res.* **20**, (1992), 6549.

[19] K. Range, E. Mayaan, L. J. Maher and D. M. York, The contribution of phosphate-phosphate repulsions to the free energy of DNA bending, *Nuc. Acids Res.* **33**, (2005), 1257.

[20] S. K. Pal, L. A. Zhao and A. H. Zewail, Water at DNA surfaces: Ultrafast dynamics in minor groove recognition, *Proc. Natl. Acad. Sci. USA* **100**, (2003), 8113.

[21] D. Banerjee and S. K. Pal, Excited-state solvation and proton transfer dynamics of DAPI in biomimetics and genomic DNA, *J. Phys. Chem. A* **112**, (2008), 7314.

[22] M. Maroncelli, J. Macinnis and G. R. Fleming, Polar solvent dynamics and electron-transfer reactions, *Science* **243**, (1989), 1674.

[23] R. Jimenez, G. R. Fleming, P. V. Kumar and M. Maroncelli, Femtosecond solvation dynamics of water, *Nature* **369**, (1994), 471.

[24] N. Nandi, K. Bhattacharyya and B. Bagchi, Dielectric relaxation and solvation dynamics of water in complex chemical and biological systems, *Chem. Rev.* **100**, (2000), 2013.

[25] L. Zhao, S. K. Pal, T. Xia and A. H. Zewail, Dynamics of ordered water in interfacial enzyme recognition: Bovine pancreatic phospholipase A_2, *Angew. Chem. Int. Ed.* **43**, (2004), 60.

[26] S. K. Pal and A. H. Zewail, Dynamics of water in biological recognition, *Chem. Rev.* **104**, (2004), 2099.

[27] E. W. Schlag, D.-Y. Yang, S.-Y. Sheu, H. L. Selzle, S. H. Lin and P. M. Rentzepis, Dynamical principles in biological processes: A model of charge migration in proteins and DNA, *Proc. Natl. Acad. Sci. USA* **97**, (2000), 9849.

[28] D. Banerjee and S. K. Pal, Ultrafast charge transfer and solvation of DNA minor groove binder: Hoechst 33258 in restricted environments, *Chem. Phys. Lett.* **432**, (2006), 257.

[29] S. Shankara Narayanan, S. S. Sinha, P. K. Verma and S. K. Pal, Ultrafast energy transfer from 3-mercaptopropionic acid-capped CdSe/ZnS QDs to dye-labeled DNA, *Chem. Phys. Lett.* **463**, (2008), 160.

[30] M. Wolter, M. Elstner and T. Kubař, Charge transport in desolvated DNA, *J. Chem. Phys.* **139**, (2013), 125102

[31] J. A. Hagen, W. Li, A. J. Steckl and J. G. Grote, Enhanced emission efficiency in organic light-emitting diodes using deoxyribonucleic acid complex as an electron blocking layer, *Appl. Phys. Lett.* **88**, (2006), 171109.

[32] H. Görner, Direct and sensitized photoprocesses of bis-benzimidazole dyes and the effects of surfactants and DNA, *Photochem. Photobiol.* **73**, (2001), 339.

[33] G. Cosa, K. S. Focsaneanu, J. R. N. McLean, J. P. McNamee and J. C. Scaiano, Photophysical properties of fluorescent DNA-dyes bound to single- and double-stranded DNA in aqueous buffered solution, *Photochem. Photobiol.* **73**, (2001), 585.

[34] C. Wan, T. Xia, H.-C. Becker and A. H. Zewail, Ultrafast unequilibrated charge transfer: A new channel in the quenching of fluorescent biological probes, *Chem. Phys. Lett.* **412**, (2005), 158.

[35] C. Z. Wan, T. Fiebig, O. Schiemann, J. K. Barton and A. H. Zewail, Femtosecond direct observation of charge transfer between bases in DNA, *Proc. Natl. Acad. Sci. USA* **97**, (2000), 14052.

[36] G. B. Behera, B. K. Mishra, P. K. Behera and M. Panda, Fluorescent probes for structural and distance effect studies in micelles, reversed micelles and microemulsions, *Adv. Colloid Interface Sci.* **82**, (1999), 1.

[37] R. Mitra, S. Sinha and S. Pal, Interactions of nile blue with micelles, reverse micelles and a genomic DNA, *J. Fluoresc.* **18**, (2008), 423.

[38] A. Adhikary, V. Buschmann, C. Muller and M. Sauer, Ensemble and single-molecule fluorescence spectroscopic study of the binding modes of the bis-benzimidazole derivative Hoechst 33258 with DNA, *Nuc. Acids Res.* **31**, (2003), 2178.

[39] S. Batabyal, T. Mondol, S. Choudhury, A. Mazumder and S. K. Pal, Ultrafast interfacial solvation dynamics in specific protein DNA recognition, *Biochimie* **95**, (2013), 2168.

[40] J. Kypr, I. Kejnovská, D. Renčiuk and M. Vorlíčková, Circular dichroism and conformational polymorphism of DNA, *Nuc. Acids Res.* **37**, (2009), 1713.

[41] R. Sarkar and S. K. Pal, Ligand–DNA interaction in a nanocage of reverse micelle, *Biopolymers* **83**, (2006), 675.

[42] T. L. Tso and E. K. C. Lee, Role of hydrogen bonding studied by the FTIR spectroscopy of the matrix-isolated molecular complexes, dimer of water, water-CO_2, water-CO and H_2O_2-nCO in solid O_2 at 12-17 K, *J. Phys. Chem.* **89**, (1985), 1612.

[43] S. S. Narayanan, S. S. Sinha, R. Sarkar and S. K. Pal, Picosecond to nanosecond reorganization of water in AOT/lecithin mixed reverse micelles of different morphology, *Chem. Phys. Lett.* **452**, (2008), 99.

[44] M. Yang, L. Szyc and T. Elsaesser, Femtosecond two-dimensional infrared spectroscopy of adenine-thymine base pairs in DNA oligomers, *J. Phys. Chem. B* **115**, (2011), 1262.

[45] H. MacDonald, B. Bedwell and E. Gulari, FTIR spectroscopy of microemulsion structure, *Langmuir* **2**, (1986), 704.

[46] T. K. Jain, M. Varshney and A. Maitra, Structural studies of AOT reverse micellar aggregates by FTIR spectroscopy, *J. Phys. Chem.* **93**, (1989), 7409.

[47] T. Kawai, J. Umemura, T. Takenaka, M. Kodama and S. Seki, Fourier transform infrared study on the phase transitions of an octadecyltrimethylammonium chloride-water system, *J. Colloid Interface Sci.* **103**, (1985), 56.

[48] S. L. Lee, P. G. Debenedetti, J. R. Errington, B. A. Pethica and D. J. Moore, A calorimetric and spectroscopic study of DNA at low hydration, *J. Phys. Chem. B* **108**, (2004), 3098.

[49] S. K. Pal, J. Peon, B. Bagchi and A. H. Zewail, Biological water: Femtosecond dynamics of macromolecular hydration, *J. Phys. Chem. B* **106**, (2002), 12376.

[50] K. Pechstedt, T. Whittle, J. Baumberg and T. Melvin, Photoluminescence of colloidal CdSe/ZnS quantum dots: The critical effect of water molecules, *J. Phys. Chem. C* **114**, (2010), 12069.

[51] I. Robel, M. Kuno and P. V. Kamat, Size-dependent electron injection from excited CdSe quantum dots into TiO_2 nanoparticles, *J. Am. Chem. Soc.* **129**, (2007), 4136.

[52] A. Makhal, H. Yan, P. Lemmens and S. K. Pal, Light harvesting semiconductor core−shell nanocrystals: Ultrafast charge transport dynamics of CdSe−ZnS quantum dots, *J. Phys. Chem. C* **114**, (2009), 627.

[53] R. K. Mitra, S. S. Sinha and S. K. Pal, Temperature-dependent solvation dynamics of water in sodium bis(2-ethylhexyl)sulfosuccinate/isooctane reverse micelles, *Langmuir* **24**, (2008), 49.

[54] A. Goto, S. Harada, T. Fujita, Y. Miwa, H. Yoshioka and H. Kishimoto, Enthalpic studies on the state of water in sodium bis(2-ethylhexyl)sulfosuccinate reversed micelles, *Langmuir* **9**, (1993), 86.

[55] N. M. Correa, M. A. Biasutti and J. J. Silber, Micropolarity of reverse micelles of AOT in n-hexane, *J. Colloid Interface Sci.* **172**, (1995), 71.

[56] S. Pal, S. Balasubramanian and B. Bagchi, Identity, energy, and environment of interfacial water molecules in a micellar solution, *J. Phys. Chem. B* **107**, (2003), 5194.

[57] S. Choudhury, S. Batabyal, T. Mondol, D. Sao, P. Lemmens and S. K. Pal, Ultrafast dynamics of solvation and charge transfer in a DNA-based biomaterial, *Chem. Asian J.* 9, (2014), 1395.

Chapter 6

Spectroscopic studies on the role of ultrafast conformational dynamics in the molecular recognition of a protein

6.1. Introduction: In all biological processes, biomolecular recognition related to small ligands is a central phenomenon. For the past 50 years, the ligand-induced conformation and change of biological macromolecules (induced-fit) proposed by Khosland has been the text book explanation of recognition events [1]. However, recent theoretical and experimental studies suggest an alternative pathway in which small ligands select and stabilize a complementary, lowest energy conformation from a pre-existing equilibrium of ground and excited states of the bio-molecules (selected-fit) [2-6]. In all of these cases, the binding interaction does not induce conformational changes. Importantly, over the past decade high resolution NMR relaxation, single molecule spectroscopy, Förster resonance energy transfer (FRET) analysis, and molecular dynamic simulations have shone more light on the conformational diversity of proteins in solution [7-17]. In recent reports, the key factor for the characteristic difference between on and off rates in the two mechanisms is concluded to be conformation and relaxation of the bio-molecules. Whether a protein binds to its ligand through a selected-fit or induced-fit mechanism can be identified by perturbing the conformational equilibrium (Figure 6.1). Several experimental strategies have been suggested, to the demonstration of the recognition pathways including mutation [18-22], which perturbs the conformational equilibrium of the involved protein. However, concise experimental demonstrations of these two pathways are sparse in the literature. This is the motivation for our present work. Furthermore, we aim to investigate biochemical strategies that involve specific mutations far from the

protein binding pockets without altering the recognition site [23]. Such mutations may alter the step-wise conformation changes required for

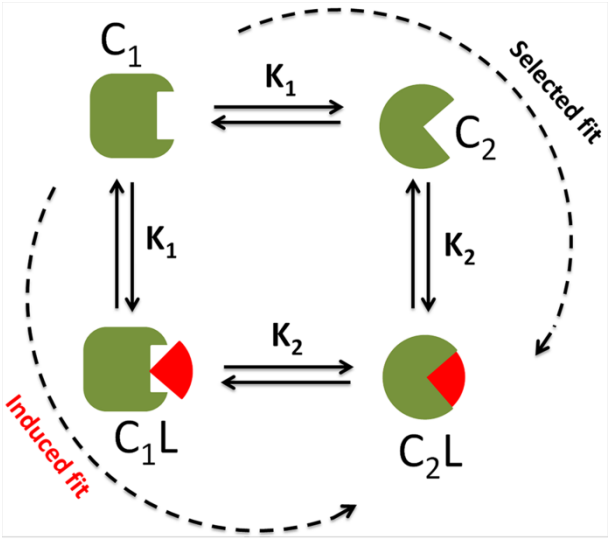

Figure 6.1. *Schematic representation of simple four state model of protein-ligand binding. C_1 and C_2 are the two conformations of the protein and L is the binding ligand. K_1 and K_2 are the corresponding binding constants.*

competent binding [24]. The calculation of conformational free energy differences in the unbound and bound state is well established but requires experimental protein structures in both the unbound and the ligand-bound state, which is challenging in most cases [6]. An alternative experimental strategy has been employed here that involves the perturbation of the host solvent to control conformational relaxations of the proteins under study. The X-ray crystal structure of α-Chymotrypsin (CHT) monomer have been studied [25] and found to be unchanged at both pH values (3.6 and 6.3) investigated [26]. However, the mobility of the water molecules at the surface of the protein is observed to change with the pH. The hydration shell of biological macromolecules plays a crucial role on their stability and in the recognition of a specific site [27]. Femtosecond-dynamical studies have provided insights into the more ordered water molecules on the overall surface of the above mentioned protein at low pH values [28]. The rigid water structure at low pH (3.6) inhibits the dynamics and functionality of proteins, whereas a mobile and

less rigid hydration surface at high pH (6.3) makes the active recognition dynamically favourable. For enzymatic activity, the dynamics of the active site is essential, however, the function and dynamics of the probe site (opposite to the active site in present case) are correlated.

In most of the biochemical reactions such as protein folding, protein-ligand interaction occur rapidly and thus, need to be triggered on very short time scales to study their kinetics [25, 29-30]. In this direction, we have studied molecular recognition (of biological systems/biomimetic) and enzyme kinetics in a microfluidics system equipped with a microscopic and spectroscopic attachment [31]. Herein, we used 8-anilino-1-naphthalenesulfonic acid ammonium salt (ANS) and CHT as model ligands and proteins, respectively. The enhancement of fluorescence intensity as a manifestation of complexation of ANS with CHT is followed along the microfluidics channel. The kinetic profile of the fluorescence enhancement of ANS with CHT at pH 3.6 and pH 6.3 along the micro-channel shows two distinct pathways. Theoretical fitting of the kinetic data in the two pH values reveal different pathways of molecular recognition of ANS by the protein CHT. In a control experiment, we studied the interaction between non-biological cetyl trimethyl ammonium bromide (CTAB) micelles with ANS under similar experimental conditions in order to rule out the role of the host solvent for the observed differential recognition pathways of CHT. We have shown here that the binding mechanism is shifting towards induced-fit from selected-fit upon increasing the ligand concentration. We also performed simulations by using COMSOL Multiphysics to interpret our experimental data.

6.2. Results and discussion:

6.2.1. Direct observation of kinetic pathways of biomolecular recognition: A simple four state model [32-34] of CHT-ANS binding in the microfluidics channel is shown in Figure 6.2. An H-shaped microfluidics channel with two inlets, one for the enzyme CHT (120 μM) in buffer at a specific pH value and another for ANS (10 μM) in the buffer solution was used to generate the time

gradient of the CHT-ANS complex along the direction of flow in the channel. The flow rates through each of the two inlets were held constant at 50 µL/minute, which corresponds to an average linear (laminar) flow of 100 µL/min in the main channel. This value of average laminar flow was obtained from the volumetric flow rate of the fluid and the cross sectional area

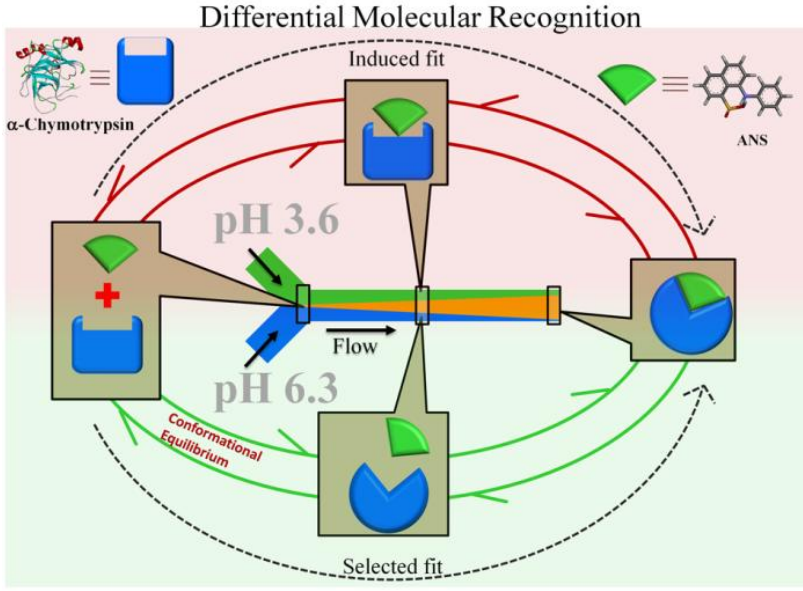

Figure 6.2. *Schematic representation of a microfluidics channel used for molecular recognition studies at different pH values in a four-state model. The difference between these two pathways is that at higher pH (6.3) the ligand (ANS) interacts with the pre-exist ensemble of protein conformations via a selected-fit mechanism, whereas at low pH (3.6) the bound protein conformation forms only after the interaction with the ligand.*

of the micro-channel. The estimated time resolution in the experimental condition along the micro-channel is 18.85 µsec/µM.

The fluorescence micrographs of the microfluidics channel corresponding to the two different experimental conditions are shown in Figure 6.3a. The blue–green emission from the ANS–CHT complex increases along the channel because ANS and CHT have time to be mixed to form the ANS–CHT complex. The intensity of the emission from the ANS-CHT complex is much higher at pH 3.6. The inset of Figure 6.3b shows the fluorescence

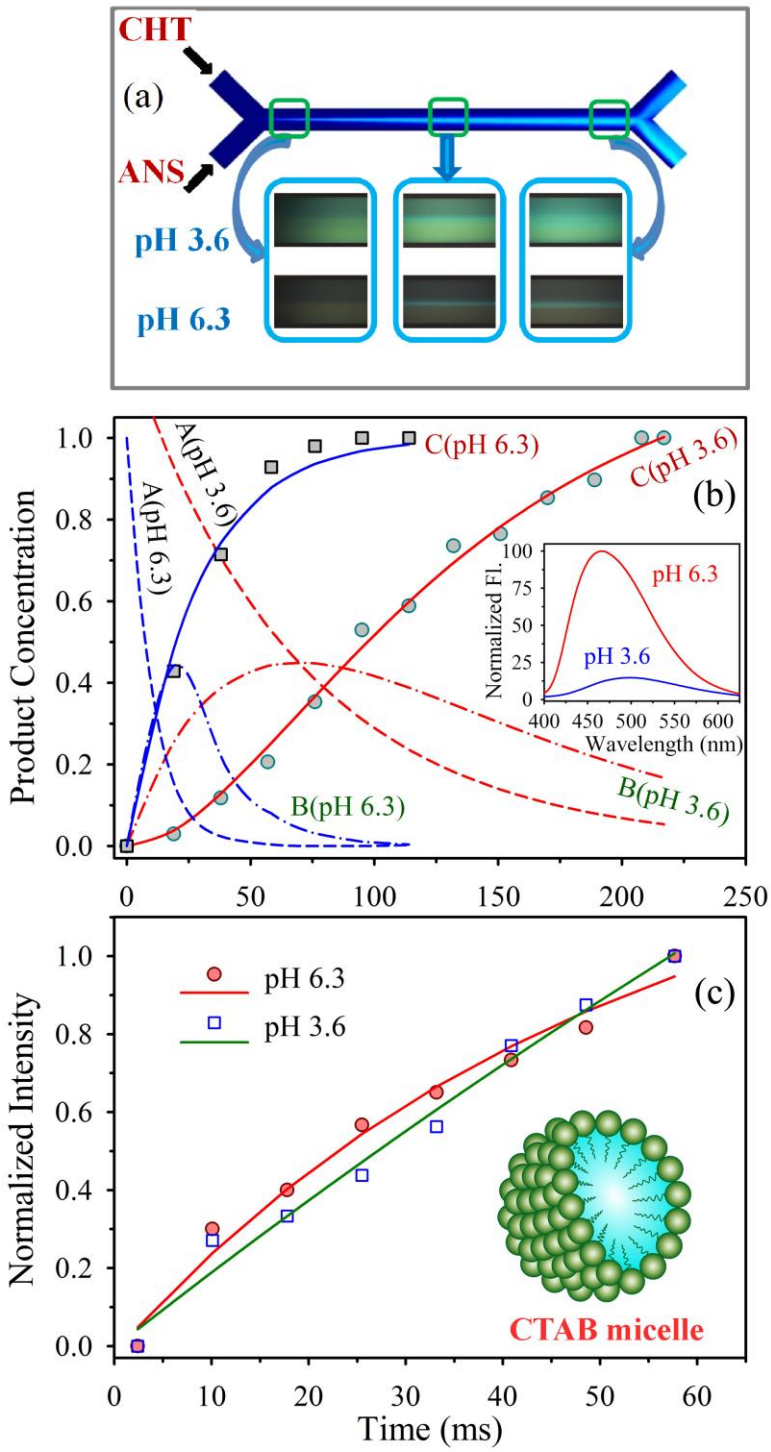

Figure 6.3. *The fluorescence and kinetics results are compared at two pH. (a) Micrographs of the microfluidics channel at different position across the channel at different pH values. (b) Evolution of the emission intensity of ANS upon complexation with CHT along the microfluidics channel (solid lines). The substrate (A) and intermediate (B) concentrations at different pH are shown with dotted lines. Steady-state fluorescence spectra of ANS with CHT at different pH are shown in the inset. (c) Molecular recognition pathways of a cationic CTAB micelle at different pH values in the microfluidics channel.*

spectra of the ANS-CHT complex with different pH buffers. The enhancement of the fluorescence quantum yield at pH 3.6 is clearly evident and is consistent with earlier studies [28, 35]. The evolution of fluorescence enhancement as a function of time along the microchanel shows two distinct pathways (Figure 6.3b).

To explain our kinetics data of experimental kinetics we have considered a simple kinetics scheme of A→B→C, with the corresponding first order rate constants of k_1 and k_2 for the formation of the intermediate (B) from the substrate (A) to the final product (C), in which the substrate A, represents the unbound (without ANS) form of the enzyme CHT; B is the intermediate state of CHT with ANS, immediately after the recognition and C is the final form of the CHT-ANS complex. Here, we have considered two important approximations; firstly k_1 is the rate of formation of the CHT-ANS complex; thus, should it be of second order. However, because the concentration of the enzyme CHT in our case is much higher than that of ANS (at least 10 times to rule out the emission of ANS itself in solvent), k_1 can be approximated as a pseudo first order rate constant. Secondly, the back reaction rates are taken to be slow enough to consider two consecutive reactions to be irreversible, which is in agreement with a steady state approximation in the system. The assumption of an almost irreversible binding of the ligand ANS with the protein CHT is supported by the earlier experimental observation that the ligand is strongly bound to the protein over the 3.6-7.0 pH range which reveals a amalgamated protein-ligand complex [35]. A unique binding site of ANS to the protein in the pH range has been explored in a X-ray crystallographic study [26]. Considering the above conditions, one may write the time evolution of [C] in the following way [36],

$$[C] = a(1 + \frac{k_1 e^{-k_2 t} - k_2 e^{-k_1 t}}{k_2 - k_1}) \tag{6.1}$$

and the concentrations of the substrate (A) and intermediate (B) can be written as

$$[A] = a e^{-k_1 t} \tag{6.2}$$

$$[B] = \frac{ak_1}{k_2 - k_1}(e^{-k_1 t} - e^{-k_2 t}) \tag{6.3}$$

in which, a denotes the initial concentration of the enzyme CHT at time t = 0. Numerical fitting of the experimental data with equation (6.1) reveals a reasonable agreement with the analytical model of the intermediate state formation. In the case of pH 6.3, the k_1 and k_2 values were obtained to be 1000 s^{-1} and 36.7 s^{-1}, respectively. On the other hand, at pH 3.6, the numerical values of k_1 and k_2 were 14.2 s^{-1} and 14.5 s^{-1}, respectively. The above analytical and approximated solutions should now be compared to decide whether the steady state approximation is valid in the context of two pathways of molecular recognition of CHT at pH 6.3 and pH 3.6. In the former case (pH=6.3), first A transforms into B rapidly and B accumulates because it disappears slowly. As the concentration of A decreases, its rate of transformation decreases, at the same time the rate of concentration of B into C increases as more B is formed, so a maximum is reached when,

$$t = \frac{\ln(k_1 / k_2)}{k_2 - k_1} \tag{6.4}$$

provided $k_1 = k_2$, from then the concentration of B decreases as shown in Figure 6.3b. The observation is consistent with the fact that a pre-selected conformation of the enzyme CHT makes complexation with the ligand ANS "fast" and only then undergoes a structural reorganization, leading to the recognition pathway on the selected-fit mechanism [6, 37]. From the magnitude of the obtained pseudo-first order reaction rate to its corresponding second order rate constant we derive a value of 10^7 $M^{-1}s^{-1}$, which is consistent with that of the reported value [38]. The first order rate constant k_2, for the structural reorganization of the enzyme is also of the same order as the reported value [38] of 10-100 s^{-1}. In the latter case (pH=3.6), when the enzyme is less flexible and biologically inactive [26, 28], the pseudo first order rate constant k_1 is much slower than that of the former case. The estimated second order rate constant is ~1.4x10^5 M^{-1} s^{-1}, which is in agreement with weak binding of ANS to the enzyme CHT at the first stage [38]. Afterward, structural reorganization

follows a similar time constant, however, it is smaller in magnitude than in the

Table 6.1. *Numerically fitted kinetic parameters.*

Concentration ratio (CHT:ANS)	k_1 (s^{-1})	k_2 (s^{-1})
10:1 (pH 6.3)	1000	36.7
10:1.5 (pH 6.3)	715.1	23.3
10:2.5 (pH 6.3)	179.5	19.9
10:3 (pH 6.3)	62.7	17.1
10:1 (pH 3.6)	14.2	14.5

former case. The molecular recognition pathway involving much weaker binding at the first stage and complexation through structural reorganization is consistent with the induced-fit mechanism.

Experimental artefacts due to the dimerization of the probe ligand at lower pH in the observation of the differential pathways of molecular recognition can be ruled out for the following reasons. Careful experiments [39] show that the ligand remains in its monomeric form at ~100 μM at pH 3, 5 and 7. The concentration of ligand used in our experiment is around 10 μM. Moreover, in a control experiment on the complexation of ANS (anionic) with cationic CTAB micelles (inset of Figure 6.3c) under similar experimental conditions, we obtained k_1 and k_2 values of 1486 s^{-1} and 19.8 s^{-1}, respectively for pH 6.3, whereas at pH 3.6 the corresponding k_1 and k_2 values are 1076 s^{-1} and 10.0 s^{-1}, respectively. This observation clearly rules out the possibility of any interference of the host buffer (of different pH) values with the differential CHT-ANS complexation kinetics at the two different pH as discussed above. Conversion of the pseudo first order rate constant k_1, to its second order counterpart reveals a value of 10^4 M^{-1} s^{-1}, which is consistent with the reported value of molecular complexation of an organic ligand with a micelle [40]. The observed similarity of the kinetic pathway in the case of CTAB micelles at two different pH values is in agreement with recognition through a selected-fit mechanism, in which the spherically symmetric micelles are always ready (in

the pre-selected conformation) to recognize the ligand ANS at first with a minor structural adjustment (k_2) following thereafter. The first order rate constants k_2 (~10 s^{-1}) are also in agreement with the structural relaxation time scale of a micelle reported in the literature [41].

Various studies [42-43] have suggested that the protein-ligand binding mechanism can be shifted from selected-fit to induced-fit upon increasing ligand concentration because in the presence of a higher ligand concentration complexation becomes more favourable, assuming an enhanced probability of complexation before the conformational transition of the protein. However, these cannot be fully confirmed without additional information on protein ligand interaction and dynamical studies of the protein. Using a molecular dynamics simulation of a model protein–ligand system, Greives et al. have shown that both the rate of the conformational transition and the concentration of ligand molecules can affect the induced-fit fraction [44]. The effect of ligand concentration on the shifting binding mechanism can be easily understood from our experiments. The fluorescence micrographs of the microfluidics channel with different ligand concentrations are shown in Figure 6.4a. It is evident from the results shown in Figure 6.4b, that the selected fit mechanism at pH 6.3 is shifted towards the induced-fit mechanism with increasing ligand at a fixed protein concentration fixed. The numerical fitting of experimental data at various ligand concentrations with equation 6.1 reveals reasonable agreement with the fact that the increasing ligand concentration leads to changes from selected-fit to induced-fit behavior. The fitting parameters are tabulated in Table 6.1 within the experimental error (±8%). The protein conformations convert into the active one in the absence of any ligand molecule and then continue in the active conformation until a ligand molecule completes the binding reaction by complexation. At a low ligand concentration, the protein is free from any ligand molecule most of the time; thus the selected-fit mechanism dominates. At high ligand concentrations, conformational changes occur followed by binding processes because most of the time the ligand

molecule will be inside the binding pocket and thus, the binding mechanism will shift towards the induced-fit mechanism [44].

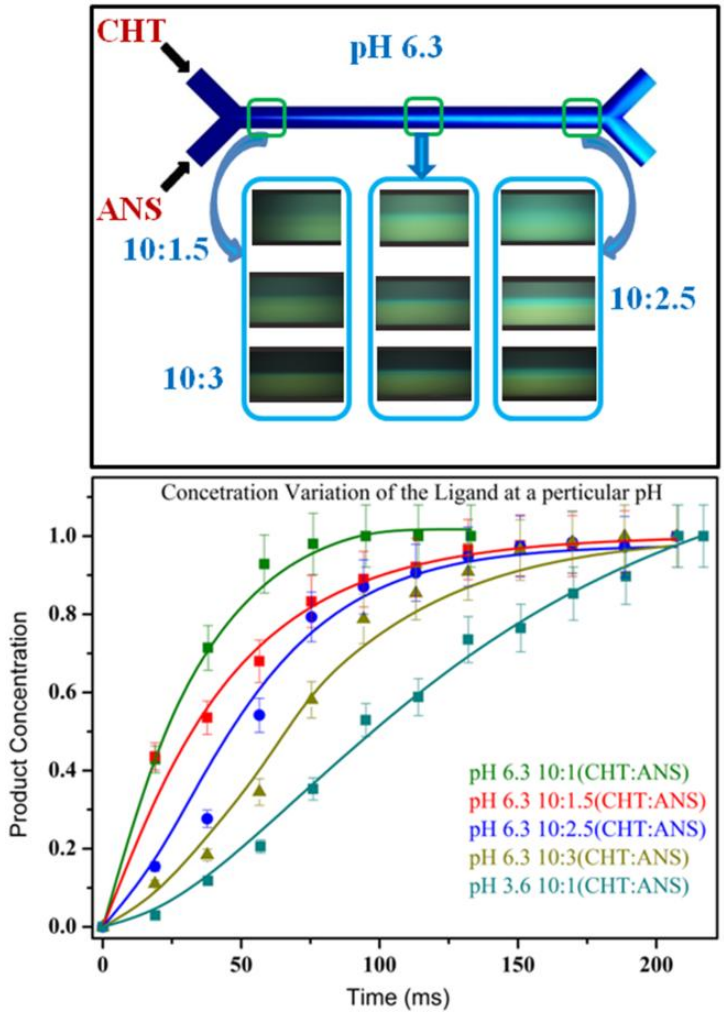

Figure 6.4. *Effect of ligand concentration on the binding mechanism (a) Micrographs of the microfluidics channel at different positions across the channel with different concentrations of ligand at a certain pH (6.3). (b) The comparison of normalised emission intensity of ANS upon binding with CHT along the microfluidics channel at different concentration of ANS at pH 6.3 and with pH 3.6.*

The experimentally observed differential molecular recognition pathways were simulated by using COMSOL Multiphysics (v4.3a) software by coupling the physics of laminar flow and reaction kinetics (Figure 6.5). A three-dimensional geometry was created based on the dimensions of the micro-channel used in our experiment-with two inlets and two outlets (H channel).

To consider species diffusion, the convection and diffusion model (transport of diluted species) was included is the fluid flow physics. The diffusion constants of CHT and ANS used were 0.5×10^{-10} m^2/s and 1×10^{-10} m^2/s, respectively as reported earlier [45-46]. The simulation was carried out with a

Table 6.2. *Kinetic parameters obtained from simulations with the COMSOL Multiphysics program.*

Concentration ratio (CHT:ANS)	k_1 (s^{-1})	k_2 (s^{-1})
10:1 (pH 6.3)	1000	29.9
10:1.5 (pH 6.3)	715.6	23.5
10:2.5 (pH 6.3)	165.5	20.3
10:3 (pH 6.3)	59.1	16.8
10:1 (pH 3.6)	14.2	14.4

flow of ANS through the lower inlet and CHT in the upper inlet. The simulation yielded a concentration profile of enzymes in the presence of a substrate gradient [47]. Figure 6.5 represents the inter-diffusional zone of the two interacting species along the channel at different times related to the spatial distribution of the interacting species at several positions in the reaction zone. For representation purpose, the initial, middle and final sections of the channel, where the simulation has been executed are shown. The inter-diffusion zone is critically governed by the molecular diffusivity of the individual species. Figure 6.5 represents a comparative observation of the rate if the fluorescence intensity changes due to the molecular recognition kinetics with diffusion limited by the molecular interaction. Figure 6.5a depicts a comparison of experimental data at pH 3.6 with the simulated data which is obtained from the induced-fit model. The contour plots representing the concentration of CHT-ANS complex at several positions along the channel and the colour bar represent the normalised concentration as shown in the insets 1, 2 and 3 of Figure 6.5(a). We have also compared the experimental data of pH 6.3 with molecular simulation data using the selected-fit model (Figure 6.5b).

By comparing the experimental results with the simulated results, one can see the interaction of ANS with CHT at different pH values follows different mechanisms. Our simulation results show that the interaction of the CHT enzyme with the ANS substrate follows the selected-fit mechanism at pH 6.3

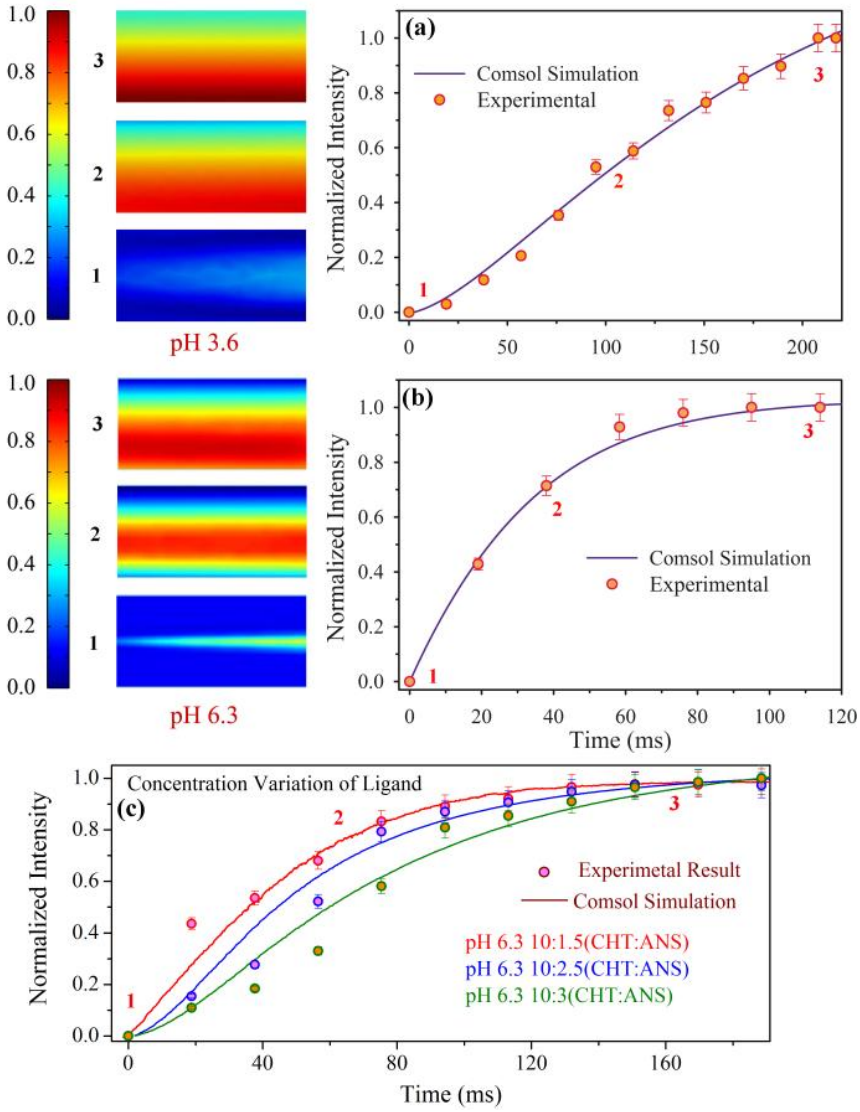

Figure 6.5. *Simulated results compared with experimental results. The simulated concentration gradient of the CHT–ANS complex at different pH values is shown in the left panel. The right panel shows the agreement of the simulation results (solid line) with that of the experimental data (scattered points) at different pH values. The shifting of the binding mechanism is shown with increasing ligand concentration at pH 6.3. Here, 1–3 represent contour plots of the complex formation at three different positions in the microfluidics channel.*

to yield k_1 and k_2 values of 1000 s^{-1} and 29.9 s^{-1}. On the other hand, at pH 3.6, k_1 and k_2 have values of 14.42 s^{-1} and 14.44 s^{-1}, respectively. A simulation of CHT enzyme with different concentration of ANS substrate at pH 6.3 as shown in Figure 6.5c yielded k_1 and k_2 values consisting with our experimental results (Table 6.2). With increasing ligand concentration a shifting of the binding mechanism can be observed by the sigmoidal shapes of the experimental data at pH 6.3. The simulated results also show sigmoidal shapes at higher concentration of the ligand although there are some deviations with the experimental results which are within the experimental error limit (±5%). Therefore, the simulated results are in reasonably good agreement with our experimental results, which suggests that the overall interaction of the ligand with the model biomimetic system can be described by simple reaction models. The molecular recognition of CHT with ANS is not simple diffusion limited but rather follows different mechanisms at different pH values [48].

6.3. Conclusion: We demonstrated two different pathways of molecular recognition of CHT by a small organic ligand ANS namely selected-fit (conformational selection) and induced-fit mechanisms in a microfluidics channel with two different pH values. While the structural flexibility of the protein at pH 6.3 triggers selected-fit, the restricted protein motion at pH 3.6 prompted the protein to adopt induced-fit of molecular recognition. We also showed that for a particular pH of 6.3 the increasing ligand concentration leads a change in binding mechanism from selected-fit to induced-fit at a fixed protein concentration. We correlated our experimental data with a simple analytical model and simulation that relyed on the steady state approximation for the generation of a product through intermediate species. Our finding might have an immediate and positive impact on efforts to designing and engineer proteins with new functions.

References

[1] D. Koshland Jr, Application of a theory of enzyme specificity to protein synthesis, *Proc. Natl. Acad. Sci. U. S. A.* **44**, (1958), 98.

[2] C.-J. Tsai, S. Kumar, B. Ma and R. Nussinov, Folding funnels, binding funnels, and protein function, *Protein Sci.* **8**, (1999), 1181.

[3] C. J. Tsai, B. Ma, Y. Y. Sham, S. Kumar and R. Nussinov, Structured disorder and conformational selection, *Proteins: Struct., Funct., Bioinf.* **44**, (2001), 418.

[4] K. A. Dill and H. S. Chan, From levinthal to pathways to funnels, *Nat. Struct. Biol.* **4**, (1997), 10.

[5] J. D. Bryngelson, J. N. Onuchic, N. D. Socci and P. G. Wolynes, Funnels, pathways, and the energy landscape of protein folding: A synthesis, *Proteins: Struct., Funct., Bioinf.* **21**, (1995), 167.

[6] T. R. Weikl and C. von Deuster, Selected- fit versus induced- fit protein binding: Kinetic differences and mutational analysis, *Proteins: Struct., Funct., Bioinf.* **75**, (2009), 104.

[7] C. Tang, C. D. Schwieters and G. M. Clore, Open-to-closed transition in apo maltose-binding protein observed by paramagnetic nmr, *Nature* **449**, (2007), 1078.

[8] Z.-L. Lu, M. Coetsee, C. D. White and R. P. Millar, Structural determinants for ligand-receptor conformational selection in a peptide g protein-coupled receptor, *J. Biol. Chem.* **282**, (2007), 17921.

[9] A. Mittermaier and L. E. Kay, New tools provide new insights in nmr studies of protein dynamics, *Science* **312**, (2006), 224.

[10] H. Frauenfelder, S. G. Sligar and P. G. Wolynes, The energy landscapes and motions of proteins, *Science* **254**, (1991), 1598.

[11] P. K. Agarwal, S. R. Billeter, P. R. Rajagopalan, S. J. Benkovic and S. Hammes-Schiffer, Network of coupled promoting motions in enzyme catalysis, *Proc. Natl. Acad. Sci. U. S. A.* **99**, (2002), 2794.

[12] K. Henzler-Wildman and D. Kern, Dynamic personalities of proteins, *Nature* **450**, (2007), 964.

[13] D. D. Boehr, H. J. Dyson and P. E. Wright, An nmr perspective on enzyme dynamics, *Chem. Rev.* **106**, (2006), 3055.

[14] A. C. M. Ferreon, J. C. Ferreon, P. E. Wright and A. A. Deniz, Modulation of allostery by protein intrinsic disorder, *Nature* **498**, (2013), 390.

[15] Lisa J. Lapidus, S. Acharya, Christian R. Schwantes, L. Wu, D. Shukla, M. King, Stephen J. DeCamp and Vijay S. Pande, Complex pathways in folding of protein g explored by simulation and experiment, *Biophys. J.* **107**, (2014), 947.

[16] M. Gruebele, Protein dynamics in simulation and experiment, *J. Am. Chem. Soc.* **136**, (2014), 16695.

[17] S. Choudhury, P. K. Mondal, V. K. Sharma, S. Mitra, V. G. Sakai, R. Mukhopadhyay and S. K. Pal, Direct observation of coupling between structural fluctuation and ultrafast hydration dynamics of fluorescent probes in anionic micelles, *J. Phys. Chem. B*, (2015).

[18] C. E. Cameron and S. J. Benkovic, Evidence for a functional role of the dynamics of glycine-121 of escherichia coli dihydrofolate reductase obtained from kinetic analysis of a site-directed mutant, *Biochemistry* **36**, (1997), 15792.

[19] G. P. Miller and S. J. Benkovic, Deletion of a highly motional residue affects formation of the michaelis complex for escherichia coli dihydrofolate reductase, *Biochemistry* **37**, (1998), 6327.

[20] L. Wang, N. M. Goodey, S. J. Benkovic and A. Kohen, Coordinated effects of distal mutations on environmentally coupled tunneling in dihydrofolate reductase, *Proc. Natl. Acad. Sci. U. S. A.* **103**, (2006), 15753.

[21] A. D. Vogt and E. Di Cera, Conformational selection is a dominant mechanism of ligand binding, *Biochemistry* **52**, (2013), 5723.

[22] A. D. Vogt and E. Di Cera, Conformational selection or induced fit? A critical appraisal of the kinetic mechanism, *Biochemistry* **51**, (2012), 5894.

[23] P. A. Romero and F. H. Arnold, Exploring protein fitness landscapes by directed evolution, *Nat. Rev. Mol. Cell Biol.* **10**, (2009), 866.

[24] S. Kumar, B. Ma, C. J. Tsai, N. Sinha and R. Nussinov, Folding and binding cascades: Dynamic landscapes and population shifts, *Protein Sci.* **9**, (2000), 10.

[25] W. A. Eaton, V. Muñoz, S. J. Hagen, G. S. Jas, L. J. Lapidus, E. R. Henry and J. Hofrichter, Fast kinetics and mechanisms in protein folding, *Annu. Rev. Biophys. Biomol. Struct.* **29**, (2000), 327.

[26] L. D. Weber, A. Tulinsky, J. D. Johnson and M. A. El-Bayoumi, Expression of functionality of. Alpha.-chymotrypsin. The structure of a fluorescent probe-. Alpha.-chymotrypsin complex and the nature of its ph dependence, *Biochemistry* **18**, (1979), 1297.

[27] P. Ball, Water as an active constituent in cell biology, *Chem. Rev.* **108**, (2008), 74.

[28] S. K. Pal, J. Peon and A. H. Zewail, Ultrafast surface hydration dynamics and expression of protein functionality: A-chymotrypsin, *Proc. Natl. Acad. Sci. U. S. A.* **99**, (2002), 15297.

[29] Y. Gambin, C. Simonnet, V. VanDelinder, A. Deniz and A. Groisman, Ultrafast microfluidic mixer with three-dimensional flow focusing for studies of biochemical kinetics, *Lab Chip* **10**, (2010), 598.

[30] S. J. DeCamp, A. N. Naganathan, S. A. Waldauer, O. Bakajin and L. J. Lapidus, Direct observation of downhill folding of λ-repressor in a microfluidic mixer, *Biophys. J.* **97**, (2009), 1772.

[31] S. Batabyal, S. Rakshit, S. Kar and S. K. Pal, An improved microfluidics approach for monitoring real-time interaction profiles of ultrafast molecular recognition, *Rev. Sci. Instrum.* **83**, (2012), 043113.

[32] S. M. Sullivan and T. Holyoak, Enzymes with lid-gated active sites must operate by an induced fit mechanism instead of conformational selection, *Proc. Natl. Acad. Sci. U. S. A.* **105**, (2008), 13829.

[33] T. Kiefhaber, A. Bachmann and K. S. Jensen, Dynamics and mechanisms of coupled protein folding and binding reactions, *Curr. Opin. Struct. Biol.* **22**, (2012), 21.

[34] E. Kim, S. Lee, A. Jeon, J. M. Choi, H.-S. Lee, S. Hohng and H.-S. Kim, A single-molecule dissection of ligand binding to a protein with intrinsic dynamics, *Nat. Chem. Biol.* **9**, (2013), 313.

[35] J. D. Johnson, M. A. El-Bayoumi, L. D. Weber and A. Tulinsky, Interaction of. Alpha.-chymotrypsin with the fluorescent probe 1-anilinonaphthalene-8-sulfonate in solution, *Biochemistry* **18**, (1979), 1292.

[36] P. Atkins and J. de Paula, 7th ed., Oxford University Press, New York, **2002**, pp. 883.

[37] D. D. Boehr, R. Nussinov and P. E. Wright, The role of dynamic conformational ensembles in biomolecular recognition, *Nat. Chem. Biol.* **5**, (2009), 789.

[38] H. R. Bosshard, Molecular recognition by induced fit: How fit is the concept?, *Physiology* **16**, (2001), 171.

[39] M. Andujar- Sánchez, V. Jara- Perez, E. S. Cobos and A. Cámara- Artigas, A thermodynamic characterization of the interaction of 8- anilino- 1- naphthalenesulfonic acid with native globular proteins: The effect of the ligand dimerization in the analysis of the binding isotherms, *J. Mol. Recognit.* **24**, (2011), 548.

[40] M. Novo, D. Granadero, J. Bordello and W. Al-Soufi, Host–guest association studied by fluorescence correlation spectroscopy, *J. Inclusion Phenom. Macrocyclic Chem.* **70**, (2011), 259.

[41] K. D. Danov, D. S. Valkovska and P. A. Kralchevsky, Adsorption relaxation for nonionic surfactants under mixed barrier-diffusion and micellization-diffusion control, *J. Colloid Interface Sci.* **251**, (2002), 18.

[42] G. G. Hammes, Y.-C. Chang and T. G. Oas, Conformational selection or induced fit: A flux description of reaction mechanism, *Proc. Natl. Acad. Sci. U. S. A.* **106**, (2009), 13737.

[43] K. G. Daniels, N. K. Tonthat, D. R. McClure, Y.-C. Chang, X. Liu, M. A. Schumacher, C. A. Fierke, S. C. Schmidler and T. G. Oas, Ligand concentration regulates the pathways of coupled protein folding and binding, *J. Am. Chem. Soc.* **136**, (2013), 822.

[44] N. Greives and H.-X. Zhou, Both protein dynamics and ligand concentration can shift the binding mechanism between conformational selection and induced fit, *Proc. Natl. Acad. Sci. U. S. A.* **111**, (2014), 10197.

[45] E. N. Vasina and P. Déjardin, Adsorption of α-chymotrypsin onto mica in laminar flow conditions. Adsorption kinetic constant as a function of tris buffer concentration at ph 8.6, *Langmuir* **20**, (2004), 8699.

[46] A. Qadeer, G. Rabbani, N. Zaidi, E. Ahmad, J. M. Khan and R. H. Khan, 1-anilino-8-naphthalene sulfonate (ans) is not a desirable probe for determining the molten globule state of chymopapain, *PloS one* **7**, (2012), e50633.

[47] S. Sengupta, K. K. Dey, H. S. Muddana, T. Tabouillot, M. E. Ibele, P. J. Butler and A. Sen, Enzyme molecules as nanomotors, *J. Am. Chem. Soc.* **135**, (2013), 1406.

[48] S. Choudhury, S. Batabyal, P. K. Mondal, P. Singh, P. Lemmens and S. K. Pal, Direct observation of kinetic pathways of biomolecular recognition, *Chem. Eur. J.* **21**, (2015), 16172.

Chapter 7

Spectroscopic investigation on the role of ultrafast allostery in specific protein-DNA recognition

7.1. Introduction: The dynamic nature of proteins and the implications for function are increasingly being appreciated [1]. The native state is now considered as a collection of energetically low-lying states with distinct conformation and dynamics, with rapid inter-conversion between them. These distinct states have detectable motions on many time-scales, including sub-nanosecond time-scales [2]. However, little is known about their functional significance. One protein function that is definitely affected by the protein dynamics, is the phenomenon of allostery [3-4]. Allosteric regulation of proteins by binding of effector molecule/macromolecules at a site other than active site has become a powerful mechanistic pathway in order to explain complex biochemical reaction following the seminal work of Monod and other investigators [5-7]. Although traditional models of allostery involve significant conformational changes, there is increasing evidence that the allostery can be mediated solely internal protein dynamics without significant conformational changes [8-12]. An early seminal work by Cooper and Dryden clearly demonstrated that the effect arises out of possible changes in both high-frequency anharmonic and low-frequency highly correlated motions of individual atoms in response to the effector binding [13-14]. In reality, effector induced changes to both the mean conformation and dynamics are to be expected [15-17].

Transcription factors from a notable class of proteins where allostery plays an important role. Allostery in transcription factors is mostly known for small molecules that induces change in transcription regulatory properties of transcription factors [18]. A few cases have been reported in which the DNA sequence itself plays the role of an allosteric ligand and changes the functional outcome in terms of gene regulation [19]. However, little is known about the role of dynamics in such

situations. Because transcription factors bind to a large number of sequences in the genome and affect the final outcome in a sequence-dependent manner, we decided to explore how two distinct DNA binding sequences affect the protein dynamics. In this study, we have used *E. coli* galactose repressor (GalR) as a model protein and its two operator target sequences O_E and O_I as effectors. O_E is immediately upstream to two promoters P_1 and P_2 of gal operon; O_I is separated from O_E by 114 bp and is in fact located inside the first structural gene, GalE [20]. GalR, like other DNA binding proteins, possesses a helix-turn-helix motif [21] and represses transcription upon binding to the two separated operator sites [20, 22], O_E and O_I. Useful feature of the repressor protein is that it is in the class of single tryptophan residue containing protein (Trp165), and thus offers excellent opportunity for the spectroscopic investigation of the intrinsic tryptophan probe. Much evidence suggests that the binding of the repressor protein to the target DNA sequences is a dimer [19, 23-24]. Although high resolution X-ray crystallographic/NMR structures of the repressor protein (GalR) and its complexes are not available, the protein is concluded to be similar in structure and function to another repressor protein, the Lac-repressor [25-27]. We constructed a homology model of GalR by using the I-TASSER serve [28]. It is very likely that binding of the GalR dimer to the operator DNAs (O_E and O_I) facilitate conformational and dynamical changes, thereby leading to allosteric interactions involving additional protein-protein or protein-DNA interactions for the tetramerization of DNA-bound GalR dimers to form a DNA loop [26, 29].

We used the single tryptophan (Trp165) of the GalR dimer as intrinsic fluorescent probe. Polarization gated fluorescence spectroscopy of Trp165 reveals the changes in local fluctuation of the protein upon interaction with operator DNAs. FRET from Trp165 to a covalently labeled cysteine-reactive extrinsic probe IAEDANS [5-({2-[(iodoacetyl)amino]ethyl}amino)naphthalene-1-sulfonic acid] at the C-terminal [30] explored intra-protein dynamics of the protein and its complexes. Polarization gated picosecond resolved fluorescence studies of AEDANS were performed to observe the significant structural rearrangement in the C-terminal domain (active site) of the repressor protein upon protein-DNA complexation

(effector site). In order to reconfirm the location of the AEDANS and structural differences between GalR-O_E / O_I complexes, we used FRET from AEDANS (donor) to the acceptor FITC (fluorescein-5-isothiocyanate) attached with the operator DNA, which is bound to N-terminal domain of the GalR [31-32]. The distribution of the donor−acceptor distances in the protein-DNA complexes clearly revealed change in overall protein dynamics upon interaction with the different operator DNAs. Clearly, our results provide an idea of structural and dynamical change of GalR upon recognition of different DNA sequences, which is crucial for deeper understanding of protein dynamics in allosteric driven protein-protein interaction to form a DNA loop.

7.2. Results and discussion:

7.2.1. Modulation of ultrafast conformational dynamics in allosteric interaction of Gal repressor protein with different operator DNA sequences: The steady state emission spectra of Trp165 in Gal-repressor protein dimer (GalR) and AEDANS labeled GalR are shown in Figure 7.1a upon excitation at 283 nm. AEDANS bound to GalR has a large overlap in its excitation spectra with the Trp165 of unlabeled GalR emission spectra, reflects the high possibility of serving as a good donor–acceptor (D–A) pair as shown in the inset of Figure 7.1b (overlap integral value of 4.22×10^{14} M^{-1} cm^{-1} nm^4). The decrease in steady-state fluorescence of Trp165 in AEDANS labeled GalR relative to that of unlabeled GalR reveals an energy transfer from Trp165 (donor) to the AEDANS (acceptor) through dipole−dipole coupling as evident from Figure 7.1a. Picosecond resolved fluorescence transients of Trp165 at 350 nm (excitation at 283 nm) in the native GalR and AEDANS labeled GalR are shown in the Figure 7.1b. A significant faster component of 110 ps (33%) in the time resolved fluorescence decay of the Trp165 residue in case of AEDANS labeled GalR compared to native GalR (two longer time components) is clearly evident from the figure. The average life-time of Trp165 decreased from 2.30 ns in GalR to 1.15 ns in AEDANS labeled repressor as tabulated in Table 7.1. The energy transfer efficiency was calculated to be 50% following the procedure detail described in section 2.5.1

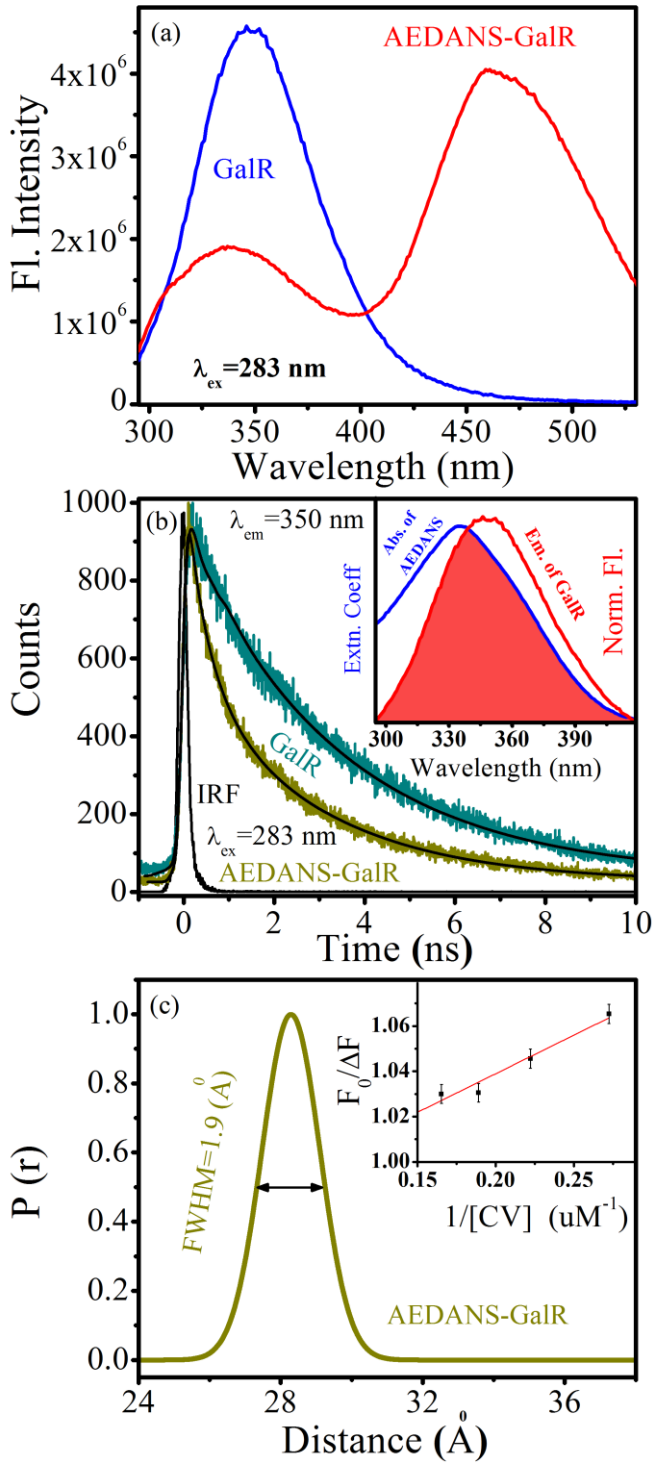

Figure 7.1. *(a) Steady state emission spectra of Trp165 in GalR and AEDANS labeled GalR (excitation at 283 nm). (b) Picosecond resolved fluorescence transients of Trp165 in GalR in absence and presence of AEDANS. Inset shows the spectral overlap of Trp165 emission and AEDANS absorption. (c) Distribution of donor−acceptor distances in labeled GalR. Inset shows modified Stern-Volmer plot of $F_0/\Delta F$ against 1/[CV] for the AEDANS quenching with different concentration of CV. Straight line the linear with 0.5% error, yields intercept 0.97. F_0 is the initial fluoroscence and ΔF= F_0-observed fluoroscence at a perticular quencher concentration.*

and as a consequence both the calculated Förster distance (R_0) and Trp165–AEDANS distance are found to be same which is 28.3 Å. Homology modeled structure of GalR (performed with I-tasser software) [28] with the tryptophan and cysteine residues highlighted is shown in Figure 7.2. It is evident from the modeled structure that the distance between Cys155 and Trp165 is 26.33 Å. Our experimental observation of

Table 7.1. *The fluorescence lifetimes (τ_i) of tryptophan residue in different systems. λ_{em}=350 nm λ_{ex}=280 nm.*

System	τ_1 (%) ps	τ_2 (%) ns	τ_3 (%) ns	τ_{avg} ns
GalR	280 (33)	3.33 (67)	-	2.30
GalR-AEDANS	110 (33)	0.49 (33)	2.79 (34)	1.15
GalR-O_E	220 (40)	3.06 (60)	-	1.92
O_E-GalR-AEDANS	70 (85)	2.20 (15)	-	0.39
GalR-O_I	190 (45)	2.32 (53)	-	1.36
O_I-GalR-AEDANS	70 (87)	2.23 (13)	-	0.28

Trp165- AEDANS distance (28.3 Å) indicates that the probe (AEDANS) is specifically attached to Cys155 (Figure 7.2), thus ruling out the possibility of inter-protein FRET. The distribution of donor−acceptor distances in the labeled protein [33] (without interaction of operator DNA) having the full width half maxima (FWHM) of 1.9 Å. In order to investigate heterogeneity in the AEDANS labeling to cysteine residues in GalR protein, we have performed the well known fluorescence quenching experiment [34-35]. Using crystal violet (CV) as the fluorescence quencher of AEDANS due to excited state energy transfer from AEDANS to CV, we have obtained a series of steady state emission spectra of has also been shown in Figure 7.1c revealing the internal fluctuation of the native AEDANS labeled GalR protein with increasing concentration of CV. Inset of Figure 7.1c shows the constructed modified Stern-Volmer plot of $F_0/\Delta F$ against 1/[CV] with a intercept of 0.97. The observation indicates that 97% of the fluorescence of the probe AEDANS is explicitly from one type of environment, consistant with the fact that the probe essentially attached to one cystein residue i.e. Cys155.

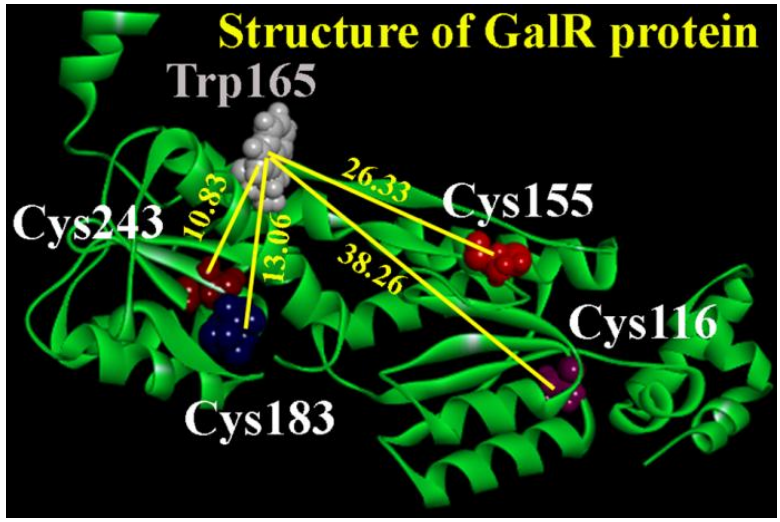

Figure 7.2. *Homology model of GalR showing the distances [Å] between the tryptophan and cysteine residues.*

In order to study protein dynamics alteration of GalR upon recognition of different DNA sequences of O_E and O_I operators, we have employed FRET study of unlabeled O_E/O_I bound AEDANS labeled GalR relative to that of unlabeled GalR as shown in Figure 7.3a and Figure 7.3b respectively. A sub-hundred picosecond (70 ps) component arises for both O_E and O_I cases as a consequence of efficient energy transfer from tryptophan to AEDANS might be due to crucial rearrangement of protein conformation in the C-terminal domain to bring Trp165 and AEDANS in close proximity for both the cases (Table 7.1). The calculated Trp165–AEDANS distance for the two complexes, GalR-O_E and GalR-O_I are found to be 20.5 Å and 20.7 Å, respectively and R_0 values are 28.3 Å for both the GalR-O_E and GalR-O_I systems. The distribution of donor−acceptor distances in the operator bound AEDANS labeled protein has also been calculated and shown in Figure 7.3c revealing the relatively less broadening in the case of operator bound GalR compared to native GalR. Although O_E and O_I bind to the GalR with similar affinity, there is small but comparatively different distance distribution for the two protein-DNA complexes. The observation indicates that the domain fluctuation is relatively less in the O_I complex (FWHM = 1.1 Å) than in the O_E complex (FWHM = 1.2 Å) [36]. Actually, DNA binding (to protein) 'repairs' the packing defect of tightly packed

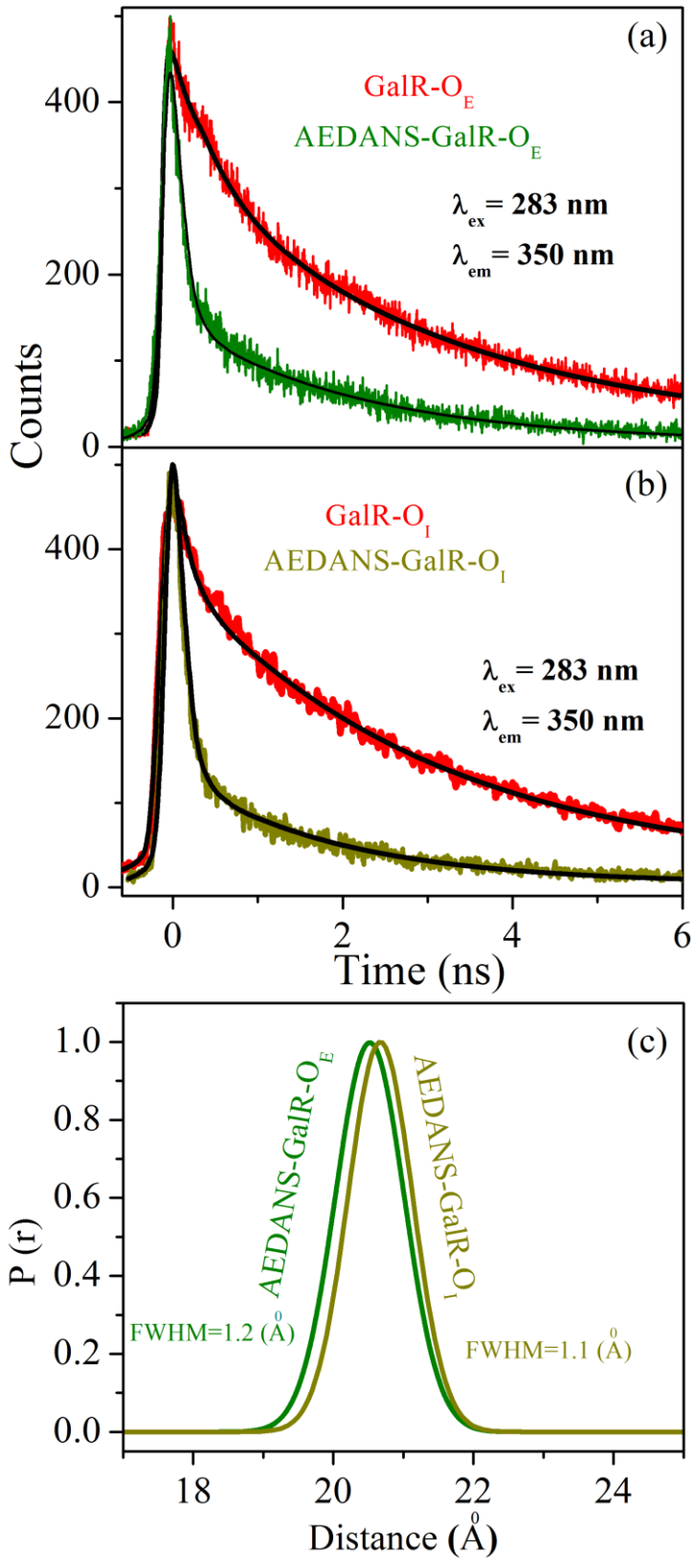

Figure 7.3. *(a) Picosecond resolved fluorescence transients of Trp165 in unlabeled and labeled GalR in presence of O_E operator DNA. (b) Picosecond resolved fluorescence transients of Trp165 in unlabeled and labeled GalR in presence of O_I operator DNA. (c) Distribution of donor−acceptor distances in both O_E/O_I-repressor complexes.*

protein, thus leading to global protein fluctuation with associated entropy loss [6, 37]. In principle, the entropic contribution includes changes both in its internal conformational entropy and in translational and rotational entropy [38-40]. Earlier reported simulation [41] and experimental [42] studies indicate that protein domain fluctuation could reflect significant residual conformational entropy.

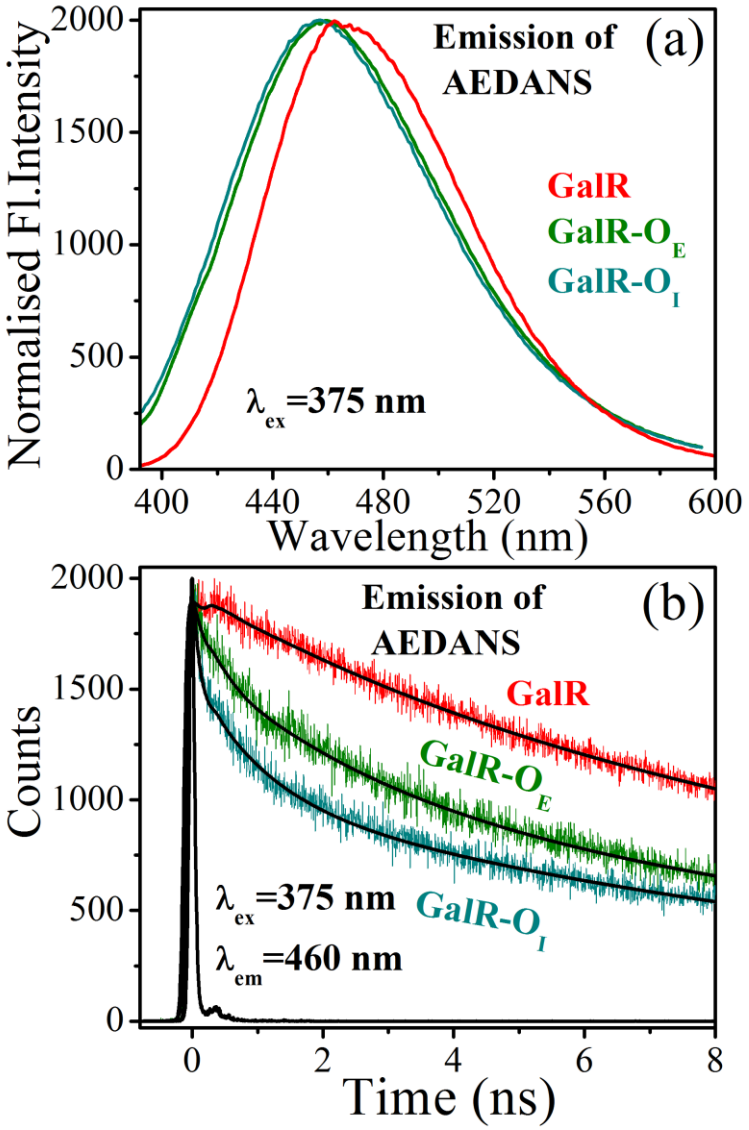

Figure 7.4. *(a) Steady state emission spectra of AEDANS attached with both GalR and O_E/O_I bound Gal repressor complexes (excitation at 375 nm). (b) Fluorescence transient of AEDANS in labeled GalR and O_E/O_I-Gal repressor complexes.*

For further confirmation of the structural fluctuation of the GalR protein upon interaction with operator DNA, we performed steady state and dynamical studies of

the AEDANS attached to Cys155, residing in the C-terminal domain of GalR. Figure 7.4a shows emission spectra of AEDANS present in both GalR and O_E/O_I bound GalR. A slight blue shift in emission spectra of AEDANS (excitation at 375 nm) in the O_E/O_I–GalR complexes (457 nm) compared to the probe in native GalR (461 nm) confirms the shifting of the probe towards the less polar environment of the dimer protein molecule [43]. Insignificant difference between the emission spectra of the probe in the O_E–GalR and O_I–GalR complexes is consistent with the fact that the immediate environment of the AEDANS remains similar in both the complexes. The fluorescence transients of AEDANS detected at 460 nm (excitation at 375 nm) in native GalR and O_E/O_I bound GalR complexes as depicted in Figure 7.4b. The fluorescence decay of AEDANS labeled GalR–O_I complex (90 ps, 42%) is found to be faster compared to those in the case of AEDANS labeled GalR-O_E (260 ps, 30%) complex (Table 7.2), similar to tryptophan residue fluorescence transient detected at 350 nm (Table 7.1). The faster decay of AEDANS in the labeled GalR in presence of O_E/O_I DNA clearly reveals a structural fluctuation in the C-terminal domain of the repressor protein. A clear differential excited state dynamics of AEDANS at the C-terminal of GalR upon interaction with two different operator DNAs is evident from our experiment. It has to be noted that the shorter excited state lifetime of AEDANS in GalR upon recognition with O_I compared to those with O_E could also

Table 7.2. *The fluorescence lifetimes (τ_i) of AEDANS attached to Cysteine residue in different systems. λ_{em}=460 nm λ_{ex}=375 nm.*

System	τ_1 (%) ps	τ_2 (%) ns	τ_3 (%) ns	τ_{avg} ns
AEDANS-GalR	-	1.63 (16)	15.42(84)	13.21
AEDANS-GalR-O_E	260 (30)	2.80 (27)	15.90 (43)	7.70
AEDANS-GalR-O_I	90 (42)	1.00 (21)	12.50 (37)	4.80

be due to excited state electron transfer dynamics [44], which are also significantly different for recognition by two operators.

In order to study rotational flexibility of the native and operator bound protein, we have investigated the polarization gated fluorescence spectroscopy of

AEDANS in GalR in absence and presence of O_E and O_I operator DNA as shown in Figure 7.5. Numerical fitting of fluorescence anisotropy of GalR protein with multi exponential decay function reveals 100 ps (9%), 1.0 ns (13%) and 30 ns (78%). While the first two time components are due to local motion of the probe attached to GalR , the 30 ns component is consistent with a global tumbling motion of the protein [19].

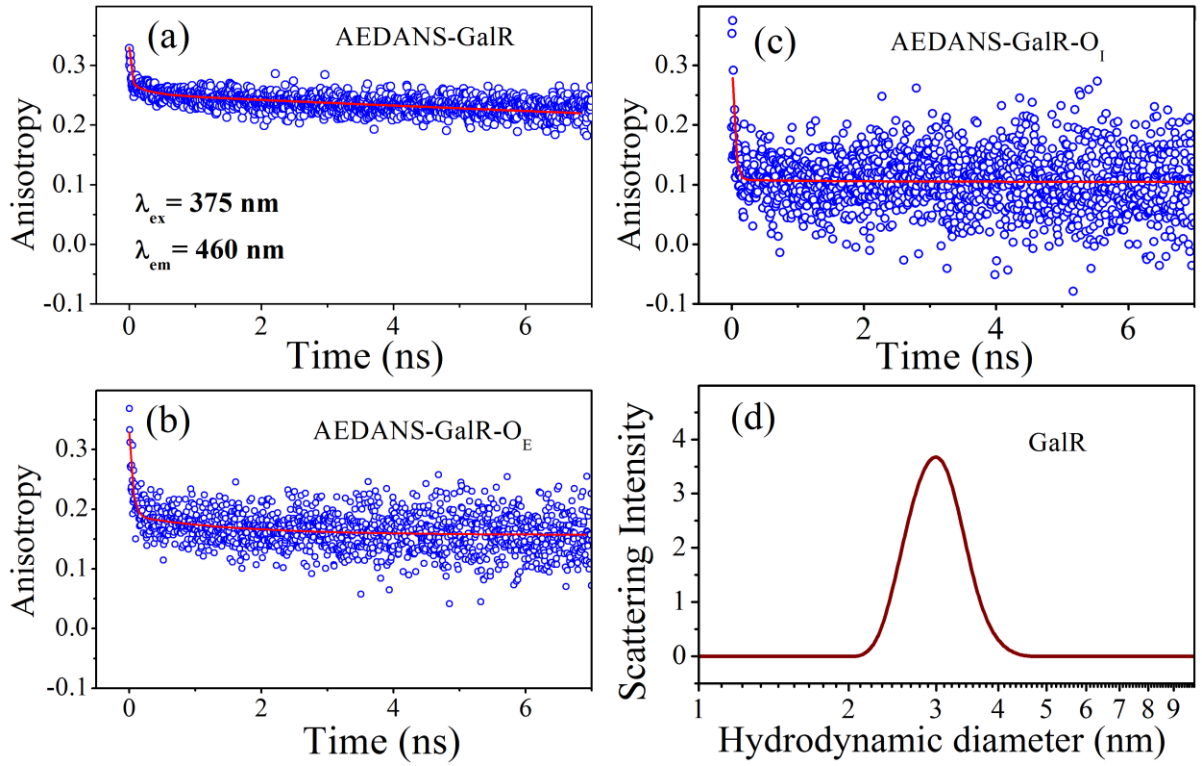

Figure 7.5. *Fluorescence anisotropy of AEDANS in (a) labeled GalR (b) labeled GalR- O_E operator DNA complex and (c) labeled GalR- O_I operator DNA complex. (d) Typical DLS signals (scattering intensity) for GalR protein is presented. Excitation at 375 nm and emission at 460 nm for all the systems.*

We have fixed the longer time constant of 30 ns during the fitting. Upon complexation with O_E operator DNA the local motion of the probe is represented by two time constantans of 50 ps (37%) and 200 ps (20%) as shown in Table 7.3. However, in case of O_I complexation local motion is merged to one component of 50 ps. The observation clearly indicates that the flexibility of the AEDANS (bound to cysteine residue) in the C-terminal domain of GalR protein upon complexation with O_I operator is much higher than that of O_E operator DNA complex (Figure 7.5). It is

Table 7.3. *Rotational time scales of AEDANS attached to Cysteine residue in different systems. λ_{em}=460 nm and λ_{ex}=375 nm.*

System	τ_1 (%) ps	τ_2 (%) ns	τ_3 (%) ns
AEDANS-GalR	100 (9)	1.0 (13)	30.0 (78)
AEDANS-GalR-O_E	50 (37)	0.20 (20)	30.0 (43)
AEDANS-GalR-O_I	50 (58)	30.0 (42)	-

worth mentioning that the broader domain fluctuation as measured from Trp165-AEDANS FRET distance distribution in the case of GalR-O_E complex is not due to the local physical motion of energy acceptor (AEDANS) as the local motion is slower compared to that in GalR-O_I complex. We have observed that the local motion of the energy donor Trp165 remains unaltered in the case of GalR upon complexation with both the operator DNA O_E and O_I. While the domain fluctuation is higher in case of O_E complex due to larger contribution from conformation entropy, particular residue fluctuation is higher in case of O_I complex could be due to rotational entropy contribution [38, 45]. Both the fluctuations are very crucial in case of allosteric signalling with GalR protein for higher order protein-protein interaction (tetramerization) through loop formation as deletion/substitution of either O_E or O_I is reported to make the GalR protein ineffective in repression [22].

For further confirmation of the AEDANS bound cysteine location with respect to the operator DNA, we performed FRET studies from AEDANS to FITC attached to the operator DNA, as depicted by Figure 7.6a and 7.6b. A strong spectral overlap (overlap integral value of 1.32×10^{15} M^{-1} cm^{-1} nm^4) of the emission spectra

Table 7.4. *The fluorescence lifetimes (τ_i) of AEDANS attached to Cysteine residue in absence and presence of FITC for different systems. λ_{em}=460 nm and λ_{ex}=375 nm.*

System	τ_1 (%) ps	τ_2 (%) ns	τ_3 (%) ns	τ_{avg} ns
AEDANS-GalR- O_E	260 (30)	2.80 (27)	15.90 (43)	7.70
AEDANS-GalR-O_E-FITC	70 (45)	1.05 (24)	10.00 (31)	3.45
AEDANS-GalR-O_I	90 (42)	1.00 (21)	12.50 (37)	4.80
AEDANS-GalR-O_I-FITC	70 (55)	0.86 (21)	8.78 (24)	2.31

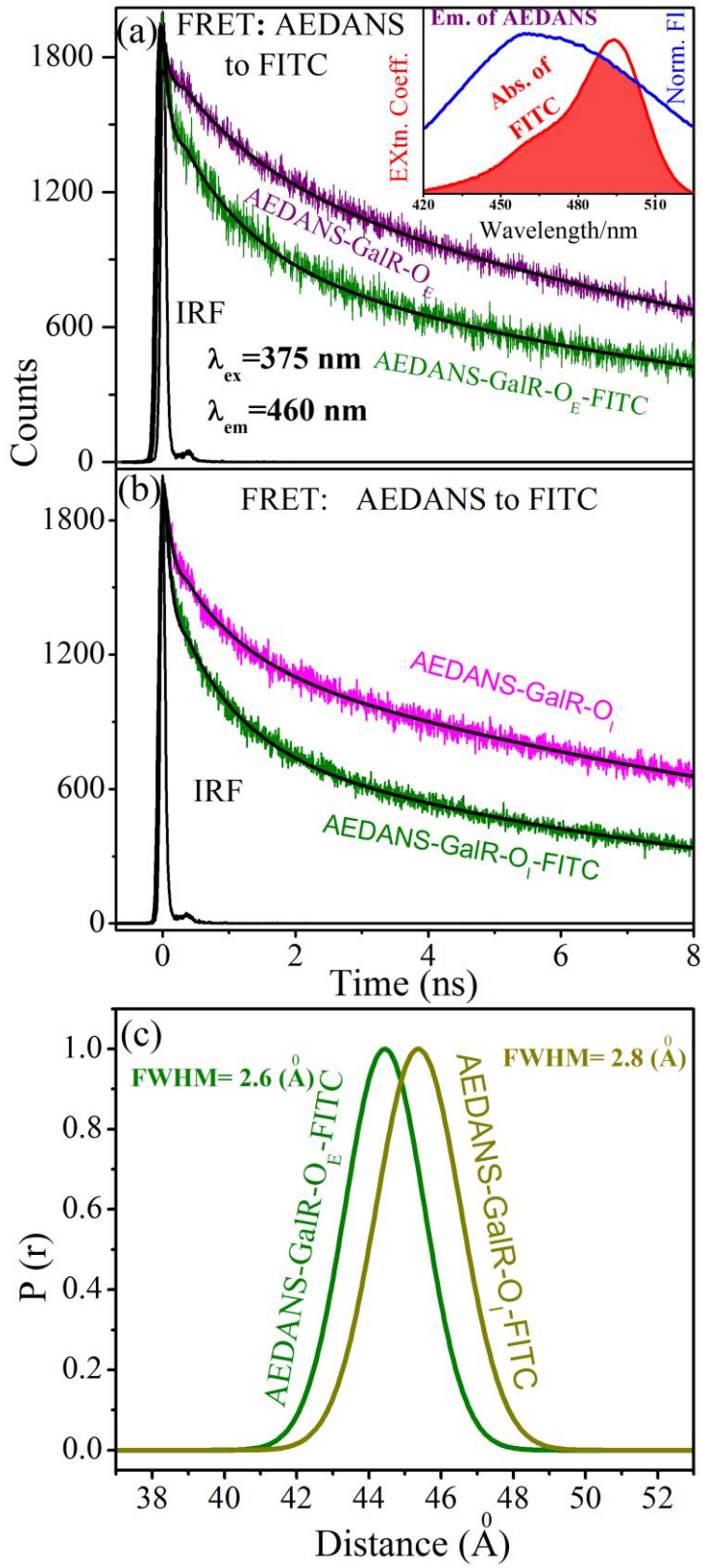

Figure 7.6. *(a) Fluorescence transient of AEDANS in the GalR at 460 nm before and after complexation with FITC labeled O_E operator DNA. (b) Fluorescence transient of AEDANS in the GalR at 460 nm before and after the complexation with FITC labeled O_I operator DNA. (c) Distribution of donor−acceptor distances in both FITC O_E/O_I- labeled Gal repressor complexes.*

of AEDANS in GalR with the absorption spectrum of FITC in O_E operator DNA reveals the possibility of energy transfer from AEDANS to FITC (Inset of Figure 7.6a). The overlap for the O_I complex remains almost same (overlap integral value of 1.52×10^{15} M^{-1} cm^{-1} nm^4). A significantly faster component of 70 ps (45%) of AEDANS arises in case of FITC labeled O_E operator-repressor complex transient detected at 460 nm compared to O_E operator-repressor complex clearly indicate energy transfer from AEDANS to FITC (Table 7.4). In the case of FITC labeled O_I-repressor complex the faster component is found to be 70 ps (55%). The distances between AEDANS-FITC in repressor- O_E/O_I complexes were found to be 44.1 Å and 45.5 Å, respectively and R_0 values are 45.97 Å for both systems. It has to be noted that the overall hydrodynamic diameter of the protein GalR is 3.1 nm (Figure 7.5d)

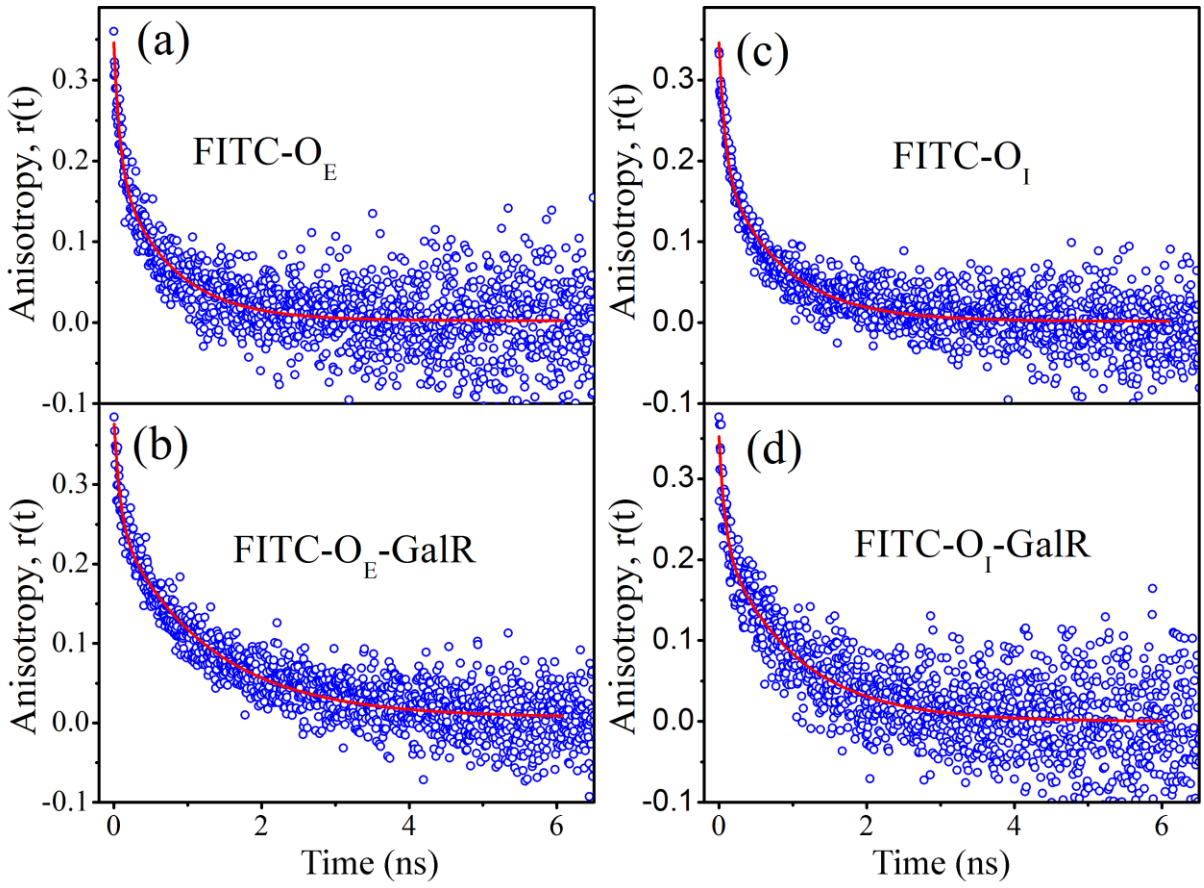

Figure 7.7. *Fluorescence anisotropy of FITC in (a) O_E operator DNA (b) GalR- O_E operator DNA complex and (c) O_I operator DNA and (d) GalR- O_I operator DNA complex. (Excitation at 445 nm and emission at 520 nm for all the systems).*

and considering the linker length 7.4 Å (for AEDANS) and 7.3 Å (for FITC) the total distance from AEDANS to FITC was calculated to be 45.7 Å, which is comparable to our measurements. Our results are also similar to the steady state FRET study performed by Adhya et al. showing the distance between C-terminal of GalR to the probe in the operator DNA is 38.6 Å [46]. In our study small but comparatively different FRET distances from AEDANS to FITC for two operator DNA-repressor complexes is evident. The difference could be due to recognition of different operator DNA which induces conformational change in the C-terminal, transmitted from N-terminal for two complexes. Taken together, the results confirm the location of the covalently attached AEDANS with cysteine residue, situated 20.5/20.7 Å from the tryptophan residue and 44.1/45.5 Å from the FITC in operator DNA for O_E - GalR/O_I-GalR complexes. We have also calculated the donor (AEDANS)–acceptor (FITC) distance distribution for the O_E/O_I-GalR complexes as shown in Figure 7.6c. Little broader distribution in case of O_I complex (FWHM = 2.8 Å) compared to O_E complex (FWHM= 2.6 Å) can be rationalised in terms of dynamical fluctuations (residual) of the host repressor protein. It has to be noted that the broadening of donor-acceptor distances might arise from the flexibility of the FITC probe in the operator DNA, which has little relevance to the intra-protein dynamics upon complexation. In order to rule out the contribution solely from the

Table 7.5*. Rotational time scales of FITC attached to O_E/O_I operator DNA in different systems. λ_{em}=520 nm and λ_{ex}=445 nm.*

System	τ_1 (%) ps	τ_2 (%) ns	τ_3 (%) ns
FITC-O_E	80 (44)	0.70 (55)	30.0 (1)
FITC-O_E- GalR	80 (12)	1.20 (85)	30.0 (3)
FITC-O_I	80 (43)	0.80 (56)	30.0 (1)
FITC-O_I- GalR	80 (36)	1.00 (63)	30.0 (1)

FITC, which is covalently attached to operator DNA in the AEDANS-FITC distance distribution, we have investigated polarization gated fluorescence of FITC upon complexation with GalR as shown in Figure 7.7. Anisotropy decays of FITC in both

O_E and O_I operator DNA (in absence of GalR protein) showed restriction in dynamics (from 700-800 ps to 1-1.2 ns) upon complexation with the repressor protein. Details of the time constants are shown in Table 7.5, thus revealing similar kinds of protein binding to both the DNAs. The overall picture which emerges from our studies is depicted in Figure 7.8.

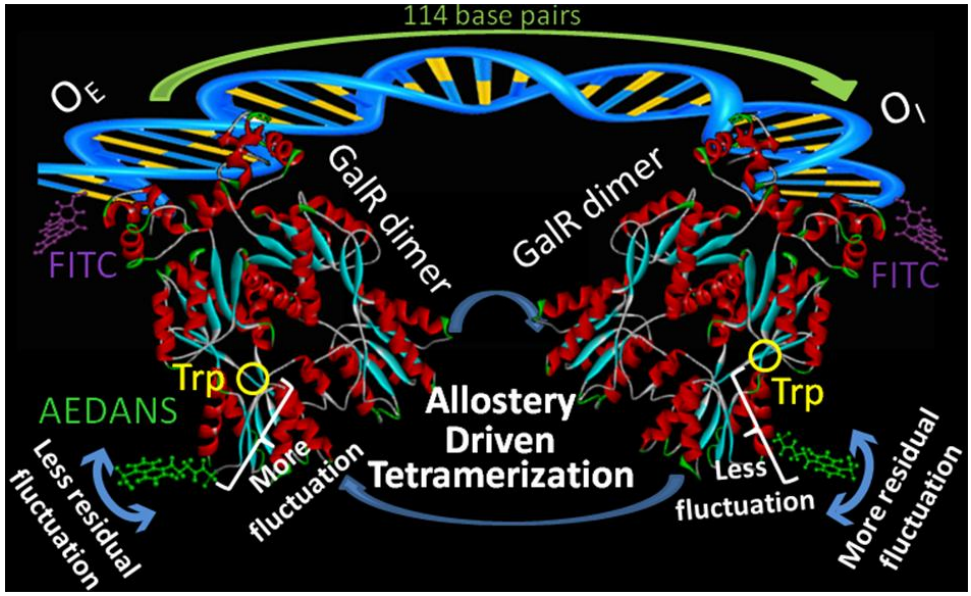

Figure 7.8. *Schematic representation of operator DNA (O_E/ O_I) bound Gal repressor protein dimer undergoing allostery-driven tetramerization. O_E operator DNA induces more domain fluctuation in the protein compared to O_I. On the other hand flexibility around AEDANS is more in case of O_I-protein dimer complex than that of O_E complex.*

7.3. Conclusion: It is increasingly clear that DNA sequences acts as allosteric ligand, in addition to its role as an anchoring point for the transcription factor. In the glucocorticoid receptor system, the DNA sequence affects the conformation and the functional outcome [47]. However, not much is known about the role of protein dynamics. Recent studies suggest that dynamics plays a role in DNA sequence dependent allostery in the lambda system as well [19]. Studies of sub-nanosecond dynamics of the repressor protein GalR upon interaction with operator DNA sequences O_E and O_I raise the possibility that key ultrafast time scales of the protein fluctuations are involved in the allosteric regulation of consequent protein-protein interaction. These studies attempt to link structural and dynamical features for the allostery driven tetramerization for a higher order nucleoprotein complex that

represses transcription of Gal operon in *E. coli* involving a DNA loop encompassing the promoter segment.

The structural aspects of the protein-DNA complexes were measured using picosecond resolved FRET, which probes distance between two fluorophore and their structural fluctuation. The studies of FRET from intrinsic Trp165 to an extrinsic probe AEDANS at the C-terminal of model allosteric repressor protein GalR reveal that intra protein fluctuation upon binding with O_I is less than that with O_E. However, for FRET between AEDANS and another extrinsic probe FITC in the operator DNAs the faster fluctuation in case of GalR-O_I complex is reflected. The differential overall protein dynamics upon interaction with DNAs of different sequence is perhaps the key feature in recognizing two C-terminal of the same protein for its biological function.

The flexibility of the C-terminal domain of the protein GalR was measured using picosecond resolved polarization gated fluorescence spectroscopy, which proves the motion of the covalently attached AEDANS to the active site (C-terminal) much away from effector site (N-terminal) of GalR. Faster orientational motions of AEDANS in GalR upon recognition with O_I compared to those with O_E are distinct from our study. For lambda repressor, we have previously shown that DNA sequences affect the protein-protein interaction through a distant domain and the protein dynamics changes concurrently. Whether these two have causal relation is not known, but appears to be likely [19, 48]. Thus differential flexibility at the active site of the protein upon recognition with two different DNA sequences could also be very crucial for interaction of two C-terminal (active sites) of the same protein for biological function of DNA loop formation in the GalR system as well. We concluded that the DNA sequence changes sub-nanosecond motions in a distant site of a transcription factor and which is likely to have functional consequence for regulation of gene expression [49].

References

[1] A. Manglik and B. Kobilka, The role of protein dynamics in GPCR function: Insights from the β_2AR and rhodopsin, *Curr. Opin. Cell Biol.* **27**, (2014), 136.

[2] W. A. Eaton, V. Muñoz, S. J. Hagen, G. S. Jas, L. J. Lapidus, E. R. Henry and J. Hofrichter, Fast kinetics and mechanisms in protein folding 1, *Annu. Rev. Biophys. Biomol. Struct.* **29**, (2000), 327.

[3] M. Karplus and J. Kuriyan, Molecular dynamics and protein function, *Proc. Natl. Acad. Sci. USA* **102**, (2005), 6679.

[4] H. Frauenfelder, B. H. McMahon, R. H. Austin, K. Chu and J. T. Groves, The role of structure, energy landscape, dynamics, and allostery in the enzymatic function of myoglobin, *Proc. Natl. Acad. Sci. USA* **98**, (2001), 2370.

[5] J. Monod, J. Wyman and J. P. Changeux, On the nature of allosteric transitions: A plausible model, *J. Mol. Biol.* **12**, (1965), 88.

[6] H. N. Motlagh, J. O. Wrabl, J. Li and V. J. Hilser, The ensemble nature of allostery, *Nature* **508**, (2014), 331.

[7] S.-R. Tzeng and C. G. Kalodimos, Dynamic activation of an allosteric regulatory protein, *Nature* **462**, (2009), 368.

[8] J.-P. Changeux and S. J. Edelstein, Allosteric mechanisms of signal transduction, *Science* **308**, (2005), 1424.

[9] N. Popovych, S. Sun, R. H. Ebright and C. G. Kalodimos, Dynamically driven protein allostery, *Nat. Struct. Mol. Biol.* **13**, (2006), 831.

[10] C.-J. Tsai, A. D. Sol and R. Nussinov, Allostery: Absence of a change in shape does not imply that allostery is not at play, *J. Mol. Biol.* **378**, (2008), 1.

[11] V. J. Hilser, J. O. Wrabl and H. N. Motlagh, Structural and energetic basis of allostery, *Annu. Rev. Biophys.* **41**, (2012), 585.

[12] T. C. McLeish, T. Rodgers and M. R. Wilson, Allostery without conformation change: Modelling protein dynamics at multiple scales, *Phys. Biol.* **10**, (2013), 056004.

[13] A. Cooper and D. Dryden, Allostery without conformational change, *Eur. Biophys. J.* **11**, (1984), 103.

[14] H. Toncrova and T. C. McLeish, Substrate-modulated thermal fluctuations affect long-range allosteric signaling in protein homodimers: Exemplified in CAP, *Biophys. J* . **98**, (2010), 2317.

[15] H.-S. Won, T. Yamazaki, T.-W. Lee, M.-K. Yoon, S.-H. Park, Y. Kyogoku and B.-J. Lee, Structural understanding of the allosteric conformational change of cyclic amp receptor protein by cyclic AMP binding, *Biochemistry* **39**, (2000), 13953.

[16] R. A. Laskowski, F. Gerick and J. M. Thornton, The structural basis of allosteric regulation in proteins, *FEBS Lett.* **583**, (2009), 1692.

[17] S. Choudhury, S. Batabyal, P. K. Mondal, P. Singh, P. Lemmens and S. K. Pal, Direct observation of kinetic pathways of biomolecular recognition, *Chem. Eur. J.* **21**, (2015) 16172.

[18] J. Kuriyan and D. Eisenberg, The origin of protein interactions and allostery in colocalization, *Nature* **450**, (2007), 983.

[19] T. Mondol, S. Batabyal, A. Mazumder, S. Roy and S. K. Pal, Recognition of different DNA sequences by a DNA-binding protein alters protein dynamics differentially, *FEBS Lett.* **586**, (2012), 258.

[20] A. Majumdar and S. Adhya, Probing the structure of Gal operator-repressor complexes. Conformation change in DNA, *J. Biol. Chem.* **262**, (1987), 13258.

[21] A. Majumdar and S. Adhya, Demonstration of two operator elements in Gal: In vitro repressor binding studies, *Proc. Natl. Acad. Sci. USA* **81**, (1984), 6100.

[22] S. Semsey, M. Geanacopoulos, D. E. Lewis and S. Adhya, Operator bound GalR dimers close DNA loops by direct interaction: Tetramerization and inducer binding, *EMBO J.* **21**, (2002), 4349.

[23] S. Batabyal, S. Choudhury, D. Sao, T. Mondol and S. Kumar Pal, Dynamical perspective of protein-DNA interaction, *Biomol. Concepts* **5**, (2014), 21.

[24] M. Brenowitz, E. Jamison, A. Majumdar and S. Adhya, Interaction of the Escherichia coli Gal repressor protein with its DNA operators in vitro, *Biochemistry* **29**, (1990), 3374.

[25] S. E. Bondos, L. Swint-Kruse and K. S. Matthews, Flexibility and disorder in gene regulation: LacI/GalR and Hox proteins, *J. Biol. Chem.* **290**, (2015), 685032.

[26] C. Zwieb, J. Kim and S. Adhya, DNA bending by negative regulatory proteins: Gal and Lac repressors, *Genes Dev.* **3**, (1989), 606.

[27] B. Von Wilcken-Bergmann and B. Müller-Hill, Sequence of GalR gene indicates a common evolutionary origin of Lac and Gal repressor in Escherichia coli, *Proc. Natl. Acad. Sci. USA* **79**, (1982), 2427.

[28] J. Yang and Y. Zhang, I-tasser server: New development for protein structure and function predictions, *Nucleic Acids Res.* **43**, (2015), 174.

[29] L. Swint-Kruse and K. S. Matthews, Allostery in the LacI/GalR family: Variations on a theme, *Curr. Opin. Microbiol.* **12**, (2009), 129.

[30] D. Ajdić and J. J. Ferretti, Transcriptional regulation of thestreptococcus mutans Gal operon by the GalR repressor, *J. Bacteriol.* **180**, (1998), 5727.

[31] C. Sonnichsen, B. M. Reinhard, J. Liphardt and A. P. Alivisatos, A molecular ruler based on plasmon coupling of single gold and silver nanoparticles, *Nat. Biotechnol.* **23**, (2005), 741.

[32] S. Weiss, Fluorescence spectroscopy of single biomolecules, *Science* **283**, (1999), 1676.

[33] S. Nag, B. Sarkar, M. Chandrakesan, R. Abhyanakar, D. Bhowmik, M. Kombrabail, S. Dandekar, E. Lerner, E. Haas and S. Maiti, A folding transition underlies the emergence of membrane affinity in amyloid-β, *Phys. Chem. Chem. Phys.* **15**, (2013), 19129.

[34] S. Lehrer, Solute perturbation of protein fluorescence. Quenching of the tryptophyl fluorescence of model compounds and of lysozyme by iodide ion, *Biochemistry* **10**, (1971), 3254.

[35] J. R. Lakowicz, *Principles of fluorescence spectroscopy*, **2013**, Springer Science & Business Media, New York, USA.

[36] S. Choudhury, P. K. Mondal, V. K. Sharma, S. Mitra, V. G. Sakai, R. Mukhopadhyay and S. K. Pal, Direct observation of coupling between

structural fluctuation and ultrafast hydration dynamics of fluorescent probes in anionic micelles, *J. Phys. Chem. B*, **119**, (2015), 10849.

[37] D. Kern and E. R. Zuiderweg, The role of dynamics in allosteric regulation, *Curr. Opin. Struct. Biol.* **13**, (2003), 748.

[38] A. J. Wand, The dark energy of proteins comes to light: Conformational entropy and its role in protein function revealed by NMR relaxation, *Curr. Opin. Struct. Biol.* **23**, (2013), 75.

[39] H.-X. Zhou and M. K. Gilson, Theory of free energy and entropy in noncovalent binding, *Chem. Rev.* **109**, (2009), 4092.

[40] M. S. Marlow, J. Dogan, K. K. Frederick, K. G. Valentine and A. J. Wand, The role of conformational entropy in molecular recognition by Calmodulin, *Nat. Chem. Biol.* **6**, (2010), 352.

[41] J. A. McCammon, B. R. Gelin and M. Karplus, Dynamics of folded proteins, *Nature* **267**, (1977), 585.

[42] F. Gurd and T. Rothgeb, Motions in proteins, *Adv. Protein Chem.* **33**, (1978), 73.

[43] S. Choudhury, S. Batabyal, T. Mondol, D. Sao, P. Lemmens and S. K. Pal, Ultrafast dynamics of solvation and charge transfer in a DNA-based biomaterial, *Chem. Asian J.* **9**, (2014), 1395.

[44] T. Mondol, S. Batabyal and S. K. Pal, Ultrafast electron transfer in the recognition of different DNA sequences by a DNA-binding protein with different dynamical conformations, *J. Biomol. Struct. Dyn.* **30**, (2012), 362.

[45] K. K. Frederick, M. S. Marlow, K. G. Valentine and A. J. Wand, Conformational entropy in molecular recognition by proteins, *Nature* **448**, (2007), 325.

[46] S. Chatterjee, Y.-N. Zhou, S. Roy and S. Adhya, Interaction of Gal repressor with inducer and operator: Induction of Gal transcription from repressor-bound DNA, *Proc. Natl. Acad. Sci. USA* **94**, (1997), 2957.

[47] S. H. Meijsing, M. A. Pufall, A. Y. So, D. L. Bates, L. Chen and K. R. Yamamoto, DNA binding site sequence directs glucocorticoid receptor structure and activity, *Science* **324**, (2009), 407.

[48] S. Deb, S. Bandyopadhyay and S. Roy, DNA sequence dependent and independent conformational changes in multipartite operator recognition by λ-repressor, *Biochemistry* **39**, (2000), 3377.

[49] S. Choudhury, G. Naiya, P. Singh, P. Lemmens, S. Roy and S. K. Pal, Modulation of ultrafast conformational dynamics in allosteric interaction of Gal repressor protein with different operator DNA sequences, *ChemBioChem* **17**, (2016), 605.

Chapter 8

Spectroscopic studies on ultrafast conformational DNA dynamics in specific protein-DNA recognition

8.1. Introduction: Protein-DNA interaction has been explored extensively without fully understanding the forces that imparts specificity [1-2]. Role of allostery in the specific protein-DNA interaction driven control of gene expression is well documented in the literature [3-7]. Dynamically driven allostery appears to be more crucial [8-10]. In a series of studies from our group, we have established that λ-repressor and Gal-repressor show altered ultrafast dynamical motions in the C-terminal domain upon operator DNA-binding in the distant N-terminal domain [11-14]. The dynamics of hydration of operator DNAs are also found to play a key role in the specific protein-DNA interaction [15-19].

In an earlier study, it was concluded that the flexibility of a target DNA may also be important for the specific DNA binding affinity [20]. Mobility of the Lac-repressor binding domain of a target DNA has been indirectly demonstrated by the observation of a mixture of B_I and B_{II} configurations about a phosphate group of the DNA moiety [21]. Although the mobility in terms of a mixture of B_I and B_{II} [22] was found to be intact upon wild type protein (Lac-repressor) binding, a significant change in the DNA mobility was observed in the target DNA upon complexation with the mutant Lac-repressor (Y7I) protein. For the Cro-protein, the increased DNA flexibility of the binding domain with CAC-bases of an operator O_R3 has been reported [20]. In the case of complexation of mutant Cro-protein (V55C) the DNA flexibility of the operator DNA has been found to be significantly reduced [23].

In the above historical context it is known that DNA flexibility plays a key role in the specific interaction with protein. However, till date the direct measurement of the flexibility of the specific protein binding region of a DNA in order to quantify the time scales associated with the flexibility has been sparsely reported in the literature and is the motive of our present work. In the present study, we have introduced a cysteine residue into the N-terminal half of the Cro-protein dimer [24] through site directed mutagenesis (G37C) and labeled the cysteine residue with the probe 5-({2-[(iodoacetyl)amino]ethyl}amino)naphthalene-1-sulfonic acid (IAEDANS). Polarization gated fluorescence of the probe reveals complexation the protein upon specific interaction with different operator DNAs (O_R3 and O_R2). The strategy of investigating the dynamical time scales in the DNA minor grooves upon interaction with specific protein using time-resolved studies is well documented [15, 25]. Polarization gated picosecond resolved fluorescence studies of DAPI (4′,6-diamidino-2-phenylindole) in minor grooves of the operator DNAs have been employed to observe the significant change in the physical motions of the probe in the operator DNAs upon interaction with the Cro-protein dimer. Picosecond resolved stokes shifts (TRES) of the well-known solvation probe DAPI in the DNA have been followed for the investigation of the environmental dynamics in the proximity of the probe [25]. The interactions of the Cro-protein with different operator DNA sequences are found to alter the significant domain fluctuation (hundreds of picosecond to nanosecond time scales) in O_R3 compared to that of the O_R2, which has crucial importance in gene regulatory network.

8.2. Results and discussion:

8.2.1. Ultrafast differential flexibility of Cro-protein binding domains of two operator DNAs with different sequences: In order to investigate how the sequence-specific DNA binding modulates protein conformation and dynamics at or near the site of protein-DNA interaction in the N-terminal half of the Cro-protein, a cysteine was introduced through site-directed mutagenesis into the

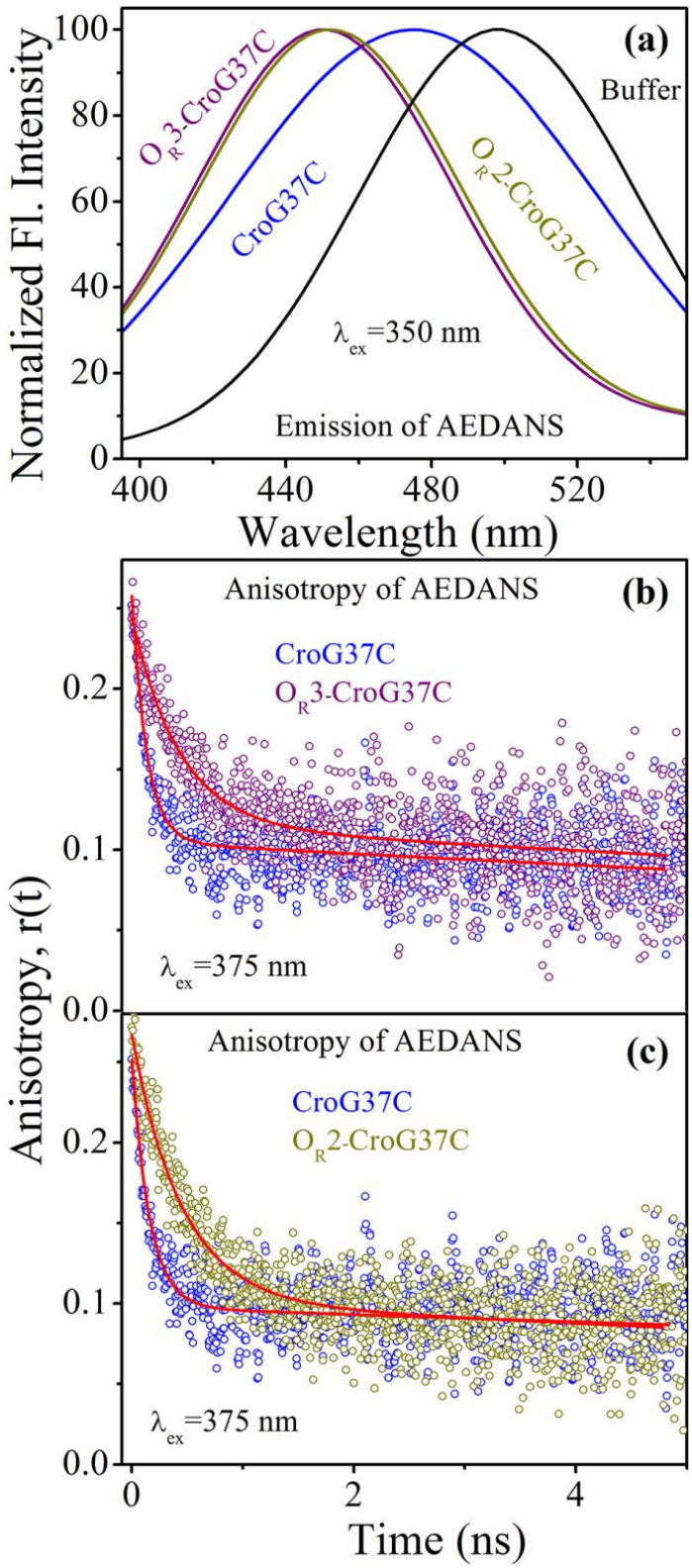

Figure 8.1. *(a) Steady-state emission spectra of fluorescence probe AEDANS in CroG37C, O_R3-CroG37C, O_R2-CroG37C, and buffer (excitation at 350 nm). Picosecond resolved fluorescence anisotropy decays of AEDANS in CroG37C, O_R3-CroG37C (b) and O_R2-CroG37C (c) are shown (excitation at 375 nm).*

N-terminal half (G37C) of the protein which is in close proximity of the protein-DNA interface. It has to be noted that the Glycine37 (G37) residue is not taking part in the Cro protein-operator DNA interaction [26-28]. The reaction of CroG37C with a sulfhydryl reactive fluorescence probe will label Cys37 exclusively due to the absence of cysteine residues in the wild-type Cro-protein. Labeling of cysteine residue with AEDANS to observe structural and dynamical properties of the protein surface is well documented in the contemporary literature [13, 29]. The steady-state emission spectra of the AEDANS group in different systems are shown in Figure 8.1a. A significant blue-shift in the emission spectrum (475 nm) of the probe in CroG37C with respect to that in an aqueous buffer solution (500 nm) indicates the shielded location of the probe in the CroG37C protein dimer (excitation at 350 nm). Further blue-shift in emission spectra of AEDANS-CroG37C upon complexation with its two DNA binding sites, O_R3 and O_R2, (450 nm) compared to that of the probe in the free CroG37C confirms further shifting of the probe towards a less polar environment of the dimer protein molecule. The observation of no significant difference between the emission spectra of the probe in the O_R3–CroG37C and O_R2–CroG37C complexes is consistent with the fact that immediate environment of the AEDANS remains similar in both the complexes.

In order to obtain a molecular picture of rotational flexibility of the free and operator-bound protein, we have investigated the polarization gated fluorescence anisotropy of AEDANS in CroG37C in the absence and presence of O_R3 and O_R2 operator DNA as shown in Figure 8.1b and Figure 8.1c. Numerical fitting of fluorescence anisotropy of CroG37C protein with multi-exponential decay function reveals time constants 160 ps (95%) and 7 ns (5%). The estimated rotational time constant(s) for the tumbling motion of Cro-protein is estimated to be 7 ns using Stokes–Einstein–Debye (SED) equation [12, 30]. During the fitting we have fixed the longer time constant to be 7 ns. The different time constants indicate the different motions (local/global) of AEDANS attached to the Cys37 residue at the N-terminal half of the CroG37C.

Upon complexation with O_R3 operator DNA, the time constants become 500 ps (96%) and 7 ns (4%) as shown in Table 8.1. However, in the case of O_R2 complexation the time components are 390 ps (96%) and 7 ns (4%). This observation clearly indicates that the mobility of the AEDANS (bound to cysteine residue) in the N-terminal half of CroG37C protein upon complexation with operator DNAs becomes restricted, may be due to the shifting of the

Table 8.1. *Rotational time scales of AEDANS attached to Cys37 residue in different systems.*

System	τ_1 (%) ns	τ_2 (%) ns
CroG37C	0.16 ±0.03 (95)	7.0(5)
O_R3-CroG37C	0.50±0.04 (96)	7.0 (4)
O_R2-CroG37C	0.39±0.02 (96)	7.0 (4)

probe into a more hydrophobic pocket of the protein, consistent with the observed anisotropy in the steady-state. However, the flexibility of the probe AEDANS in the O_R2 operator DNA complex is comparatively higher than that in the O_R3 operator DNA complex. This may indicate substantial conformational differences between the two complexes. Overall, the results of the anisotropy decay experiments indicate that residual motion at the N-terminal half of the CroG37C in the complex is DNA sequence-specific.

For further investigation of the dynamics at the protein biding domain of the DNAs, we have labeled both the operator DNAs (O_R3 and O_R2) with DAPI, a well known minor groove binder [25, 31-32]. Figure 8.2a and Figure 8.2b describe the emission spectra of DAPI bound to operators DNAs in the presence and absence of Wild-Type (WT) Cro-protein, along with the emission spectra of DAPI in an aqueous buffer solution. In presence of O_R3 (Figure 8.2a) and O_R2 DNA (Figure 8.2b), the emission maximum of DAPI (465 nm in buffer) is significantly blue shifted (O_R3 operator DNA: 448 nm, O_R2 operator DNA: 447 nm). In the presence of Cro-protein, the emission spectrum is further blue shifted in case of O_R3–Cro complex (442 nm), whereas it remains almost unaltered for the O_R2–Cro complex (445 nm). While steady state anisotropy of

DAPI bound to O_R3 remains almost constant, in the case of O_R3–Cro complex the anisotropy decreases with the increase in detection wavelength as shown in

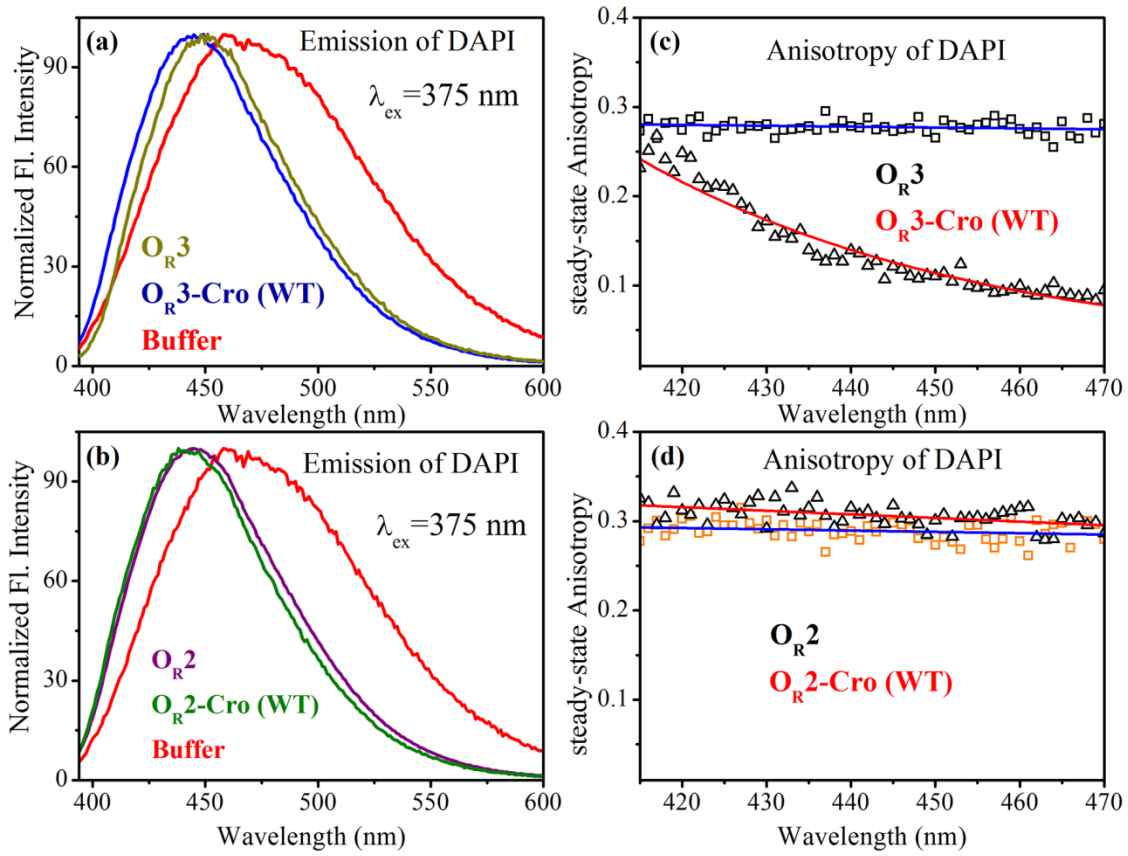

Figure 8.2. *Steady-state emission spectra of fluorescence probe DAPI in O_R3 and O_R3-Cro (Wild Type) (a) and O_R2 and O_R2-Cro (Wild Type) (b) are shown. Steady-state anisotropies of the probe DAPI in corresponding systems are shown in (c) and (d) (excitation at 375 nm). The solid lines in (c) and (d) are guide to eyes.*

Figure 8.2c. The observation can be rationalized in the following two ways. Firstly, the probe DAPI could remain in two different environments namely DNA and bulk solution, revealing less anisotropy in the red edge of the emission spectrum. Another reason could be from a single emissive species of DAPI in DNA with different degrees of solvation [33] which could come from the dynamical flexibility of the probe containing region of the DNA upon complexation with the Cro-protein. We have ruled out the former possibility by time-resolved area normalized emission spectroscopy (TRANES) as evident in the following section. However, in the case of the O_R2 operator DNA

complex, the steady-state anisotropy of DAPI remains constant upon binding with Cro (Figure 8.2d).

To investigate the conformational and structural change within the operator DNA itself in detail that occur upon interaction with Cro-protein, time-resolved anisotropy studies of the probe DAPI were performed. Bi-exponential fitting of fluorescence anisotropy of DAPI in O_R3 operator DNA yielded time component of 80 ps (13%) and 5.83 ns (87%). Upon complexation of the DNA with Cro-protein, the faster time components become 40 ps (35%), as evident from the Figure 8.3a. However, in case of O_R2 operator DNA the time constants were calculated to be 70 ps (15%) and 5.12 ns (85%) and they became 60 ps (24%) and 4.62 ns (76%) upon conjugation with Cro-protein (Figure 8.3b) as shown in Table 8.2. To validate our results we have also fitted

Table 8.2*. Rotational time scales of DAPI attached to O_R3/ O_R2 operator DNA in different systems.*

System	τ_1 (%) ns	τ_2 (%) ns
O_R3	0.08±0.01 (13)	5.83±0.2 (87)
O_R3-Cro (WT)	0.04±0.01 (35)	6.19±0.3 (65)
O_R2	0.07±0.02 (15)	5.12±0.1 (85)
O_R2-Cro (WT)	0.06±0.02 (24)	4.62±0.2 (63)

the parallel and perpendicular fluorescence decays individually by Spencer and Weber equations for all the anisotropy decays and obtained the similar rotational time scales for the corresponding systems [34] consistent with those revealed from the fluorescence anisotropy decays. The observed rotational time constants of the anisotropy decay of the both operator DNAs are consistent with our earlier studies [25]. Our results indicate that the flexibility of the probe in the minor groove of the O_R3 operator DNA in O_R3-Cro complex is higher compared to that of the O_R2-Cro complex, consistent with the steady-state anisotropy study. The decrease in the rotational time scales of the probe in the protein-operator DNA complex compared to that in the corresponding

operator DNA (O_R3) clearly reflects higher dynamical flexibility of the operator DNA upon complexation with the repressor protein leading to the exposure of the probe DAPI to the aqueous environment [35]. In fact a significant bending of the protein binding region of O_R3 compared to O_R2 with the Cro-protein has been observed previously [27, 35-36]. The increased flexibility of the binding

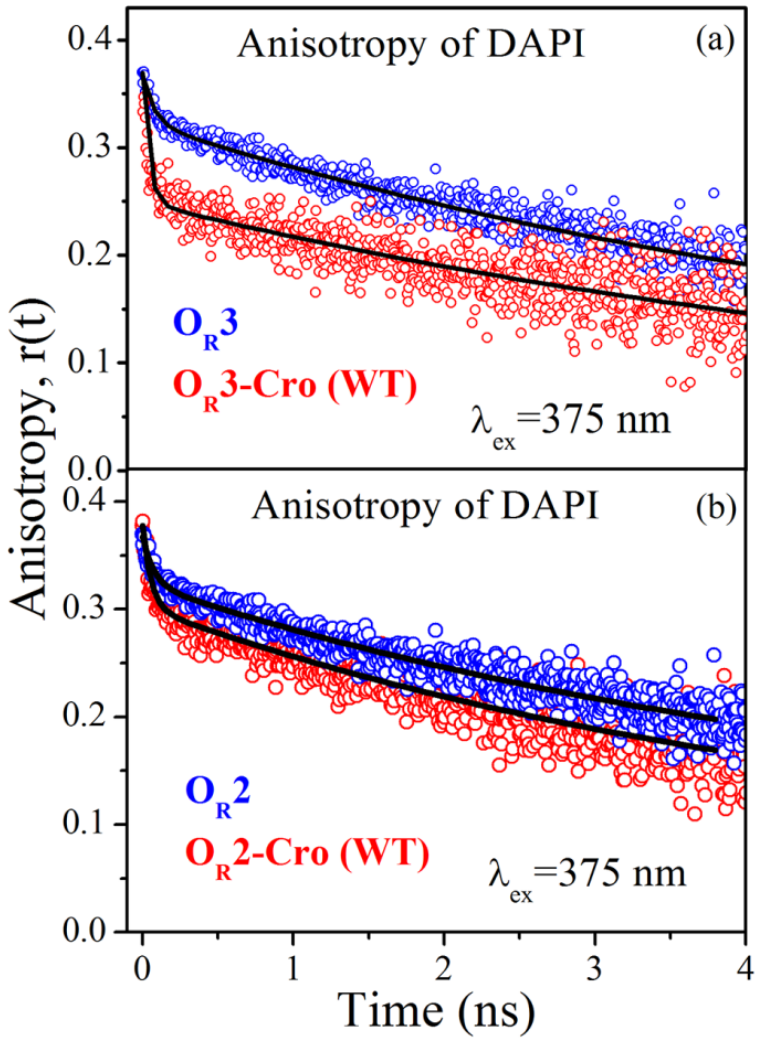

Figure 8.3. *Picosecond resolved fluorescence anisotropy decays of DAPI in O_R3 and O_R3-Cro (wild type) (a) and O_R2 and O_R2-Cro (wild type) (b) are shown.*

region, where the probe DAPI is supposed to reside (middle portion of the operator DNA), in terms of mixture of B_I and B_{II} forms of the DNA has also been evidenced in O_R3 operator [23].

After obtaining the rotation time scales of the DAPI, attached to the operator DNAs and corresponding repressor complex, we have investigated the dynamical timescales of the Cro-protein binding domain of operator DNAs at the protein-DNA interface. Picosecond-resolved fluorescence transients of DAPI bound to operator DNAs in absence and presence of Cro-protein, have been measured at a number of wavelengths across the emission spectrum of DAPI in the complex. Figure 8.4a and Figure 8.4b show the decay transient of DAPI doped O_R3 operator DNA in the absence and presence of Cro-protein at two characteristic wavelengths (extreme blue and red end of the fluorescence

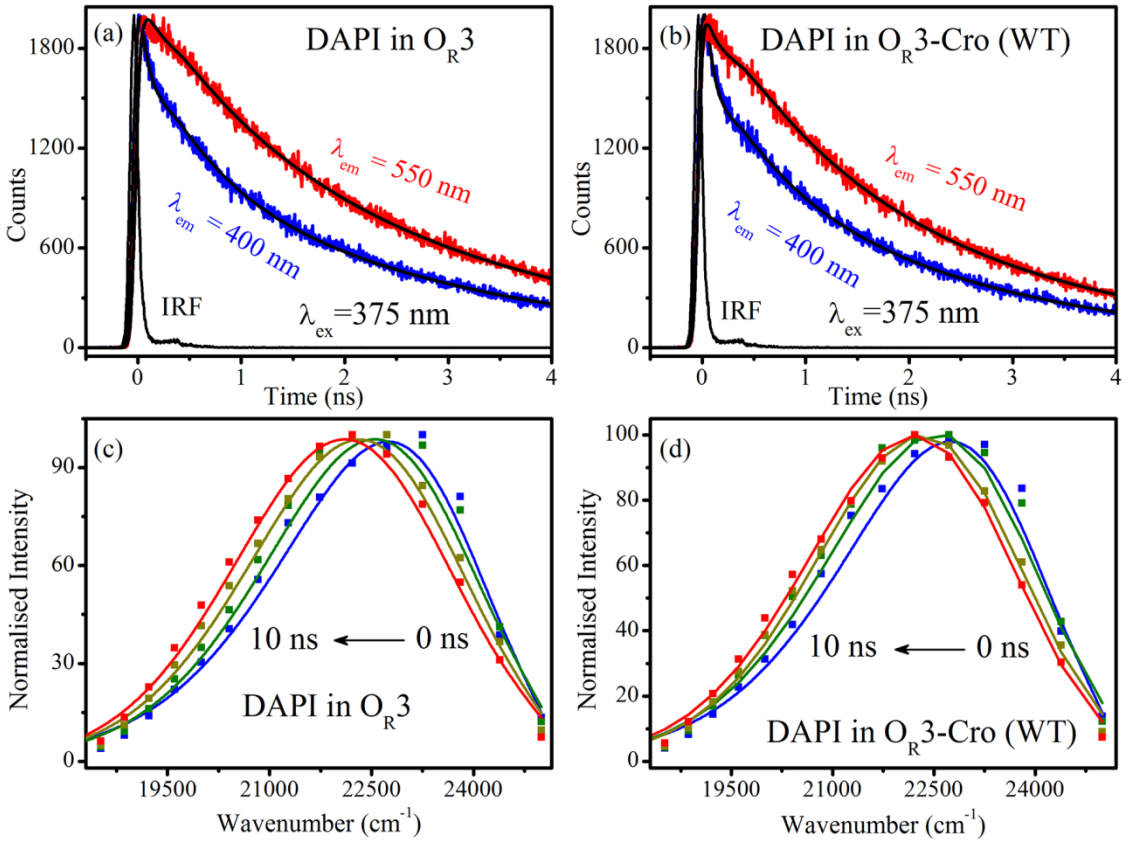

Figure 8.4. *Picosecond-resolved transient of DAPI at blue and red end of the emission spectrum in a) O_R3 and b) O_R3-Cro (wild type) complex. Time-resolved emission spectra (TRES) of corresponding systems are shown in (c) and (d).*

spectrum), respectively. An ultrafast decay component in the blue end is eventually converted into a rise component of a similar time constant in the red end for both the cases. The nature of the wavelength-dependent transients

across the emission spectrum of the probe DAPI in the DNA and protein-DNA complex signifies solvation stabilization of the probe in the DNA environments [37-38]. Figure 8.4c and Figure 8.4d show the constructed time-resolved emission spectra (TRES) of DAPI with a spectral shift of 693 cm^{-1} and 546 cm^{-1} for, O_R3 operator DNA in absence and presence of Cro-protein, respectively, in a 10 ns time window, which indicates that DAPI is stabilized due to solvation by its immediate environment in the excited state. Figure 8.5a and Figure 8.5b displays the transients of DAPI bound to O_R2 operator DNA in absence and presence of Cro-protein respectively. The corresponding TRES are plotted in

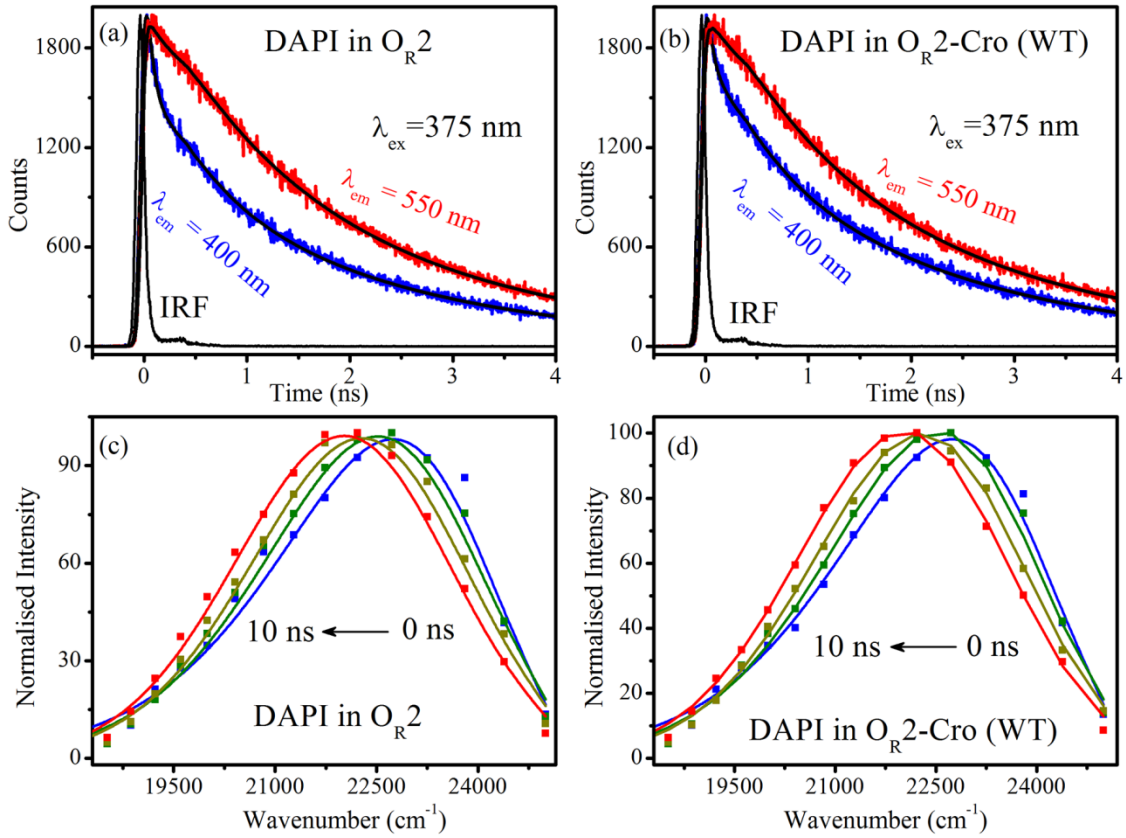

Figure 8.5. *Picosecond-resolved transient of DAPI at blue and red end of the emission spectrum in a) O_R2 and b) O_R2-Cro (wild type) complex. Time-resolved emission spectra (TRES) of corresponding systems are shown in (c) and (d).*

Figure 8.5c and Figure 8.5d with a spectral shift of 708 cm^{-1} and 722 cm^{-1} in the 10 ns window for O_R2 operator DNA and O_R2 operator DNA complex, respectively.

The solvation correlation function [C(t)] for both the DNA and its protein-DNA complex are plotted up to 10 ns as shown in Figure 8.6a and 8.6b, revealing temporal excited-state energy relaxation of the fluorophore in the DNA environments. Two-component exponential decay fitting of C(t) for O_R3 operator DNA yields time components of 0.18 (71%) and 2.0 ns (29%) and for the O_R3-Cro complex the time constants obtained are 30 ps (82%) and 1.55 ns (18%). However, in the case of O_R2 operator DNA and the O_R3-Cro complex the fitting reveals almost similar kind of decay with time constants of 220 ps

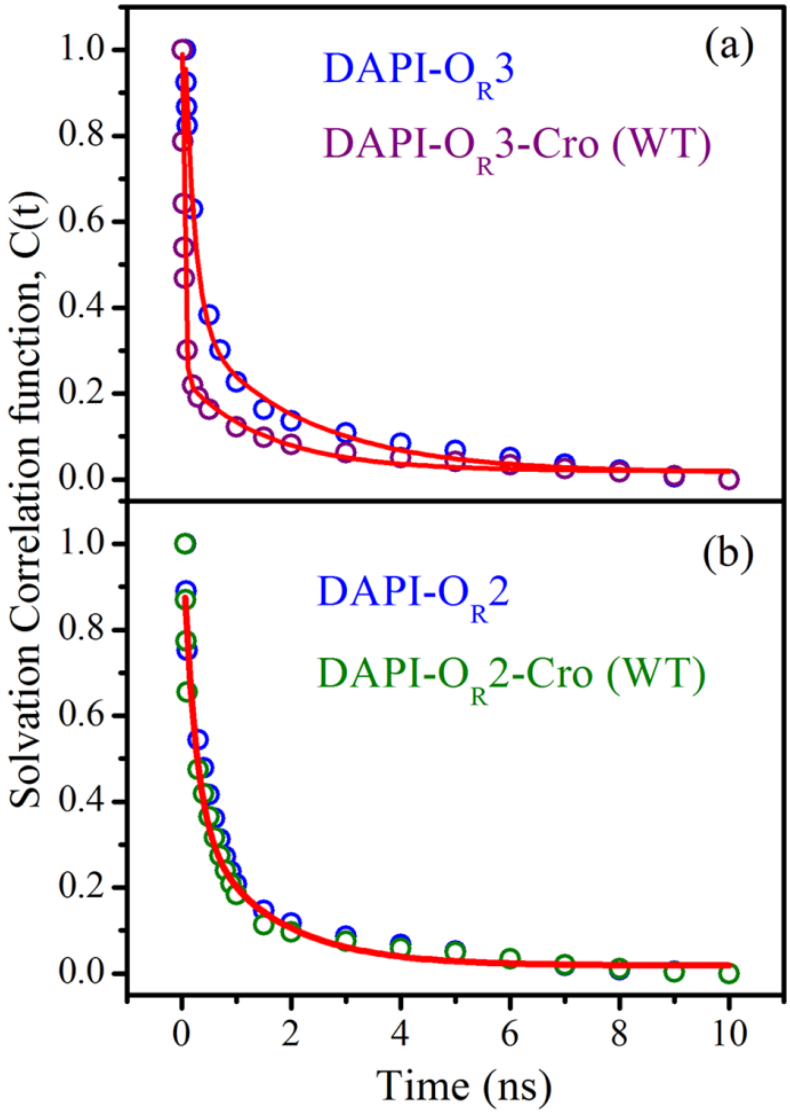

Figure 8.6. *Solvation correlation decay profiles of DAPI in O_R3 and O_R3-Cro (wild type) (a) and O_R2 and O_R2-Cro (wild type) (b) are shown.*

(66%) and 1.43 ns (34%), consistent with earlier reported results [25]. It has to be noted that due to limited time resolution, we are missing the ~1 ps component of DNA minor groove water dynamics [39-40], which is exclusively from bulk-type water in close proximity of DNA surface. However, the observed sub-hundred to few hundred ps timescales are responsible for bound type water dynamics, associated with the DNA minor groove structure [41]. The longer nanosecond time component in C(t) plot is responsible for the relaxation of DNA structural fluctuation [41]. The observation suggests minimal perturbation in the minor groove of O_R2 operator DNA upon

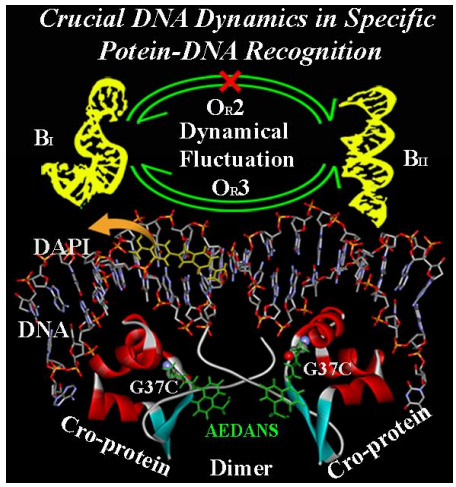

Figure 8.7*. Schematic representation of Cro-protein dimer with two operator DNAs, O_R3 and O_R2. The domain fluctuation (inter conversion of B_I to B_{II} and vice versa) of O_R3 upon complexation with the dimer is also highlighted.*

complexation with Cro-protein. However, in case of O_R3 a significant faster component arises upon interaction with Cro-protein. The observation indicates that upon strong binding with Cro-protein allows the DNA to be more flexible compared to that with the O_R2, consistent with earlier studies [20, 26].

It has to be noted that the faster component of both time resolved anisotropy and solvation of the probe DAPI in O_R3 upon complexation with Cro-protein could be rationalized in terms of DAPI population in DNA and bulk water contributing heterogeneous time scales. In order to rule out the possibility we have performed TRANES analysis of the TRESs of the DAPI in

the operator DNAs before and after the complexation with the Cro-protein. As reported earlier studies TRANES analysis which offer an iso-emissive point in the area normalized TRES, could be excellent tool to conclude the presence of two emissive species in the excited state of a molecule [42-43]. Careful analysis of the TRANES of the probe DAPI in the operator DNAs before and after the complexation with the Cro-protein does not show any iso-emissive point ruling out the possibility of two emitting species in the case of DAPI in O_R3 with the Cro-protein. Thus, the faster time scales in the physical motion (anisotropy) and environmental dynamics (solvation) of the probe DAPI clearly reveals enhanced dynamical flexibility of the protein binding region of the operator DNA O_R3 compared to that of the operator O_R2. The overall picture that comes from our present experimental studies is shown in Figure 8.7.

8.3. Conclusion: Till date, what determines the affinities of DNA-binding proteins for their target sequences is only understood in a broad sense. The least understood aspect is the entropic contributions which may fine-tune the affinity for different target sites. The entropic contributions may be in the form of conformational entropy of bound protein or DNA, the entropy of solvent molecules associated with proteins and DNA or the entropy of ion-release associated with the DNA or the protein. Even small changes in any of these components may alter the binding affinities enough to alter biological outcomes. Thus, it is important to understand the motional characteristics of proteins, DNAs and their respective hydration layers in different protein-DNA complexes. Cro-protein binds to O_R3 with approximately 3 Kcal/mole more binding energy than that of the O_R2 [44]. Cro-protein association with O_R3 is entropy driven, suggesting a significant role of the entropic component. Significant reduction of DNA relaxation time upon Cro binding to O_R3, as reported here, suggests an increase in DNA-domain entropy upon complex formation. Interestingly, such a reduction is not apparent in the case of O_R2, indicating that there may be a differential entropic stabilization of the O_R3 complex with respect to the O_R2 complex. At least a part of the differential

affinity between O_R3 and O_R2 may be accounted for by such DNA-domain dynamics.

In brief, we suggest that recognition of different DNA sequences by a transcription factor not only involves different interaction patterns of protein atoms with that of the DNA atoms, the motional freedom of the macromolecules also undergo significant changes. We propose that a full understanding of protein-DNA recognition must involve elucidation of the entropic character of the participating macromolecules and protein binding domains of the operator DNAs [45].

References

[1] S. A. Teichmann and M. M. Babu, Gene regulatory network growth by duplication, *Nat. Genet.* **36**, (2004), 492.

[2] D. S. Johnson, A. Mortazavi, R. M. Myers and B. Wold, Genome-wide mapping of in vivo protein-DNA interactions, *Science* **316**, (2007), 1497.

[3] A. Manglik and B. Kobilka, The role of protein dynamics in GPCR function: Insights from the β_2AR and rhodopsin, *Curr. Opin. Cell Biol.* **27**, (2014), 136.

[4] M. Shiina, K. Hamada, T. Inoue-Bungo, M. Shimamura, A. Uchiyama, S. Baba, K. Sato, M. Yamamoto and K. Ogata, A novel allosteric mechanism on protein–DNA interactions underlying the phosphorylation-dependent regulation of Ets 1 target gene expressions, *J. Mol. Biol.* **427**, (2015), 1655.

[5] J. A. Lefstin and K. R. Yamamoto, Allosteric effects of DNA on transcriptional regulators, *Nature* **392**, (1998), 885.

[6] H. N. Motlagh, J. O. Wrabl, J. Li and V. J. Hilser, The ensemble nature of allostery, *Nature* **508**, (2014), 331.

[7] R. Nussinov, C. J. Tsai and J. Liu, Principles of allosteric interactions in cell signaling, *J. Am. Chem. Soc.* **136**, (2014), 17692.

[8] N. Popovych, S. Sun, R. H. Ebright and C. G. Kalodimos, Dynamically driven protein allostery, *Nat. Struct. Mol. Biol.* **13**, (2006), 831.

[9] J. Monod, J. Wyman and J.-P. Changeux, On the nature of allosteric transitions: A plausible model, *J. Mol. Biol.* **12**, (1965), 88.

[10] S.-R. Tzeng and C. G. Kalodimos, Dynamic activation of an allosteric regulatory protein, *Nature* **462**, (2009), 368.

[11] S. Batabyal, S. Choudhury, D. Sao, T. Mondol and S. Kumar Pal, Dynamical perspective of protein-DNA interaction, *Biomol. Concepts* **5**, (2014), 21.

[12] T. Mondol, S. Batabyal, A. Mazumder, S. Roy and S. K. Pal, Recognition of different DNA sequences by a DNA-binding protein alters protein dynamics differentially, *FEBS Lett.* **586**, (2012), 258.

[13] S. Choudhury, G. Naiya, P. Singh, P. Lemmens, S. Roy and S. K. Pal, Modulation of ultrafast conformational dynamics in allosteric interaction of gal repressor protein with different operator DNA sequences, *ChemBioChem* **17**, (2016), 605.

[14] T. Mondol, S. Batabyal and S. K. Pal, Ultrafast electron transfer in the recognition of different DNA sequences by a DNA-binding protein with different dynamical conformations, *J. Bimol. Struct. Dyn.* **30**, (2012), 362.

[15] S. Batabyal, T. Mondol, S. Choudhury, A. Mazumder and S. K. Pal, Ultrafast interfacial solvation dynamics in specific protein DNA recognition, *Biochimie* **95**, (2013), 2168.

[16] Y. Levy and J. N. Onuchic, Water mediation in protein folding and molecular recognition, *Annu. Rev. Biophys. Biomol. Struct.* **35**, (2006), 389.

[17] D. U. Ferreiro, I. E. Sánchez and G. de Prat Gay, Transition state for protein–DNA recognition, *Proc. Natl. Acad. Sci. USA* **105**, (2008), 10797.

[18] Y. Yang, Y. Qin, Q. Ding, M. Bakhtina, L. Wang, M.-D. Tsai and D. Zhong, Ultrafast water dynamics at the interface of the polymerase–DNA binding complex, *Biochemistry* **53**, (2014), 5405.

[19] S. Choudhury, S. Batabyal, P. K. Mondal, P. Singh, P. Lemmens and S. K. Pal, Direct observation of kinetic pathways of biomolecular recognition, *Chem. Eur. J.* **21**, (2015), 16172.

[20] Y. L. Lyubchenko, L. S. Shlyakhtenko, E. Appella and R. E. Harrington, Ca runs increase DNA flexibility in the complex of .Lambda Cro protein with the O_R3 site, *Biochemistry* **32**, (1993), 4121.

[21] C. Karslake, M. V. Botuyan and D. G. Gorenstein, Phosphorus-31 NMR spectra of oligodeoxyribonucleotide duplex Lac operator-repressor headpiece complexes: Importance of phosphate ester backbone flexibility in protein-DNA recognition, *Biochemistry* **31**, (1992), 1849.

[22] M. Trieb, C. Rauch, B. Wellenzohn, F. Wibowo, T. Loerting and K. R. Liedl, Dynamics of DNA: B_I and B_{II} phosphate backbone transitions, *J. Phys. Chem. B* **108**, (2004), 2470.

[23] J. D. Baleja and B. D. Sykes, A nuclear magnetic resonance study of the DNA-binding affinity of Cro-repressor protein stabilized by a disulfide bond, *Biochem. Cell Biol.* **72**, (1994), 95.

[24] P. J. Darling, J. M. Holt and G. K. Ackers, Coupled energetics of λ Cro-repressor self-assembly and site-specific DNA operator binding I: Analysis of Cro dimerization from nanomolar to micromolar concentrations, *Biochemistry* **39**, (2000), 11500.

[25] D. Banerjee and S. K. Pal, Dynamics in the DNA recognition by DAPI: Exploration of the various binding modes, *J. Phys. Chem. B* **112**, (2008), 1016.

[26] R. G. Brennan, S. L. Roderick, Y. Takeda and B. W. Matthews, Protein-DNA conformational changes in the crystal structure of a lambda Cro-operator complex, *Proc. Natl. Acad. Sci. USA* **87**, (1990), 8165.

[27] W. Anderson, D. Ohlendorf, Y. Takeda and B. Matthews, Structure of the Cro repressor from bacteriophage λ and its interaction with DNA, *Nature* **290**, (1981), 754.

[28] Y. Takeda, A. Sarai and V. M. Rivera, Analysis of the sequence-specific interactions between Cro-repressor and operator DNA by systematic base substitution experiments, *Proc. Natl. Acad. Sci. USA* **86**, (1989), 439.

[29] J. Fang, A. Mehlich, N. Koga, J. Huang, R. Koga, X. Gao, C. Hu, C. Jin, M. Rief and J. Kast, Forced protein unfolding leads to highly elastic and tough protein hydrogels, *Nat. Commun.* **4**, (2013), 2974.

[30] T. Köddermann, R. Ludwig and D. Paschek, On the validity of Stokes–Einstein and Stokes–Einstein–Debye relations in ionic liquids and ionic-liquid mixtures, *ChemPhysChem* **9**, (2008), 1851.

[31] J. Riedl, R. Pohl, N. P. Ernsting, P. Orság, M. Fojta and M. Hocek, Labelling of nucleosides and oligonucleotides by solvatochromic 4-aminophthalimide fluorophore for studying DNA–protein interactions, *Chem. Sci.* **3**, (2012), 2797.

[32] J. Kapuscinski, DAPI: A DNA-specific fluorescent probe, *Biotech. Histochem.* **70**, (2009), 220.

[33] A. Chattopadhyay, A. Arora and D. A. Kelkar, Dynamics of a membrane-bound tryptophan analog in environments of varying hydration: A fluorescence approach, *Eur. Biophys. J.* **35**, (2005), 62.

[34] D. O'Connor, *Time-correlated single photon counting*, **2012**, Academic Press, USA.

[35] D. A. Erie, G. Yang, H. C. Schultz and C. Bustamante, DNA bending by Cro protein in specific and nonspecific complexes: Implications for protein site recognition and specificity, *Science* **266**, (1994), 1562.

[36] C. Torigoe, S.-i. Kidokoro, M. Takimoto, Y. Kyogoku and A. Wada, Spectroscopic studies on λ Cro protein-DNA interactions, *J. Mol. Biol.* **219**, (1991), 733.

[37] S. Choudhury, P. K. Mondal, V. K. Sharma, S. Mitra, V. G. Sakai, R. Mukhopadhyay and S. K. Pal, Direct observation of coupling between structural fluctuation and ultrafast hydration dynamics of fluorescent probes in anionic micelles, *J. Phys. Chem. B* **119**, (2015), 10849.

[38] S. Choudhury, S. Batabyal, T. Mondol, D. Sao, P. Lemmens and S. K. Pal, Ultrafast dynamics of solvation and charge transfer in a DNA-based biomaterial, *Chem. Asian J.* **9**, (2014), 1395.

[39] S. K. Pal, L. Zhao and A. H. Zewail, Water at DNA surfaces: Ultrafast dynamics in minor groove recognition, *Proc. Natl. Acad. Sci. USA* **100**, (2003), 8113.

[40] S. K. Pal, L. Zhao, T. Xia and A. H. Zewail, Site-and sequence-selective ultrafast hydration of DNA, *Proc. Natl. Acad. Sci. USA* **100**, (2003), 13746.

[41] E. B. Brauns, M. L. Madaras, R. S. Coleman, C. J. Murphy and M. A. Berg, Measurement of local DNA reorganization on the picosecond and nanosecond time scales, *J. Am. Chem. Soc.* **121**, (1999), 11644.

[42] A. Koti, M. Krishna and N. Periasamy, Time-resolved area-normalized emission spectroscopy (TRANES): A novel method for confirming emission from two excited states, *J. Phys. Chem. A* **105**, (2001), 1767.

[43] S. Rakshit, R. Saha, P. K. Verma and S. K. Pal, Role of solvation dynamics in excited state proton transfer of 1-naphthol in nanoscopic

water clusters formed in a hydrophobic solvent, *Photochem. Photobiol.* **88**, (2012), 851.

[44] P. J. Darling, J. M. Holt and G. K. Ackers, Coupled energetics of λ Cro-repressor self-assembly and site-specific DNA operator binding II: Cooperative interactions of Cro dimers, *J. Mol. Biol.* **302**, (2000), 625.

[45] S. Choudhury, B. Ghosh, P. Singh, R. Ghosh, S. Roy and S. K. Pal, Ultrafast differential flexibility of Cro-protein binding domains of two operator DNAs with different sequences, *Phys. Chem. Chem. Phys.* **18**, (2016), 17983.

List of Publications

1. **S. Choudhury**, P. K. Mondal, V. Sharma, S. Mitra, V. Garcia-Sakai, R. Mukhopadhyay and S. K. Pal, Direct observation of coupling between structural fluctuation and ultrafast hydration dynamics of fluorescent probes in anionic micelles, *J. Phys. Chem. B* **119,** (2015), 10849.
2. **S. Choudhury**, S. Batabyal, T. Mondol, D. Sao, P. Lemmens and S. K. Pal, Ultrafast dynamics of solvation and charge transfer in a DNA-based biomaterial, *Chem. Asian J.* **9,** (2014), 1395.
3. **S. Choudhury**, S. Batabyal, P. K. Mondal, P. Singh, P. Lemmens and S. K. Pal, Direct observation of kinetic pathways of biomolecular recognition, *Chem. Eur. J.* **21,** (2015), 16172.
4. **S. Choudhury**, G. Naiya, P. Singh, P. Lemmens, S. Roy and S. K. Pal, Modulation of ultrafast conformational dynamics in allosteric interaction of Gal repressor protein with different operator DNA sequences, *ChemBioChem* **17,** (2016), 605 (Cover Article).
5. **S. Choudhury,** B. Ghosh, P. Singh, R. Ghosh, S. Roy and S. K. Pal, Ultrafast differential flexibility of Cro-protein binding domains of two operator DNAs with different sequences, *Phys. Chem. Chem. Phys.* **18,** (2016), 17983.

*6. S. Batabyal, **S. Choudhury**, D. Sao, T. Mondol and S. K. Pal, Dynamical perspective of protein DNA interaction, *Biomol. Concepts* **5,** (2014), 21.

*7. P. Singh, **S. Choudhury**, G. K. Chandra, P. Lemmens and S. K. Pal, Molecular recognition of genomic DNA in a condensate with a model surfactant for potential gene-delivery applications, *J. Photochem. Photobiol. B* **157,** (2016), 105.

*8. S. Batabyal, T. Mondol, **S. Choudhury**, A. Mazumder and S. K. Pal, Ultrafast interfacial solvation dynamics in specific protein DNA recognition, *Biochimie* **95,** (2013), 2168.

*9. T. Mahata, A. Kanungo, S. Ganguly, E. K.Modugula, **S. Choudhury**, S. K. Pal, G. Basu and S. Dutta, A benzyl moiety in a quinoxaline-based scaffold acts as a DNA intercalation switch, *Angew. Chem. Int. Ed.* **55,** (2016), 7733.

*10. A. Mathew, E. Varghese, **S. Choudhury**, S. K. Pal and T. Pradeep, Efficient red luminescence from organic-soluble Au25 clusters by ligand structure modification, *Nanoscale* **7,** (2015), 14305.

*11. K. R. Krishnadas, T. Udayabhaskararao **S. Choudhury**, N. Goswami, S. K. Pal and T. Pradeep, Luminescent AgAu alloy clusters derived from Ag nanoparticles: manifestations of tunable Au(I)-Cu(I) metallophilic interactions, *Eur. J. Inorg. Chem.* **5,** (2014), 908.

*12. D. Bagchi, S. Chaudhuri, S. Sardar, **S. Choudhury**, N. Polley, P. Lemmens and S. K. Pal, Modulation of stability and functionality of a phyto-antioxidant by weakly interacting metal ions: Curcumin in aqueous solution, *RSC Adv.* **5,** (2015), 102516.

*13. S. Ghosh, H. Remita, P. Kar, **S. Choudhury**, S. Sardar, P. Beaunier, P. S. Roy, S. K. Bhattacharya and S. K. Pal, Facile synthesis of Pd nanostructures in hexagonal mesophases as promising electrocatalyst for ethanol oxidation, *J. Mat. Chem. A* **3,** (2015), 9517.

*14 G. Naiya, P. Raha, M. K. Mondal, U. Pal, R. Saha, **S. Choudhury**, S. Batabyal, S. K. Pal, D. Bhattacharyya, N. C. Maiti and S. Roy, Conformational selection underpins recognition of multiple DNA sequences by proteins and consequent functional actions, *Phys. Chem. Chem. Phys.* **18,** (2016), 21618.

*15 M. Khatun, **S. Choudhury**, B. Liu, P. Lemmens, S. K. Pal and S. Mazumder, Resveratrol-ZnO nanohybrid enhanced anti-cancerous effect in ovarian cancer cells through ROS, *RSC Adv.* **6**, (2016), 105607.

* Not included in the thesis.